# Analysis and Assessment of Masonry Arch Bridges

Justin Robinson BEng

Doctor of Philosophy

University of Edinburgh
March 2000

# Abstract

The importance of masonry arch bridges to the transport infrastructure throughout Europe is unquestionable. However with ever increasing axle loads present on today's roads, and new European directives increasing the required load carrying capacity of these structures, the need for an accurate and reliable method of arch bridge assessment has never been more important. The current methods of arch bridge assessment have been shown to be conservative, resulting in unnecessary and costly repair work or replacement of structures. The research described in this thesis is an element of an on-going study into soil-structure interaction, a very important factor for the accurate assessment of arch bridges.

This investigation, furthering study into the effects of soil-structure interaction, is undertaken with a variety of methods and techniques which are described in this thesis. These include model bridge testing, investigating different load types and fill heights, monitoring of full scale structures and subsequent analysis investigating thermal effects, comparison of the present arch bridge assessment methods linked with an actual arch bridge assessment programme and the development of new numerical modelling methods of arch assessment. Thus an investigation using discrete element analysis methods has been conducted, with comparison with finite element methods and physical models.

A new technique for arch bridge assessment has been introduced, based on the discrete element analysis performed in this thesis. This method allows the inclusion into an analysis of soil-structure interaction effects and the possibility to include many other 3-D effects.

# Declaration

This thesis is submitted to the University of Edinburgh for the degree of Doctor of Philosophy. The work submitted in this thesis has been composed by myself, under the supervision of Dr David A. Ponniah, unless otherwise referenced within the text.

The following papers published in journals or conference proceedings were derived from the work in this thesis. A set of these papers is bound, where possible, with the thesis and may be found in Appendix D. The numbering sequence does not follow that of the thesis but follows the page numbering of the original journal or proceedings as appropriate.

1. Robinson, J.I., Ponniah, D.A. and Prentice, D.J. Soil pressure measurements on a multi-span brick arch. Proceedings of the Seventh International Conference on Structural Faults and Repair, Edinburgh, 1997.

2. Robinson, J.I., Prentice, D.J. and Ponniah, D.A. Temperature effects in a new brickwork arch bridge. Proceedings of the Seventh International Conference on Structural Faults and Repair, Edinburgh, 1997.

3. Robinson, J.I., Prentice, D.J. and Ponniah, D.A. Thermal effects on a masonry arch bridge investigated using ABAQUS. Proceedings of the Second International Arch Bridge Conference, Venice, 1998.

4. Robinson, J.I., Thavalingam, A., Ponniah, D.A., Bicanic, N. Computational framework for discontinuous modelling of masonry arch bridges. Submitted to Computers and Structures.

5. Robinson, J.I., Thavalingam, A., Ponniah, D.A., Bicanic, N. Comparative prediction of the collapse load for masonry arches including backfill interaction. Corrected and resubmitted to Masonry International. March 2000.

6. Robinson, J.I., O'Flaherty, M, Stewart, P. and Ponniah, D.A. Comparative assessment of masonry arch assessment methods. Under preparation.

7. Prentice, D.J., Robinson, J.I. and Ponniah, D.A. Stress distribution in an instrumented double span brick arch bridge. Under preparation.

# Acknowledgements

The author would firstly like to acknowledge the assistance and guidance given during the course of this thesis of his supervisor, Dr. David A. Ponniah.

The funding for the research was provided by the EPSRC and the University of Edinburgh, through payment for the supervision and teaching of undergraduate students. Without this financial support the project would not have been completed.

Significant assistance has been obtained from Prof. Nenad Bićanić from the University of Glasgow and Dr. Appapillai Thavalingam, in the field of discrete element analysis.

The author is also indebted to Murray Innes, Stuart Wallace, Paul Huyton, George Karidis, Micheal O'Flaherty and Paul Stewart who, in the course of studying for their respective final year Honours thesis, helped with experimentation, analysis of results, comparative studies and arch bridge assessments which form parts of this thesis. Many thanks are also due to Richard Boyd and James Jarvis for solving the many "easy" problems involved in the presentation of this thesis.

Lastly and most importantly I would like to thank my parents for the many types of support they have so kindly offered throughout this extended period of research.

# Contents

# List of Figures

# List of Tables

# Notation

The definitions of the symbols used in this thesis are given below. Roman characters are given first, followed by Greek characters. Symbols are also defined where they first appear in the text. Where overlap of definitions has occurred the meaning will be evident from the context in which it is used.

## Roman characters

| | | |
|---|---|---|
| $A$ | - | area of the cross section |
| $d$ | - | thickness of the arch barrel |
| $d_a$ | - | thickness of the arch barrel at abutment |
| $d_c$ | - | thickness of the arch barrel at crown |
| $\underline{D}$ | - | displacement matrix |
| $D_{mag}$ | - | displacement magnification factor |
| $e$ | - | void ratio |
| $E$ | - | Young's modulus of elasticity |
| $F_b$ | - | barrel factor |
| $F_c$ | - | condition factor |
| $F_d$ | - | depth factor |
| $F_f$ | - | fill factor |
| $F_j$ | - | joint factor |
| $F_m$ | - | material factor |
| $F_{mo}$ | - | mortar factor |
| $F_p$ | - | profile factor |
| $F_{sr}$ | - | span/rise factor |
| $F_w$ | - | width factor |
| $\underline{F}$ | - | force matrix |
| $f$ | - | limiting stress |
| $h$ | - | depth of fill at crown, including surfacing |
| $H_{max}$ | - | maximum horizontal thrust |
| $I$ | - | moment of inertia of the cross section |

$k$ - friction coefficient
$K_a'$ - coefficient of active earth pressure
$K_o'$ - coefficient of at rest earth pressure
$K_p'$ - coefficient of passive earth pressure
$\underline{K}$ - stiffness matrix
$L$ - arch span
$M$ - bending moment
$p$ - point load
$q^{ave}$ - average contact stress
$q^{max}$ - maximum contact stress
$r$ - radius of arch intrados *or* correlation coefficient
$r_c$ - rise at midspan
$r_q$ - rise at quarter span
$r^2$ - coefficient of uniformity
$R$ - reaction force
$T$ - axial force
$T_e$ - coefficient of thermal expansion
$W$ - point/failure load
$W_p$ - provisional axle load
$W_m$ - modified axle load
$x$ - horizontal distance from crown

## Greek characters

$\gamma$ - bulk unit weight
$\lambda_i$ - contact force for iteration $i$
$\phi$ - angle of shearing resistance
$\sigma_c$ - uniaxial compressive strength
$\sigma_1$ - major principal stress
$\sigma_2$ - minor principal stress
$\sigma_n$ - normal stress
$\rho$ - density
$\rho_m$ - masonry density
$\rho_f$ - fill density
$\rho_s$ - surfacing or road density
$\tau$ - shear stength
$\omega$ - uniformaly distributed load

# Glossary of terms

Some of these definitions are taken from British Standard BS 6100[7] and BD/21,[8] Glossary of building and Civil Engineering terms and from the British Standard BS 5390,[9] Code of practice for stone masonry.

| | |
|---|---|
| Abutment | The body, usually of masonry, which provides the resistance to the thrust of the arch. |
| Arch ring | The load bearing part of the bridge. |
| Backing | Material, usually of lower quality, used to fill in or give support behind the arch structure. |
| Bedding plane | The plane of stratification of the stone. |
| Bond | Arrangement of masonry units so that the vertical joints of one course do not coincide with those of courses immediately above or below. |
| Buttress | A pier at right angles to a wall, built to help the wall resist earth or arch thrust or water pressure. |
| Dead load | Loading due to the weight of the materials forming the structure or structural elements. |
| Dressing | Surface finish to a stone produced by working. |
| Efflorescence | Crystalline deposit on the surface of masonry after evaporation of water that has carried soluble salts from within. |
| Extrados | The outer convex curve of an arch. |
| Face | Exposed surface of a structure or masonry unit. |
| Footing | A widening of any structure at the foot to improve stability. |
| Gothic | Pointed arch. |
| Haunch | The lower section of the arch ring towards the springing. |
| Haunching | see Backing |
| Hydraulic (lime) | Mortar which is able to set and harden under water. |
| Intrados | The inner (concave) curve or an arch. |
| Keystone | Central voussoir at the crown of an arch. |

| | |
|---|---|
| Masonry | Construction made from stone, bricks or blocks. |
| Overbridge | A bridge over the facility in question, e.g. a canal overbridge is one over a canal. |
| Parapet | Upward extension of a spandrel wall above road surface level. |
| Pier | In intermediate support between adjoining bridge spans or a thickened section located at intervals along a wall to strengthen it. |
| Pointing | The finishing of joints in mortar as the work proceeds or the filling with mortar of the joints in a wall from which the bedding or jointing mortar has been removed. |
| Rib | A band of masonry projecting from the soffit of the arch. |
| Rise | Vertical height from springing level to the crown of the intrados. |
| Saddle | A concrete slab cast over an arch to strengthen it or to distribute loads upon it. |
| Skew arch | Arch whose longitudinal and transverse axes are not at right angles. |
| Spalling | Flaking from the face of a masonry unit caused by frost, crystallisation of salts or mechanical action. |
| Spandrel wall | A wall parallel to the road carried on the arch extrados. |
| Springing | Plane from which an arch springs. |
| Under-bridge | A bridge under the facility in question, i.e. a road under-bridge is one under and carrying a road. |
| Underpinning | Providing new, deeper support under a wall or column without removing the superstructure. |
| Vault | Arched ceiling over a void or any space covered by arches. |
| Viaduct | A road or railway bridge over a valley consisting of a series of spans carried on piers. |
| Voussoir | Wedge shaped masonry unit in an arch. |
| Wing wall | A wall at the abutment of a bridge which extends beyond the bridge to retain the earth behind the abutment. |

# Chapter 1

# Introduction

## 1.1 General introduction to masonry arch bridges

### 1.1.1 The masonry arch bridge

Wherever we travel we are bound to encounter bridges as part of a transport infrastructure, and for many centuries the masonry arch bridge appears to have been the dominant form. Figure 1.1 shows the basic structural elements which make up a masonry arch bridge. For each type of bridge, but in particular the masonry arch, there exists a relationship between the structural form of a bridge and the materials used for its construction. The masonry arch makes use of materials with little or no tensile strength and relies on their ability to resist compression. Stone is very weak in tension, and until the discovery of the arch, could only be used for very short spans. Any load applied to a bridge is transmitted through the road pavement to the fill and then distributed through the fill material onto the arch extrados. The arch barrel then transmits these distributed forces through its structure back into the fill and into the abutments through the springings. Hence arch bridges push their supports outwards, and this has to be resisted by forces produced by the ground pressing against the abutments or pier foundations. Generally, the smaller the span of the arch, the less horizontal force is exerted. Larger spans have in general only been possible in more recent times, although some medieval examples of these 'segmental arch' (so called because the wide arch forms only a segment of a circle) still exist today, for example the Ponte Vecchio in Florence (completed 1356).

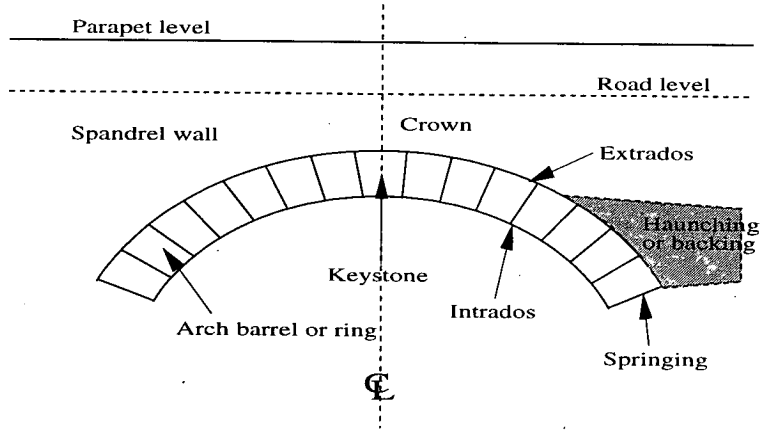


Figure 1.1: Salient parts of an arch bridge

The strength of masonry arches is highly dependent upon the strength of the arch barrel, which is generally built with strong dressed masonry units or brickwork. Arch strength is also very dependent upon the fill material used to transmit load to and from the arch barrel. This fill material can be variable in its nature and material properties and may often contain voids or unexpected material such as backing. Due to the present nature of arch assessment, namely finding the load capacity of an arch, it is the nature of the fill which is sometimes most difficult to identify.

Arch bridges are thought as being very simple structures; however the method by which the structure transmits applied loads to its supports is complicated to analyse or assess. These difficulties have meant that, even today, masonry arch bridge assessment methods are in many cases either over-complicated or over-simplistic and as yet cannot be fully relied upon for accurate assessment.

### 1.1.2 History of construction

The masonry arch has been known to exist in various forms for many thousands of years and has been shown to be in constant general use up to the present time. The Romans were undoubtedly the first major exploiter of arched forms in construction, with many examples of their work still existing today, paying testament to the durability and popularity of such structures. Changes in the importance of the symbolism and the functionality of differently shaped arches over the years demanded changes in the type of arch being constructed. Many of the theories of arch bridge analysis and construction came to fruition in the period between 1850 and 1880. The major driving force for this was the industrial revolution occurring throughout Europe and the United States at this time, leading to the need for a large transportation infrastructure; an example of the is the the increase in the the railway network by 700% in the same period.[10] During these years the nature of civil engineering also changed, due to the size of construction work required - greater than any person, company or even country could manage alone. A majority of the masonry arches existing today were constructed around this period; the transport infrastructure of many European countries relied greatly on this type of structure.

The requirement for a structure to get from one place to another in a single

span dictates the conceptual design of a bridge.[1] (*Here conceptual is assumed to mean from an original idea.*) Masonry bridges are very complicated structures, with many criteria being identified as being important for their design and construction, as shown in Figure 1.2.

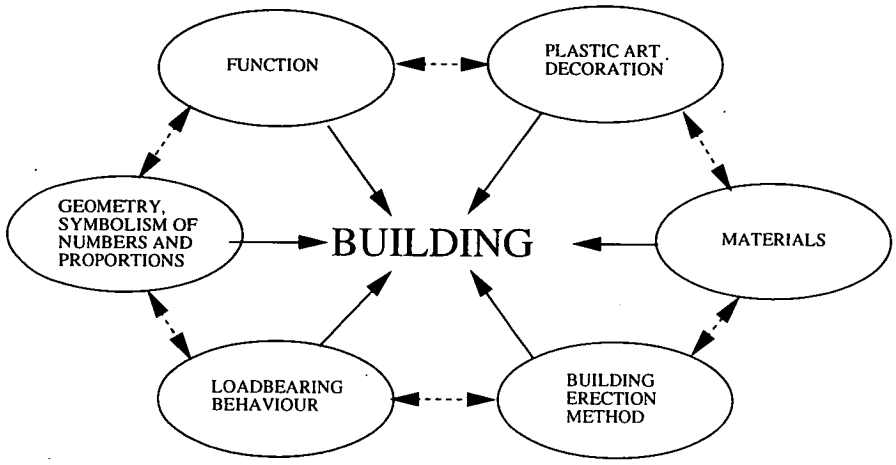


Figure 1.2: Criteria influencing a conceptual bridge design (after Falter *et al*[1])

A good illustration of the conceptual method of design is in the design and construction of many of the 18th and the 19th century bridges in Venice.[11] The construction of a these bridges is a combination of natural, (i.e. the situation in Venice in the 18*th* century, with the city being divided largely by the lack of bridges), scientific and social criteria all having effect on the final design. Movement of most materials therefore required the use of flat bottomed boats. To enable the use of boats required vaulted bridges structures. The arch was designed mainly for canal use, rather than any other design method, leading to the semicircular shape most commonly seen today.

Masonry arch construction constitutes about 70% of the bridges in Venice: this is strange in view of the apparent vulnerability of this type of structure to movement of the foundations, a particular problem in this city. Many innovations were used to help prevent this: vertical loads were reduced by using lighter baked voussoirs and by the omission abutments from the design. Builders had proven rules for construction that came from experience gained over many years; this led to many natural innovations and refinements used to cope with problems encountered. Large foundation slabs and piles were used to prevent the abutments from washing away; a hydraulic mortar with superior mechanical properties allowing for arch movement and the use of specific stone, which was both frost resistant and of

low porosity, were introduced. Another important point raised was the ability of mortar to harden over time. The gradual removal of the supporting scaffolding allowing redistribution of forces without loss of material while the mortar was still hardening. Figure 1.3 shows a representation of this supporting structure.

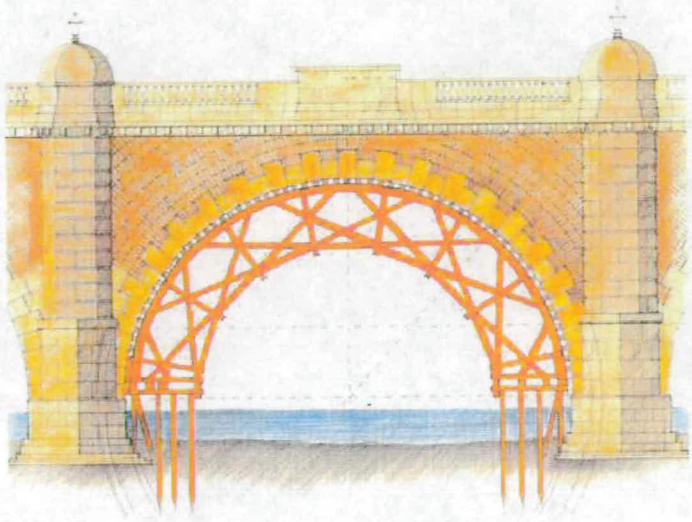

Figure 1.3: Representation of arch under construction

The fact that masonry arch bridges have been in existence for such a long time has meant that they store in their structures a wealth of construction knowledge from the various civilisations who built them; thus their conservation and documentation is also of great importance. Its structural continuity through the years, withstanding technical and natural changes, provides evidence of the influence of this type of structure. Building these structures has always been, and will continue to be, a dynamic process, constantly changing and improving. Therefore bridges of this type require preservation, not only as an important part in the infrastructure of an area, but also as part of the cultural landscape. Bridges of this type exist throughout the world and form parts of many historical transportation systems.[12] It has been suggested that bridges act as a group in the infrastructure of an area. As such they should be treated together, not separately, receiving maintenance and protection together, as single bridges do not always qualify for such cover.

Although the history of the masonry arch bridge is a glorious one, its construction type has been considered in certain areas as being something from the past. The historic awareness of many of the material and construction techniques have disappeared from modern bridge design, new methods have replaced old and 'new'

theories are still being formulated. Bridge documentation is therefore a useful way of gaining insight into how and why construction methods were used and how bridges were originally designed. For these reasons the Interdepartmental Centre of Engineering for Heritage, University of Naples[13] "Federico II", aims to catalogue many of these structures on the Internet$^{TM}$.

The replacement of less durable structures by longer lasting ones has been one of the significant things to have happened to bridge design over the centuries. However, many modern materials used in bridge construction have proved to have shorter lives. Bridges built by the Romans are still standing, but both reinforced and pre-stressed concrete bridges of more modern construction have already experienced many problems. During recent years the UK has begun to realise that masonry arch bridges may, in some circumstances, offer a practical alternative to more conventional steel and reinforced concrete construction.[14] Masonry arches offer proven longevity and low maintenance costs, with several examples of two thousand year old masonry bridges still in use today. The growing importance of environmental influences on bridge design in recent years highlights the requirement for the use of sensitive and appropriate materials. Masonry arches are generally considered to be more aesthetic than their modern alternatives, their pleasing appearance and durability of masonry bridges has encouraged a renaissance in arch construction, which has been supported by the Highways Agency and Local Authorities responsible for the maintenance of the UK bridge stock.

## 1.2 Present bridge assessment methods

When a client primarily asks for a bridge assessment, this will take the form, in the first instance, of a desk study and subsequently of an arch inspection and assessment to find the load carrying capacity of the structure. (The load carrying capacity of a bridge is defined as the vehicle loading that a structure can carry with reasonable probability that it will not suffer serious damage.) The carrying capacity shall be assessed relative to vehicles of up to 40/44 tonnes gross weight.[8] The British Standards which give criteria for the assessment of highway bridges and structures are BD 21/97[8] and BA16/97. The latter is advisory in nature, giving principles and methods deemed to satisfy criteria in the Standards.

The bridge inspection required before any assessment should verify the form of construction, the dimensions of the structure and the nature and condition of the structural elements, noting any signs of distress and their cause. Special care should be taken to find the density and dimensions used to estimate the nominal load, $Q_K$. For this to be done trial holes or bore-holes may be required. In practice however these are not normally employed, since conservative material properties are often used to give conservative assessments. Further investigations would only be required should these initial assessments highlight a possible problem. Use should also be made of all existing information pertaining to the structure, such as as-built drawings, soil data and past inspection reports. The initial bridge inspection, which at present usually takes only one day to perform, produces a quantity of information, which cannot be said to be excessively accurate, since many parameters are difficult to obtain. Using a more scientific approach at this first inspection stage would, it is felt, reduce the need for further inspection and assessment work and so save both on time and money. This first phase, costing about £500 per bridge, is only superseded if the initial assessment has shown the structure to be 'unsafe'.

A special section in the code relating to masonry arch bridges includes a list of criteria that should be included in an initial inspection of masonry arch structures. This information is also required for the current MEXE method. At present correction factors are applied in the presence of more than one span, the type and size of piers, breaking loads, the skew of the bridge and fatigue due to stress concentrations. Parapets and spandrel walls have numerous unknown effects, many of which are beneficial to the strength of the arch. The non-inclusion of these is potentially conservative. At present spandrel walls are assessed separately from the arch barrel and are not assumed to support or strengthen the latter. The assessment of spandrel walls is based on results from a visual survey only . The quantified effect of all these positive factors is, however, very complicated and at present cannot be accurately included into present assessment methods.

A special case has been put forward for the assessment of masonry arches over other bridge types, suggesting the use of the modified MEXE assessment method rather than of limit state analysis methods. The assessment methods used today, thanks to their conservative nature, are undoubtedly affecting the actual bridges that they are meant to be protecting. The sensitivity of each assessment method to its input parameters is in many cases unknown. Guidance for the assessment

of masonry arches comes from several sources;

- BD21/97[8] & BA16/97
- TRL reports[15]
- Books, state of art review from TRL[4]
- Conference publications.

Should a bridge assessment programme show a structure to be inadequate, one of the following actions could be taken:

- vehicle weight or lane restrictions could be applied, (in many cases requiring subsequent monitoring);
- should the bridge be incapable of carrying even the lowest level of load listed in the code it would be closed;
- if replacement or strengthening of the structure were required, anything done to these structures would have to retain the original character of the bridge, since it has been acknowledged that arch bridges are part of our cultural heritage.

All of these actions will result in expense to various groups: thus avoiding them by accurate arch assessment is vital.

At the moment many of the new masonry arch assessment methods offer no apparent improvement in relation to the modified MEXE method and they are distrusted, due mainly to their relative difficulty of use. It is important that industry becomes more involved in the use and evaluation of assessment methods in order to determine the relative usefulness of each.[16] This, it is felt, would help researchers develop and evolve new methods of analysis in the future which will be more accurate and just as dependable and universally accepted. The modified MEXE method, the recommended method of assessment before any others, determines the value for the allowable axle load, which can be compared to the live loading vehicle weights required in the code.

For a masonry arch assessment programme to be considered successful, it should:

- correctly predict the load carrying capacity and failure modes of a structure;
- allow assessment at a reasonable cost both in money and time;
- properly consider all the parameters that influence load capacity;
- allow progressive investigation of borderline bridges; and
- be suitable for improvement with additional knowledge.

Many of these are not allowed for with the current assessment methods available today.

There are two reasons which cause concern for modern masonry arch bridge assessment. Firstly the majority of the bridge stock of this country was not originally designed to carry the large loads required today; secondly the present assessment methods are not particularly suited to their analysis at these loads. It is a testament to the structure of masonry arch bridges that they have been able to cope with these increasing loads. The deficiencies in the present assessment methods for arch bridges are researched in this thesis as part of an ongoing series of studies investigating the theories behind modern arch assessment. Some of these shortcomings have previously been identified as being the omission of soil-structure interaction effects and three dimensional effects, which have been shown to contribute to the strength of the structure.

Also as part of this thesis new analysis methods, such as new finite element and discrete element computational methods, are introduced and investigated in order to assess their suitability for arch bridge assessment. The ever increasing processing power of modern computers has meant that new methods are increasingly being used in arch analysis. These methods have been chosen in order that arch bridges can be investigated and the contribution of other effects to the strength of the arch quantified.

## 1.3 Outline of thesis

A brief summary of the research programme presented in this thesis is outlined below, subdivided into different chapters for each area investigated.

**CHAPTER 2 - Literature review**

A summary of published literature is included, partly to give the reader the background knowledge useful for understanding the research and also to introduce the theory and research conducted by others in the fields being investigated here. This includes an introduction to the field of arch bridge assessment, giving the reader sufficient insight to understand the various methods of assessment being investigated. Sections on computational methods, relevant experimental work and soil-structure interaction have also been included. The literature review has been divided into sections which allow the work to be referenced with greater ease.

**CHAPTER 3 - Comparison of modern assessment methods**

Four of the most commonly used masonry arch bridge assessment methods are introduced, giving details of the theory behind each and explaining how each is performed. A parametric study has been performed for each method to understand more fully the technique and to allow comparisons to be made between each package. An assessment programme for a number of bridges in the Lothian region is also to be included: this comprises comparisons between the different assessment methods used.

**CHAPTER 4 - Double span brick arch tests**

A series of double span arch tests has been conducted at the University of Edinburgh. This chapter describes further tests performed on an instrumented brick arch bridge. The exhaustive series of tests includes testing with increased load levels and increased fill heights for a series of line load tests. Further, a complete series of patch load tests has also been completed for two fill heights and load levels. Comparisons with previous tests are presented.

**CHAPTER 5 - Thermal analysis of Kimbolton Butts bridge**

A thermal analysis with a finite element (FE) package is presented, and the results compared with measurements taken from an instrumented bridge. The modelling includes both 2-D and 3-D methods to incorporate the entire bridge structure.

**CHAPTER 6 - Discontinuous modelling of masonry arches**

The feasibility of using discontinuous analysis formulations for the assessment

of masonry arch bridges has been investigated. It has been postulated that the discontinuous nature of masonry arches could make this type of assessment method particularly suitable. Two different discrete methods of arch analysis are investigated and compared with an actual failure load test. A continuum analysis method, which also models some of the discontinuities involved, has been performed.

### CHAPTER 7 - Conclusions

A list of the conclusions are presented together to give an overview of the main findings of the research.

### CHAPTER 8 - Recommendations for further work

Areas for further investigation, emanating from the research presented and considered significant by the author, are presented here.

# Chapter 2

# Literature review

## 2.1 Introduction

Throughout the last two millennia, on a worldwide scale, arch bridges have continually been designed and constructed. These arches, many of which are still standing, pay testament to the strength and durability of this type of structure. Despite this amount of time, it has only been relatively recently that scientific research into these structures has been documented. It is therefore unfortunately inevitable that a large amount of useful information to do with masonry arch bridges has been lost, almost certainly forever.

This section therefore contains an overview of the work from the past 350 years. It was felt important to do this as an introduction to the methods of arch analysis and assessment and the relevant theories behind each, in order to give an overview of the subject being investigated. Since many of the theories have evolved over time to get to their present levels, it was felt important to give the history of this process in order that the different methods can be more fully understood. Many methods of arch analysis have been introduced over the years, each evolving, either increasing or decreasing in popularity over the many years that this process occurs. Included in this section is a review of relevant bridge tests and subsequent analysis and assessment methods that are used later in this thesis; also included are sections on soil-structure interaction, new discrete element methods of assessment and the new design techniques that are used presently.

The understanding of soil-structure interaction and its beneficial effects have partially been understood, but due to their influence on the strength, stability and design of arches the knowledge of how and why these interactions occur is still at an early state. The ability of present assessment methods and packages to model these effects is based on assumptions, therefore further investigation is required to improve current knowledge in the subject.

## 2.2 Theoretical Work

A review of the relevant literature for the following sections has already been covered in detail by Page,[4,17,18] Heyman,[2] Fairfield[19] and later by Prentice.[20] A brief summary of the relevant literature is presented below.

### 2.2.1 Empirical methods

These are believed to be the basis for most bridge construction up to the end of the $19^{th}$ Century. Due to the obvious problems involved with the construction of arch bridges a series of useful empirical "rules" for construction were formulated. Generally these methods did not take into account the properties of materials but were based on observation of the traditional bridge stock, which had been proven by time to be safe. Factors of safety were however employed on a subjective basis to give some confidence in stability.

It was Rankine[2] who first documented these empirical relationships for British practice for calculating the arch ring thickness $d$, as shown in Equation 2.1.

$$\begin{aligned} d &= 0.105 \times \sqrt{r} \qquad (Single - span) \\ d &= 0.126 \times \sqrt{r} \qquad (Multi - span) \end{aligned} \tag{2.1}$$

where $r$ is the radius of curvature of the arch intrados. Other relationships were available for direct ratios for the ring thickness to either the span, $L$, or the radius of curvature, Equation 2.2.

$$d = 0.138 \times \sqrt{r + \frac{L}{2}} + 0.061 \tag{2.2}$$

Work by Stephenson and later by Baker[2] gave numerous equations relating the required to the actual dimensions for the arch barrel thickness at both crown and springing, thickness of intermediate piers and many other dimensions. The main problem with this type of analysis was the large number of these equations, some requiring factors of safety, others producing different values for the same input dimensions.

A recent concise paper on the subject was published by Corradi[21] which introduces many of the aspects that were considered in the $19^{th}$ Century. Rules for the laying out of the intrados, the ring thickness of the keystone voussoir and the springings, abutments and piers and the maximum arch span are all considered. Many examples for each required dimension are given and although only a few received significant recognition, this led to confusion in design, showing the need for a code of practice. It was concluded that the most popular methods were those that provided answers, instruments and elementary methods for bridge design, even if the theory behind them was not rigorous or exactly relevant.

## 2.2.2 Elastic methods

### 2.2.2.1 Early development

The earliest documented work relating to arches was that by Robert Hooke[2] in 1675, with his work into the "mathematical and mechanical" behaviour of arched structures, with this he stated:

"as hangs the flexible line, so but inverted will stand the rigid arch."

It has been shown that, not surprisingly, Hooke did not fully understand the problems inherent in this type of analysis and could not solve the problem statically. Work using calculus tried to prove the theory, and although mistakes were made, a simple arch made from spheres, was shown to be self-supporting. Polini,[2] whilst working on St Peter's dome, stated that stability of the structure would be assured if "our chain can be found to lie entirely within the thickness of the arch." He showed this theory to be correct by loading a flexible chain with weights proportional to each segment's self weight, showing that the line of thrust did lie within the shape of the arched dome.

This type of analysis was also studied significantly by La Hire[2] between 1695 and 1731, again looking at the statics of an arch ring, assuming solid and, wrongly, frictionless voussoirs. His solution was the creation of a funicular polygon, or line of thrust for the arch based on the self weight of each voussoir. To create the funicular polygon the static forces are balanced and the reactions resolved. Starting at a support and working progressively inwards, a triangle of forces is

calculated, producing the thrust lines for each section, from which the funicular polygon is constructed. This work is further outlined below and forms the basis of many of today's mechanism methods of analysis. This line of thrust was first shown experimentally by Barlow[2] in 1846, who, with the aid of removable mortar joint inserts, showed the path of the thrust line by removing the unnecessary inserts. Couplet's[2] work further linked and improved upon thrust line and stability analysis of arches.

## THE FUNICULAR POLYGON

This well known tool assumes an arch with vertical forces acting on it, relating to dead and live loading, as shown in Figure 2.1(a). This enables the reactions and the horizontal component of the compression for the arch to be found. Starting at one support a force diagram can be drawn for the first springing to get a theoretical value and direction of the compressive force $C_1$ acting in the arch at that point. This can then be performed for each joint until the funicular polygon shown in Figure 2.1(c) has been completed. The pole $O$ of the force polygon is taken at a distance $H$ from the vertical line, and the lines radiating from $O$ give the inclinations of the various portions of the thrust line. If this line of thrust lies within the arch, then the structure is assumed to be stable. This method can obviously involve the weights of the voussoirs and any given loading. It is the choice of horizontal component of the compression ($H$) which has the effect on the shape of the polygon and so is directly linked to the dimensions of the actual bridge being analysed.

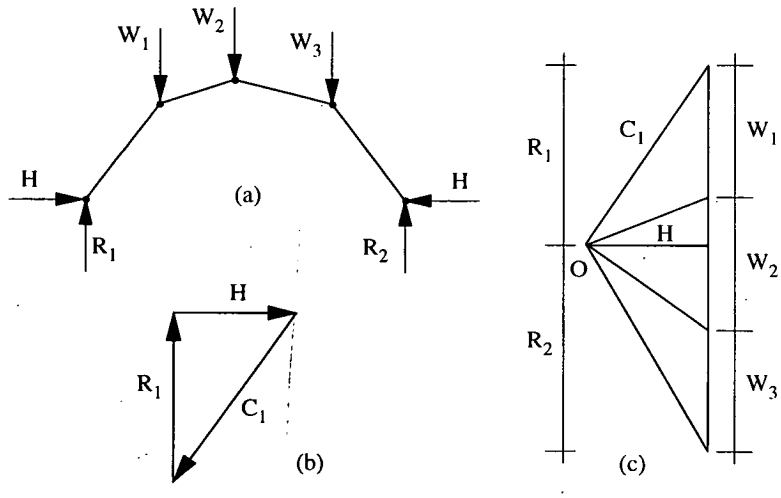


Figure 2.1: The formation of the funicular polygon (after Heyman[2])

Consolidation of the previous work by Villarceau[2] in 1854 helped devise a method to ensure the centre line of the barrel coincided with one of the possible lines of thrust for any state of loading: from this work tables of examples were devised. This method did not find the actual line of thrust for a particular load case but only required the arch centre line to coincide with one of the many possible lines of thrust for stability to be satisfied.

In 1952, almost one hundred years later, this work was repeated by Inglis[22] when he represented this method by a series of equations for calculating the line of thrust and so the barrel centre line. Fuller[2] in 1874 used the funicular polygon method of analysis with improvements, using the "middle third rule" to give some factor of safety to the work. Equation 2.3 represents a family of curves with parameter, $h$. A practical example of this work, is for a specific span, L, and total height $(a+h)$, the value of $h$ could be chosen by the designer. This method is illustrated in Figure 2.2, and Equation 2.3.

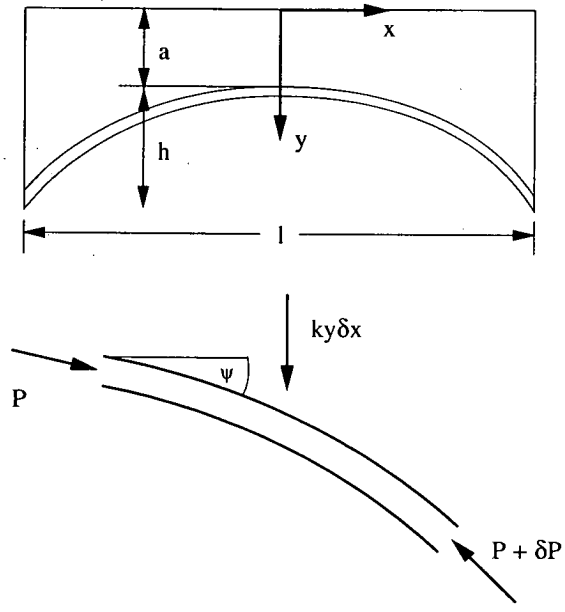


Figure 2.2: Arch centre line method of design (after Heyman[2])

$$y = a\ cosh\left(\frac{2x}{l}\ cosh^{-1}\left(\frac{a+h}{a}\right)\right) \tag{2.3}$$

The arch centre line is found so that it coincides with the thrust line resulting from the loading case. To build to this specification is of course another matter, proving

to be of great difficulty, especially for longer spans. This method however gives no information on the required thickness of arch to ensure safety and stability due to other loads.

Castigliano[2] in 1879 based a new method of analysis on the middle third rule. This states that if the line of thrust, idealised as point loads, lies outside the middle third of the arch barrel thickness, tension occurs in the adjacent half, leading to instability. The reason why the middle third has been chosen is illustrated in Figure 2.3, which shows by simple elastic theory why, for a rectangular section, a third is commonly taken as the safe limit. The vertical load is idealised as a point load and as its position moves away from the centre line of the block, the stress at the base varies. When the load reaches a third of the width this is the limit when the whole section is still in compression. Outside this limit tension must be present in the section and since masonry has little or no tensile strength, the section can be discounted.

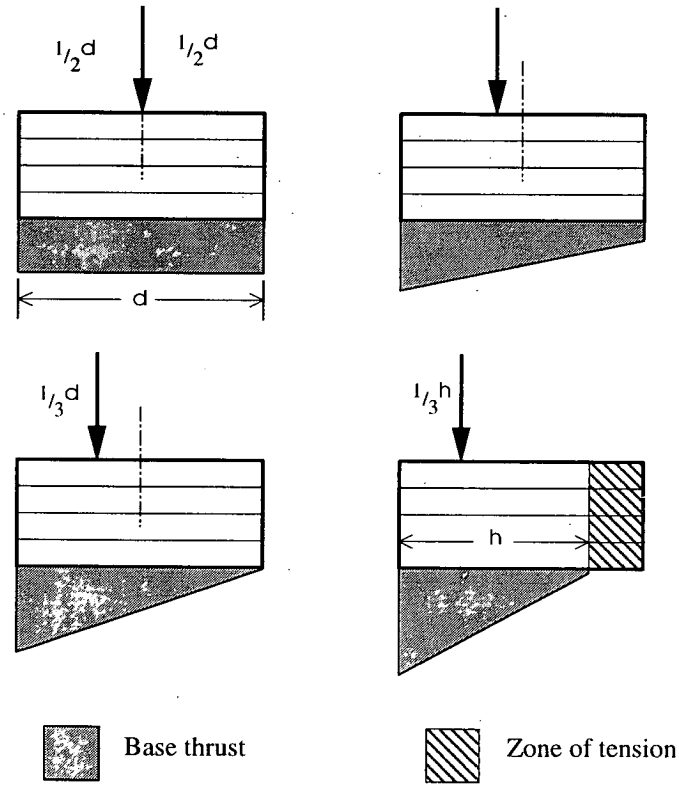


Figure 2.3: The middle-third rule

This method was further improved by removing any part of the arch barrel in tension, and then repeating the calculation until the line lies within the remaining

middle third. This produces a lower bound solution for the thickness of the arch barrel.

#### 2.2.2.2 Further development

The Military Experimental Establishment, MEXE[8,23] assessment method for the classification of masonry arch bridges was first introduced just after the second World War. It is based on early work by Pippard,[2] detailed by Heyman,[2] that pioneered this method. Pippard noticed that small movements at the abutments would normally produce hinges, making the arch a statically determinate structure. However he ignored the central hinge and simplified the structure arch as a two-pinned rib, shown in Figure 2.4. MEXE is probably the most commonly used assessment method for arch bridges, the theory behind which has been extensively discussed and, although proven to be an unsatisfactory assessment method in many ways, it is still is the simplest and most trusted method used by practising engineers.

By making numerous assumptions, Equations 2.4 & 2.5 were formulated, calculating dead load thrust and bending moments at the crown. Some of the assumptions made were:

- the arch is parabolic in shape
- the crown load point is not the most critical position but assuming an increase in capacity due to soil-structure interaction effects, this increased the capacity suitably
- the fill applies only vertical load, it has no structural strength
- fill has the same unit weight as the arch barrel
- The thrust line must lie within the middle half of the barrel thickness, providing limited compressive strength and an unspecified tensile strength.

$$H = \frac{l}{a}\left(\sigma l h\left(\frac{a}{21} + \frac{h+d}{4}\right) + \frac{25}{128}W\right) \tag{2.4}$$

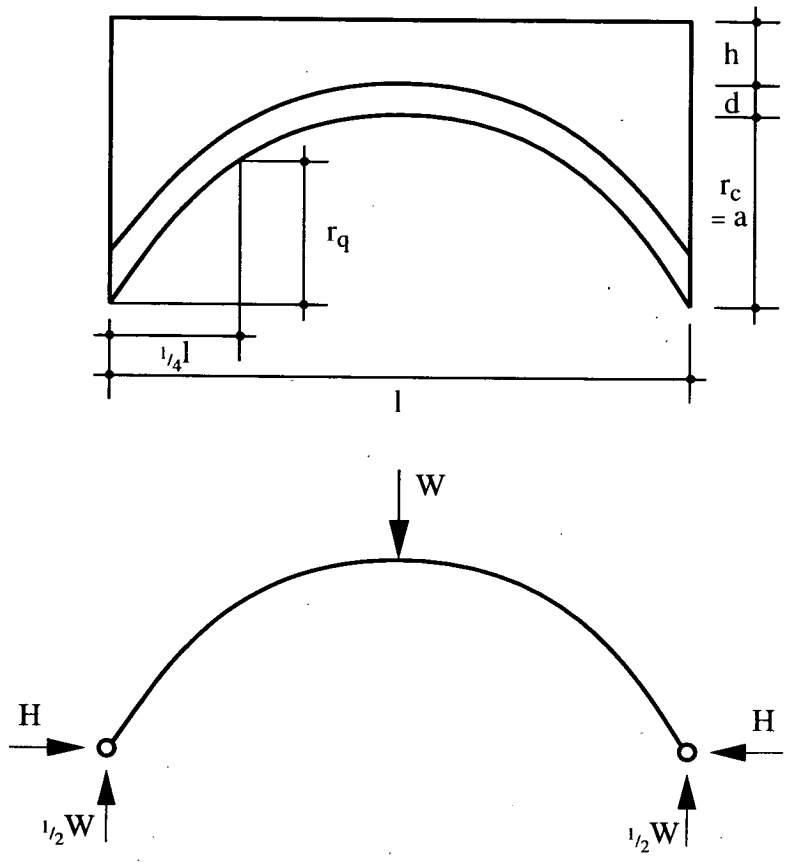


Figure 2.4: Two-pinned rib (after Pippard[2])

$$W = \frac{\left(\frac{256fhd}{l}\right) + 128\sigma lh\left(\frac{a}{28d} - \frac{1}{21} - \frac{h+d}{4a}\right)}{\left(\frac{25}{a} + \frac{42}{d}\right)} \tag{2.5}$$

It is then possible to derive the maximum load that would be supported by the arch. Pippard constructed tables from which $W$ could be found for the different arch dimensions of $l$, $d$ and $h$. The MEXE method found that it could represent Equation 2.5 by a nomogram. MEXE will be further introduced and discussed later in Section 3.2.1 of this thesis. BD 21/97[23] represents the modified MEXE method as it presently stands. The points of concern are mainly to do with the basis of the modification factors and the way in which they are used, without taking into account factors that have been proven to have significant effects. MEXE, for these reasons, tends to give conservative and, in some cases, illogical results.[16,24]

Hughes and Bridle[25–27] have both published papers relating to their own assessment method for arch bridges. Although this method is based on the Castigliano elastic method it has been extended to give a failure load for a given arch and load case. This method includes important soil-structure interaction effects, with the use of horizontal forces acting directly on the arch. Forces and moments are found for each load, areas of tension are removed and progressive iterations are performed until convergence to a safe solution is achieved. Further loading configurations are computed until convergence no longer occurs, this is assumed to be the failure load and position for the bridge. Good correlation with model and full scale tests was found for this method of analysis.

Further work has been completed employing various computational methods using pinned elastic methods,[25,28] these however contradict many of today,s assumptions relating to arch bridges: that failure load decreases with increasing dead load, that fill contribution is minimal and that the compressive and especially the tensile strength are the main defining factors of failure. These methods are also time consuming if the process of load distribution and critical load point are to be established. These will be discussed later in Section 2.3.1. Heyman[29] draws caution to elastic methods of analysis which rely on the arch supports, often an unknown factor, to provide known reactions. He states that when centring is removed there has to be a change in the span, generally outwards for single-spans but which can be inwards for multi-span structures. These movements will produce large movements in the calculated thrust line and may form a cracked state of the masonry. This cracked state does not weaken the structure, in fact it is only responding in its nature to the external effects.

### 2.2.3 Plastic methods

#### 2.2.3.1 Early development

La Hire[4] in 1695 performed a static analysis of arches concluding that an ideal arch, without the presence of any fill, could not stand without the presence of friction to give it stability. He continued this work and returned to this problem in 1712, considering the way that arches failed. Couplet[2] used much of this background work, noting that friction would lock the voussoirs together against sliding but not preventing hinge formation. He also assumed that the voussoirs

would not fail in crushing, as he ignored this effect in his work. This early work used three basic assumptions which were required for plastic analysis:

- masonry has zero tensile strength
- it has infinite compressive strength
- there is no sliding between voussoirs.

From this work Couplet found the arch thickness that a semicircular arch would require to support its own weight and in doing this he correctly predicted the collapse mechanism. He also related the arch radius,$R$, to the arch thickness, $t$, to give a safe ratio of 0.106. The position of the internal hinges has been shown by Heyman[2] with the use of Equation 2.6 to occur at the angle $\beta$ from the crown of $58^o49'$. Couplet also considered other arch problems with other arch shapes, together with the problem of pier stability required to resist these forces. Much of this work has subsequently been confirmed experimentally by Danyzy.[2]

$$\beta \cot \beta \left( \frac{2\beta \cos \beta + \sin \beta \cos^2 \beta + \sin \beta}{2\beta \cos \beta + \sin \beta \cos^2 \beta - \sin \beta \cos \beta} \right) = \frac{\pi}{2} \tag{2.6}$$

Further work by Coulomb[2] simplified the problem by considering only half an arch and finding two equations for the horizontal thrust $H$, required to maintain equilibrium. To do this he needed a hinge between the crown and the springing. He formulated two equations for the maximum and minimum values of thrust which would allow hinges to form at either the arch intrados or extrados, thus finding limits between which the thrust must lie. From this trial and error method the critical cross-section can be found when the two thrusts give a unique solution. This is illustrated in Figure 2.5.

#### 2.2.3.2 Further development

Until relatively recently this form of plastic mechanism approach, (discussed above), for the assessment of arch bridges has been ignored. It was not until Pippard,[2,4] between 1936 and 1962, that this method returned to prominence.

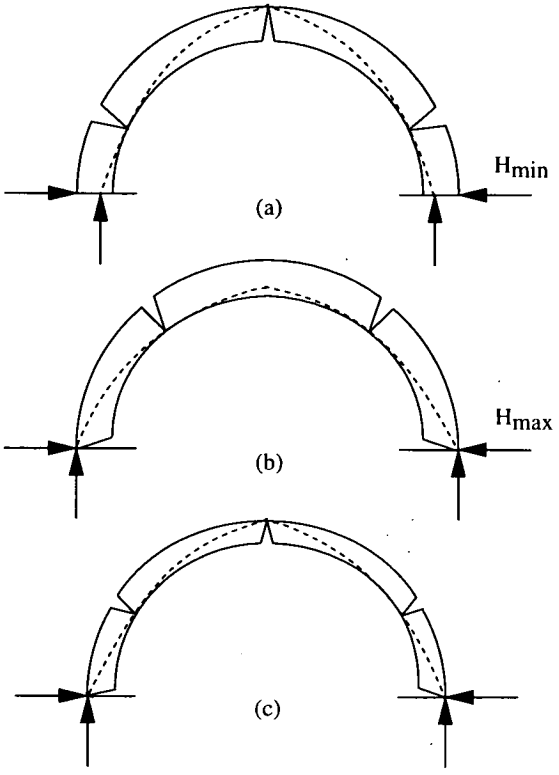


Figure 2.5: Plastic method of analysis (after Heyman[2])

However since this time a large quantity of research has been completed. This work analyses a four hinge mechanism, with one hinge under the applied load and another at the adjacent springing, as represented in Figure 2.6. Heyman formulated a tabular form of calculation to find the position of the other hinges, taking into account the self weight of the fill and the arch units. He was then able to find the failure load from static analysis, which he verified as an upper bound solution with extensive experimentation. His early tests to collapse, with smooth steel and mass concrete voussoirs, helped to derive the present day MEXE assessment method. Heyman[2,30–34] is another prolific author of relevant papers in plastic mechanism methods. He further simplified previous equations and tabular methods by assuming the critical loading point at the quarter span and the position of the hinges, giving an approximate equation for the required ring thickness. A factor of safety to account for the imperfect assumptions is however required, as either a load or a geometrical factor. These factors are represented in Equation 2.7,

$$\begin{aligned} Geometrical\ safety\ factor &= \gamma_{geom} = \frac{t}{t_{min}} \\ Load\ safety\ factor &= \gamma_{mech} = \frac{F}{G} \end{aligned} \tag{2.7}$$

where $t$ is the actual thickness, $t_{min}$ is minimum theoretical thickness required for stability, $F$ is the minimum point load and $G$ is the total weight. A relationship between this geometric and load factor has been further discussed by De-Rubeis,[35] where comparisons between the two have been performed and explained. Graphs of collapse load, as arch thickness and load position are varied, revealed curves previously documented.[34] This has also been performed for different arch shapes producing interesting relationships.

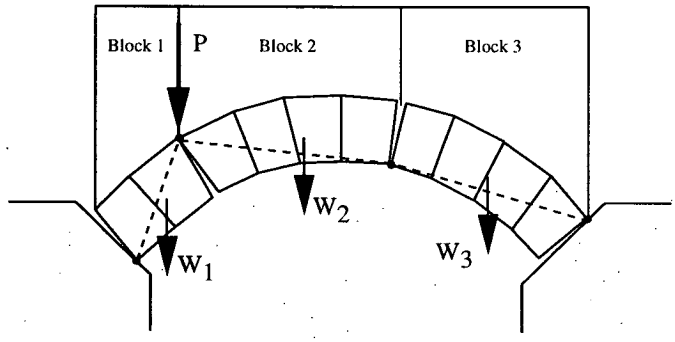


Figure 2.6: Mechanism method of analysis

Harvey *et al*[36–38] has done more work on mechanism methods, with the development of a computer based package, ARCHIE. This package has the important inclusion of soil-structure interaction effects of both load dispersal and earth pressures, represented by horizontal forces calculated from input coefficients of earth pressures. This was done to give more realistic failure load results compared to previous mechanism methods, which ignore these effects. Mechanism methods tend to give the correct failure mode, but drawbacks have been noticed, particularly for deep arches with the inclusion of unknown soil parameters. ARCHIE, one such method, is discussed in detail later in this thesis.

Another mechanism method introduced by Crisfield & Packham[39] made further modifications to the standard mechanism method. A compressive yielding at hinges was allowed, resulting in the formation of hinges inside the arch barrel and a friction angle for the fill, allowing lateral resistance. This method was also

computerised, allowing relatively easy computation of the lowest collapse load. A more in depth discussion of the package is given by Page.[4]

Other developments have been made to increase further the reliability of this method with the inclusion of lateral soil pressure by Cabrera *et al.*[40] By dividing the arch into vertical slices with the area and centroid calculated for each section, the method requires forces and moments to be resolved about the first three hinges, and finding the unknowns. This gives an upper bound solution, which, if the position of the fourth hinge is varied, will give the required solution.

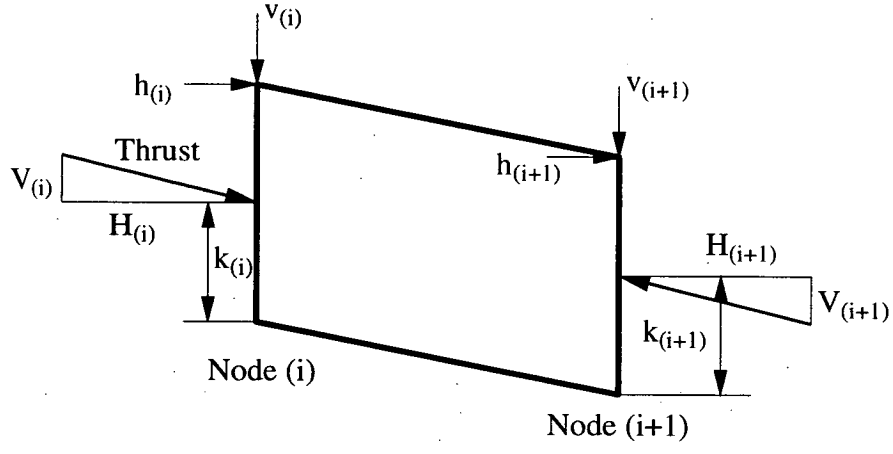


Figure 2.7: Element forces

Lateral soil pressure is applied with nodal lateral loads, which are a function of depth and density of fill, and the coefficient of lateral soil pressure. These lateral loads are taken into account when moments are taken. The ratio of lateral soil pressure to vertical pressure is considered to lie between the lower active and upper passive limits, as in Equation 2.12. The value of earth pressure at rest is unknown, however Rankine proposed a steady state coefficient of:

$$K'_o = 1 - sin\phi \tag{2.8}$$

He found that varying the input value for $K'_o$ produced a change in the factors of safety under dead load, depending directly upon the type of bridge tested. The author looked at two bridges, Bargower & Bridgemill, whose shapes represent extremes of span:rise ratio. An increase in $K'_o$ increased the factor of safety for

the Bargower bridge by pushing the hinges towards the springings, and reducing the thrust line at the extrados hinges, thereby producing the increase in failure load. Bridgemill produced a decrease in the factor of safety for the same increase in $K'_o$, with the thrust line already at the intrados the change thereby producing a less stable state. The author concludes that the inclusion of lateral earth pressure does not always produce conservative assessment, but does give a more realistic prediction of the arch thrust and therefor the factor of safety.

#### 2.2.3.3 Mortar and masonry strength

Boothby[41] considers the differences between the block and mortar controlled failure mechanisms. For the block controlled mechanism, suggested by rigid plastic analysis, failure occurs only when the line of thrust goes outside the arch ring in alternating order, producing the failure mechanism: this provides the lower bound solution. The upper bound solution is produced by equating the potential energy of the failure system, shown in Figure 2.8 and Equation 2.9, where $\delta$ is the vertical displacement of the load and $\delta_i$ is the vertical displacement of the centroid of the $i$'th segment.

$$-P\delta + W_1\delta_1 + W_2\delta_2 + W_3\delta_3 + \ldots = 0 \tag{2.9}$$

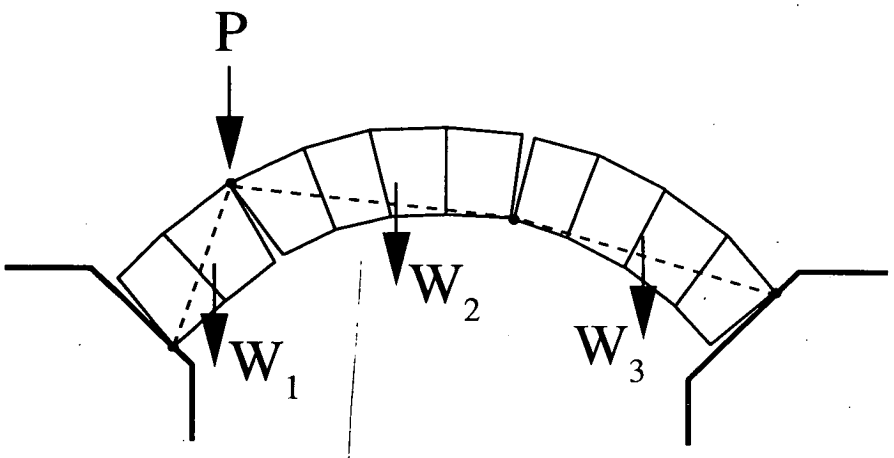


Figure 2.8: Four pin failure mechanism

The mortar mechanism involves yield surfaces with linear hardening, which in practice is the more common mode of failure in older structures, where the mortar

is generally wet and weak. Failure is due to a complicated relationship between the axial thrust and the internal moment between each block, both of which are non-linear. The yield function of the section shown in Figure 2.9, is given by the interaction shown in Equation 2.10, where $P_0$ is the maximum axial force and $M_0$ is the maximum moment, each relating to the compressive yield strength, $\sigma_0$, of the mortar.

$$f(P,M) = \frac{1}{4}\left(\frac{M}{M_0}\right) + \left(\frac{P}{P_0}\right)^2 - \left(\frac{P}{P_0}\right) \leq 0 \tag{2.10}$$

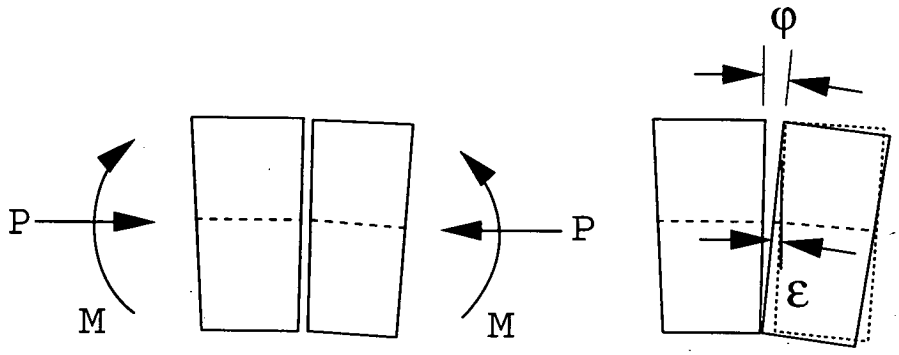


Figure 2.9: Mortar joint displacement coordinates

From the yield strength the yield surface is calculated; this surface can also be represented with a linear approximation. The gradient of this force/moment approximation is represented by $\bar{e} = \epsilon/\varphi$, which is the eccentricity of the hinge from the centre of the arch barrel. If the compressive yield strength is exceeded for a section, linear hardening is included, which will help stabilise the structure, due to the energy dissipated by the plastic deformation of the joint. This method has been computerised by the author since it requires second order conditions to be considered. The method is simplified by identifying stable states of specific mechanisms and then using the lower and upper bounds of the load to identify the unstable mortar mechanisms. Then the energy state of the total system can be determined using various equations; this will suggest whether the system has achieved increased stability.

It is concluded that mortar controlled mechanisms are usually initiated at lower loads than required for plastic collapse, but this load increases due to hardening effects. The weakness of such mortar compensates for the brittleness of the

masonry units in many structures, where failure is initiated in the mortar long before ultimate failure will occur. These beneficial effects offered by weak mortar are thought to be inbuilt in older structures, rather than being produced accidentally.

Gilbert[3] has considered a case where the compressive strength of the masonry is investigated, allowing a rectangular compressive stress blocks to form at the hinges. This type of failure occurs with high strength voussoirs with lower strength mortar joints. To account for the masonry crushing an iterative procedure was utilised, the first stage of which calculates the failure using internal forces with no crushing allowed; the area required to withstand this stress can be calculated from the crushing strength. Two values of reducing the effective ring thickness were investigated, shown in Figure 2.10.

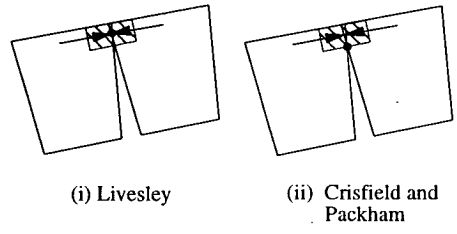


Figure 2.10: Location of hinges by two method (after Gilbert[3])

The difference between the two methods lies in the reduction in the effective ring thickness between iterations. In practice the second method converges slightly more rapidly than the first. An interesting conclusion to the paper is that multi-ring and multi-span arches are effected less by changes in the crushing strengths than single span arches.

#### 2.2.3.4 Limit analysis

Limit analysis, previously applied to other structures, was first introduced to arch bridges by Kooharian[42] in 1953. It was assumed that the linear distribution of stress previously introduced as the middle third rule (Section 2.2.2.1) has been proven by Pippard[2] to be over-conservative. This method involves constructing a funicular polygon for the arch, however it is the choice of pole point that causes the difficulty, as this point cannot be assured to be the critical point, providing the lowest failure load.

There are two fundamental theorems underlying limit analysis. Firstly that if a stable, statically admissible state can be found, this represents a lower bound solution to the problem, but not necessarily the most critical solution. Exactly how safe this value is would give one the upper bound solution. The second theorem is concerned with finding the precise value of collapse load, from a collapse mechanism. This upper bound theorem state has the condition where the work done by external loads is equal to that done by internal forces, zero assuming plastic failure conditions. The mechanism requires four hinges but the placement of these is again the difficult aspect. For this reason both limit theorems are applied to problems, depending upon what is required from the analysis. Limit state analysis is applicable to masonry arch bridges, but the methods must be rigorous and conform to principles in BD 21/97.[8]

Clemente[43] makes the same assumptions as above. If any safe equilibrium condition can be found, then the structure is assumed to be statically safe;[29] this line may not be the actual thrust line. For an arch with a line of thrust in equilibrium with the dead loads the minimum thickness of arch that is required can be determined by gradually reducing the arch thickness in an iterative process until failure. However for a semicircular arch the positioning of the hinges is not as certain as that pertaining in more parabolic arches. A parametric study investigating the span/rise ratio and weight and height of fill has been performed by the author. This results in a large influence from the weight of fill for both arch shapes, while the height of fill has differing effects for each structure.

Following on from previous work by Melbourne,[44] Sinopoli[45,46] tried developing boundary theorems for kinematic and static approaches, using rigid block limit state analysis. Melbourne developed a method based on the mechanism method, where equilibrium equations were developed, based on an imposed displacement. The static method considers a generic voussoir of half an arch, and states ranges for thrust, with reference to the rotational equilibrium for the arch intrados and extrados. The kinematic method is based upon equilibrium occurring when the work of the dead load is zero, for an infinitesimal change in configuration of the arch due to a failure mechanism. It works on the assumption that there is no sliding and that there can be no inter-penetration of voussoirs: these are not unreasonable assumptions. Although a sliding failure has been considered the friction angle required is small enough for it to be neglected in this study. Kinematic methods provide the equilibrium boundaries as a function

of geometry and the applied loads. Each method includes the use of unilateral constraints, which describe the method by which the voussoirs are not allowed to inter-penetrate each other, resulting in the relative displacement between voussoirs being greater than, or equal to, zero. The kinematic approach analyses the arch considering only the active forces, for which lower and upper bound solutions can be obtained to give the collapse mechanism. The static method uses the reaction forces at the springings to determine the limits of admissible thrust at the crown, thus obtaining the collapse mechanism.

#### 2.2.3.5 Theoretical models and analysis

Como[47] looked at arches from a slightly different point of view. He still assumed a no compression, no tension model which initially results in the structure being indeterminate, but allows the settlement that must naturally occur to produce a mechanism, this allows for the static analysis of arches. The author shows, through a series of equilibrium equations, that a horizontal movement at the springing of a single-span will produce a static state and a settlement of a pier; for a multi-span structure it will produce the kinematic state. An outwards movement of the springing has been shown, in work by Coulomb,[2] to result in a thrust line with the shortest span and the highest rise. This results in the minimum possible value of thrust among all the statically admissible options. For a vertical movement of the pier it has also been shown that the mechanism formed produces the maximum settlement reaction for all kinematicaly admissible reactions, and the minimum statically admissible reaction.

Harvey[48] discusses the basic assumptions used in assessment of arch bridges. These are that the supporting structure of the bridge is not considered, but only load-fill, arch-fill and arch-spandrel interactions are taken into account. In many cases the influence of the spandrel walls and particularly their relatively large inherent stiffness compared to that of the fill has been ignored. This particular influence, is by its nature, often complicated and therefore not well understood. Alternative stress paths have been argued and test results seem to suggest these alternative and unconsidered mechanisms. The author also states that analysis of the structure in two dimensions, considering only arch and fill, is conservative. However earlier he states that alternative stress paths can produce different failure modes that are not presently considered. Many of the present methods

of assessment do not consider spandrel wall stiffness to affect the mechanism of collapse and the actual contributions that this part of the structure actually makes.

## 2.3 Computational Work

Although numerical methods for arch assessment have been used for some time, it is only relatively recently that computational methods of analysis have been powerful enough to be used economically. Theoretical assessment methods have been successfully computerised, greatly saving on time and increasing accuracy, but these have been documented and discussed previously.[2,4,19,20] Only where these methods are relevant to work in this thesis will the method be further reviewed. These methods include research into the predominant factors affecting 2-D and 3-D analysis, enabling other bridge properties and parameters to be investigated: these include spandrel walls, the number of spans and bridge skew. In this section a brief introduction is given to the commonly used finite element methods relating to arch bridges and other more specific research. A subsection on the use of discrete elements has also been included for completeness, as this relatively new type of analysis in included in this thesis.

### 2.3.1 Finite element (FE) methods

A relatively recent development in the analysis of masonry arch bridges has been the use of finite element techniques. Early efforts had been made by Towler and Sawko[49,50] when they showed the potential by computing load deflection curves and collapse loads for an arch modelled with 1-D beam elements to represent the arch barrel. The fill at this stage only acted as a dead load and no further soil-structure interaction effects were modelled. Crisfield and Wills[28,51] later introduced non-linear spring elements in order to try to model the resistance from the soil, as shown in Figure 2.11. The spring stiffness is termed the sub-grade modulus, and is initially pre-compressed to the equivalent at rest

pressure. The maximum horizontal pressure is limited by the active or passive pressures depending upon the type of movement of the arch. These terms are further explained in Section 2.5.2.1. This non-linear behaviour was required to produce realistic collapse loads, more recently attempts have been made to model the fill directly.

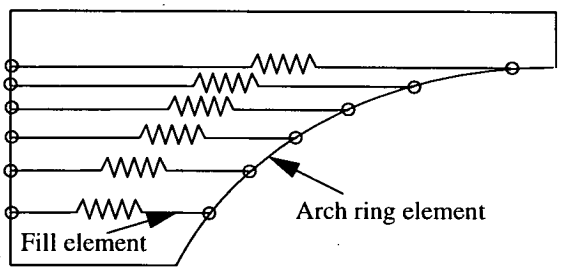


Figure 2.11: 1-D arch and fill elements (after Page[4])

Work by both Bridle and Hughes[26] introduced the Cardiff/TRL assessment package, CTAP, based on an elastic cracking Castigliano approach. Equation 2.11 shows the general formulation for strain energy, resulting from the bending moment, $M_i$ and axial force, $T_i$ acting on elements due to arrangement of loads.

$$U = \int_0^L \frac{M_i^2 \delta l_i}{2EI_i} + \int_0^L \frac{T_i^2 \delta l_i}{2EA_i} \tag{2.11}$$

This equation can be differentiated to find the forces and moments throughout the structure. Once this has been done, data is available to calculate the deflections due to the moment at any point, together with the change in length due to the direct load. Stresses are then calculated and, if zones of tension are found to exist, a new section without these areas is adopted for the next iteration, until convergence is achieved for this load level. Increasingly larger load level are iterated progressively until convergence is no longer possible, and the failure load has been achieved. The model assumes linear elastic behaviour in compression and zero strength in tension. Good correlation with full scale tests to failure and finite element methods was observed.

Another such method uses a non-linear generalised matrix formulation, (GMF), for curved members with variable cross section. The GMF method is an extension of work by Mari[52] for the non-linear analysis of masonry construction; a full

derivation of the matrix methods used for this analysis may be found in work by Molins.[53] The contribution of spandrel walls and fill is included by the use of tapered members joined to the arch ring. This method produced adequate estimates of failure loads and mechanisms and further comparative tests are presently under way.[54]

Choo *et al*[55,56] modelled the arch ring differently, using tapered elements allowing failure in both tension and compression, resulting in zones having no further structural stiffness but still contributing to the arch compressive strength. For an applied load, the effective arch ring depth is calculated, taking into account the redistribution of forces due to zones of either tension or high compression and structural deflection, as shown in Figure 2.12. Iteration is continued until convergence satisfies a criteria based on a percentage of the initial ring depth. This is the starting position for the next load increment to be applied. Loading is increased until convergence is no longer possible and the collapse value is reached. Fill is modelled as springs and a dispersal angle $\phi$ is used to distribute the applied load onto the arch barrel. The computer based program MAFEA, used by British Rail, is based on the above method of no tension in the arch ring and passive horizontal resistance from the soil fill.

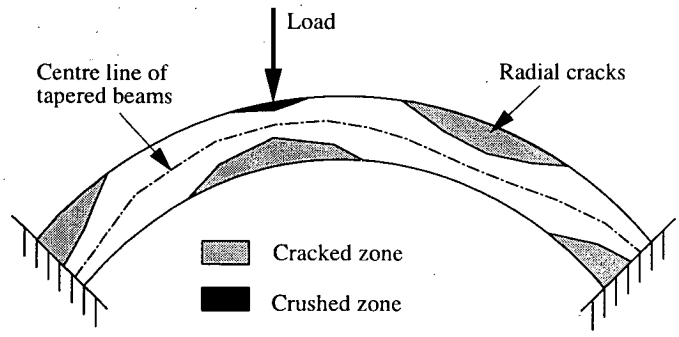


Figure 2.12: Arch ring comprising tapered beam elements (after Page[4])

### 2.3.2 Further work

Many computational assessment methods have been developed since the increase in computer power, allowing for more sophisticated analysis to be performed. Much of this work has been performed to verify test results mentioned previously, as well as allowing more specific bridge parameters to be investigated.

A paper by Hodgson *et al*[57] involved modelled destructive load tests investigating the effect of ring separation of single span multi-ring arches. The model was developed using the commercial package, ANSYS (1995), using three-dimensional (3-D) solid elements to represent the arch. The elements allow cracking, crushing and ring separation when the shear stress exceeded the shear bond strength.

Hodgson *et al*[57] tested two nominally identical bridges, each with two brick work rings. The first was constructed with wet sand joints allowing ring-separation while the second was constructed with mortar bonded joints forming a complete arch ring. The initial failure tests produced a 50% increase in the failure load of the ring without ring separation. From deflection data collection it was noted that the flexibility of the structures increased non-linearly with increased load. The arch with built-in ring-separation had less stiffness than the equivalent arch due to the lack of composite behaviour. This highlighted the importance for an analytical model to have the ability to detect the propagation of ring-separation and correctly model its effects. This behaviour is started by a plastic rather than a brittle failure mechanism, suggesting that ring-separation state can be active before any visible circumferential cracks are visible. The parameters which define the mortar joints are its stiffness and its yield stress, both of which were known.

The solid section used in the analysis allows for 3-D compressive failure to occur, at which point the area has no stiffness in further calculations. Cracks are also allowed for where the tensile stress state criterion has been reached, and a plane of weakness is created. Again this is done by reducing the stiffness of the section to zero, allowing the yield stress to be maintained and not falling to zero. Modelling of the multi-ring aspect was achieved using gap elements, several of which had to be used simultaneously in order to create the correct mortar effect. An idealised unit width of arch was modelled on the loading characteristics of the original models. Horizontal forces were applied to the model in accordance with a Rankine pressure distribution using a value for $K_p = 4.5$. A value lower than that calculated was used since the deflection required to produce full passive pressure would fail the structure.

The computer models produced limited results, although the load-deflection response of the actual failure tests could be reproduced by varying the material properties. However the non-linear response could be better reproduced using discrete rings in each case. The choice of material property was also a problem

for Cardinale *et al.*[58] when trying to model a multi-span masonry arch bridge with frame and shell elements. Material properties were obtained by performing suitable site and laboratory tests. The analysis proved to be very dependent on the elastic modulus, $E$, which was varied to replicate actual tests. Another author presently studying 3-D masonry arch structures using centrifuge models and finite element analysis methods is Sicilia.[59] The analysis uses a macroscopic approach, utilising several elements for every block and every mortar joint. Macro-models at the moment require a simplified hypothesis and can not be as accurate as micro-models, but their main advantage lies in the enormous reduction of the computational cost.

#### 2.3.2.1 Mortar joints investigated

Rosson *et al*[60] looked at the importance of the properties, and not necessarily the strength, of the mortar joints that bond voussoirs in a masonry arch. Older mortar joints tend to be made from mortar consisting of sand and lime which differ considerably from the modern Portland cement mortars. These sand-lime mortars exhibit relatively low elastic yield strength and therefore high ductility and energy absorption. They also exhibit a linear hardening behaviour, which is of importance in view of the nature of the masonry arch. This mortar has been modelled with a Drucker-Prager material model, with tension cut-off and a limit on the allowed hardening. With a series of models a yield envelope for this material in terms of the moment produced by the applied load were obtained. Assuming a linear hardening relationship for the mortar, new moment thrust envelopes were obtained, showing increasing hardening effects as the eccentricity of the load was reduced or the load was increased. This has been related to actual model tests, reviewed in Section 2.4.2. It was concluded that this method produced a suitable shakedown state for the masonry structure due to repeated loads, the type of load that such bridges undergo every day.

Another computer-based program to model the mechanism failure of a simple arch has been devised by Ashour.[61] The method utilises a numerical technique, equating the internal energy dissipated in the arch by the masonry to the external work done by the loads in order to find the arch capacity. For the internal work to have any effect, the masonry is assumed to have the modified Coulomb failure criteria with a tension cut-off.[62] The tension required is assumed to be 5% of the

compressive strength. With this simplified model a computationally inexpensive method of analysis, which correlates well with previously conducted laboratory tests, has been produced.

#### 2.3.2.2 Interactive assessment

There has been a general move towards more interactive assessment methods which, by their nature, tend to be more accurate: this allows for direct influence from an assessing engineer. Kumar[5] presents a method by which an arch assessment can be altered by using elastic analysis and then subsequent placement of hinges to find the ultimate load when sufficient hinges have been placed. This is an attempt to make the computational assessment techniques less like black boxes and more interactive and understandable and reduce the differing solutions provided by the present computer-based assessment techniques. Using conventional notation shown in Figure 2.13 for the equilibrium of an example arch section, the relationship between the force and moment capacity can be calculated.

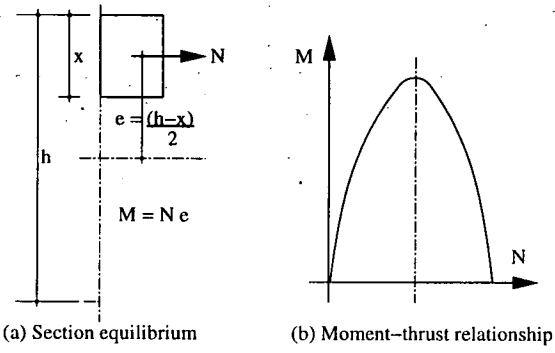


Figure 2.13: Force on an arch section (after Kumar[5])

An elastic computer analysis programme can be used to find the moment and force at a section due to an applied load. The placement of hinges can now be performed using the failure criterion thus achieved. If sufficient hinges are produced to form a mechanism, then failure is said to occur. The elastic analysis resulted in higher moments being found to occur than the above convention suggests, leading to a reduced capacity of the structure. By the placement of the hinges at the new moment capacities and re-analysis, the strength of the bridge was increased. Although this method increases computational time it does, however, produce

more realistic results and a better understanding of the arch behaviour than is presently available.

Another interactive method has been introduced by Ridley-Ellis[14] to enable the design of an optimum arch shape. The method, MOAD, allows the initial dead load profile of an arch to be obtained. The model uses input parameters to produce a profile which best suits a particular situation. Constant ring thickness and constant fill depth is assumed to allow stresses within the arch to be calculated and checked. The model is based upon principles already introduced by Villarceau[2] and Inglis.[22] This method seems useful for practising engineers, since it gives guidance for the design of arch bridges and is thus useful for their future construction. This method is presently available in a free down-loadable state on the Internet.

### 2.3.3 Discrete element analysis

It has been postulated that many aspects of a masonry arch bridge would make analysis with discrete element methods particularly suitable. The joints between voussoirs represent the main plains of weakness of arch bridges, allowing blocks to slip and the formation of hinges. Arch/fill interaction due to the load and arch movement are allowed for by these methods. The reliability of the simple numerical model, composed of rigid elements connected by frictional joints, has been verified by comparison with classic limit analysis.[42] The governing numerical parameters for this type of analysis are defined here as the *stiffness* and the *friction* of the contacts.

Early concepts of discrete element methods were proposed by Goodman *et al*[63] for the simulation of jointed rock masses in a combined discrete and finite continuum approach. Further changes were introduced by Cundall,[64] with a continuum behaviour treated as a special limiting case. Cundall's[65,66] work has moved into different areas of research, investigating smaller scale problems of granular assemblies, although the discrete method utilised is essentially the same for both types of analysis. Known early as *distinct element methods* with the inclusion of deformity of material the term *discrete element methods*, DEM, became accepted.

Most DEM's tend to use the same initial concepts, solving equations of motion

using an explicit time-stepping scheme. They tend also to use force histories as a consequence of contacts between discrete elements, produced by a penalty method, where the contact force is proportional to the inter-penetration. This in turn produces new equations of motion for the next time step. Improvements have been included, such as deformity of solid material, more complex contact interaction laws and failure or fracturing criteria controlling solid material behaviour. This has required the use of sophisticated searching algorithms to ensure contact detection, and data representation techniques have been employed to store data in an efficient manner.[63,67] The shape representation of elements and the contact detection algorithm have been shown by Hogue[68] to greatly influence the flexibility, accuracy and efficiency of an analysis.

Early discrete element methods treated a structure as a large number of interacting parts with changing spatial geometry and therefore contacts. Rigid blocks were initially utilised, but recent work has allowed for deformity of the blocks, using some sort of discrete and finite element approach. The deformation of individual discrete elements was initially dealt with by subdivision of the element into triangular constant strain zones, allowing more accurate changes in strain to be observed. An alternative suggested by Williams[69] was the use of discrete body deformation mode shapes. Shi,[70] in a similar context, used polynomial approximation of the strain field for the centroid movement for each discrete body. These new methods tend towards almost meshless formulations, where continuum and dis-continuum modelling are very similar.

Discrete element analysis has been used for many different applications, from flow of granular material to discontinuities and fracture of rock and concrete.[71] Ng[72] has investigated the small strain response of a 3-D granular soil which, as such, does not relate directly to arch bridges, but the soil materials are similar and as such this paper is of interest. Another approach introduced by Munjiza[73] was the modelling of fragmentation of a continuum due to applied stresses, having the advantage of that fact that modelling of the continuum can be initially coarse, becoming finer only in areas of high deformation or strain gradient. The method works by considering a continuum splitting apart when the load carrying capacity of a crack of area reduces to zero. In this way discrete elements consisting of finite elements are created.

The discrete element methods used in this thesis will be more fully introduced

in a later Chapter, as it was felt that the description of the method would be of more relevance at that point. With particular attention to the discontinuous deformation analysis, DDA,[70] method a large amount of work has been performed on this package. Cheng[74] discussed early problems with the DDA package and introduced modifications and improvements to the original method, so that certain problems could be overcome, allowing the program to become a practical analysis tool for general problems. Jing[75] presents DDA including its principles, governing equations, solution techniques and contact representation and detection algorithms. Further extensions to the initial DDA method have been included by Lin *et al*,[76] introducing an improved contact algorithm, adding block fracturing and sub-blocking capabilities. Block contacts have been modelled using an Augmented Lagrangian Method instead of the original penalty method. This allows block contacts to be found more accurately. Block fracturing algorithms have also been implemented into DDA, using Mohr-Coulomb failure criterion to allow one block to be broken into smaller blocks.

An attempt was made by Owen *et al*[77] to model an arch bridge structure with finite and discrete elements to represent the discrete and composite nature of actual bridges. The work aimed to continue to develop procedures for assessing the strength of damaged masonry and the efficiency of repair strategies. An idealised two-span bridge has been modelled, with masonry units represented by deformable discrete elements and the fill with spherical discrete elements. This structure was subjected to abnormal vehicular loading to determine the load distribution throughout the structure. Another finite/discrete element package has been used to investigate ring separation of another problem investigated by TRL.[77] This paper however does not state either what packages were used in each type of analysis, or the contact properties used in the analysis, which define the discrete elements in particular. Melbourne[78] used a finite element analysis with different brick/mortar elements and the use of interface elements. Although this is a finite element method, the use of interface elements with prescribed strengths provided the necessary discrete failure mode. With these types of analysis a very good correlation between the numerical predictions and experimental results have been achieved.

Mirabella *et al*[79] used another discrete code, *UDEC*, previously used to model blocky-rock systems (Cundell *et al*[80]) to model an arch structure. The arch was divided into blocks connected by elastic contacts. Two types of load were

applied, the first moving a particular block with a given velocity, and the second moving a support to change the horizontal support reaction, which in turn causes the failure mechanism. The presence of backfill was represented by static loads acting on the arch extrados, with the confining forces calculated from the weight of the soil slice above the block. No load dispersal or soil structure interaction other than dead load is considered or allowed for. The presence of this backfill would considerably increase the failure load as previous studies have shown. A parametric study was performed on the dimensional and numerical parameters used, the results of which are listed below:

- *Contact stiffness* was shown to have no influence on the failure load or mechanism, as limit analysis theorems suggest.
- *Friction angle* has a marked effect of the failure load and at lower values the failure mechanism involves some sliding as well as hinges being formed.
- *Number of blocks* in the model has a very small effect on the failure load, thought mainly to be due to allowing a slightly different failure mechanism to occur.
- The progressive reduction of the *thickness/span ratio* produces a reduction of the failure load until the arch is no longer stable under self-weight alone.
- *Arch shape* was shown to have differing effects on the failure load for the various types of load applied.

The use of discrete elements to investigate arch bridges is still at an early stage, and it is felt that there is scope for improvements on the promising early research. This type of analysis enables the investigation of many of the factors effecting the strength of arch bridges such as arch/fill interaction, failure mechanisms, spandrel walls and other 3-D effects.

## 2.4 Experimental Work

Experiments have undoubtedly been used, going back to Roman times, to test theories of stability, geometry and strength of arches. Since then, experiments have provided valuable insight into specific factors effecting bridge structures. The new experimental work on arch bridges, generally split into two groups (full scale tests and model tests), will be outlined in this section. Much of this experimental work is now done in conjunction with validation using modern computational assessment methods.

### 2.4.1 Field tests

The taking measurements in order to monitor and assess structures has advantages and disadvantages over smaller scale model tests. The main advantage is that the results being obtained from these tests are actual results from real structures. Previous field tests have provided valuable information about specific structures, but since they are in the field a problem lies in the obtaining of sufficient specific information from these tests. The opportunity to monitor full scale bridges has been decreasing for some time, due to problems of cost, practicality and availability. A series of these load tests on redundant arch bridges was performed by the Transport Research Laboratory between 1984 and 1994.[4] These tests have been used widely as a method of calibration for many of the modern analysis programs.

Hughes *et al*[81] have performed a series of tests on a bridge in Gwynedd, the results from which have been presented with comparisons between recorded and predicted stress and strain. The tests use a flat-jack strain relief testing technique; this is interesting because serviceability loading states are investigated. The method measures the displacement at a particular mortar joint, effectively monitoring the strain. Then with the use of a flat-jack, which replaces the mortar in a joint, the stress required to restore the original strain state can be calculated. This value is assumed to be the original stress for the dead load state. Live load simulations were also performed and the pressure required to obtain the locally measured strains is recorded. The stress results produced similar distributions to the predicted analysis. The predicted strains are generally much larger than the

Further tests were conducted by Boothby *et al*[85] on five masonry arch bridges, varying in span from 2.5 to 11.5m, and having different aspect ratios. Each arch was again instrumented with LVDT's to measure the effect of load on the displacement of the arch intrados. Cracks present before the tests were also monitored with similar LVDTs. An adequate number of readings was taken to record sufficient information for each type of loading used. Trucks were used to load the structures, although the size of bridge affected the type of loading applied. An attempt was made to make the tests as uniform as possible.

If the linearity of the load-deflection response is affected, then the structure of the arch ring is assumed to be damaged.[84] Lower loads generally produced linear responses; the use of higher loads stopped the linear response and some inelastic displacement remained in the arch ring. A finite element model, created using ANSYS, was used to correlate the displacement data. It was also aimed to locate the thrust line, to aid with the mechanism analysis. Isoparametric elements were used for the voussoirs, while the joints were made from gap and hinge elements in an attempt to model the discrete block structure. The soil resistivity was also accounted for with the use of cable elements along the exterior of the arch barrel. A parametric study was performed on the modulus of elasticity of the voussoirs and the stiffness of the cable elements, and suitable values were chosen to replicate the actual recorded displacement data. The model then had to be matched to the different types of bridge that had been tested. It was concluded that the F.E. analysis was capable of modelling low loads, but could not replicate non-linear displacement responses. The author concluded that the non-linear response results were due to damage to the structure of the bridge rather than to the formation of hinges, since this formation was allowed for in the model. It was concluded that the non-linear responses of the structures were due to damage to the voussoirs or mortar, rather than by elastic thinning of the arch ring.

### 2.4.2 Model-testing

An extensive range of tests has been performed by various authors on model arch bridges, with each set of tests looking at different parameters. These tests have however been either conducted or reviewed previously by Fairfield[19] and subsequently by Prentice.[20] Previous research has investigated such factors as soil-structure interaction,[38] flat arches, multi-spans and arch ring separation.[86]

Therefore only the recent published model tests are reviewed in this section.

The influence of fill material and masonry type has been investigated by Hughes *et al*[87] with a series of centrifuge tests. These allow the self weight of the model to be varied to produce stresses as would be found in a full scale test. An instrumented $\frac{1}{6}$-scale model of a prototype bridge was constructed, with care taken at each stage to replicate all scale effects, such as fill, brick and mortar sizes. Instruments measured stresses, strains and deflections of both the fill and arch barrel. The failure load and formation of hinges compared well with the prototype test. The effects of changing the brick, mortar and fill properties were then investigated. Reducing brick and mortar strength produced a reduction in the failure load, while changing the fill type also has a significant effect. The effect of changing either the mortar or the brick alone was, unfortunately, not investigated here: this would have given a guide to the relative effect of each. The author then goes on to relate this work to the currently available assessment techniques previously examined in Section 1.2. Only the present mechanism and cracking elastic methods are considered as these are the only ones to incorporate the above parameters. Parametric studies investigating the theoretical property changes for soil and brick have been included, with some interesting findings. The mechanism method produced good results, even though based on compressive failure, which rarely occurred in the tests. The elastic cracking analysis confirms the presence of full passive pressure as found in the actual tests.

Experimental validation of flat arch analysis techniques has been conducted by Peng *et al*[88] with the construction and testing of a brick-work model arch. Displacement was recorded using LVDT's, loading was applied at $\frac{1}{4}$-span using hydraulic loading jacks. The failure mode of the structure was initiated by separation of the spandrel walls and the arch ring, before the formation of any visible hinges within the arch ring. The final failure occurred when the spandrel walls rotated outwards and fell away from the model.

The structure was modelled using LUSAS, a finite element package using eight noded isoparametric elements throughout. The package produced good comparative results, with the majority of cracking occurring at $\frac{1}{4}$-span. The parametric study found that the elastic modulus of the brick work, $E$ in $GNm^{-2}$ and uniaxial compressive strength, $\sigma_c$ in $Nmm^{-2}$ increased the predicted ultimate load as each of these parameters increased. These effects however were not

particularly sensitive. Although the package under-predicted the failure load, further improvements have been suggested to improve the model.

#### 2.4.2.1 Soil-structure interaction

In a series of tests to destruction specifically to determine soil-structure interaction effects, Davey[89] found that soil-structure interaction increased the capacity of the bridge significantly from the capacity when the soils strength was ignored. This gave an obvious need for these interactive effects to be modelled in any bridge analysis, because to ignore such effects would be to underestimate the capacity.

Although soil-structure interaction has been shown to be an important aspect of the structure of the arch bridge, little work has been done solely investigating this interaction phenomenon for bridges. Ponniah[90–92] investigated this soil arch system and the four modes of soil-structure interaction:

- load dispersal
- lateral earth pressure redistribution as the arch ring deforms
- mobilisation of circumferential shearing resistance
- arching behind displaced sections of the arch ring.

This work was continued at the University of Edinburgh by Fairfield[19,93–97] who, through a series of small and full scale model tests and field tests investigated soil-structure interaction effects directly for arch bridges. The small scale tests produced a number of conclusions, showing both load dispersal and lateral earth pressure distribution solely from soil structure interaction. From the large scale tests both dead load and live load soil stress distributions were measured and favourably compared to theoretical predictions, again allowing the investigation of load dispersal through the fill and lateral earth pressure distribution around the arch. A larger load dispersal than predicted by BD21/97[23] was found to occur. Shear stresses were recorded around the extrados and related to displacement of the arch barrel. These displacements also produced some mobilisation of the passive pressures previously mentioned.

Further investigations of the soil-structure interaction of multi-span tests were performed by Prentice[20,98–102] at the University of Edinburgh. This work was to continue that done previously and relate the geotechnical theories previously discussed for single spans to the behaviour of multi-span arch bridges. For this the author performed a similar series of small scale timber model tests, large scale double span brick arch tests and the monitoring of a new brick-work arch. He related many of these tests to finite element analysis and other types of bridge analysis used today.

Harvey *et al*[38] carried out a series of tests on model arches in order to investigate soil-structure interaction effects. The paper concludes that soil-structure interaction was evident from pressure changes of the 48 soil pressure cells used in the structure. This interaction was produced from arch movement into the fill material on the side of the arch away from the load. Any effect of soil-structure interaction on the side below the load is complicated by the presence of the load masking these effects. This is the same for most of the previously mentioned model arch tests. One exception to this is the small scale timber tests by Prentice,[20,100] but here pressure readings were not recorded. An effort has been made to relate deflection to stress relief later in this thesis.

#### 2.4.2.2 Repair and strengthening

Sumon[103] presents two load tests on the same bridge to investigate ring separation and the subsequent effects of the repair work performed. The nature of the test was more by accident than by design, resulting from the bridge being involuntarily loaded to failure during elastic tests; however the tests were useful in testing a repair method. The test bridge had no spandrel walls or road surfacing. Instrumentation of the structure was performed using displacement and vibrating wire strain gauges. The other important factor is that the bridges have an inbuilt ring separation. Restoration of the structure was performed using stainless steel mesh repair (SSMR), forming a series of continuous bars along the soffit. Elastic tests produced little interesting information. The failure tests were performed using a knife edge load, positioned at the quarter-point. The failure load of the repaired and reinforced arch occurred at a 38% larger load than the simple arch. A good discussion is presented on the failure mechanism and the way in which it propagated during the test. The definition of failure and collapse in this example

are not clear, although the bridge condition is well explained during the test. It is however clear that the reinforced and repaired arch is stronger and stiffer then the original arch.

Another series of model tests assessing the increase in load carrying capacity from a sprayed layer of concrete to the arch soffit was presented by Peaston & Choo.[104] The eight arches tested were identical, spanning 2.5 $m$, with a standard load test, applied at the quarter point to obtain the load carrying capacity. All subsequent arches were tested elastically, at 80% of their estimated capacity applied repeatedly in a cyclic loading for four million cycles. Half the samples failed before the cyclic loading had been completed. The surviving arches were allowed to recover and then strengthened with a sprayed mortar, to various depths, and allowed to cure. These arches were then load tested to failure. This resulted in increases in capacity, which occurred as the mortar layer depth was increased. A large increase in capacity was produced in these tests, for a relatively small increase in the arch ring thickness.

Comparisons made with the modified MEXE method produced, not unsurprisingly, conservative values of the ultimate load capacity. This is without taking into account any reduction in the condition factor due to the previous loading. The span of the arches is however within the suggested range for the MEXE method. A 2-D finite element programme, including the modelling of the strengthening mortar, was used to give an upper and lower bound solution for the completely bonded and un-bonded joint in the arch. The test results compared favourably with the un-bonded solution, although it was commented that during the tests no evidence was observed of mortar de-bonding.

## 2.5 Soil structure interaction

Soil-structure interaction has been researched since the beginning of soil mechanics, however specific arch bridge research is still at an early stage. Work comes from the need to understand how structures and soil interact for a given engineering problem. The following section presents the new work pertaining to interaction

in the arch bridge field. Initially arches were treated as retaining structures and then later their properties were linked to that of buried pipes and culvert. Soil structure interaction is an inevitable mechanism that occurs with almost every structure. An engineer may choose to ignore this mechanism, but the interaction will take place and its effects may be more that envisaged.[105] Prior to 1970 design practice tended to consider the ground and structure in relative isolation, which is what in fact occurs today with arch bridges. In early work most of this interaction was considered only for structures sitting on top of a soil and then affecting the soil below, which is of course an important aspect of bridge design, (Thorburn[105]).

In later publications on the subject, Thorburn,[106,107] there is a beginning of an attempt try to understand the importance of this interaction with respect to tunnels, underground openings, retaining walls and buried structures. By this period there were two distinct categories of interaction: structure supported by ground and ground supported by structures. These earth retaining structures are of interest here, since the structures are integral components of the soil-structure system, deriving both loading and support from the soil. Strain and time dependent forces and movement cause variations in ground pressure, and the retaining structure responds to these changes to maintain a state of balance. Importance is drawn to the initial *in situ* stresses, together with structural movements on lateral soil pressure. Of particular interest is work done on buried structures, where interactive effects, both applied and resisted by the surrounding ground, are depended upon for strength and structural behaviour.

### 2.5.1 Soil-structure interface

For most of the comparative studies carried out later in this thesis an interface between dry sand and the bricks and mortar is of particular interest. Full scale tests have been carried out on buried structures, retaining walls and actual arch bridges, although little conclusive evidence has been proposed concerning the soil-structure interface. Many measurements have been presented regarding the separate properties of the masonry arch material and that of the fill, although very little to do with the properties of the interface under dead and loaded conditions.

A paper by Viladkar[108] discusses modelling the interface for soil structure interaction

studies and suggests ways in which this interface can be improved. The author states that a thorough understanding of the actual structure is essential and that the stiffnesses of these interfaces are of great importance. For continuum element analysis problems there is still a large difference between linear and non-linear interactive analysis. This is further discussed by Runesson[109] and Goshy.[110] The use of an interface element has an appreciable influence on the shear stresses along the interface although, since interface effects are still not fully understood, this results in modelling being very complicated and difficult. In the most recent international arch bridge conference[111] little consideration was given to soil-structure interaction effects.

## 2.5.2 Structures supporting soil

### 2.5.2.1 Retaining walls

The earliest work performed by Coulomb[19] looked at the thrust soil exerts on earth retaining structures and the yield criteria of soil. Both of these form the basics for much of the modern soil-structure interaction analysis. This early work was later linked to arched bridges, but was not done so at the time.

Information available is generally on the relationship between earth pressure and movement relating to retaining walls. Figure 2.14 shows results of tests in which a rigid wall was rotated into and away from a dry sand backfill.[112] The results are presented in terms of the coefficient of horizontal earth pressure $K$, derived from thrust plotted against wall rotation. Other similar relationships have also been obtained more recently (Carder *et al*[113] & Katona et al[114] & CIRIA[115]). The relative movements required to produce the limiting active and passive conditions will depend on the structure, the soil and the initial stress state prior to any movement. This movement is of great interest to this research, since very few studies have been found which give a similar relationship for an arch bridge structure. The consideration of the relative movement required to achieve the soil thrust is of great importance.

The horizontal pressure applied to arch structures is found by applying the appropriate Rankine coefficient to the vertical pressure from the weight of the overlying soil. The coefficient depends on the type of movement of the structure,

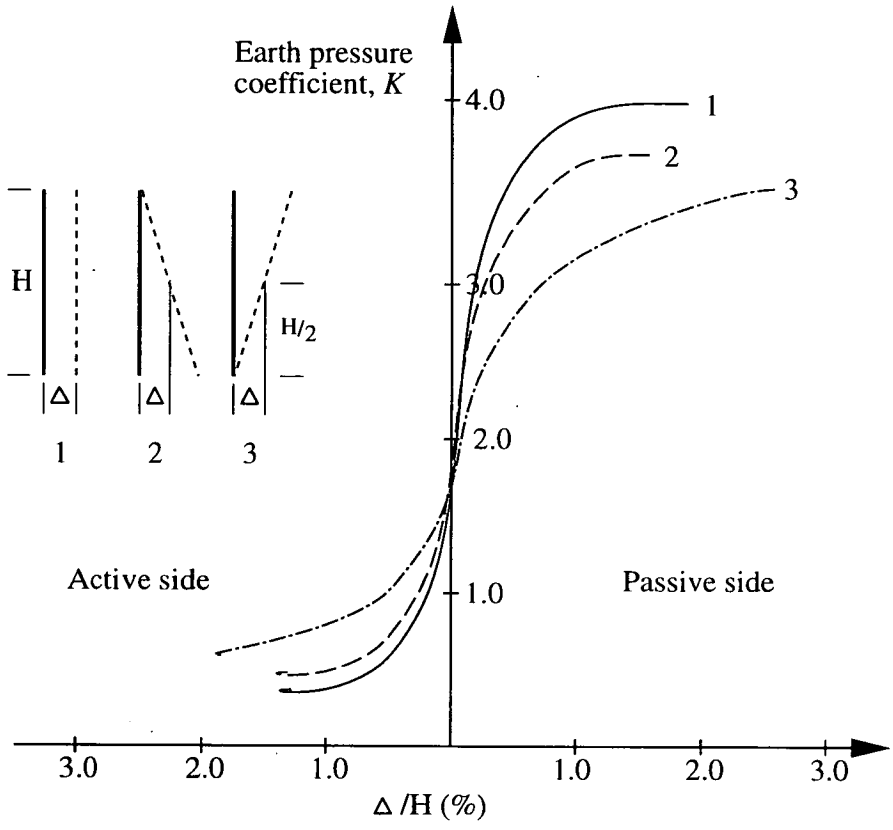


Figure 2.14: Development of active and passive pressure coefficients for a rough wall (after Berry *et al*[6])

moving into the soil (passive coefficient, $K_p$), stationary (at rest coefficient, $K_o$) or moving away from the soil (active coefficient, $K_a$). These coefficients are generally calculated from the internal friction angle ($\phi$) as shown in Equation 2.12.

$$K_p = \frac{1+\sin\phi}{1-\sin\phi} \qquad K_o = 1-\sin\phi \qquad K_a = \frac{1-\sin\phi}{1+\sin\phi} \tag{2.12}$$

The amount of movement required to develop these pressures fully has been studied, but much of this work has been subsequently questioned. Other work previously reviewed[19] is also of relevance, investigating many types of finite element and small and large scale model tests to examine this interaction. Zones of movement were interpreted from the model tests and pressure distribution investigated with the finite element methods. Comparisons with the theoretical pressure distributions of Coulomb, Jaky and Spangler have also been made. These comparisons were found to be ineffective in predicting pressure changes, although

elastic analysis using two dimensional elements was found to give good correlation of the stress states.

Viladkar,[108] following previous work by Buragohain and Pande, has modelled the soil-structure interface, with particular use of interface elements. Three noded isoparemetric beam interface elements were used to model the problem, which accounts for axial interaction between the different element types used in the analysis. The paper concludes that these interface elements are essential in trying to understand the realistic nature of the problem. The tangential and normal stiffness of these elements is important and have a large effect on the shear stresses along the interface.

#### 2.5.2.2 Buried structures

This type of structure varies between rigid concrete and flexible thin-walled steel culvert. The rigid structures are designed so that the permissive material properties are not exceeded, while for the thin structures deflection is a main design criteria, altering the distribution of soil pressure on the structure due to interactive effects. There are two main reasons for this interaction to occur:

- the altered stress state around the culvert due to the difference in material properties of the structure and the soil
- the distortion resulting in the redistribution of pressure around the structure.

A large amount of work has been performed on soil surrounded structures, and has been previously reviewed in detail by Fairfield.[19] The fact that this research links well with arch bridge soil-structure interaction makes it of interest here. Other factors listed as affecting the interaction of the soil-structure system include:

- shape of the structure and construction techniques
- loading condition
- relative stiffness of the soil.

The complexity of this problem however results in a soil-structure system that is difficult to analyse properly. A main criteria for this interaction is obviously the stiffness of the structure, since this directly affects the interaction produced: many such structures are classified by this factor.

## 2.6 Concluding remarks

This review has briefly covered the long and dynamic history of masonry arch bridge design, analysis and construction. It is hoped that this insight has given the reader an overview of the various topics relevant to today,s arch bridge assessment methods and the problems inherent with them. It is one of the aims of this thesis to understand more fully the problems with modern assessment methods.

For all the efforts into the assessment of masonry arch bridges it still appears that the current assessment methods widely used throughout the UK underestimate the strength of this type of structure. The inability to accurately assess these structures has meant the gradual decline in this type of construction. It has been shown that present methods of assessment are conservative, resulting in the over-designing these structures, in increasing the initial cost and thus making them less likely to be a chosen solution to a problem.

In this literature review many methods of masonry arch assessment have been introduced: four of these methods are subsequently used in this thesis for a comparative study and a bridge assessment. The methods used are:

- the modified MEXE method, an empirical method with modification factors,
- ARCHIE, a mechanism based programme,
- CTAP, an elastic, no tension analysis, and
- MAFEA, a finite element model.

For this reason the specific theory behind each method has not been fully explained in this section: it is introduced in more detail in the relevant chapter.

A great deal of research seems to have been performed trying to make the present assessment methods more accurate, including affects such as spandrel walls and arch/fill interaction. Little work has been performed previously however with the powerful tool of discrete element analysis, a package which initially seems well suited to the arch bridge problem.

# Chapter 3

# Comparisons of modern computational assessment methods

## 3.1 Introduction

By the beginning of 1999 all the bridge structures in Britain should have been assessed, to verify that they meet the requirements made by the EC directive aimed at a common European transport policy. The directive required that the maximum axle load be increased from a value of 38 tonnes to 40 and 44 tonnes.[8] These larger vehicle weights were introduced due to pressure to have larger vehicles on our roads. Any bridge failing to meet these new requirements will need strengthening or have a weight restriction imposed.

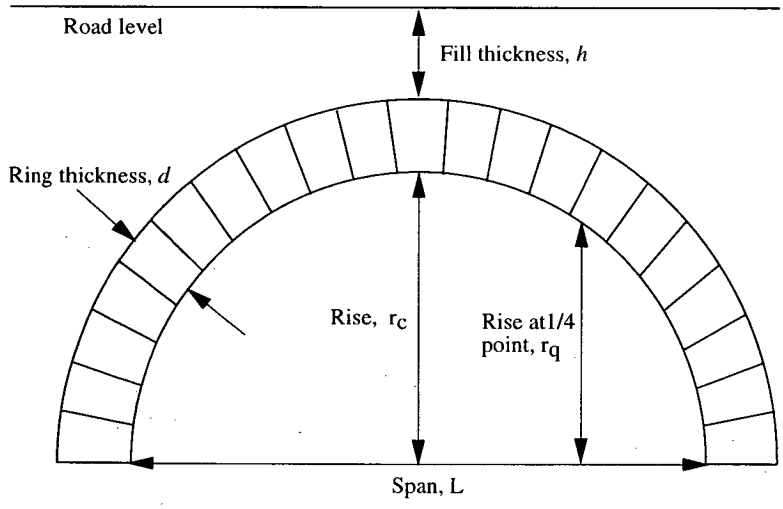


Figure 3.1: Definition of arch bridge dimensions

During the summer of 1997 the bridge stock of East Lothian council were to be assessed for these new axle loads. This assessment required an initial inspection in order to obtain the main external dimensions of each bridge; the span ($L$), the rise at the crown ($r_c$) and quarter point ($r_q$), the thickness of the arch barrel ($d$) and the depth of fill ($h$). These measurements were then used to perform a modified MEXE assessment using the most severe modification factors, producing an initially conservative assessment. Any structure passing this initial assessment would be assumed to be safe and therefore not requiring further inspection. Any bridge not passing this first assessment was then re-assessed to find the actual modification factors that would be re-applied to obtain the final capacity. A second assessment package, ARCHIE, was also used to obtain a second opinion of each bridge capacity. Again conservative input variables were used to give an initial conservative assessment and any failures re-investigated. Re-assessment of

the bridge involved coring of the arch barrel to investigate the ring thickness, the masonry strength values and look for the presence of backing.

In this section four commonly used bridge assessment methods are introduced and investigated. These methods include the MEXE and ARCHIE assessment packages mentioned above, and two others, CTAP and MAFEA. All of these have been briefly introduced in Chapter 2, but each will be covered in more detail here. Firstly a parametric study was performed with each assessment method, investigating how changes in dimensional and material parameters affect the failure load produced. This was performed to give a greater insight into how each method behaves, and how the different methods compare. Secondly each package was used to perform an arch assessment on the East Lothian bridge stock, with comparisons again being made between the packages.

## 3.2 Assessment packages considered

### 3.2.1 The modified MEXE assessment method

The MEXE method is documented in BA 16(DMRB 3.4.4): The assessment of highway bridges and structures and BD 21/97, volume 3, section 4.[8,116] These codes deal primarily with the inspection and assessment of the strength of the arch barrel. It ignores the affects on strength provided by such elements as the wing walls, spandrel walls, foundations etc. These items are dealt with under the Advice Notes. The modified MEXE method is used to estimate the carrying capacity of arches spanning up to 18m, but for spans over 12m it becomes increasingly conservative compared to other methods, and as such is not recommended.[23] It is also accepted that the method is not suitable for arches which are flat, noticeably deformed or heavily skewed. BD 21/97 states that where the ring depth is less than the depth of fill, results should also be confirmed by more rigorous methods. MEXE is also not intended for multi-span arches unless piers are very short and stocky, although British Rail have adapted the method with the addition of an abutment factor.[4]

The modified MEXE assessment is based on an empirical method set out in "Military Load Classification (of civil Bridges) by the Reconnaissance and Corre-

lation Methods[117]". It includes results from past experience, and has been found to be reliable for the range of vehicles conforming to the Construction and Use Regulations. The original assessment is in terms of a maximum allowable axle load on an axle forming part of a double axle bogie. Factors are given which can convert this result to other axle configurations.

#### 3.2.1.1 Theory

The modified MEXE method is based upon an empirical formula using solely the arch dimensions. The arch is assumed parabolic in shape, with $\frac{r_q}{r_c} = \frac{3}{4}$, and have a span to rise ratio, $\frac{L}{r_c} = 4$, and built of good quality masonry, with well pointed undamaged joints. With these dimensions and using a series of equations, factors based on dimensional and qualitative properties of the actual bridge are then applied to the result from Equation 3.1. Information is also required about the type and condition of material used in the bridge structure, the type of construction and the condition of the structure. A full list of information required can be found in the relevant parts of the code.

#### 3.2.1.2 Provisional Assessment

The provisional axle load, $W_p$, can be found by substituting $(d+h)$ and $L$ either into a nomogram or into the following expression:

$$W_p = \frac{740(d+h)^2}{L^{1.3}} \tag{3.1}$$

This equation should only be used within the suggested dimension limits stated earlier. This provisional axle load is then modified by the following modification factors.

#### 3.2.1.3 Modification Factors

1. Span/Rise Factor ($F_{sr}$). This takes account of the arch shape, which would affect the overall strength. With a span to rise ratio of 4 or less the factor

is assumed to be 1, but for ratios greater than 4 reference should be made to Fig 3/3 in the code. Where the span/rise factor is:

$$F_{sr} = \frac{L}{r_c} \tag{3.2}$$

2. Profile Factor ($F_p$) This is to take account of the fact that elliptical arches are not as strong as segmental and parabolic arches. The ideal profile of a parabolic has been taken, where the rise at the quarter points, $r_q = 0.75r_c$. The profile factor $F_p$ can be again calculated by either Fig 3/4 in the code or by the following expression:

$$F_p = 2.3\left(\frac{r_c - r_q}{r_c}\right)^{0.6} \tag{3.3}$$

3. Material Factor ($F_m$). This factor is an expression which looks at the depth of the fill and the height of the arch barrel, and relates these to their own factors, the fill factor $F_f$ and the barrel factor $F_b$, which can both be found in Tables in the code. There are special notes also in the code pointing out special things to look for and to take account of. The material factor can be obtained from the following expression:

$$F_m = \frac{(F_b \times d)(F_f \times h)}{d + h} \tag{3.4}$$

4. Joint Factor ($F_j$). To take account of the general size and condition of the joints. The joint factor can be obtained from the following expression:

$$F_j = F_w \times F_d \times F_{mo} \tag{3.5}$$

Where $F_w$ = Width factor, $F_d$ = Depth factor, $F_{mo}$ = Mortar factor. These factors can be obtained from Tables within the code.

5. Condition Factor ($F_c$). The previous factors are based more on quantitative information obtained from the bridge, where as the condition factor depends more on an objective assessment of the importance of the various cracks and

deformations which may be present, and how they are counter-balanced by good materials and workmanship. the factor varies between 0 and 1.0 and depends upon two criterion, defects affecting the stability and load carrying capacity of the arch barrel, and those which don't. A fuller description of this may be seen in the code. Care must be taken to dissociate these from the material, joint and condition factor discussed earlier.

#### 3.2.1.4 Modified axle load

All of the previous modification factors are then brought together with the provisional axle load calculated earlier in order to produce the modified axle load. This presents the allowable loading on an arch from a double axle bogie configuration with no 'lift-off' from either axle. Thus the modified axle load, $W_m$ can be obtained from the following expression:

$$W_m = F_{sr} \times F_p \times F_m \times F_j \times F_c \times W_p \tag{3.6}$$

To obtain values for other axle configurations the modified axle load is multiplied by an axle factor $F_a$. This can be found in the relevant code and is solely dependent on the span. The modified MEXE method spreadsheet used in the parametric study and arch assessment programme is shown in Appendix A.

### 3.2.2 The ARCHIE assessment method

The Archie package for masonry arch analysis was first introduced in 1983 by Harvey,[118] who originally designed the software due to shortcomings he saw in other assessment methods. The package contains three main additions to the mechanism method previously introduced:

1. The line of thrust is modified to a zone of thrust to take account of material strength

2. The mechanism method was structured to take account of the level of knowledge of the various aspects of the bridge structure. The programme

was therefore designed to calculate the required ring depth for a particular position and value of load.

3. The soil fill acts not just as a stabilising dead weight and a distributing medium for the applied load, but also contributes an element of horizontal pressure.

ARCHIE comes in a version with an option to input the dimensional data for the analysis and another option allowing the analysis of the problem with variation of quantitative properties such as material strength and density.

#### 3.2.2.1 Data set programme

ARCHIE allows the bridge dimensions to be input and saved under a specific name for later analysis. The general arch shape is the first option where it offers various options to choose from circular, three centred or gives the option of entering data points separately to allow less common arch shapes to be analysed. Next the number of sections or voussoirs required in the arch ring is selected. The span and rise are then input in units of millimetres as well as the chainage and elevation of the springings and elevation of the pier. This gives the general shape of the arch barrel. The next option is to input the road profile data, this gives the option of choosing the number data points to be used and the position of these points are entered also in millimetres. The general shape of the arch has now been completed and the next thing requested are the bridge material data. These properties include; arch dimensions, material strengths, material density, friction angle for the soil, the position and force from backing and a factor of passive pressure.

Little information is required from the bridge survey to do with the type and condition of material used, the type of construction and the condition of the structure apart from the depth of mortar loss. Information that can be obtained about the general appearance of the structure is not included into the analysis. There is no provision in the package to be able to apply factors such as would be used in MEXE, this results in constant failure loads independent of a visual examination.

#### 3.2.2.2 Load set programme

Archie contains three main load set options, lift-off loads, non lift-off loads and restricted loads. Each has the option of choosing either single, double or triple axles with either left or right lift-off, or left or right heavy loads respectively. These load cases will not be looked at in this parametric study as it is not relevant but the inclusion of these are useful for normal bridge assessment. It is also possible to specify types and ranges of load that are not previously included. Load files were written to cover the range of expected failure loads at 1 ton intervals in order to perform the parametric study. Where failure loads were not an exact multiple of the intervals, results were interpolated to give more exact answers. A partial safety factor of 3.4 is applied to the single axle load.

The lane width parameter can also be varied at this point, if the measured width is less than $5m$, with the distribution width being given by Equation 3.7.

$$Distributed\ \ width = 1.5 + h + vehicle\ \ width \tag{3.7}$$

#### 3.2.2.3 Provisional Assessment

For the provisional assessment the salient values from the Bargower bridge test were input to get a constant bridge case. An initial analysis was performed on the structure to find the load at which the line of thrust was no longer restrained within the arch barrel. This value was recorded and then used as a base value for all subsequent analyses investigating the parameters.

### 3.2.3 The CTAP assessment method

The Cardiff TRRL Assessment Programme (CTAP) assessment package was developed by Bridle and Hughes[25,26] in Cardiff at the University of Wales. It is based firmly on a Castigliano type elastic analysis as has previously been described. This method has been extended to produce a theoretical failure load for an arch structure and represents the main factors of behaviour for a two-dimensional arch and its passive horizontal interaction with the fill material

for different arrangements of applied loading.

The basic theory is that the bending moments and forces in the arch barrel can be found for any arch geometry and loading configuration. The strain energy ($U$) resulting from these can then be determined from Equation 3.8 by numerical integration.

$$U = \int_0^L \frac{M^2 dl}{2EI} + \int_0^L \frac{T^2 dl}{2EA} = \sum_{i=1}^{n} \frac{M_i^2 \delta l_i}{2EI_i} + \sum_{i=1}^{n} \frac{T_i^2 \delta l_i}{2EA_i} \tag{3.8}$$

This is a natural extension of previous work to include axial deformation which can be significant for certain arch geometries. Shear deformation could also be included but was found to have little contribution. This analysis assumes no abutment movement and the determination of $H_A$, $V_A$ and $M_A$, the reactions at the abutment, are found by differentiating Equation 3.8. Equation 3.9 is used to determine the deflections of the arch due to the moment and the applied load.

$$\begin{aligned} \delta x_p &= \sum_0^{x_p} \frac{M_i(y_p - y)\delta l_i}{2EI_i} - \sum_0^{x_p} \frac{T_i cos\theta \delta l_i}{2EA_i} \\ \delta y_p &= \sum_0^{y_p} \frac{M_i(x_p - x)\delta l_i}{2EI_i} - \sum_0^{y_p} \frac{T_i sin\theta \delta l_i}{2EA_i} \end{aligned} \tag{3.9}$$

Numerical integration is used to find the forces and moments in each section. New sections are adopted by removing areas of tension within the arch ring. Passive and active soil loading is applied to the arch from the deflection information and the input linear soil model between each step. Iteration is employed to progressively thin the arch ring, in each case only the area in compression is considered and the process repeated until convergence. If a failure load is required the load is incremented and the forces and moments re-iterated. If no solution can be found then the arch has failed so the load increment is reduced until a solution is found, which gives the collapse load.

Before any analysis can be performed the operator must create data files containing information required for the arch analysis. This information is entered under one of the four entry headings listed below;

**Arch geometry** All arch dimensions are entered including lane width, road angle and number of elements that should be used for the analysis. Arch thickness at the crown and abutment are both required. A choice of arch shapes also needs selecting as to which best represents the arch under assessment.

**Arch material** Material property data are entered including elasticity, bulk density and monitoring strength.

**Fill material** Fill and road surface property data are entered, including sub-grade reaction, density and soil pressure coefficients used to calculate soil loading. Since $h$ was relatively large for Bargower, the high dead load caused excessive thinning of the arch ring bringing about failure due to dead load. Subsequently $h$ was reduced by half before the parametric study could be performed.

**Loading type** Two main options exist. The increasing load case allows the initial load value and type to be input and the manner in which it is incremented towards failure is specified. The travelling load case allows a specified load to move across the entire span of the bridge in a specified number of moves. The distribution angle can also be input, assumed to be 1:2 as specified in the code.[23] The increasing load case option was used to allow the position of load to be fixed in most cases.

The various data files must now be saved before any analysis is carried out. The present package came with Bargower data already installed, a list of the salient values used in the analysis is provided in Table 3.5.

### 3.2.4 The MAFEA assessment method

The MAFEA (Masonry Arch Finite Element Analysis) assessment method was developed jointly by British Rail Research and the University of Nottingham to cope with the shortcomings they saw in other assessment methods. Primarily developed for the assessment of railway bridge structures, an option exists to alter the loading conditions to suit axle loading to allow comparison with the other packages. The present package comes with a series of five reports that

provide the documentation for the MAFEA software.[119] The series comprises an introduction to the method, a user guide, a parametric study, a comparison to arch collapse tests and recommended material properties.

The quantity and complexity of input data required is large, however predefined data within the package can be utilised to produce an effective assessment. Despite being the most comprehensive of the packages used here, MAFEA is versatile and easy to learn and use due to it graphical nature and its menu driven command structure.

MAFEA divides the masonry arch bridge into two main elements: the arch barrel representing the main load bearing part of the structure, and the fill material. The barrel is assumed to have no tensile capacity and the fill assumed to be non-structural although it can resist movement of the barrel. MAFEA models the arch barrel with tapered beam elements as shown in Figure 2.12. These elements allow for both rigid body movement, changes in sectional properties and material failure. In this way two types of failure, a crushing and a stability case can both be modelled.

#### 3.2.4.1 Data entry

MAFEA works by requiring the thrust line to remain within the modelled arch barrel, if haunching is present the thickness of the barrel can be nominally increased. Material properties such as density, elasticity and compressive strength are required, although for the fill, the friction angle and coefficients of earth pressure are also required. The entering of both the friction angle and the coefficients allows the maximum passive pressure to be fixed rather than always calculated.

MAFEA requires assessment and serviceability factors available from BD 21/97, although default setting exist for each within the package. The arch barrel and fill material properties require to be saved in an input file, and must be completed before the arch definition can take place. An analysis control file also requires data for the soil model, initial load step, distribution angle, type of distribution and factors relating loading and crack convergence. Vehicle definition including the various axle configurations and the type of axle applied has also to be defined. For this study a single axle with a $300mm$ contact length was used with a lane

width of $2.5m$.

The final input section to complete is the arch definition. Arch dimensions, shape and the number of elements required to model the arch ring are all specified here. Once this input information has been completed the user would build the mesh with the chosen number of elements and go on to perform the analysis.

The number of elements used can have an affect on the failure load, with the minimum number of elements that produce a constant collapse load being the optimum value to use. Many other analysis control options exist which determine the way the programme will analyse an arch problem. These are discussed in the series of reports and codes, and for the case of this study have been kept at their default values throughout.

Generally it is suggested that an arch assessment is performed with the material parameters given in the reports. However for this parametric study material properties were known . In most cases material properties are generally not known so MAFEA provides 'Unknown' material types for such situations. These material types represent a worst case scenario giving a conservative initial assessment, if more favourable values are to be used a more thorough site investigation would be required to justify them. Unique to MAFEA safety factors exist for many of the parameters, the default values for which are given in Table 3.1

| Parameter | Stability | Crushing |
|---|---|---|
| Barrel density | 0.8 | 1.15 |
| Barrel elasticity | 2.0 | 2.0 |
| Fill density | 0.8 | 1.2 |
| Fill elasticity | 2.0 | 2.0 |
| Friction angle | 1.3 | 1.3 |
| Lateral passive pressure | 2.0 (Tested) | 1.0 (from $\phi$) |

Table 3.1: Partial safety factors for MAFEA material properties

Bargower bridge data, with which the parametric study was performed, required the arch barrel crushing strength to be increased to stated values to allow for both types of failure to be predicted. The lowest failure load from the two cases was chosen as the critical value.

## 3.3 Parametric study

### 3.3.1 Overview

Although each of the four methods of arch bridge assessment have been used for some years it was still necessary to perform a parametric study on each in order to properly understand the different ways in which each package performed. For this reason an independent study was performed on each package to try to find the key parameters and understand why they are significant by relating their affects to the analysis method. Bargower[84] bridge was chosen to give suitable values for the parametric study to be performed, since material properties and dimensions are all well known. A full set of graphs from the parametric study are presented in Appendix B. Any variations from the standard input data required by the different packages will be recorded in the text. Arch profiles will be assumed to be segmental throughout this study, with the rise at the quarter span derived where not available from Equation 3.10.[4] The general range for $r_q/r_c$ of $0.7 \rightarrow 0.866$ encompasses all arch shapes required here.

$$r_q = \frac{\sqrt{L^4 + 4L^2r_c^2 + 16r_c^4} - L^2}{8r_c} + \frac{r_c}{2} \tag{3.10}$$

Parameters will be varied, where possible, in order to investigate each package and to identify the parameters which have greatest affect on the assessed capacity of the arch. The sensitivity to each parameter was investigated by keeping all other parameters constant while repeating the analysis with different values for the parameter being considered. Graphs were plotted of collapse loads against the range of each parameters tested to investigate the sensitivity to each parameter. The working ranges investigated are detailed in Tables 3.3 to 3.6. This investigation will enable an assessing engineer to target site investigations and material testing to determine the critical properties for each assessment package. Criteria governing the degree of accuracy required for each parameter are also determined. For each package a spreadsheet was devised giving the input parameters used to produce a series of failure loads.

### 3.3.2 MEXE

Firstly a spreadsheet was designed that would calculate the modified axle load from a constant provisional axle load, for a series of different modification factors. All of the dimensional and condition values input into this spreadsheet were then varied to investigate the single and combined affects on the final modified axle load. The affects of this study are discussed in the following sections and the graphs are presented in Appendix B, Figures B.1 and B.2.

#### 3.3.2.1 Variation of modification factors

**Variation of the barrel and fill factors** As previously discussed the material factor is made up from two factors and two dimensions. The barrel factor is one of these variable that goes into the material factor that is then applied to the provisional axle load. It is a factor obtained directly from a table, and as such is subjective. It is only a rough guide as to the choice of barrel material to choose from. The barrel factor is one of four numbers obtained from a table, which then goes into the material factor.

A similar result is also produced by the variation of the fill factor, which also is one of the factors that combines into the material factor. The factor is again obtained from a table, but does not vary over such a large range as the barrel factor, the range being from 1.0 to 0.5. The explanation of the fill material is not wide and a common problem during a survey is that the bridge fill material is difficult to examine unless cores samples or trial pits are used. Because the depth of fill is generally greater than the depth of the arch barrel the smaller range of fill factor actually produces a 34% reduction in the modified axle load. For this reason the fill factor is a very significant factor. As both the barrel and fill factors are combined using Equation 3.6, a comparison has also been completed with both factors being varied.

**Variation of the width, mortar and depth of joint factors** The joint factor which is applied to the provisional axle load is made up from three other factors, each chosen from tables and so having a set range of values and being open to interpretation. The first factor is the width of joint factor, this has three

values varying from 1.0 to 0.8 in steps of 0.1 mm, depending upon the measured thickness of the mortar joint. The range of values produces a 20% reduction in the modified axle load. The next factor, the mortar factor has an even smaller range of values of either 1.0 or 0.9, and does not seem to be very relevant to the final axle load. This range of results obviously gives a 10% reduction in the modified axle load. The third factor is the depth of joint factor, which is obtained from a table but is the factor most affected by an engineers discretion. The range lies between 1.0 for properly pointed joints to as low as is decided if the joints are insufficiently filled for more than one tenth the thickness of the barrel. A value of 0.6 was chosen here to be small enough. This range of factors produced a reduction in the modified axle load of 40%, again a very significant reduction for such an insignificant parameter, that is easily remedied by re-pointing.

**Variation of the defects and unfavourable defect factors** The quantitative condition factor is produced from the combination of a defects factor, and a factor for unfavourable defects not affecting the stability of the arch barrel. These are both combined giving a condition factor that varies between 1.0 and 0. A low factor for a bridge in poor condition, while 1.0 being used for an arch barrel in good condition with no defects. In the Standards there exists various examples of poor arch barrel conditions and defects that would influence the load capacity of the structure. The relationship between the condition factor and the defect factors therefore produces a linear relationship. When this is done and the defect and unfavourable defect factors combine to greatly reduce the modified axle load. As there is little guide to the values that should be used an over conservative value chosen would have a large affect on the final outcome of an analysis.

#### 3.3.2.2 Variation of bridge dimensions

**Variation in the depth of fill and ring thickness** Firstly the depth of fill has been varied while keeping all the other factors including the ring thickness constant. This has the affect of increasing the combined height $(d+h)$ used in the provisional axle load calculations and also the span/rise factor, the profile factor and the material factor. Reducing the depth of fill by 40% actually reduces the modified axle load by 45%, the reduction again being linear. The ring thickness was also varied, this affects several of the factors. If it is varied alone then a

reduction in the ring thickness only of 50% produces a reduction in modified axle load of 45%. Another combination of the two values is one that leaves the total crown thickness, $(d + h)$ constant, so if the ring thickness is increased by a finite amount then the same amount is reduced from the fill thickness. In this way the provisional axle load is unchanged and only the material factor is affected directly. Again for a reduction in depth of fill of 40% actually produces an increase in modified axle load of almost 17%. While the same reduction in ring thickness of 50% only reduces the axle load by just over 14%. Within the code when the depth of fill at the crown is greater than the thickness of the arch barrel, the results should be confirmed by an alternative and more rigorous assessment method.

**Variation of the rise at 1/4 span** This value affects the profile factor only but is not directly related, see Equation 3.3. For values of $r_q/r_c$ of less than 0.75 the profile factor is 1.0, reducing to 0 when $r_q/r_c$ equals 1.0. By using the equation and plotting rise at 1/4 span against modified axle load the table in the code is produced. Increasing $r_q$, i.e. $r_q/r_c$ increasing towards 1.0, the profile factor quickly reduces, losing half its value when $r_q$ is only 92% the value of $r_c$. As said earlier when $r_q$ is 75% the value of $r_c$ the profile factor has increased to 1.0 and cannot go any higher. In this way the shape of the arch has a very large affect on the modified axle load, and so small errors in the measurement of $r_q$ can have a large influence on the output from an analysis.

**Variation of the span** The bridge span affects the provisional axle load calculation and also the span/rise factor. As the span increases the reduction in modified axle load decreases. For a reduction in span from the starting distance of $10.45m$, of 50% making the span equal to $r_c$, this increases the modified axle load by 133%. If the span is made even shorter then the modified axle load increases by larger and larger amounts. For an increase in span of 29%, making the span just below the upper range of the MEXE method, the decrease in the modified axle load is 28%. The relationship between span and modified axle load for this case is:

$$y = 153x^2 - 43.17x + 354.82 \tag{3.11}$$

Where $y$ = Modified axle load (tonnes), $x$ = Span ($m$). This again shows how dependent on accurate measurement the modified axle load can be, with accurate measurement being important.

**Variation of the rise at the crown** The rise has a very large affect on the modified axle load of the bridge. For a very small difference in value produces a very large difference of the modification factors. The rise at the crown affects the profile factor and also the span/rise factor, but does not have any affect on the provisional axle load. When $r_c$ is less than $r_q$, less than $4.52m$, which is not likely, then the profile factor reduces to zero. When $0.75r_c \leq r_q$ or greater the profile factor take the value of 1.0, for these values $(L/r_c)$ is less than 4 and so the span/rise factor is again equal to 1.0, producing no difference. If $(L/r_c)$ is greater than 4, for values of rise less than $L/4$, the span/rise factor would change, but for these values $r_q/r_c$ is already at 1.0 so setting the profile factor to zero, resulting in a zero modified axle load. When the region that is influenced is investigated more closely then some interesting points are revealed. The main zone of interest for this part of the study is for rises above $r_q$ and below $(r_q/0.75)$. The variation in this part of the graph is very marked the closer that $r_c$ approaches $r_q$.

## 3.3.3 ARCHIE

In this section the variables that affect the outcome of an analysis are identified and investigated. The following dimensions and properties have been investigated and the results from these analysis follow.

### 3.3.3.1 Variation of the position of loading

This was the first parameter that was chosen to be looked at for the chosen bridge. The total span of the bridge was 10.45 $m$, and this entire range was analysed in equal intervals, with points of interest being investigated with more resolution. The maximum failure load being at the springings of the structure, a local maximum load at the centre of the span and the minimum failure load of 44.2 tonnes achieved at a load position of 7100 $mm$. The failure curve was also symmetrical about the centre line of the span. Once this minimum failure load

had been found for this single axle load case, this position of loading was chosen to be kept as the constant load position for all future tests in this parametric study.

#### 3.3.3.2 Variation of the material properties

The range of all the material properties varied in this study are listed in Table 3.4, along with the % change in the failure load produced by a 25% change in the parameter being investigated. This was only performed if the variation of the parameter being investigated produced a linear response in the failure load. If the response in the failure load was non-linear then a more descriptive explanation of the variations is produced. The range of material properties tested with the package is thought to represent the real life variation on input values that would be used.

**Masonry strength** Masonry strength was varied from its original value of 11 $N/mm^2$, and the relationship between this and the failure load was shown to be almost linear, over the entire range. There is a slight decline in the failure load as the masonry strength increases, and for an average increase in masonry strength of 25% the failure load increases by only 5%.

**Masonry density** The change over the entire range of masonry density's tested was linear and for an average increase of 25% in the property produces only a 1.84% increase in the failure load. A direct relationship between the masonry density and the failure load is not produced for this study, but these variations could be due to the analysis method used.

**Fill density** This variation produced a much greater change in the failure load recorded, a 25% increase in the fill density produced a 20.3% linear increase in the failure load. For the problem being investigated the height of fill is quite large, a factor of 2.5 greater than the thickness of the masonry, but the failure load increase is much greater than this factor, showing that the fill density is an important parameter requiring an accurate site investigation.

**Surface density** The surface density range investigated here is similar to that of the fill, but due to the thickness of the surface being only $200mm$, a factor of 8.8 times smaller than the fill depth, it is expected that the affect on the failure load be reduced by a similar amount. From the results the % difference in failure load is much less than this, 20 times smaller than the increase produced by the fill density. The relationship is again linear which enables direct relationship in this manner.

**Angle of internal friction for soil** Again a linear relationship is shown for the variation in the phi value for soil, in this case a 25% increase in the phi value produces a 13.9% decrease in the failure load. This shows that the phi value is an important parameter due to the way in which it is obtained, and the variation that can be found from a particular investigation.

**Factor of passive pressure** This is the soil resistance for the specified problem. The value set acts as a cut-off, so if the value is set too low then the calculated passive pressure may be less than the at-rest value, therefore the package automatically uses a input figure. Using a figure less than this therefore results in no change in the final failure load. At some value of factor of passive pressure, depending upon the other properties there is a marked increase in the failure load up to a maximum value of 69.3 tonnes for a factor of 0.275. In the operational manual for this package it is suggested that a value of greater than 0.3 should not be used. How these values are chosen is not obvious, and when values greater than 0.3 are used the failure load drops again to about the failure load at lower factor values. Full passive pressure is only developed as a results of significant movement, up to 10% of the embedded depth of the arch barrel, although small displacements produce rapid results up to about half passive pressure, a factor of 0.5 here. The significant movement required for higher factors is not really incorporated into this method.

#### 3.3.3.3 Variation of the bridge dimensions

The range of dimensions that can be analysed using this package was investigated and the following properties were investigated. The height and rise of the span,

the depth of overlay, surfacing and mortar loss and the ring thickness and the ring thickness factor are all investigated here.

**Rise** From the original height, the parameter was varied, but could only be reduced in value from original 5220 $mm$, due to the package not allowing anything greater than the original semi-circular shape to be analysed. From this analysis the failure load can be shown to be not directly proportional to variation of rise. The actual relationship can be shown to be close to:

$$F = ar_c^2 + br_c + c \tag{3.12}$$

Where $r_c$ is the rise of the arch barrel at the crown and F is the failure load at the particular value. As the rise decreases the increase in failure load increases by the above relationship.

**Span** When varying the span the position of the load has to be considered carefully. The positioning of the load is done using a distance from the left hand springing towards the right. If this value is kept constant as in all the other parametric tests then a curved line is produced, due to the load getting closer to the crown and so increasing the failure load, as shown, as the load traverses the span. From the original problem the position of the load was calculated as a percentage of the total span, and this percentage value used for each subsequent span to position the load correctly. When this was done a straight line graph was produced, showing for a 25% increase in the span produced a 20.2% increase in the failure load. A significant increase, but due to the ease with which the span is measured this should not be a problem in real life.

**Ring thickness** This part of the analysis required some care at the data input stage, as it was required to keep the fill height constant for the new ring thickness values. This was done by varying the height of the road surface by the same amount by which the ring thickness was changed. If only the input ring thickness was changed this resulted in a curved line with the fill thickness change affecting the results. The graph of ring thickness against failure load is not quite a straight

line graph, and so it is difficult to work out what a 25% increase in the ring thickness would have on the failure load . The curve again seems to be constantly changing and so an equation of best fit can be drawn, the resulting equation is as follows:

$$F = ah^2 + bh + c \tag{3.13}$$

Where $h$ is the average depth of fill including surfacing and $F$ is the failure load. Over the middle range a 25% increase in the ring thickness produces a 36% increase in the failure load. This is true for the tested range. This is again a significant percentage that greatly affects the failure load, and so careful measurement is required.

**Ring thickness factor** The relationship between this parameter and the failure load is again linear, with the 25% increase in the ring thickness factor producing a 19.9% increase in the failure load. The ring thickness factor relates the ring thickness at the crown to the thickness at the abutments.

**Depth of fill** A linear plot is again produced showing the direct relationship between depth of fill and failure load, for a 25% increase in the depth of fill producing a 15.8% increase in the failure load.

**Depth of surfacing** The depth of surfacing has been varied here keeping everything else constant, thus resulting in the total depth of fill increasing over the arch barrel, i.e. the finite factor added to the depth of surfacing has not been taken from the depth of overlay or fill. The relationship to the failure load is again linear, with the 25% increase resulting in a 2% increase in the failure load. This represents a small factor for quite a large increase in the parameter, so accurate measurement of this value relative to others is not as important.

**Depth of overlay** The original arch problem did not contain an overlay value, however a 25% increase in the depth of overlay produces only a 1% increase in

the failure load. No further investigation was considered for the depth of overlay or the depth of surfacing since the % changes are so small.

**Depth of mortar loss** This is a linear relationship again with a 25% increase in the depth of mortar loss producing a 5.7% decrease in the failure load. Relating the change in mortar loss to the original barrel thickness would be more meaningful in this case, with an increase in mortar loss representing 11.4% of the total barrel thickness, producing a decrease of 18.5% of the original failure load. This represents a significant figure, with only a small change in the measured mortar loss resulting in a large difference in the final failure load.

### 3.3.4 CTAP

In this section the dimensional and property parameters that could influence the outcome of an analysis were identified and investigated. The results obtained are summarised in Table 3.5. The programme gave the failure output in $kN/m$ which required converting into tonnes by the use of Equation 3.14

$$W\ (Tonnes) = \frac{CTAP\ output\ \times\ Lane\ width}{9.81\ \times \gamma_{fl}} \tag{3.14}$$

Where $\gamma_{fl} = 3.4$. Since the affect of varying the of lane width is calculated from this equation a linear response is the only possible outcome.

#### 3.3.4.1 Variation of load position

The load position was varied to find the worst position of loading for future tests. This was done manually by changing the load position in the data file and running the analysis. A similar distribution of failure loads is produced as produced by the other packages already discussed. The distribution is symmetrical about the centre of the span but gives a much flatter distribution in this same area, making the lowest failure load not as clear as with other packages.

#### 3.3.4.2 Variation of the bridge dimensions

In varying the span the loading position had to be fixed at effectively the same place representing a percentage of the total span. This position was fixed using results from the previous ARCHIE parametric study. Increasing the span increased the failure loads linearly. Span could not be tested for less than $10.45m$ since the assessment shape had been chosen as circular. The rise at the crown had a large affect on the failure load with flatter arches having increased affect in increasing the failure load.

Varying the fill thickness has only a minor influence, up to a point where the extra dead weight causes excess thinning of the arch ring; producing a large drop in failure loads. This relates back to initial problems encountered with the initial data set-up in Section 3.2.3 to do with arch stability.

The ring thickness both at the crown and the abutment both had a large affect on the failure load, with the latter being the more influential of the two for the range tested. This result has significant implications to bridge surveys, as often with larger spans accurate measurement of the thickness at the crown is sometimes difficult. However as long as accurate measurements are recorded at the abutments the output from the package should be fairly accurate.

#### 3.3.4.3 Variation of material properties

Arch elasticity had a minor linear affect on the failure load although at values less than $7 \times 10^5\ kN/m^2$, failure loads reduced significantly, these are however considered unrealistic values. The monitoring stress used in the analysis has no affect on the failure load for the elastic analysis since a failure mechanism with material crushing is not considered.

Masonry density had very little influence on the failure load, while increasing the fill density resulted in a linear increase. It would be expected that increasing the dead load would increase the amount of thinning occurring in the arch ring, however it is thought that this increase would also increase the uniform compression in the ring giving more stability. The road bulk density and thickness both had very little affect on failure load.

The sub-grade modulus has no affect on failure load up to a critical value of $13000kN/m^3$ at which point the load falls dramatically. The soil pressure coefficients all have a significant influence on the failure loads. $K_p$ has a linear affect on the failure load, while $K_o$ and $K_a$ have a limited affect until raised over 0.15, at which point the failure load falls dramatically. For this reason if a CTAP analysis was to be performed for real structures it is vital to obtain accurate values for the pressure coefficients if the assessment is to give any level of confidence.

### 3.3.5 MAFEA

Although Report 3 within the MAFEA documentation[119] is itself a parametric study, it was still felt important to perform a study to provide a clearer understanding of the package and allow direct comparisons to be made with the other packages. Within the parametric study results are presented in a similar fashion as presented in this thesis. Two sets of results are plotted, one for the stability case and the other for crushing failure. This was done to identify areas where failure loads may coincide or overlap.

#### 3.3.5.1 Variation of load position

The package automatically traverses the arch during an analysis increasing the load at each defined point until failure. This information can be saved to a designated file from which a plot can be obtained. The worst position for the load was at $4.13m$ from the springing, and the capacity was seen to increase again towards the centre of the span.

#### 3.3.5.2 Variation of bridge dimensions

The span has a significant linear affect on the failure load, while the rise has a large influence, which is not linear, and given the large value for crushing strength used for the analysis means that accurate measurement of the rise is important. Variation in fill depth has some affect but a peak is reached where any further increase in the depth does not lead to a further increase in failure load.

The ring thickness at the crown and the abutments was investigated separately and together. Over the range it was found that varying $d_c$ had little affect while varying $d_a$ had a large influence on the failure load. When varying both the parameters at the same time a similar trend was observed as varying $d_a$ alone suggesting that great care be taken in the measurement of this value. Increasing the lane width produced a linear increase in failure loads, this, as explained earlier, is due to the load being distributed over a longer length.

#### 3.3.5.3 Variation of material properties

The elastic modulus of the arch and the fill in particular have very little influence on the failure loads. The arch elastic strength does, for lower values, have an increasing affect and for that reason has to be given some importance. The use of specific values, without actual tests to provide such information, is a possible problem with this type of package. The variation in crushing strength relates to the masonry and not to the individual blocks within the structure. For the crushing failure case there is an obvious cut off where the bridge fails under dead load, up until this point the failure loads change linearly. The collapse modes change particularly in this case from a stability failure to crushing. Masonry density for the range tested is shown to have very little affect on the output. Fill density however does have a much greater linear affect although the response of the package for a shallower arch would be expected to be different.

The variation of the soil parameters is somewhat unnecessary as the assessing engineer can keep $K_p$ low and have a separate friction angle for the soil to ensure conservatism. MAFEA uses $K_p$ to find $K_a$ with $K_o$ calculated from $\phi$. It was found that for larger passive pressure factors failure loads were affected but only for values greater than 1.0. Increasing the friction angle for the soil actually reduced the capacity of the arch for crushing case and had little affect on stability. Since only $K_p$ is shown to have any real affect, great care must be taken in choosing values for this factor.

The number of elements used to model the arch was also varied as it is known that this can greatly affect the output failure load. The optimum number required for an arch analysis is the minimum number that no longer influences the failure load. In this case it can be seen that as the number of elements increases the

load levels off, although the optimum number of elements required has still not been reached for either failure case. In performing this study 35 elements were used, although this would not supply the optimum failure load. The number of elements would however allow relatively quick analysis to be performed and should produce reliable results.

### 3.3.6 Discussion of parametric study

The parametric study completed for this thesis has highlighted some of the differences that exist between the assessment methods. Tables 3.3 to 3.6 show the various failure load ranges for each parameter. The gradients obtained from the plots in Appendix B allow comparisons between packages to be made more easily. Table 3.2 gives a combined comparative view of how a change in each parameter affects the failure load produced. Column *A* indicates the importance with which a change in each parameter has been judged to affect the failure load. Each parameter has been classed in order of importance to that package and also relative to the others. This is achieved by analysing the change in failure load which was affected by a change in the parameter. Care must be taken to ensure that this change in parameter does not miss any induced affects. Hence this method is not solely a numerical classification, but also a subjective judgement made considering the failure load range and the range of the parameter. Column 'B' demonstrates the affect which an increase in the parameter has on the failure load produced, an increase or decrease. The meaning of the numbers and symbols in Table 3.2 are:

- 1 - Accuracy of *primary* importance to package
- 2 - Accuracy of *secondary* importance to package
- 3 - Accuracy of *tertiary* importance to package
- + - Indicates increase in failure load for increase in parameter
- - - Indicates decrease in failure load for increase in parameter
- None - Indicates no affect in failure load for increase in parameter

| Parameter varied | Package | | | | | | | |
|---|---|---|---|---|---|---|---|---|
| | MEXE | | ARCHIE | | CTAP | | MAFEA | |
| | A | B | A | B | A | B | A | B |
| Span | 2/1 | - | 2 | + | 1/2 | + | 1/2 | + |
| Rise at centre | 2 | +/- | 1 | - | 1 | - | 1 | - |
| Ring thickness | 2 | + | 1 | + | 1 | + | 1 | + |
| Ring thickness at crown | *** | *** | *** | *** | 2 | + | 3 | + |
| Ring thickness at abutment | *** | *** | *** | *** | 1 | + | 1 | + |
| Fill thickness | 2 | + | 2 | + | 2 | - | 2 | +/- |
| Ring thickness factor | *** | *** | 2 | + | *** | *** | *** | *** |
| Passive pressure factor | *** | *** | 2/3 | +/- | 1 | + | 2/1 | + |
| At Rest pressure factor | *** | *** | *** | *** | 1 | - | *** | *** |
| Active pressure factor | *** | *** | *** | *** | 1 | + | *** | *** |
| Masonry strength | *** | *** | 2 | + | *** | *** | 1 | + |
| Arch elasticity | *** | *** | *** | *** | 3 | + | 3 | + |
| Fill elasticity | *** | *** | *** | *** | *** | *** | 3 | - |
| Masonry density | *** | *** | 3 | + | 3 | - | 3 | + |
| Fill density | *** | *** | 3 | + | 2 | + | 2 | + |
| Surfacing density | *** | *** | 3 | + | 3 | - | *** | *** |
| Phi for soil | *** | *** | 3 | - | *** | *** | 3 | - |
| Surfacing depth | *** | *** | 3 | + | 3 | None | *** | *** |
| Depth of mortar loss | *** | *** | 2 | + | *** | *** | *** | *** |
| Depth of overlay | *** | *** | 3 | + | *** | *** | *** | *** |

Table 3.2: Summary of combined parametric study

- *** - Indicates where a parameter is not required for each assessment method

An example of this is a discussion of the influence of ring thickness for the different packages. The importance of the ring thickness can be seen in Table 3.2. MEXE when considering $d$ in calculating the $W_p$ only considers the total crown thickness, $(d+h)$ despite the fact that the arch ring is likely to have a greater load capacity than the fill material. The ring thickness is treated separately for $F_m$ but this has a smaller affect. The two packages which allow variation of $d$ between the crown, $d_c$ and the abutment, $d_a$, both consider $d_a$ to be of greater importance. For such an important parameter however it is rare to obtain an accurate measurement of the ring thickness unless a core is taken. Measurements on the extremes of the arch may be inaccurate, as shown in Figure 3.2. In conclusion the affect of the ring thickness is of primary importance to all but the MEXE method.

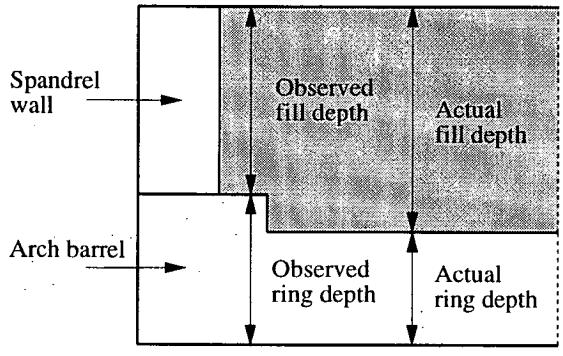


Figure 3.2: Cross section through arch barrel

The rise was also found to be an important dimensional parameter apart for the MEXE method. It affects the way in which the packages analyse and also affects $L/r_c$. In MEXE it also has differing affects due to the nature of the package relating parameters to an optimal value of $L/r_c = 4$. MEXE tends to favour steeper arches, however the other packages increase the capacity for shallower arches.

For both MEXE and ARCHIE an increase in fill thickness raises the capacity of the bridge, while for the other methods a similar increase can have an opposite affect. This is due to some of the methods thinning the arch ring under dead load, while others treat the affect only as a dead load without soil structure interaction.

CTAP and MAFEA produce very similar relationships to dimensional variations, mainly due to similarities in the method of analysis. Both removing areas of tension in the arch ring and assuming similar soil pressure models. CTAP solely has the soil pressure coefficients as of primary importance. This apparent sensitivity makes the accurate assessment of a structure difficult since determining the pressures or $\phi$ from tests is infrequently performed and at best not accurate. For a large number of bridge assessments soil testing is seldom performed and is not considered to be economically viable.

MAFEA is most affected by crushing strength values, the only material property considered to be of *primary* importance. Hence a close approximation of this value is pivotal in attaining accurate results from this package.

MEXE has certain advantages over the other packages in including the condition of the bridge with a factor derived from a site visit. Other packages allow for cracking, material failure and missing mortar but do not allow for other factors which must have an influence on the failure load of the structure, examples are given in the relevant codes.[23] MEXE allows for the inclusion of all these affects with the use of factors which however are still very subjective.

Extending this study to understand how changes in parameters would affect failure loads for shallower arches would be an interesting, but it was felt outside the scope of the present investigation.

| Parameter varied | Range tested | Failure load range | Gradient of curve | | | |
|---|---|---|---|---|---|---|
| | | | Maximum | Range | Minimum | Range |
| $L$ | 10.45–15.45 | 42.6–70.8 | -7.9 | 10.45–11.45 | -4.2 | 13.45–15.45 |
| $r_c$ | 1.75–5.22 | 70.8–91.4 | 22.5 | 1.75–2.5 | -8.3 | 3.00–5.22 |
| $d$ | 0.7–1.4 | 70.8–127.8 | 81.4 | 0.7–1.4 | - | - |
| $d$ ($d+h$ constant) | 0.7–1.4 | 70.8–82.7 | 17.1 | 0.7–1.4 | - | - |
| $h$ | 1.06–1.76 | 38.7–70.8 | 45.9 | 1.06–1.76 | - | - |
| $h$ ($d+h$ constant) | 1.06–1.76 | 70.8–82.7 | -17.1 | 1.06–1.76 | - | - |
| $F_b$ | 0.7–1.5 | 58.8–78.0 | 23.9 | 0.7–1.5 | - | - |
| $F_f$ | 0.5–1.0 | 55.8–88.8 | 60.1 | 0.5–1.0 | - | - |
| $F_w$ | 0.8–1.0 | 62.9–78.6 | 78.7 | 0.8–1.0 | - | - |
| $F_d$ | 0.6–1.0 | 42.5–70.8 | 73.3 | 0.6–1.0 | - | - |
| $F_{mo}$ | 0.9–1.0 | 63.7–70.8 | 70.8 | 0.9–1.0 | - | - |
| $F_c$ | 0.32–0.8 | 35.4–88.5 | 110.6 | 0.32–0.8 | - | - |

Table 3.3: Summary of MEXE parametric study

| Parameter varied | Range tested | Failure load range | Gradient of curve | | | |
|---|---|---|---|---|---|---|
| | | | Maximum | Range | Minimum | Range |
| Load position | 0–10.45 | 26.0–50.5 | *N/A* | *N/A* | *N/A* | *N/A* |
| $L$ | 10.45–14.00 | 26.0–32.6 | 1.9 | 10.45–14.00 | - | - |
| $r_c$ | 1.75–5.22 | 26.0–116.7 | -49.7 | 1.75–2.75 | -7.3 | 5.00–5.22 |
| $d$ | 0.5–0.9 | 15.1–41.9 | 88.0 | 0.85–0.90 | 48 | 0.5–0.55 |
| $h$ | 0.25–4.00 | 16.5–40.7 | 6.5 | 0.25–4.00 | - | - |
| Masonry strength | 1–15 | 2.9–26.9 | 7.6 | 1-3 | 0.2 | 13-15 |
| Masonry density | 19–31 | 25.5–26.2 | 0.06 | 19–31 | - | - |
| $K_p$ | 0–0.45 | 23.6–40.8 | *N/A* | *N/A* | *N/A* | *N/A* |
| Fill density | 16–26 | 20.4–29.6 | 0.9 | 16-26 | - | - |
| Surfacing density | 16–26 | 25.8–26.2 | 0.01 | 16–26 | - | - |
| Surfacing depth | 0.15–0.275 | 25.6–26.6 | 8.0 | 0.15–0.275 | - | - |
| $\phi$ soil | 29–36 | 24.4–27.1 | -0.3 | 29–30 | -0.4 | 34-36 |
| Depth of mortar loss | 0.01–0.08 | 25.4–21.2 | -60.0 | 0.01–0.08 | - | - |
| Depth of overlay | 0.01–0.08 | 26.1–27.1 | 14.3 | 0.01–0.08 | - | - |
| Lane width | 2.50–3.50 | 26.0–36.7 | 10.7 | 2.50–3.50 | - | - |

Table 3.4: Summary of ARCHIE parametric study

| Parameter varied | Range tested | Failure load range | Gradient of curve | | | |
|---|---|---|---|---|---|---|
| | | | Maximum | Range | Minimum | Range |
| Load position | 0–10.45 | 21.8–131.0 | *N/A* | *N/A* | *N/A* | *N/A* |
| $L$ | 10.45–14.00 | 21.8–52.9 | 9.4 | 10.45–12.00 | 7.0 | 13.0–14.0 |
| $r_c$ | 1.75–5.22 | 21.8–468.9 | -589 | 1.75–2.00 | -23.3 | 4.5–5.22 |
| $d$ | 0.3–1.0 | 0.0–64.2 | 220 | 0.7–1.0 | 0 | 0.3–0.6 |
| $d_c$ | 0.3–1.0 | 13.6–28.1 | 20 | 0.3–1.0 | - | - |
| $d_a$ | 0.3–1.0 | 0.0–47.8 | 180 | 0.6–0.7 | 0 | 0.3–0.5 |
| $h$ | 0.25–1.40 | 1.6–23.5 | -3.5 | 0.25–1.40 | - | - |
| Lane width | 2.5–3.5 | 21.8 | 8.7 | 2.5–3.5 | - | - |
| $E_a$ | 500–1500 | 3.1–21.8 | 0.074 | 500–700 | 0.005 | 700–1500 |
| Monitoring stress | 1.0–15.0 | 21.8 | 0 | 1.0–15.0 | - | - |
| $\rho_m$ | 19.0–31.0 | 21.6–22.2 | -0.05 | 19.0–31.0 | - | - |
| Subgrade modulus | 5000—25000 | 1.0–21.8 | 0 | 5000–25000 | - | - |
| $K_p$ | 0.0–0.6 | 9.9–67.3 | 110 | 0.0–0.2 | 85 | 0.4–0.6 |
| $K_a$ | 0.0–0.175 | 0.0–26.8 | 100 | 0.1–0.16 | -20 | 0.0–0.1 |
| $K_o$ | 0.0–0.2 | 0.0–21.8 | -3.5 | 0.0–0.17 | - | - |
| $\rho_f$ | 16.0–26.0 | 16.4–25.2 | 0.88 | 16.0–26.0 | - | - |
| $\rho_s$ | 16.0–26.0 | 21.6–22.0 | -0.03 | 16.0–26.0 | - | - |
| Road thickness | 0.1–0.4 | 21.8 | 0.0 | 0.1–0.4 | - | - |

Table 3.5: Summary of CTAP parametric study

| Parameter varied | Range tested | Failure load range | Gradient of curve | | | | |
|---|---|---|---|---|---|---|---|
| | | | Maximum | Range | Minimum | Range | Collapse mode |
| Load position | 0–10.45 | 50.2–646.5 | $N/A$ | $N/A$ | $N/A$ | $N/A$ | Stability |
| $L$ | 10.45–14.00 | 50.2–79.0 | 10.2 | 10.45–14.00 | - | - | Stability |
| $r_c$ | 1.75–5.22 | 53.8–424.7 | -194.0 | 1.75–3.00 | -36.8 | 4.82–5.10 | Stability |
| $h$ | 0.25–2.00 | 43.2–52.9 | -11.0 | 1.50–2.00 | 7.8 | 0.25–1.50 | Stability |
| $d$ | 0.6–1.0 | 0.0–131.1 | 638.0 | 0.6–0.65 | 277.7 | 0.65–1.00 | Stability |
| $d_c$ | 0.55–0.70 | 49.5–51.7 | -10.0 | 0.55–0.70 | - | - | Stability |
| $d_a$ | 0.7–1.0 | 50.2–125.9 | 252.3 | 0.7–1.0 | - | - | Stability |
| Lane width | 2.5–3.5 | 50.2–70.2 | 20.0 | 2.5–3.5 | - | - | Stability |
| Arch elasticity | 1000–20000 | 17.8–52.1 | 0.006 | 1000–3000 | 0.000 | 10000–20000 | Stability |
| Fill elasticity | 5–50 | 46.6–53.4 | -0.15 | 5–50 | - | - | Stability |
| Crushing strength | 10.0–30.0 | 0.0–50.2 | 62.2 | 12–13 | 0.25 | 15–30 | Crushing |
| $\rho_m$ | 19.0–31.0 | 48.7–51.8 | 0.26 | 19.0–31.0 | - | - | Stability |
| $\rho_f$ | 16.0–26.0 | 33.9–63.0 | 2.9 | 16.0–26.0 | - | - | Stability |
| $K_p$ | 0.0–3.7 | 50.2–139.1 | 32.9 | 1.0–3.7 | 0.0 | 0.0–1.0 | Stability |
| $\phi$ soil | 29–40 | 47.9–50.5 | -0.2 | 29–40 | - | - | Stability |
| Number of elements | 30–70 | 29.3–58.8 | -1.7 | 30-35 | -0.5 | 60–70 | Stability |

Table 3.6: Summary of MAFEA parametric study

## 3.4 Masonry arch assessment

### 3.4.1 Introduction

In this section the ninety-nine bridges that were assessed in East Lothian were processed using the four assessment packages already introduced in Section 3.2. Of the data gathered there were ten multi-span bridges which for the purpose of this study have been treated as individual spans. This has already been shown to be conservative but is necessary for the comparison. Other structures with spans less than $2m$ were also surveyed although an assessment was not required. It is important to understand that the failure loads, $W_m$ in MEXE, are not the actual predicted failure loads for the bridge, but values which allow comparisons between packages. For example there is no provision to vary the lane width within MEXE, although the other packages contained this parameter which had to be kept constant.

The failure load produced for each package was related back to the input parameters by SPSS, a statistical analysis package available for windows. It was an aim of this analysis to obtain a general formulae for each package relating the input dimensional parameters to the predicted failure load.

### 3.4.2 Data collection

Arch dimensions were recorded for the bridges by two final year students, Michael O'Flaherty and Paul Stewart, in the course of studying for their respective honours thesis whilst working for East Lothian Council. Where the lane width falls below $5m$ the crossing of the bridge should be restricted to one vehicle at a time allowing full distribution width to be used as shown in Section 3.2.2.2. Since the data collected was initially only the dimensional information for each bridge other factors used in the packages had to be kept constant and at realistic values to give comparable results. The MEXE assessments performed for East Lothian Council were performed initially with the worst case factors, only structures failing this analysis required a second site visit to find actual modification factors with which to re-analyse the bridges.

The input parameters used in the subsequent analysis for each package are given in Table 3.7. The blanks indicating parameters which are not required for each specific package. The choice of pressure coefficients for the CTAP package was difficult due to the apparent sensitivity of the package to these values. In correspondence with Hughes,[16,24,27] it was suggested to obtain conservative failure loads from the package to use the values given in the Table 3.7. Only failure loads for single axle loading configuration have been investigated here.

| Parameter | Units | Package | | | |
|---|---|---|---|---|---|
| | | ARCHIE | CTAP | MAFEA | MEXE |
| Ring thickness factor | - | 1.0 | - | - | $F_b = 1.0$ |
| $K_p$ | - | 0.1 | 0.6 | 0.1 | $F_f = 0.7$ |
| $K_o$ | - | - | 0.5 | - | $F_w = 0.9$ |
| $K_a$ | - | - | 0.4 | - | $F_m = 0.9$ |
| Masonry strength | $N/mm^2$ | 3.0 | 3.0 | 3.0 | |
| $E$ arch | $N/mm^2$ | - | 1500 | 1500 | $F_d = 0.9$ |
| $E$ fill | $N/mm^2$ | - | - | 30.0 | $F_c = 0.8$ |
| Masonry density,$\rho_m$ | $kN/m^3$ | 20.0 | 20.0 | 20.0 | - |
| Fill density,$\rho_f$ | $kN/m^3$ | 18.0 | 18.0 | 18.0 | - |
| Surface density,$\rho_s$ | $kN/m^3$ | 23.0 | 23.0 | - | - |
| $\phi$ soil | $^o$ | 35.0 | - | 35.0 | - |
| Surfacing depth | m | 0.1 | 0.1 | - | - |
| Distribution angle | $^o$ | 27 | 27 | 27 | - |
| Wheel size | m | - | 0.3 | 0.3 | - |
| Sub-grade modulus | $kN/m^3$ | - | 9000 | - | - |

Table 3.7: Arch bridge assessment input parameters

Since MAFEA considers both stability and crushing cases both were investigated in order to find the lower failure load. MAFEA recommends properties to be used with a provisional assessment and these are the values which have been adopted here. Although some of the values used are obviously conservative these values are recommended if the properties of materials are not known, which is often the case in actual arch bridge assessment problems.

### 3.4.3 Discussion of results

Table 3.9 lists the arch assessment results produced from the analysis of all surveyed dimensional data. The results have provisionally been ordered in ascending failure loads predicted by ARCHIE. From examination of this table it becomes clear just how much variation in results there is. Figure 3.3 has also been constructed to show the failure loads produced by each assessment package relative to ARCHIE. This allows trends to be more clearly identified.

The MEXE analysis tends to produce consistently low results, again related to the PAL load limit and the application of constant modification factors. ARCHIE produces what appears to be the most consistent set of failure loads along with MAFEA whose trend seems to be quite similar. There are several exceptions within the MAFEA assessment (zero failure loads produced) when the arch fails under its own dead load. These initial failures are generally for arches with abnormally high span:ring thickness or span:rise ratios. CTAP produces a good comparison with ARCHIE for lower loads but produces large failure loads for arches with shallow profiles and large fill depths. This is due to the elastic cracking analysis struggling to fail the structures since crushing failure is not considered. If the load/stress plots for each bridge were analysed then a stress cut-off could be used to identify a failure load. This is however somewhat subjective and considered out-with the aims of this assessment. The other packages considered produced failure loads, which in about one quarter of the bridges analysed, whi8ch were lower than that required by the EC vehicle weights for a single axle load.[8]

CTAP seems to have problems predicting failure loads for the stronger bridges towards the end of the table. Many of these arches have large fill depths and are shallow in profile, ($L/r_c$ high), for which the likelihood of crushing failure is increased. CTAP does not have the ability to consider this type of failure as the elastic cracking analysis method used is unable to fail the bridge. It is suggested that to obtain more sensible failure results the load stress plots for each bridge be examined to indicate problem areas. This is still a subjective method and requires a long time to perform and as such is outside the bounds of this thesis which is investigating the packages with specific input conditions. This is felt to be slightly unfair to the method but with the number of bridges being considered it was felt that this was the only practical way to proceed.

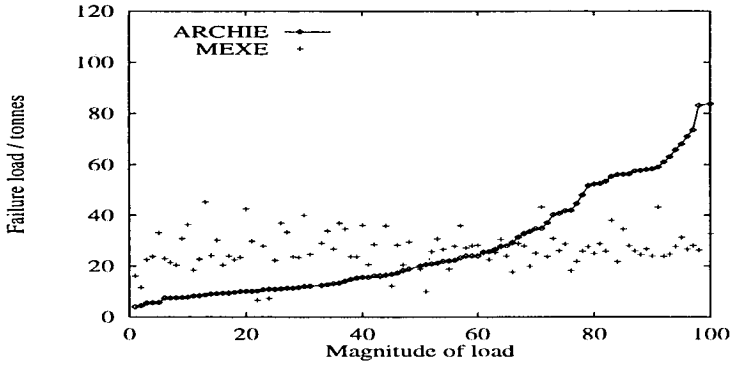


(a) ARCHIE and MEXE analysis

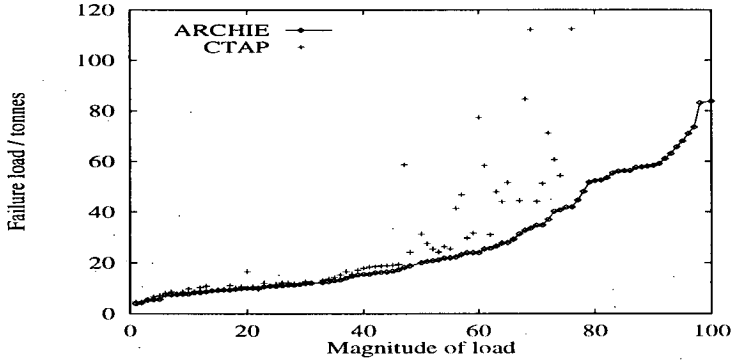


(b) ARCHIE and CTAP analysis

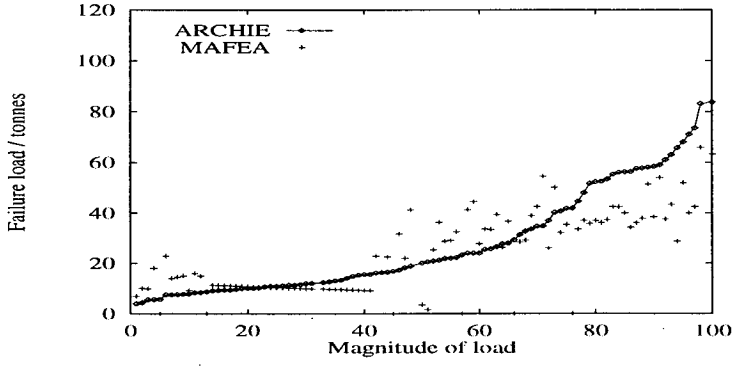


(c) ARCHIE and MAFEA analysis

Figure 3.3: Failure load results from the arch bridge assessment programme

### 3.4.3.1 Statistical analysis

The statistical package, SPSS for windows was used to assess the failure loads using a non-linear regression analysis. Failure loads were related to the four most significant dimensional parameters; span, rise, ring thickness and fill thickness. The form of the relationship produced is shown in Equation 3.15

$$W = k \times L^A \times {r_c}^B \times d^C \times h^D \tag{3.15}$$

where the constants $A$-$D$ and $k$ being solved for by using SPSS to find the relationship produced. Table 3.8 presents the results from this analysis. In order to determine the degree of fit between the dimension based equation and the predicted results graphs were plotted for each of the assessment methods, as shown in Figure 3.4. A line was also drawn to indicate the position of an ideal correlation. The correlation coefficients, $r^2$, obtained are also shown in Table 3.8 to give a numerical value for the accuracy of the correlation. The closer the degree of correlation the closer $r^2$ is to unity.

| Variable | Package | | | | |
|---|---|---|---|---|---|
| | ARCHIE | MEXE | MEXE($W_p \leq$70) | CTAP | MAFEA |
| a | -1.406 | -0.127 | -1.057 | -0.292 | -1.035 |
| b | -0.410 | 0.083 | 0.222 | -0.878 | -0.324 |
| c | 2.423 | 0.280 | 1.037 | 1.735 | 1.633 |
| d | 0.262 | 0.156 | 0.744 | 0.364 | 0.619 |
| k | 1722.92 | 43.83 | 760.72 | 328.71 | 631.55 |
| $r^2$ | 0.755 | 0.286 | 0.828 | 0.544 | 0.580 |

Table 3.8: Results of the SPSS analysis

The MEXE analysis is limited by the code to 70 tonnes, although the provisional axle load is found primarily from the bridge dimensions the correlation of results is quite poor. Another analysis was however performed considering only the bridges for which $W_p$ was below this initial upper limit. This new set of results showed a much greater correlation to the failure loads.

ARCHIE shows a high correlation to the predicted failure loads. This was helped by the consistency of results achieved by this package. CTAP however only

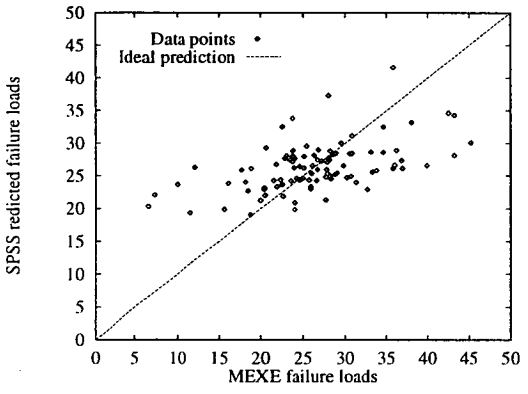


(a) MEXE correlation

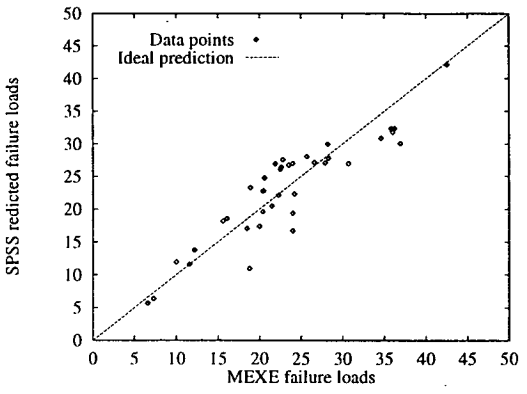


(b) MEXE correlation ($W_p \leq 70$ tonnes)

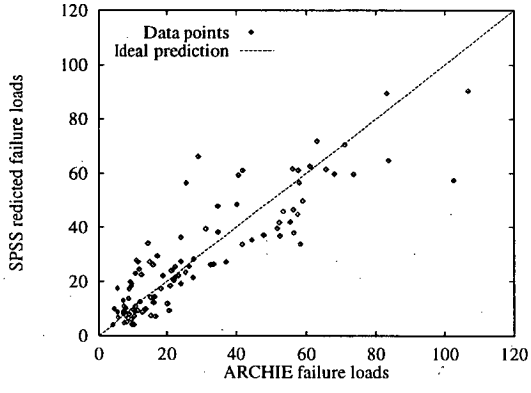


(c) ARCHIE correlation

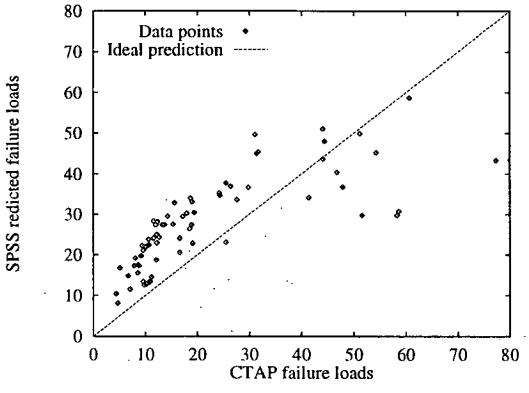


(d) CTAP correlation

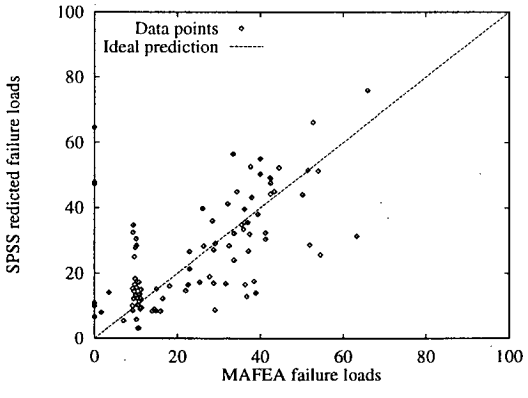


(e) MAFEA correlation

Figure 3.4: Correlation of each package to the SPSS predicted failure loads

produced meaningful results for the first seventy bridges as previously explained, the falsely high values were ignored for this analysis. Relatively good correlation occur for the lowest predicted failure loads but the results are inconsistent at the higher failure loads.

MAFEA produced the largest variation between the dimensionally predicted failure load and that of the package. A group of points seem to occur for a predicted failure range of between 9 and 11 tonnes, the reason for this being that the predicted results are taking into account factors that cannot be included into such a general relationship as Equation 3.15. The fact that some packages do not fit this dimensional relationship actually infers that these packages are taking into account potentially beneficial effects that are not included by this simple relationship.

In order to demonstrate the effect of each parameter graphs have been constructed for each package. Figures 3.5($a$)-($d$) show the sensitivity of each package to each parameter with some interesting results. The relative sensitivity for each package has been found for the range of parameters from the survey, and is simply the dimension to the corresponding power. The MEXE sensitivity is based on the factor produced for the restricted range again. It is clear from the results that the ring depth is the most sensitive parameter for the assessment methods analysed since the change of dimension produces the largest range of results. This again points to the ring thickness being a key parameter in any bridge survey.

Graph 3.5(b) shows clearly how MEXE has a significant inverse sensitivity to the other packages for a variation in the rise, with MAFEA being the least sensitive to a variation in this value. CTAP shows a similar variation of sensitivity to change in span to the other package but still is significantly different. All package treat ring thickness to be an important parameter, ARCHIE the most and MEXE the least as already shown by the parametric study. The fill thickness all have similar sensitivity ranges as the ring thickness but the order is reversed.

The MEXE regression analysis for the restricted range ($W_p < 70$), produces Equation 3.16 which upon closer inspection is very similar to Equation 3.1, seen earlier in this section for calculating $W_p$ for the MEXE method.

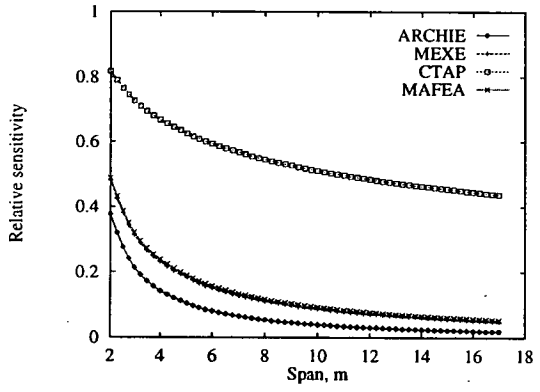


(a) SPSS sensitivity to span

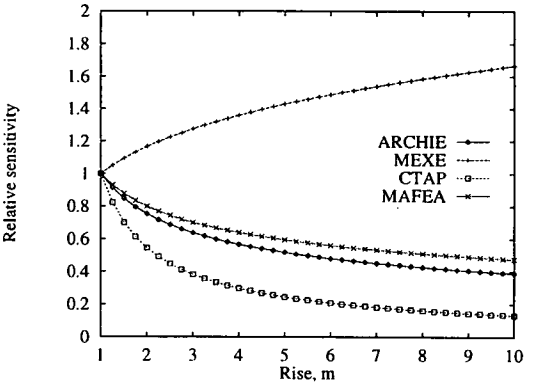


(b) SPSS sensitivity to rise

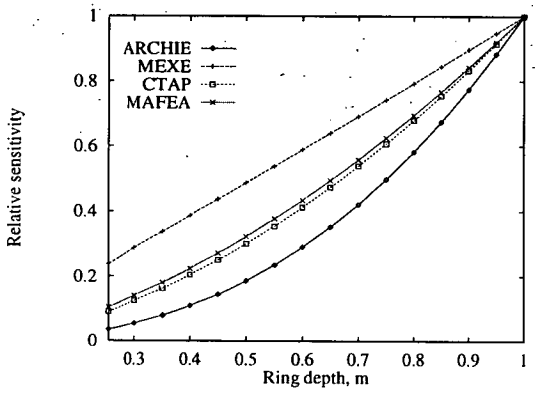


(c) SPSS sensitivity to ring thickness

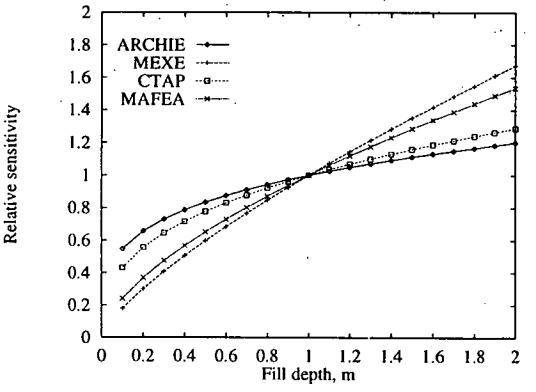


(d) SPSS sensitivity to fill depth

Figure 3.5: Effect of change of parameter on sensitivity of package

$$W = 760.7 \times \left( \frac{r_c^{0.22} \times d^{1.037} \times h^{0.744}}{L^{1.057}} \right) \tag{3.16}$$

The development of such equations for each assessment method could provide the assessing engineer with an extra tool to assist with their work. Such a simple relationship could easily be completed in the field and could help to highlight bridges which are likely to require careful surveying of key parameters, the parameters varying upon the assessment method being utilised. This would save both time and resources if the need to revisit a structure in order to duplicate an initial assessment could be stopped.

## 3.5 Conclusions

Despite the importance of masonry arch assessment in maintaining a safe transport network throughout the UK there still exist uncertainties in many of the assessment methods used today. These uncertainties undoubtedly have many effects on the assessment of and subsequent remedial work and reconstruction of these bridges. Strengthening work whether being unnecessary or necessary will inevitably be very expensive in both the long and short term and has the effect of making such structures unpopular in modern design procedure. The fact that new assessment methods have been introduced indicates that previous methods of assessment are not perfect, and the fact that the previous methods are still used in a primary assessment must present a dichotomy of the assessment methods.

Further work must be performed to try to improve correlation between the existing techniques of assessment and at present it is equally important that more than one method is utilised whenever an assessment programme is undertaken. This would eliminate the risks of overestimating or underestimating the strength of arch bridges but in itself raises important questions to do with consistency and safety of present assessment methods. From the results it is clear that the more each method of assessment utilises the significant parameters effecting the failure load the more accurate the method becomes. Including such important arch parameters into an assessment is vital for a accurate assessment. Some of the main points raised by this research are:

- MEXE is sensitive to fill depth and relatively insensitive to ring thickness when compared to the other three packages.
- MEXE considers flatter arches to be relatively weaker in comparison to the other packages which consider this shape important for increased strength.
- CTAP does not give conservative results for flat or very strong arches.
- Where masonry strength is used it is a sensitive parameter especially for MAFEA when large structures are assessed.
- ARCHIE gives the most consistent set of results for the range of bridges investigated in the arch assessment programme.
- There is a large variation in some of the failure loads produced by what should be consistent assessment packages.
- There is scope for the improvement of modern assessment methods, particularly in an interactive role.
- For borderline cases, alternative methods are advocated in preference to the present modified MEXE method.

Table 3.9: East Lothian arch failure load predictions

| Bridge Name | Span (m) | Rise (m) | Ring (m) | Fill (m) | ARCHIE tonnes | MEXE tonnes | CTAP tonnes | MAFEA tonnes |
|---|---|---|---|---|---|---|---|---|
| GIFFORD VILLAGE | 7.67 | 3.02 | 0.36 | 0.367 | 4.00 | 16.10 | 4.70 | 7.00 |
| BLANCE BURN | 3.40 | 1.40 | 0.335 | 0.085 | 4.40 | 11.60 | 4.40 | 10.10 |
| JANEFIELD | 2.40 | 1.05 | 0.30 | 0.20 | 5.50 | 22.60 | 5.10 | 9.90 |
| SMEATON | 4.46 | 2.02 | 0.30 | 1.13 | 5.60 | 23.80 | 6.70 | 18.10 |
| KEITH | 7.30 | 3.69 | 0.41 | 0.82 | 5.70 | 33.10 | 7.10 | 0.00 |
| PENCAITLAND (1) | 3.60 | 1.60 | 0.30 | 1.10 | 7.50 | 23.00 | 8.10 | 22.90 |
| FASENY | 7.34 | 2.14 | 0.45 | 0.319 | 7.50 | 21.50 | 8.60 | 14.00 |
| TYNINGHAM DAM | 6.10 | 1.55 | 0.40 | 0.30 | 7.60 | 20.40 | 7.90 | 14.50 |
| QUARRYFORD | 6.00 | 2.52 | 0.42 | 0.78 | 7.70 | 30.80 | 8.60 | 15.00 |
| LINTON LINN (1) | 12.45 | 4.18 | 0.49 | 0.91 | 7.80 | 36.20 | 9.80 | 9.20 |
| GARVALD | 6.13 | 1.63 | 0.44 | 0.216 | 8.30 | 18.50 | 8.80 | 16.00 |
| OLDHAMSTOCKS | 10.10 | 4.26 | 0.56 | 0.45 | 8.40 | 22.80 | 10.30 | 14.90 |
| LINTON LINN (2) | 12.50 | 4.26 | 0.49 | 1.17 | 8.70 | 45.20 | 10.90 | 0.00 |
| HADDINGTON RAILWAY | 8.60 | 1.57 | 0.40 | 0.58 | 9.10 | 24.20 | 9.20 | 11.30 |
| SALTOUN (1) | 4.32 | 1.27 | 0.36 | 0.46 | 9.20 | 30.20 | 9.40 | 11.215 |
| BOLTON | 4.04 | 1.325 | 0.42 | 0.20 | 9.40 | 20.40 | 9.60 | 11.131 |
| SALTOUN (2) | 10.53 | 3.99 | 0.59 | 0.44 | 9.40 | 24.00 | 11.20 | 11.046 |
| TYNE WATER (3) | 3.91 | 1.43 | 0.44 | 0.21 | 9.70 | 22.50 | 10.10 | 10.962 |
| ROCKVILLE | 4.47 | 1.548 | 0.46 | 0.241 | 10.00 | 23.50 | 10.70 | 10.877 |
| DUNGLASS NEW | 26.33 | 6.91 | 0.86 | 1.48 | 10.10 | 42.50 | 16.60 | 10.792 |
| MORHAM | 4.70 | 1.83 | 0.47 | 0.40 | 10.10 | 29.80 | 10.60 | 10.708 |
| WEST SALTOUN | 15.63 | 2.24 | 0.60 | 0.11 | 10.20 | 6.60 | 9.60 | 10.623 |
| WHITTINGHAME (1) | 9.75 | 2.911 | 0.57 | 0.456 | 10.70 | 27.90 | 12.10 | 10.538 |
| SAMUELSTON | 21.40 | 3.38 | 0.75 | 0.13 | 10.90 | 7.30 | 10.90 | 10.454 |
| UGSTON | 8.60 | 1.28 | 0.40 | 0.61 | 10.90 | 22.30 | 11.60 | 10.369 |
| SMEATON RAILWAY (1) | 7.90 | 1.68 | 0.43 | 0.68 | 11.10 | 36.90 | 12.20 | 10.285 |
| PENCAITLAND (2) | 5.40 | 1.20 | 0.35 | 0.75 | 11.30 | 33.30 | 12.20 | 10.20 |
| "STATION ROAD " | 3.365 | 1.502 | 0.37 | 0.871 | 11.30 | 23.70 | 12.00 | 10.115 |
| ALDERSTON HOUSE (1) | 2.50 | 1.16 | 0.33 | 0.70 | 11.60 | 23.40 | 11.60 | 10.031 |
| SMEATON RAILWAY (2) | 7.85 | 1.65 | 0.43 | 0.76 | 12.00 | 39.90 | 12.70 | 9.946 |
| ALDERSTON HOUSE 2 | 2.50 | 1.08 | 0.33 | 0.58 | 12.10 | 24.60 | 12.30 | 9.862 |

*continued on next page*

| Bridge Name | Span (m) | Rise (m) | Ring (m) | Fill (m) | ARCHIE tonnes | MEXE tonnes | CTAP tonnes | MAFEA tonnes |
|---|---|---|---|---|---|---|---|---|
| TYNE WATER (2) | 4.01 | 1.46 | 0.47 | 0.30 | 12.40 | 29.00 | 13.30 | 9.777 |
| GILCHRISTON | 5.50 | 1.22 | 0.38 | 0.69 | 12.70 | 33.80 | 13.70 | 9.692 |
| GLENKINCHIE | 3.69 | 1.331 | 0.39 | 0.673 | 13.10 | 26.70 | 14.30 | 9.608 |
| MERRYHATTON | 9.10 | 1.60 | 0.44 | 1.00 | 13.30 | 36.80 | 15.30 | 9.523 |
| GIFFORD | 12.07 | 2.87 | 0.63 | 0.644 | 14.10 | 34.60 | 16.60 | 9.438 |
| ALDERSTON HOUSE 3 | 2.50 | 1.15 | 0.36 | 0.68 | 14.80 | 23.70 | 15.60 | 9.354 |
| TENTH GREEN | 2.30 | 1.00 | 0.30 | 0.80 | 15.30 | 23.70 | 17.20 | 9.269 |
| BROXBURN A1087 | 7.64 | 1.64 | 0.52 | 0.54 | 15.60 | 36.00 | 18.00 | 9.185 |
| SPILMERSFORD | 20.45 | 3.42 | 0.775 | 0.72 | 15.60 | 20.60 | 18.50 | 9.10 |
| ORMISTON STATION | 4.24 | 1.47 | 0.46 | 0.64 | 16.20 | 28.50 | 18.70 | 22.90 |
| BLACKHALL | 3.11 | 0.45 | 0.25 | 0.29 | 16.30 | 15.60 | 18.90 | 16.50 |
| HOPES HOUSE | 6.90 | 1.30 | 0.47 | 0.59 | 16.50 | 35.80 | 19.00 | 22.60 |
| WATERLOO | 21.95 | 3.52 | 0.88 | 0.30 | 16.80 | 12.20 | 19.10 | 0.00 |
| STENTON | 4.27 | 1.43 | 0.55 | 0.19 | 17.30 | 28.30 | 19.40 | 31.70 |
| LITTLE KNOWES (SOUTH) | 3.75 | 0.71 | 0.35 | 0.28 | 18.30 | 20.50 | 58.60 | 22.00 |
| WHITTINGHAME (2) | 4.70 | 1.52 | 0.43 | 1.15 | 18.90 | 29.50 | 24.20 | 41.30 |
| COLSTON WATER | 12.30 | 1.25 | 0.60 | 0.62 | 20.10 | 18.90 | 31.40 | 3.50 |
| GRANTS BRAES | 15.50 | 1.57 | 0.71 | 0.26 | 20.60 | 10.00 | 27.60 | 1.60 |
| FILTER STATION | 5.33 | 0.92 | 0.44 | 0.41 | 20.90 | 25.70 | 25.50 | 25.40 |
| THORNTON BURN | 5.50 | 1.34 | 0.56 | 0.26 | 21.20 | 30.70 | 24.30 | 36.30 |
| INCH | 5.16 | 0.985 | 0.465 | 0.34 | 21.90 | 26.60 | 26.40 | 28.80 |
| SETON FARM | 3.40 | 0.833 | 0.43 | 0.065 | 22.00 | 18.80 | 25.50 | 29.10 |
| ALDERSTON HOUSE 4 | 2.75 | 0.84 | 0.32 | 0.67 | 22.30 | 27.80 | 41.40 | 32.50 |
| DUNGLASS OLD | 10.00 | 4.45 | 0.70 | 4.00 | 23.30 | 35.80 | 46.80 | 0.00 |
| HUMBIE DEAN (1) | 2.92 | 0.93 | 0.34 | 0.82 | 24.00 | 27.20 | 29.80 | 41.30 |
| THORNTON | 5.80 | 2.78 | 0.62 | 2.04 | 24.00 | 28.00 | 31.70 | 44.50 |
| CROOK ROAD | 5.80 | 0.89 | 0.46 | 0.48 | 24.00 | 28.20 | 77.30 | 27.80 |
| LOCH | 2.09 | 0.76 | 0.25 | 0.94 | 25.50 | 25.10 | 58.30 | 33.60 |
| CUDGEL HOUSE | 3.06 | 1.52 | 0.50 | 1.02 | 25.70 | 22.50 | 31.10 | 33.40 |
| GAMUELSTONE | 3.20 | 1.11 | 0.34 | 1.36 | 26.60 | 25.40 | 47.90 | 39.40 |
| SPILMERSFORD APPR'CH | 6.12 | 1.04 | 0.47 | 1.03 | 27.80 | 30.50 | 44.10 | 26.40 |

*continued on next page*

| Bridge Name | Span (m) | Rise (m) | Ring (m) | Fill (m) | ARCHIE tonnes | MEXE tonnes | CTAP tonnes | MAFEA tonnes |
|---|---|---|---|---|---|---|---|---|
| LUGGATE BURN | 3.32 | 0.86 | 0.46 | 0.10 | 28.00 | 24.00 | 51.60 | 36.70 |
| GOSFORD SANDS | 3.35 | 0.25 | 0.42 | 0.907 | 29.30 | 17.70 | 119.90 | 0.00 |
| NEWLANDS | 3.68 | 1.13 | 0.48 | 0.64 | 31.40 | 28.90 | 44.40 | 28.50 |
| SMEATON TROWS | 3.03 | 0.67 | 0.33 | 0.67 | 32.80 | 27.90 | 84.60 | 29.20 |
| LYARS | 3.84 | 0.75 | 0.46 | 0.135 | 33.60 | 20.00 | 112.20 | 38.90 |
| WEST LATCH | 2.20 | 0.91 | 0.37 | 0.67 | 34.70 | 25.10 | 44.10 | 42.50 |
| EAST BEARFORD | 6.15 | 1.60 | 0.72 | 0.36 | 34.80 | 43.20 | 51.20 | 54.50 |
| SPOTT 1 | 5.00 | 0.74 | 0.42 | 1.43 | 37.00 | 23.80 | 173.70 | 26.10 |
| ST. LAWRENCE HOUSE | 4.59 | 1.44 | 0.605 | 0.79 | 40.20 | 30.80 | 60.70 | 50.10 |
| GOLF | 2.00 | 0.85 | 0.40 | 0.40 | 40.70 | 26.10 | 54.30 | 32.20 |
| SPOTT 2 | 5.60 | 0.91 | 0.54 | 0.80 | 41.80 | 28.70 | 150.90 | 35.40 |
| LITTLE KNOWES (NORTH) | 2.56 | 0.29 | 0.38 | 0.50 | 41.90 | 18.20 | 112.40 | 0.00 |
| PARK HILLS | 4.24 | 0.55 | 0.48 | 0.29 | 44.60 | 21.90 | 149.90 | 33.60 |
| BROOMRIGG | 3.08 | 0.53 | 0.40 | 0.32 | 48.00 | 25.90 | 149.90 | 37.10 |
| MORHAM BANK | 2.70 | 0.57 | 0.37 | 0.47 | 51.70 | 27.70 | 149.90 | 35.90 |
| LEASTON | 2.74 | 0.49 | 0.37 | 0.49 | 52.30 | 25.00 | 149.90 | 37.00 |
| PILMUIR | 2.15 | 0.60 | 0.31 | 0.58 | 52.50 | 28.80 | 149.90 | 36.20 |
| MAINSHILL | 2.36 | 0.42 | 0.36 | 0.32 | 53.40 | 25.90 | 149.90 | 37.40 |
| BILSDEAN (1) | 6.10 | 1.58 | 0.65 | 1.25 | 55.30 | 38.00 | 149.90 | 42.50 |
| PEFFER BURN | 3.60 | 0.50 | 0.50 | 0.60 | 56.00 | 21.80 | 149.90 | 42.40 |
| BILSDEAN (2) | 6.13 | 1.28 | 0.66 | 1.19 | 56.20 | 34.60 | 149.90 | 40.00 |
| SANDYFORD B6369 | 2.79 | 0.66 | 0.35 | 1.00 | 56.30 | 28.00 | 149.90 | 34.30 |
| HARELAW | 2.64 | 0.51 | 0.37 | 0.56 | 57.50 | 26.00 | 149.90 | 36.10 |
| MILL LADE (2) | 2.45 | 0.40 | 0.40 | 0.408 | 57.70 | 24.50 | 149.90 | 37.90 |
| ALDERSTON HOUSE 5 | 2.50 | 0.89 | 0.42 | 0.75 | 58.00 | 26.80 | 149.90 | 51.40 |
| BRANXTON | 2.23 | 0.43 | 0.34 | 0.13 | 58.30 | 24.00 | 149.90 | 38.50 |
| TRANENT RAILWAY | 7.50 | 1.70 | 0.80 | 1.20 | 59.00 | 43.20 | 149.90 | 54.00 |
| NORTH MARVINGSTON | 2.65 | 0.44 | 0.41 | 0.63 | 61.00 | 23.90 | 149.90 | 37.60 |
| MILL LADE (1) | 2.50 | 0.40 | 0.44 | 0.35 | 63.00 | 24.70 | 149.90 | 43.40 |
| BLACKFORD | 2.31 | 0.40 | 0.435 | 0.14 | 65.70 | 27.70 | 149.90 | 28.80 |
| TYNEHOLM HOUSE | 2.40 | 0.79 | 0.48 | 0.18 | 68.00 | 31.30 | 149.90 | 51.90 |

*continued on next page*

| Bridge Name | Span (m) | Rise (m) | Ring (m) | Fill (m) | ARCHIE tonnes | MEXE tonnes | CTAP tonnes | MAFEA tonnes |
|---|---|---|---|---|---|---|---|---|
| MORHAM MAINS | 2.20 | 0.43 | 0.39 | 0.56 | 71.00 | 26.70 | 149.90 | 40.00 |
| PENSHIEL | 2.24 | 0.73 | 0.40 | 0.59 | 73.50 | 28.10 | 149.90 | 42.50 |
| MORHAM MAINS | 2.23 | 0.45 | 0.42 | 0.81 | 83.10 | 26.30 | 149.90 | 65.90 |
| LUFFNESS CULVERT | 2.00 | 0.55 | 0.42 | 0.18 | 83.70 | 32.70 | 149.90 | 63.30 |
| TRANENT ACCESS | 2.43 | 0.94 | 0.37 | 2.42 | 102.50 | 23.70 | 149.90 | 155.20 |
| SPITTALRIGG | 2.15 | 0.71 | 0.46 | 0.61 | 106.70 | 28.20 | 149.90 | 52.70 |

# Chapter 4

# Double span brick arch tests

## 4.1 Introduction

Continuing on from work previously presented by Fairfield[19] and Prentice,[20] further tests have been performed on the double span brick arch described previously. The dimensions, constituent materials, instrumentation and load positions are as previously described by Prentice. Instrumentation was installed on the extrados and intrados of both arches and within the sand fill to monitor the values of normal and shear stresses, displacements and total pressure respectively. Different load levels, fill heights and load types were investigated during a series of tests undertaken over a period of two years. Consistency between these and previous tests would allow direct comparisons of the results obtained. The results from these tests represent a significant set of data with which to compare to future assessment and analysis packages, to aid in their development.

These new tests required the design and construction of a new load type, and the change in fill height by 100%, requiring extra shuttering to the side of the bridge. In all cases the load was applied to the top surface of the fill and the instruments were monitored to allow the stresses and displacements throughout the structure to be quantified. An indication of the load dispersal was found from measurements and the extent of the soil structure interaction could be established. The use of the patch load allowed 3-D affects of loading to be investigated providing a large quantity of potentially useful information.

## 4.2 Experimental set-up

The bridge dimensions and instrumentation have remained mostly unchanged since the work performed by Prentice.[20] Only significant differences between the experimental methods are outlined in this section.

### 4.2.1 Bridge construction

The bridge has been constructed with the same salient dimensions as the structure shown in Figure 4.1. The arch barrels are each formed of a single ring of 41 class B engineering bricks set on their sides to a total thickness of $102.5mm$, with a

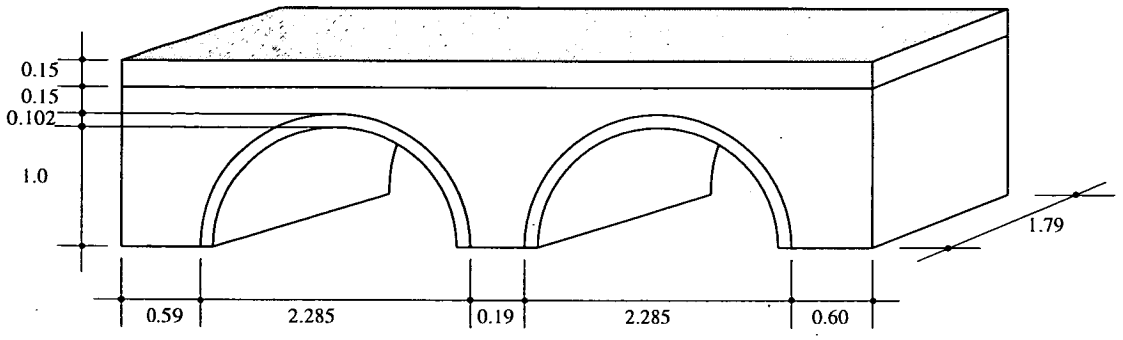


Figure 4.1: Schematic diagram of salient dimensions

nominal $10mm$ mortar bond. The barrel was laid in English bond with half brick cut every second course for the facing of the arch ring.

The intermediate support is designed as an infinitely stocky pier to allow no lateral displacements during any of the tests. The bridge as closely as possible represents a 2-D slice through an arch barrel, to best aid with comparisons to previous tests and computer analysis work. For this reason spandrel walls have been neglected since this would have a large 3-D affect on the structure. $18mm$ thick timber sheets are used to retain the fill. These timber sheets are suitably separated from the arch barrels to ensure minimal affect on the strength and response of the structure. End retaining walls are also utilised to contain the fill material and are positioned at a sufficient distance to ensure they have no influence on the load dispersal of the structure. Polythene strips were attached to the structure and the retaining walls to minimise friction between the walls and the fill and to contain the fill material.

For the placement of the shear and normal cells in the arch extrados pockets were precut to ensure a flush fit. Cables were passed through the bricks and connected to a data-logger placed close to the bridge structure. The fill pressure cells were placed in predefined position during the placement of the fill at the required depths. A more detailed description and further discussion of the instrumentation and data logging equipment is presented in section 4.2.3.

| Parameter | Symbol | Fairfield | Prentice | Units |
|---|---|---|---|---|
| Density | $\sigma$ | 1515 | 1517 | $kg/m^3$ |
| Shear resistance angle | $\phi$ | 40 | 34 | $^o$ |

Table 4.1: Fill material properties

### 4.2.2 Material properties

#### 4.2.2.1 Fill material

The fill material used in this series of tests is similar to that used by Fairfield and identical to that used by Prentice. The fill in both cases is very similar and test have been performed previously to determine their properties, required for later analysis of results. In situ density and angle of shearing resistance have been found previously and are presented in Table 4.1, the difference between the shear resistance angle seems large but has been explained.

#### 4.2.2.2 Arch barrel and mortar

The characteristic strength of the bricks used in the bridge was kept constant throughout, and from test was found to have a strength of $42.2N/mm^2$. Since most tests on the bridge are within the elastic limit of the structure then the significance of this value is seen to be minor. A standard mortar mix of 1:1:6, cement:lime:sand was used with Ferocrete quick drying cement to reduce the time of construction.

### 4.2.3 Instrumentation

In order to monitor the bridge during loading a combination of instrumentation was used. Although the equipment installed in the bridge has already been documented in previous work[19,20] it was felt important to introduce the different types of instrumentation used in order to make the explanation of results and comparisons easier. Figure 4.2 shows the placement of the instrumentation inside the bridge prior to the tests performed.

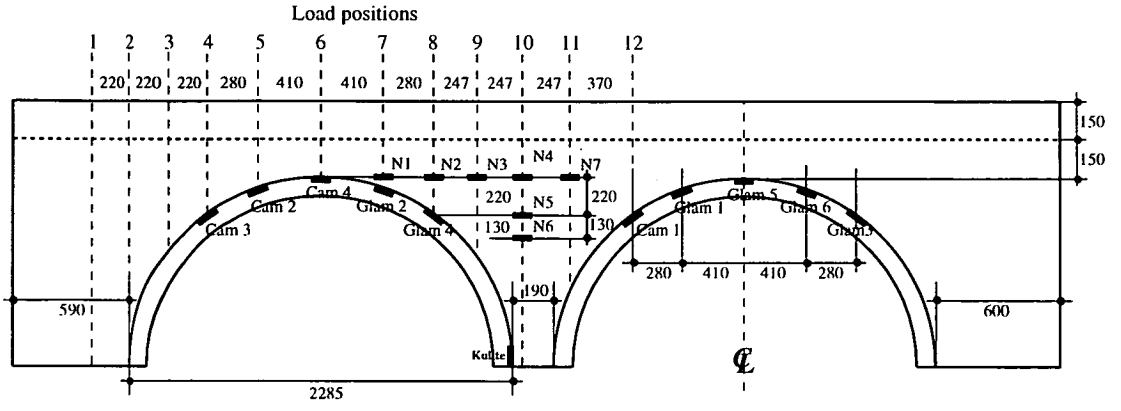


**Cam 3** Cambridge cell No. 3

**Glam 3** Glamorgan cell No. 3

Note: All dimensions are in mm

Figure 4.2: Position of all instrumentation

**Loading cells**: The role of these cells is to monitor the amount of load applied through the loading arms, and therefore the pressure applied to the top of the bridge. The cells used have been calibrated several times during the testing period and have been shown to be reliable and accurate. The placement of load cells is detailed in Figure 4.4.

**Stress cells**: Two types of cells were used in the arch bridge, a Cambridge (Cam) earth pressure cell and a very similar Glamorgan (Glam) cell. These cells are used to measure normal and shear stresses applied to the arch extrados resulting from the applied load. Four Cambridge and Six Glamorgan cells were placed in the arch barrel as shown in Figure 4.2. Two of the cells, Cam1 and Glam1 occasionally gave erroneous readings so results from these cells have to be used with caution.

**Fill pressure cells**: Pressure changes created in the sand fill were measured using soil pressure cells measuring normal pressure only. A total of seven gauges were used in the fill, five placed at the same height to measure the lateral pressure distribution within the soil. The remaining gauges were placed at varying depths along the bridge centre line.

In addition, a Kulite cell was positioned at the base adjacent to arch 1. The Kulite cell is aligned vertically to measure lateral pressure in the soil. The object of the Kulite cell was to test that the central pier did not move, important since very small displacements can result in large changes in arch behaviour.

**Deflection gauges**: These are placed under the bridge touching the arch intrados to coincide with the stress cells shown in Figure 4.2. The gauges are orientated to measure deflection perpendicular to the intrados allowing deflections to be associated with the measured stresses. Twelve gauges were used, one under each of the stress cells and an additional two aligned equidistant along the transverse line under gauge Cam2. These were placed to measure any eccentricity in deflection of the bridge due to applied loads.

### 4.2.4 Method of loading

The object of loading the bridge is to model a vehicle axle or wheel by applying a distributed load over a designated area. This loading method is similar to applying a knife-edge load (KEL) or wheel load, which are precluded for practical reasons. During the series of tests performed on the bridge two different types of load were used. Firstly the previous line load tests were repeated using a similar loading beam set-up, shown in Figure 4.3, but with an increased load level. Secondly, a new test was designed and performed to test the reactions of the bridge to a patch load. The size of the patch was the first variable, the choice of which being affected by several criteria:

- Size of the bridge structure
- Load level to be achieved
- Shear failure of the soil fill
- Corresponding codes for patch loads

Calculations and codes of practice[121] were consulted resulting in a square contact area of $300mm$ sides being chosen with the same applied pressure. The patch is being used to represent a single nominal wheel alternative to UDL and KEL. A new load level was to be tested using a maximum applied pressure of 82 kPa, compared to the 41 kPa previously. It was decided to do this to test the structure further into its elastic range and possibly into the plastic range.

The second patch load type selected was to further test the response of the bridge to the application of a 3-D load type. This is to say that the distance the load

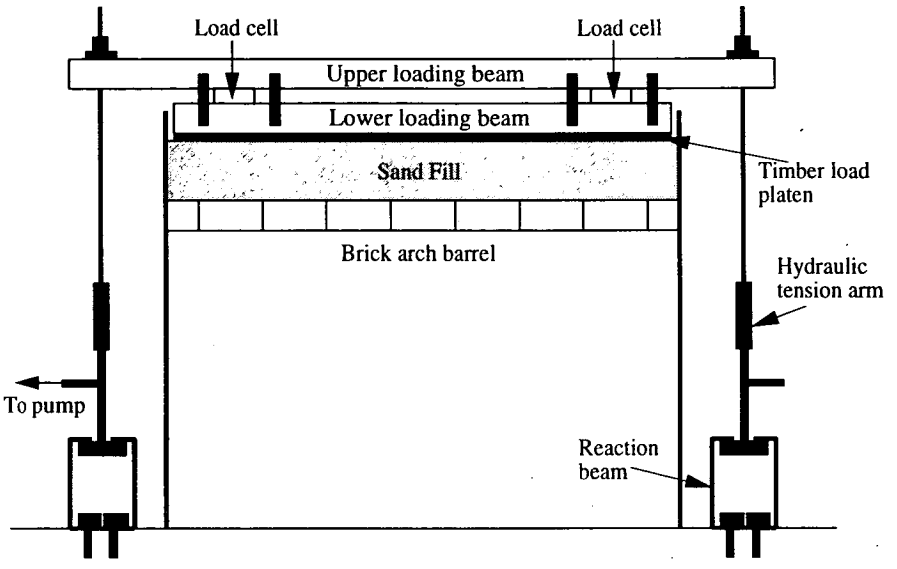


Figure 4.3: Section showing line loading apparatus

was applied away from the line of the cells could be varied in order to get a representative 3-D response of the bridge. For this type of test the loading system had to be changed as shown in Figure 4.4($b$). For the patch load tests a single pump was attached to both hydraulic tension arms in order that the load could be better controlled. The ball bearing is there to ensure that the load is vertical and that no uneven loading is induced by the loading method. For this to occur the timber platen and the sand surface must be as horizontal as possible before each test.

Each of these types of test required slightly different loading set-ups, however two hydraulic arms were utilised in each case to keep the applied load vertical and balanced. The difference between the line load and the patch load tests required changes only to the lower loading beam, load cell, load platen and the method by which the pumps were attached to the tension arms. An illustration of how this varied is shown in Figure 4.4.

## 4.3 Experimental programme

Over the research period the tests shown in Tables 4.2 and 4.3 have been conducted for the load cases, fill heights and load levels listed. Increasing the load

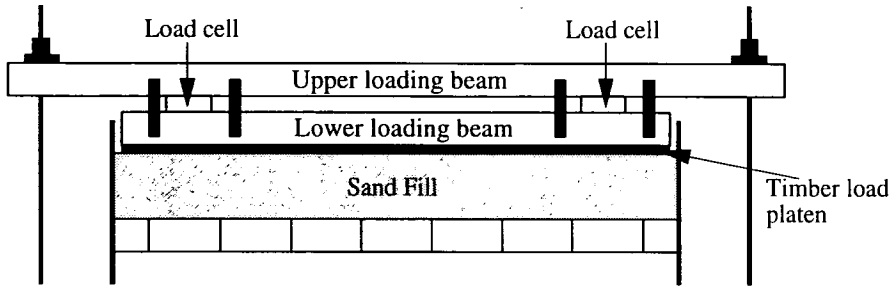


(a) Line loading set-up

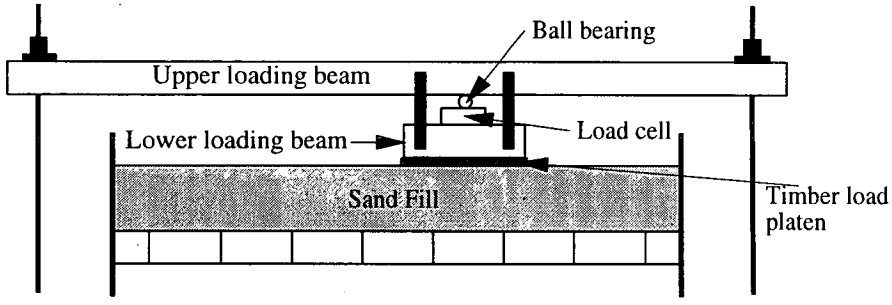


(b) Patch loading set-up

Figure 4.4: Different loading set-up for load types

levels was seen to be important since this would indicate the linearity of response of the bridge, while increasing the fill height would investigate this parameter, each related to the different load type being tested.

The load levels were chosen to represent $\frac{1}{3}$ and $\frac{2}{3}$ of the collapse load of the similarly proportioned single span. To achieve these load levels a sensible load increment had to be determined which took into accounting the dead load of the loading structure.

The position of the 12 line load tests is indicated in Figure 4.2 and the patch load tests coincide with these positions as shown in Figure4.5. Each set of 36 patch load tests is made up form three lines of 12 tests. Loading line $A$ indicates the position of the instrumentation within the bridge, while lines $B$ and $C$ represent a displacement of one patch width away from the line of cells. This allows each test to be given a grid reference to record the test date. In this way a thorough three-dimensional understanding of the bridge can be built up. This will allow a database of results allowing comparison to be made with computational methods

of analysis.

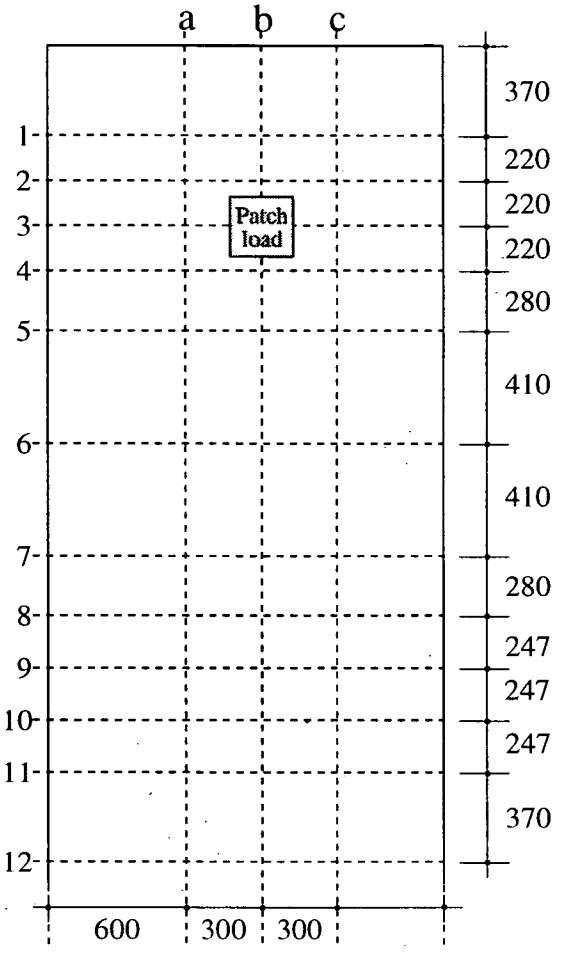


Figure 4.5: Position of patch loads application

For each test all instrumentation was recorded when no load was applied to the bridge, for the dead load case (with loading beams in place) and for the static loading cases (load increments applied). The loading was applied in six equal increments until the desired level was achieved, or cracks were seen to be forming. It was important to wait for a 10 minute period to allow for stresses and displacements to dissipate throughout the structure between each new load increment before measurements were taken. This period coincided with the time taken for the data logger to process the data collected from the previous load increment.

| Year of test | Positions tested | | | Total |
|---|---|---|---|---|
| | Load level = 41 kPa Fill height = 150 mm | Load level = 82 kPa Fill height = 150 mm | Load level = 82 kPa Fill height = 300 mm | |
| 1997 | - | $1 \rightarrow 12$ | - | 12 |
| 1998 | - | - | $1 \rightarrow 12$ | 12 |
| Total | 12 | 12 | 12 | **24** |

Table 4.2: Summary of line load tests performed

### 4.3.1 Tests performed

A complete series of line load tests were performed in 1997 and 1998 covering all loading position. In 1997 the tests were performed at an increased contact stress of 81 $kPa$ and in 1998 after the height of fill over the arches has been increased a further series of tests was performed as indicated in Table 4.2.

A complete series of patch load tests was initially performed in 1996 covering all loading position on the surface of the fill, shown in Figure 4.5. These tests were performed to the same contact stress, 41 $kPa$, as the original line load tests to allow direct comparisons to be made. From these tests several conclusions could be drawn as to the structural response of the bridge.

In 1997 all positions along loading line 'a' were tested with an increased load level of 82 $kPa$. Also included were all positions on transverse loading lines 3, 6 and 7. Further tests were not completed due to lack of time and a belief that information gained from these further tests would be minimal. In 1998 after the height of fill over the arches has been increased a further series of tests with an load level of 82 $kPa$ was performed as indicated in Table 4.3. Using the higher load level of 82 $kPa$ was felt to be safe for the bridge, although care was taken when loading to ensure that the structure was not permanently damaged.

These tests represent a body of work which contains a large amount of data to do with 3-D affects, and the way in which the structure responds to this type of loading. This 3-D affect will be investigated further in later sections where comparisons will be made to this body of work.

| Loading Line | Positions tested | | | Total |
|---|---|---|---|---|
| | Load level = 41 kPa Fill height = 150 mm | Load level = 82 kPa Fill height = 150 mm | Load level = 82 kPa Fill height = 300 mm | |
| **A** | 1 → 12 | 1 → 12 | 1 → 12 | 36 |
| **B** | 1 → 12 | 5, 6 & 7 | 4, 5 & 9 | 18 |
| **C** | 1 → 12 | 6 | 4 & 9 | 15 |
| Total | 36 | 16 | 17 | **69** |

Table 4.3: Summary of patch load tests performed

## 4.4 Experimental Results

### 4.4.1 Overview of results presented

The results obtained from each test were initially analysed using Excel spreadsheet packages. Calibration for the cells had been performed previously[100] to determine the values recorded at the cell. A set of tests results is presented in the Appendices in the form of a graph. Discussion of these results is undertaken in the following subsections. The results presented and discussed are generally grouped according to the type of load and the type of cell being discussed. For the Cambridge and Glamorgan cells the results are also grouped according to the arch on which the cells are positioned. Stresses on arch 1 are measured by cells Cam3, Cam2, Cam4, Glam2 and Glam4 and arch 2 by cells Cam1, Glam1, Glam3, Glam5 and Glam6. The soil pressure cells are grouped according to their position in the fill. Cells N1, N2, N3, N4 and N7 being termed 'horizontal cells' and cells N4, N5, N6 and the Kulite cell being termed the 'vertical cells', due to their alignment. The load test results presented are split into section depending upon the load level, fill height or load type being tested.

For each set of tests performed a repeatability test has also been conducted in order to validate the method of loading, the instrumentation measurements and that the structural stability of the bridge had not been permanently damaged during the testing period.

### 4.4.2 Influence Lines

In order to analyse the many test results which have been produced in a more meaningful way, influence lines have been constructed. Influence lines are used to compare the large amount of data produced in a standard format which can be easily understood. Each influence line graph presents the maximum reading for each type of instrumentation as the load position is varied. If the load was considered to move progressively from loading position 1 to 12, the influence line would represent change in reading for the cells shown. The load position related to each instrument reading is indicated on the $x$-axis by the distance from loading line 1. Measurements are as shown in Figure 4.2.

Influence lines have been grouped together in order to make comparisons between the change in parameters easier to examine. Line load results are grouped in order to compare the change of parameters progressively, for the initial load level, the increase in load level and then the subsequent increase in fill height at the increased load level. Similar graphs are presented in Section 4.6 for the patch load test results.

### 4.4.3 Theoretical distribution of contact stress

During the analysis of results higher measured stresses were recorded than the applied load at the fill surface. This section is included to explain the presence of such high recorded readings. It is commonly assumed that the stress distribution at the soil/footing interface is uniform if the load is applied axially. It has however been shown by Henry[122] that for a rigid footing on cohesionless soil the stress distribution reaches a maximum beneath the centre of the footing. The fall in the stress at the edges is attributed to lateral movement of particles, made possible due to the absence of shearing resistance, (confining pressure), at the edges due to zero overburden stress.

Observations on rigid footings reported by Rodstein[123] revealed that the stress distributions below the platen are roughly elliptical beneath the centre, rising to peaks about $\frac{1}{6}$ of the width from the edge and falling to zero at the edges.

This theory suggests that pressure distribution below the centre of a rigid strip load is initially parabolic. Therefore calculating the maximum contact stress $q^{max}$ directly under the the load can be performed. Consider Figure 4.6, where an idealised strip with an average stress, $q^{ave}$ has been applied, the resulting stress distribution would be a parabolic, with the two areas equal to the total load applied. Several assumptions have been made;

- the loading platen is inherently stiff
- the sand fill comes into contact with every part of the platen

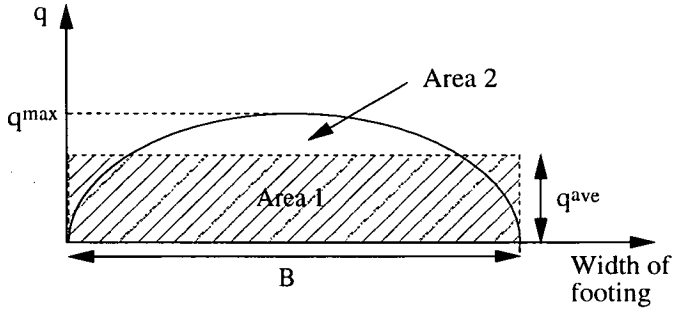


Figure 4.6: Stress distribution below a rigid footing

The applied load is constant and equal to each area for the average and parabolic stress levels, therefore Area 1 must be equal to Area 2. If the parabola has the Equation 4.1 and solving for the limits which are known:

$$q = ax^2 + bx + c \tag{4.1}$$

To find the area under the parabola we have to integrate the equation and solve for the known limits. Equating the two areas which are equal, the average contact stress to the maximum theoretical stress is given by:

$$Area\ 2 \quad = \int_0^B \left(ax^2 + bx\right) dx \Rightarrow \left[\frac{ax^3}{3} + \frac{bx^2}{2} + d\right]_0^B \tag{4.2}$$

$$\mathbf{q^{max} = 1.5 \times q^{ave}} \tag{4.3}$$

Equation 4.3 shows that the maximum stress at the surface is 1.5 times the average applied stress, the value generally used during stress calculations. If the stress variation was not in fact parabolic but linear then $q^{max} = 2 \times q^{ave}$. This theory is backed up by the results obtained during the series of tests performed.

Finding the contact stress distribution for a square patch load requires a slightly more sophisticated method, with the inclusion in a third dimension. The average applied stress is $q^{ave}$, and the lengths of the sides are $\alpha$ and $\beta$.

If the first parabola for the first side, of length $\alpha$, has the equation:

$$z = Ax^2 + Bx + c \tag{4.4}$$

Solving again for the known limits this then gives Equation 4.5;

$$z = \frac{4q^{maxy}}{\alpha}\left(x - \frac{x^2}{\alpha}\right) \tag{4.5}$$

Where $q^{maxy}$ has its own parabolic equation:

$$\begin{aligned} & q^{maxy} = Dy^2 + Ey + c \\ where \quad & D = -\frac{4q^{max}}{\beta^2} \quad and \quad E = \frac{4q^{max}}{\beta} \\ \Rightarrow \quad & q^{maxy} = \frac{4q^{max}}{\beta}\left(y - \frac{y^2}{\beta}\right) \end{aligned}$$

Therefore

$$\begin{aligned} z &= \frac{16q^{max}}{\alpha\beta}\left(y - \frac{y^2}{\beta}\right)\left(x - \frac{x^2}{\alpha}\right) \\ when \quad \alpha = \beta = B \quad &\Rightarrow z = k\left(y - \frac{y^2}{B}\right)\left(x - \frac{x^2}{B}\right) \\ where \quad k &= \frac{16q^{max}}{B^2} \end{aligned} \tag{4.6}$$

This time the total volume under the curve is equal to the total force applied to the footing. To find the volume under this curve it is required to double integrate the equation, for the patch which is square and has sides of length B.

$$\begin{aligned} Volume &= q^{ave}\alpha\beta = \int_0^{\alpha}\int_0^{\beta} z\, dx\, dy \\ Volume &= q^{ave}B^2 = \int_0^{B}\int_0^{B} z\, dx\, dy \end{aligned} \tag{4.7}$$

By integration of the above equation and solving for the known limits, this results in;

$$\begin{aligned} Volume &= \frac{16q^{max}B^2}{36} = q^{ave}B^2 \\ &\Rightarrow \quad \mathbf{q^{max} = 2.25 \times q^{ave}} \end{aligned} \tag{4.8}$$

A further check was also performed for the numerical analysis in order to check $q^{max}$ and the total volume obtained. The results from this analysis directly correlated to the above calculations. Figure 4.7 shows the contact stress bulb produced. The maximum stress obtained, $q^{max}$, at the centre of the contact surface is 2.25 times the average stress used in calculations.

## 4.5 Discussion of line load tests results

Since line load tests on the structure have been performed and discussed in detail previously the new reason for interest is the increase in load level and change in the fill height.

### 4.5.1 Increased load level

From previous tests a load level of 41 kPa, representing $\frac{1}{3}$ of the single span failure load, was used at all load positions. Increasing the load level to 82 kPa required great care in order not to permanently damage the structure. For this reason the most critical load positions were tested last. For loading positions 4

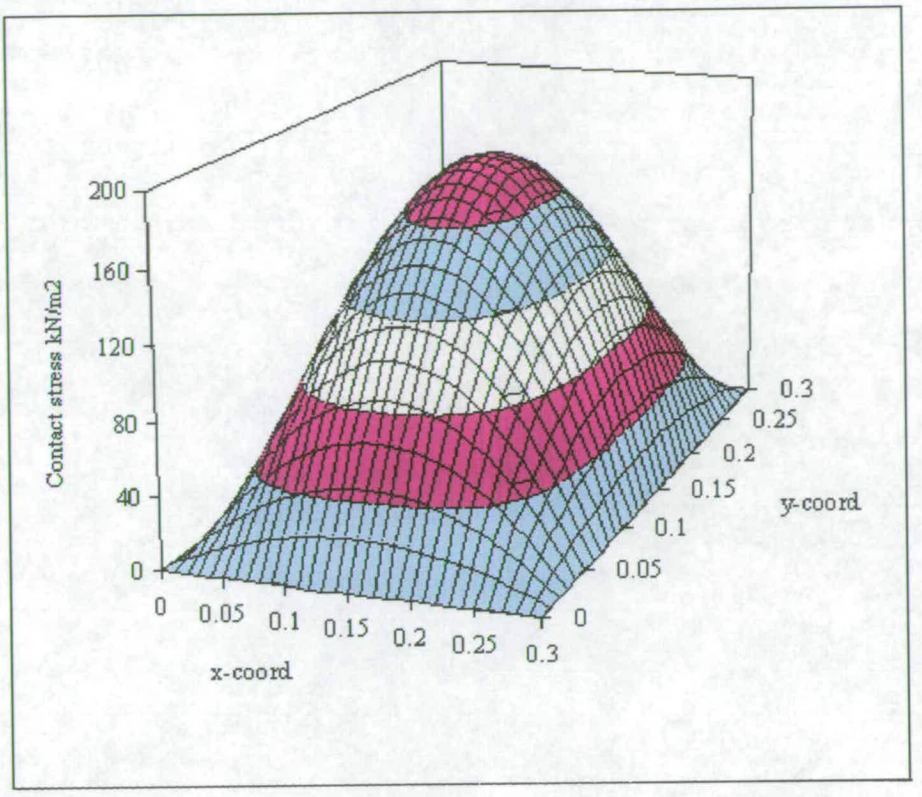


Figure 4.7: Stress distribution below a rigid square platen

$\rightarrow$ 7 it became apparent that the full load level would not be reached without endangering the bridge structure. At these position loading was suspended at 61 kPa, at these levels visible hinges formed in the arch barrel, closing again upon load removal.

Figure 4.8($a$) shows the normal stress influence line graph for arch 1. It is clear that largest normal stress is located at the crown since this is the point of least fill cover. A greater degree of load spread is visible further away from the crown, again an affect of the fill height between the load and the arch extrados. The normal stress readings are also clearly not symmetrical even though the load positions and levels are symmetrical about the centre span. This result has some implications since the only parameter producing this affect would be the presence of the second arch.

The measurement of shear stresses by the Cambridge and Glamorgan cells is a measure of the component of the force measured parallel to the arch barrel. The orientation of cells is not uniform throughout the bridge and consequently, negative and positive readings can be recorded for stresses acting in the same

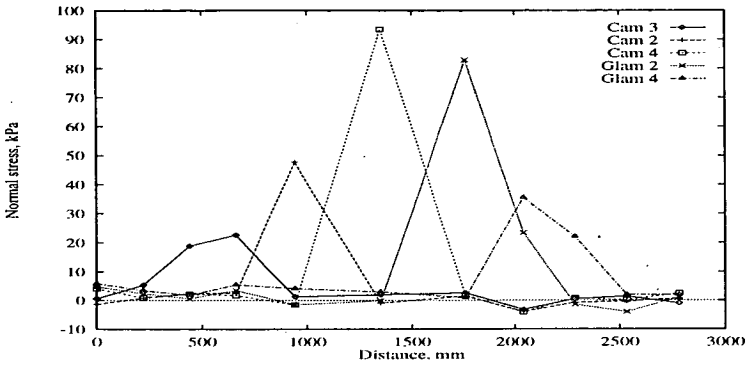


(a) Fill height = 150 mm, applied load = 61 kPa

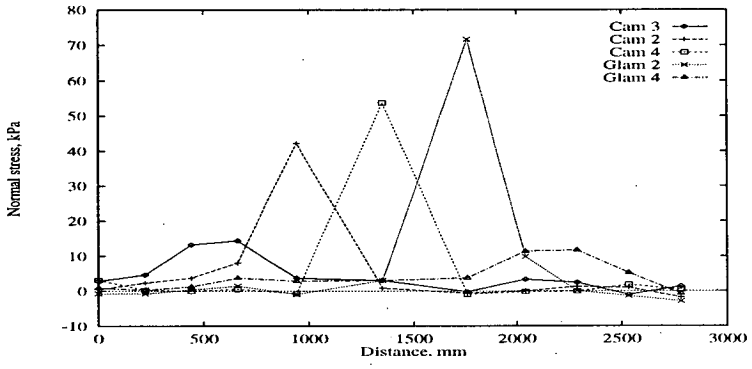


(b) Fill height = 300 mm, applied load = 61 kPa

Figure 4.8: Normal stress on Arch 1

direction. For this reason Table 4.4 indicates the direction the fill slides over the barrel for a positive cell reading.

Figure 4.9($a$) shows the shear stress influence line for arch 1. The largest positive shear stress is encountered for load position 5, and the most negative change in stress is for $Cam4$ when the load is over the centre of span 1. These results are more meaningful when compared with recorded arch displacement reading which indicate clearly how these changes in stress have been created. Again the change in shear stress shows some signs of being symmetrical but the different sides are still obviously different.

Figures 4.12($a$) & 4.13($a$) are the influence lines for the soil pressure cells. It is clear that the maximum pressure change occurs when the load is directly over the relevant cell. There is little load spread observed for the cells at a depth of 150 mm, but for the pressure cells at greater depth, cells 5 & 6, fill pressure

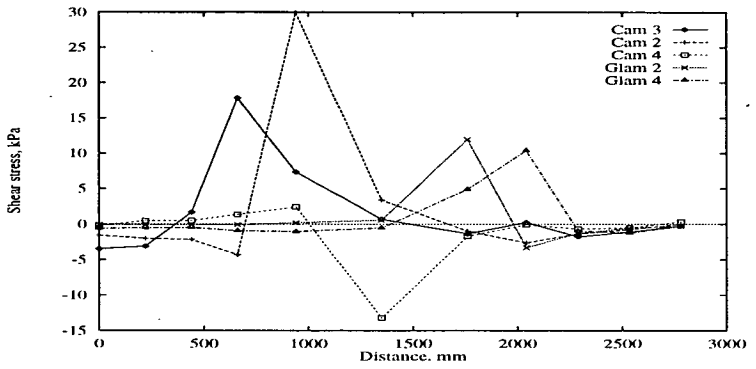


(a) Fill height = 150 mm, applied load = 61 kPa

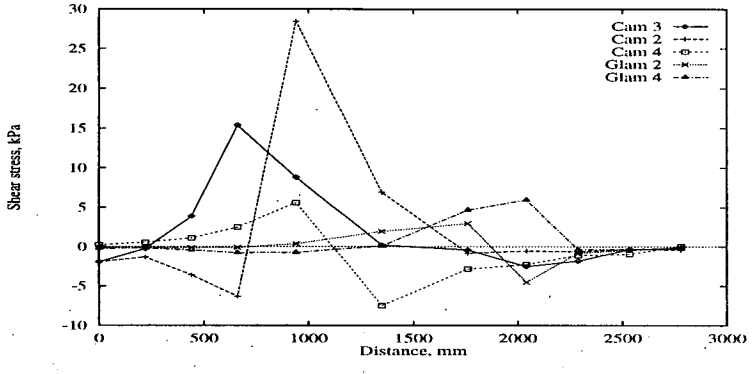


(b) Fill height = 300 mm, applied load = 61 kPa

Figure 4.9: Shear stress on Arch 1

distribution is clearly observed. The proximity of the semi-rigid boundary to the pressure cell is also seen to affect the measured pressure. The horizontal soil cells are all at the same depth, therefore the difference between each reading can only be explained by the proximity of the arch.

The Kulite cell for the first time indicates a change in pressure normal to the arch extrados, these changes are very small but occur over a greater range of applied load positions. It is not clear if the change in pressure is due to the applied load directly or from arch movement. Since changes in pressure occur when the applied load is at load positions 4 and 5 this indicates some arch movement influence.

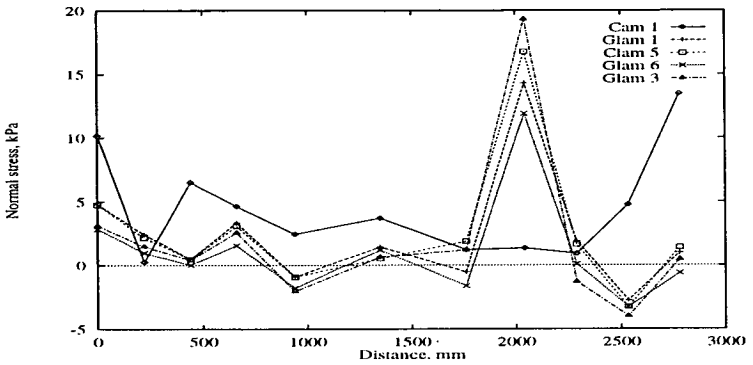


(a) Fill height = 150 mm, applied load = 61 kPa

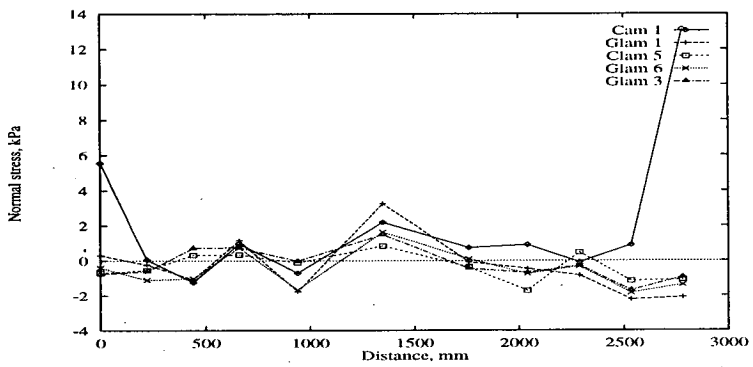


(b) Fill height = 300 mm, applied load = 61 kPa

Figure 4.10: Normal stress on Arch 2

### 4.5.2 Increased fill height

The results for this section are presented in the form of influence line graphs showing loading position against maximum measured stress as the load traverses the bridge. The results are presented according to the arch on which the cells were placed for both normal and shear stresses.

#### 4.5.2.1 Glamorgan and Cambridge cells

Normal stress results show a linear response of measured stress with increase in applied load for all results except the more extreme loading positions where influence is not directly from the load. The absence of a trend for loading positions 1 and 11 can be attributed to movements of the arch barrel changing the stress

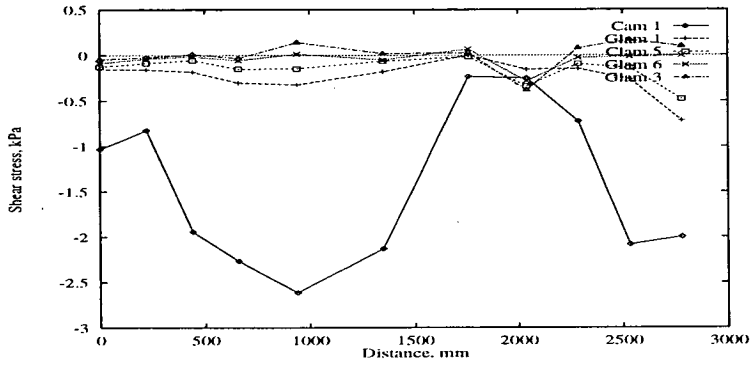


(a) Fill height = 150 mm, applied load = 61 kPa

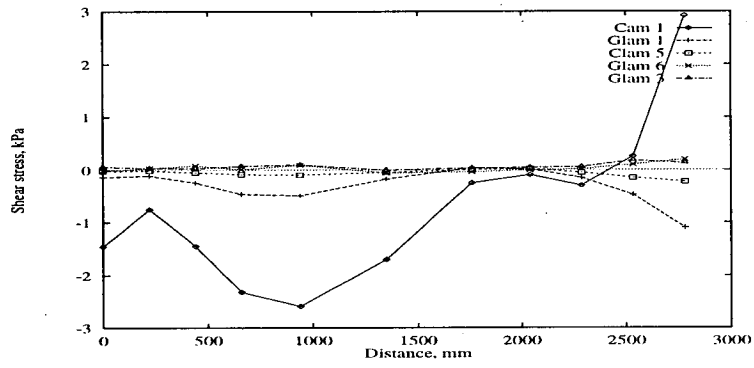


(b) Fill height = 300 mm, applied load = 61 kPa

Figure 4.11: Shear stress on Arch 2

distributions at the arch-fill interface. It is evident that the stresses recorded in arch 1 are higher than in arch 2, mainly because arch 1 is the primarily loaded arch. For this reason the trends between the cell pressure readings and the applied loading will not be as pronounced. There is less fill between the load and the arch and so the load is not being distributed as much, and movement of the first arch will also promote further load distribution.

Figure 4.8($b$) shows the influence lines for arch 1 for the cells on the extrados of that arch. It can be seen that a number of distinct peaks are present as the load traverses the arch. The maximum readings are all measured when the load is directly over each specific stress cell. The difference in the values observed can be attributed to the depth of fill over the arch barrel at each point and also to the position of the cell on the arch. The lack of symmetry must be attributed to variation in the manner which the stresses are carried by the fill,

| Arch 1 | Cam3 | Cam2 | Cam4 | Glam2 | Glam4 |
|---|---|---|---|---|---|
| Rotation | ACW | ACW | CW | CW | CW |
| Arch 2 | Cam1 | Glam1 | Glam5 | Glam6 | Glam3 |
| Rotation | ACW | CW | ACW | ACW | CW |

Table 4.4: Definition of a positive shear stress reading

| Fill height (mm)<br>Applied load ($kN/m^2$) | 150<br>61 | % of applied load | 300<br>61 | % of applied load |
|---|---|---|---|---|
| Cam3 | 22.6 | 37 | 14.4 | 24 |
| Cam2 | 47.8 | 78 | 42.3 | 69 |
| Cam4 | 93.5 | 153 | 53.7 | 87 |

Table 4.5: Comparison of maximum recorded values for the change in parameter

affected by the lack of symmetry of the model. It can be inferred that the stress distribution through the fill is different for the abutment side to the pier side. Measured deflections below these cells are all similar for the maximum recorded stress values. The second arch is having a greater affect on measured stresses as the load increases. Glam2 for some reason presents a higher reading than any of the others. This may be due to a rogue cell reading although the cell does load in a linear fashion and otherwise compares well with other cells, giving some confidence in the result.

The normal stresses for arch 2 cells, shown in Figure 4.10($b$), are significantly less than those measured for arch 1. A number of observations can be made from the readings to determine the manner by which the arch carries the applied load. The maximum value recorded is for Cam1, this cell being the closest to the applied loads. Similar readings are recorded for cells in arch 1, a similar distance away from the applied load which gives some reliability in the results. Other peaks can be explained by the fact that the arch sways, shown by deflection results, transferring load to the second arch through the fill. These reading can only be due to load being dispersed through the fill into arch 2. When compared with deflection readings it clearly shows that the second arch moved away from the loaded arch.

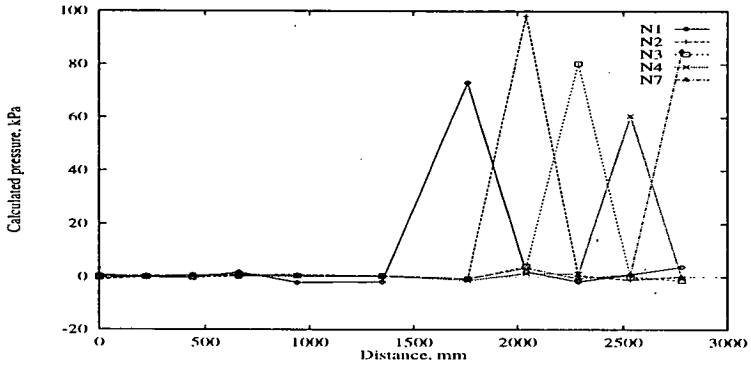


(a) Fill height = 150 mm, applied load = 61 kPa

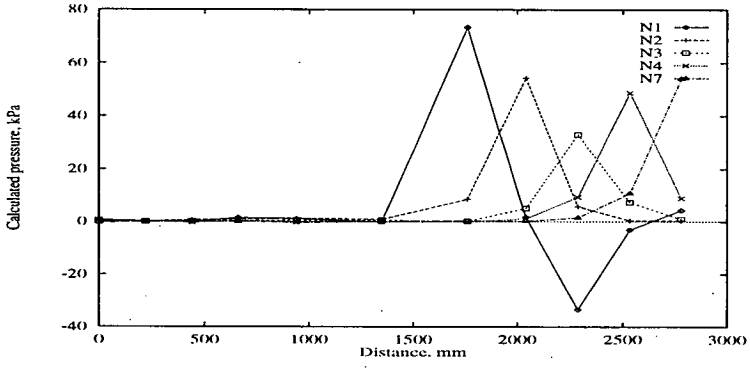


(b) Fill height = 300 mm, applied load = 61 kPa

Figure 4.12: Horizontal soil cells, influence lines (1997-1998)

Figure 4.9($b$) shows the shear stress influence lines for arch 1. The shear stress cells generally show a trend that an increase in the applied load leads to an increase in the shear stress. This trend is not however always linear and is often curved, especially prevalent for the cells on the second arch. It is again immediately clear that the magnitude of the shear stresses measured for arch 1 are greater than those for arch 2. A good way to understand the influence line graphs is to look further at the results obtained for loading line 5. A peak value of 28 kPa is recorded at Cam2, the cell directly under the load. This positive stress indicates that the fill is shearing down the face of the arch at this point. The remaining cells measure values of: 8.8 kPa for Cam3, 5.6 kPa for Cam4, 0.4 kPa for Glam2 and -0.7 kPa for Glam4. With reference to Table 4.4 these results indicate the fill being pushed away from the load and onto and along the arch barrel. Similar observations can be made for the other loading positions.

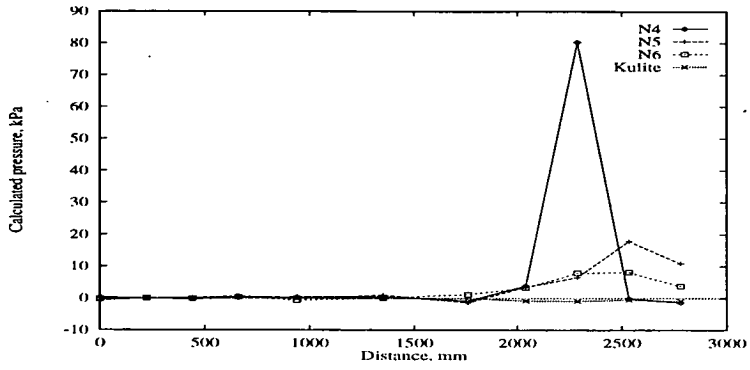


(a) Fill height = 150 mm, applied load = 61 kPa

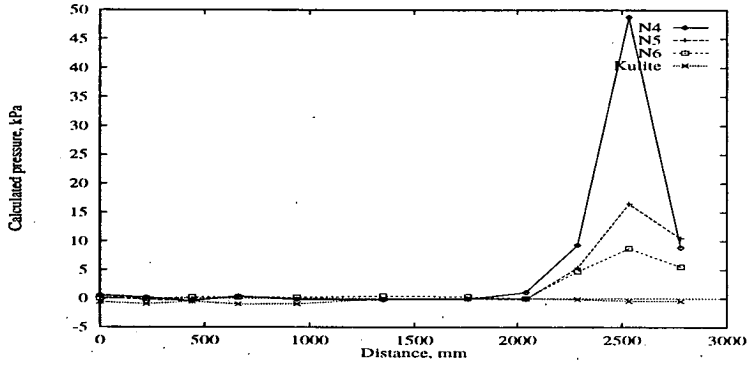


(b) Fill height = 300 mm, applied load = 61 kPa

Figure 4.13: Vertical soil cells, influence lines (1997-1998)

For loading position 6 the results are not initially what would be expected. Since the load is applied over cell Cam4 it would be assumed that the shear stress would 'spread' evenly over the arch resulting in no change in shear stress. This is however the cell which gives slightly the largest change in shear stress. The reading for the adjacent cells indicate symmetrical responses but not in magnitude. These results indicate again that there must be a difference between the restraint from the abutment and pier sides of the arch in question.

Graph 4.9($b$) shows a similar lack of symmetry which goes some way to explaining the previous lack of symmetry for the normal stress results. The inference is that the shear component from the applied load is high for loading position 4, resulting in a reduced normal stress. The opposite can be inferred for the measured values at Glam2. The difference in behaviour may be due to the fill in the centre of the bridge dissipating stresses less effectively than the fill at the abutments

because of the pressure constraining affects caused by the second arch. It may also be inferred that the abutment side of arch 1 is stiffer, restricting displacement towards the pier side and increasing normal stress. The low shear stress at the centre of the span is as expected and compares well with previous tests.

#### 4.5.2.2 Soil pressure cells

From inspection of graphs 4.12($b$) and 4.13($b$) it can be seen that the pressures measured in the cells are small until the load is applied close to the line of cells. At this point the zone of influence from the load starts to enter the area of the cells. This results in an interesting affect which allows the distribution of the load through the fill and the subsequent pressure changes produced by arch movement to be constructed. It would be easier with a greater number of pressure cells to get a better distribution but this could in itself affect the pressure distribution through the fill material.

The stress distribution across the bridge for the different loading positions is best illustrated in Figure 4.12($b$). It becomes clear that the maximum pressure readings are recorded by the cell when the loading position is directly over the cell. With the increased fill height the cells positioned adjacent to the directly loaded cell are more affected, due to greater load dispersal. The measured cell pressure being higher than the applied load has already been explained in Section 4.4.3.

**Aside**: *Stress distribution through soil has been studied by various authors. Boussinesq*[124] *considers a homogeneous, isotropic soil and determines the stress distribution at a point below an applied load. Influence charts have been derived in order to make this process easier. From these charts the vertical stresses calculated for a section of fill form bulbs of equal stress when plotted. For each bulb of equal pressure a constant ($\leq 1$) relates the change in pressure at some point below the applied load. These constants can be used to evaluate the stress in the soil for a known vertical and horizontal distance from the load application.*

*Further Westergaard*[124] *has investigated situations where the soil is anisotropic, considering a situation where there was a rigid boundary within the bulbs of pressure created by the applied load. He concluded that the stresses experienced will be greater with the presence of the rigid boundary.*

It is conceivable that the arch barrels could be considered as being a rigid boundary which would affect the pressure bulbs. It is evident from the results obtained that this is in fact the case. Cells closer to the arch barrel should register higher cell pressures due to the arch acting as a rigid boundary. This affect is clearly shown by the cell readings for N1 and N7, the cells closest to the arch barrels giving the highest readings.

Soil pressure cell N1 indicates a similar response to the other cells apart from when the load is placed at loading positions 9 and 10, where negative pressures are recorded. This indicates a pressure decrease in the fill occurring in the area of the fill. This is difficult to explain since only an arch movement away from the soil in this area can explain the resulting stress release. Small hairline cracks were evident during the loading of these positions and obtaining a consistent loading stress was difficult. However these reasons do not explain the pressure release unless locked in pressure was being dissipated by arch movement. Measured pressure decreases from cells N1 to N3 as Westergaard predicted but rises again for cells N4 and N7. The reason for the increase in readings for loading positions 10 and 11 is initially uncertain since the depth of fill between the load and arch in greater. There are two possible reasons for this behaviour:

1. The pressure recorded for cell N3 is a rogue result. If it was larger then Westergaard's predicted behaviour is followed.

2. The arch barrel is affecting the pressure distribution to give the measured value. A different pressure path is occurring resulting in the low reading.

Similar observation have been observed for the vertical line of cells shown in Figure 4.13($b$). Again the observed results suggest the soil pressure measured decreases with depth of fill and horizontal distance from the point of application of the load, as would be predicted by Boussinesq. With the load on the remote side of the arch the cells show very little consistent response although arch movement, resisted by the fill, is observed. Maximum readings are again recorded with the load directly overhead, reducing as the load moves away from the line of cells.

A small decrease in pressure for the Kulite cell is recorded and shows a small distribution of the applied load through the fill at the cell position. No visual cracks were observed in the region of the cell during any of the tests and it is

felt unlikely that any pier movement occurred. It is felt that the decrease in pressure is due to a a slight movement of the arch away from the fill, mobilising the active pressures. The pressures recorded are small but indicate clearly a variation dependent upon loading position. The largest pressure measurements occur for loading positions which produce greatest sway in the arch.

#### 4.5.2.3 Formation of hinges

Due to the increased load levels it was foreseen that hinges would start to form during the loading process. The formation of these hinges is not an indication that the bridge is fast approaching collapse but is redistributing the applied load. Since multi-span arches have been shown to be more flexible it was feared that the increased loading might prove dangerous. For this reason the critical positions were tested last. When cracks, however small were identified the test was immediately suspended, and the load removed.

For the structure to collapse it requires a minimum of four hinges to form a mechanism. This type of collapse was predominant since no crushing failure of the arch material had been indicated in any of the tests. The formation of excessive cracks could signify that the arch had reached its serviceability limit state and the cracks were weakening the structure.

The tests for the worst load cases were performed with great care and at a reduced load increment so any build up of stresses would be more gradual. Even at these reduced values minute cracks were visible which closed again after the loading was removed. The position and size of the cracks are indicated in Figure 4.14.

## 4.6 Discussion of patch load tests results

Patch load tests have not been performed on the structure previously and have been introduced earlier in Section 4.2.4. In this section the results obtained from the series of test shown in Table 4.3 are discussed. For the later tests performed only differences between the original results and the affect of the change of parameter will be discussed to reduce replication. There is however for the first time a transverse loading affect which will require some introduction.

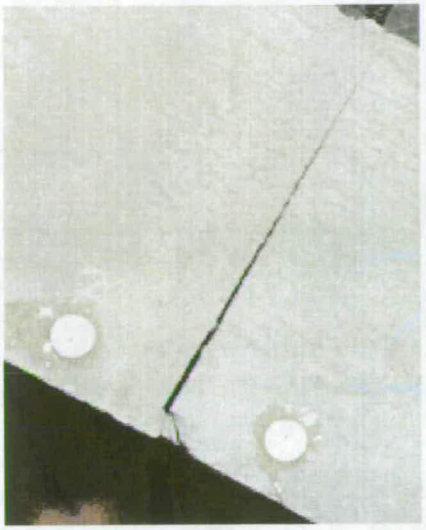

(a) Hinge 1

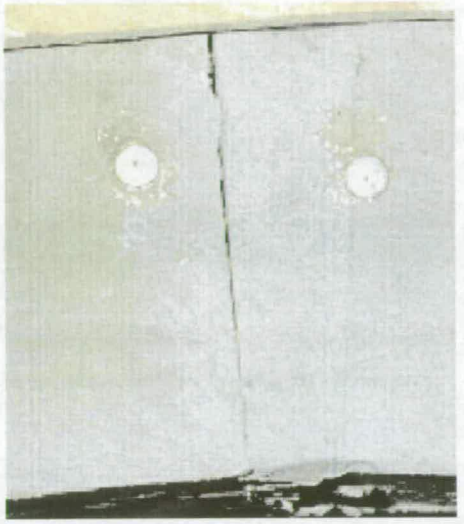

(b) Hinge 2

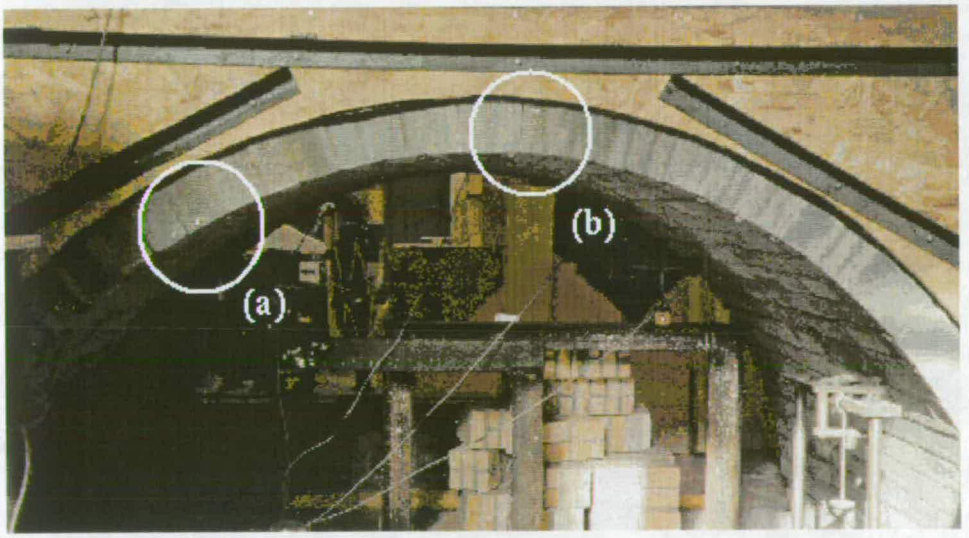


(c) Bridge elevation

Figure 4.14: Picture of visible cracks and positions

More than 70 patch load tests have been performed over a period of 2 years, resulting in information being obtained for changes in load level, fill height, loading position and a transverse loading affect. The results from these patch load tests are presented in Figures 4.15 to 4.25.

## 4.6.1 Normal stress

### 4.6.1.1 Transverse loading

Initial normal stress results show a linear response to the applied load when applied along loading line $A$. With loading lines $B$ and $C$ the response to the load is no longer linear. As the load moves away from the line of cells the stress measured quickly reduces, as would be expected. Since the original fill height was only 150 $mm$ many of the readings obtained can only come from distribution of the applied load through the structure. This provides useful information as to the response and nature by which the arch reacts with the fill to applied loads.

Figure 4.15 shows the typical normal stress results for arch 1 for the different loading lines. These results provide a good representation of the behaviour that is experienced for arch 1. Figure 4.15($a$) shows a similar response to the line load tests already discussed. Slightly different peak responses are recorded for cells Cam4 and Glam2 but these are quite small and may be due to the different load type.

For loading lines $B$ and $C$ it is clear that the recorded stresses are greatly reduced than when the load was applied directly above the line of cells. The peak value recorded for loading line $B$ is for cell Glam2, while for loading line $C$ is cell Glam4. Load dispersal through the fill would infer that influence directly from the applied load would have little affect on the measurements for loading lines $B$ and $C$. The influence would however be greater for the deeper cells, like Cam3 and Glam4, and less for the crown cell Cam4. This affect is shown in Figure 4.15$b$ and $c$. For Cam4 a pressure reduction is experienced for loading positions 5$b$ and 5$c$, this is due to movement of the arch away from the fill, displayed by displacement results. The two sides of the arch also shows some symmetry, an increase in stress being induced by either arch movement or direct load influence onto the arch.

#### 4.6.1.2 Increasing load level

Figure 4.16($b$) again shows how the response of the cells is again not symmetrical, with the largest stress being measured by Glam2. For the loading positions either side of this maximum reading normal stress values are recorded, again giving some confidence in these results.

For this increased load level the transverse loading positions were also partially tested for loading positions 5, 6 and 7. Particularly at the crown the measured change in normal stress reduced almost to nothing, while for the positions either side of this the stress reduced by almost 80%. This must be an affect of the amount of fill covering the arch in each case. Table 4.6 shows that doubling the load level increases the measured stress acting on the arch by two, as would be expected since the load/stress lines are still linear. Distribution of the load in the transverse direction is again seen to be very minimal, not surprising since load dispersal in this direction cannot be affected by the load level applied.

#### 4.6.1.3 Increasing fill height

Figure 4.16($c$) shows the typical normal stress results for arch 1 and loading line $A$. These positions provide a good representation of the behaviour that is experienced for arch 1. The stress rises uniformly with the applied load. It should be noted that the peak values are reduced with the increased fill height. It can also be noted from the results shown in Table 4.6 that doubling the fill height has the affect of reducing the measured stress. It would be expected that the reduction in measured value would increase for the cells closer to the crown as the fill increase represents a greater increase in the total fill level. This is shown by the figures presented in the table.

With the increase in fill level there seems to be a greater load dispersal in the transverse direction than observed previously. This affect can only be due to the larger load dispersal of the extra fill since load levels are kept constant.

| Fill height (mm) | Applied load ($kN/m^2$) | Cam3 | | Cam2 | | Cam4 | |
|---|---|---|---|---|---|---|---|
| | | Max stress | % of applied | Max stress | % of applied | Max stress | % of applied |
| 150 | 41 | 18.1 | 44 | 44.5 | 108 | 74.6 | 182 |
| 150 | 82 | 36.2 | 44 | 100.6 | 122 | 122.9 | 150 |
| 300 | 82 | 24.8 | 30 | 52.1 | 64 | 87.5 | 107 |

Table 4.6: Comparison of maximum recorded normal stresses

### 4.6.2 Shear stress

#### 4.6.2.1 Transverse loading

The same pattern can be seen here as for the normal stress charts with loading line $A$ having the largest stresses, reducing as the load goes away from the line of cells. With consultation with Appendix B it can be seen that arch 1 results tend to be larger, however the second arch loading is meaningful since this shows how the arch is obviously redistributing the load through the structure.

It is also clear that the response of the cells around the arch is not symmetrical. Figure 4.17($a$) shows this fact clearly as well as the phenomenon by which the stress changes sign from the peak position and then goes to the opposite direction as the load traverses the bridge. The high shear stress values relate to the reduced normal stress values as previously mentioned during the line load results. Graphs $b$ and $c$ also show these affects. For these graphs cells Cam3 and Cam2 give the largest readings for loading positions 3-5. This may be due to the arch being more flexible, pushing into the pier side than the abutment side. This extra movement allowing greater change in shear stress and the reduction in normal stress.

The stresses developed on arch 2 are sometimes as large as stresses on arch 1. Theses stress changes are due to arch movement redistributing the load, the zone of this movement increasing the further away from the load you are. Therefore it is foreseeable that higher stresses may be recorded in the secondary arch rather than in the transverse direction.

| Fill height (mm) | Applied load ($kN/m^2$) | Cam3 | | Cam2 | | Cam4 | |
|---|---|---|---|---|---|---|---|
| | | Max stress | % of applied | Max stress | % of applied | Max stress | % of applied |
| 150 | 41 | 11.7 | 29 | 24.0 | 59 | -7.5 | 18 |
| 150 | 82 | 28.0 | 25 | 49.3 | 52 | -17.3 | 21 |
| 300 | 82 | 18.2 | 22 | 31.7 | 39 | -15.0 | 18 |

Table 4.7: Comparison of maximum recorded shear stresses

#### 4.6.2.2 Increasing load level

Figure 4.18($b$) shows how the increase in load influences shear stress measurements. Few conclusions can be drawn since the distributions are identical apart from the magnitude of the stress, which is doubled. For loading position 8 an interesting phenomena occurs with the fill shearing down the arch for Glam4 and up the arch for Glam2. The movement of the fill in this area into the arch ring is producing this change, fill pushing down the face of Glam4 and up Glam2.

#### 4.6.2.3 Increasing fill height

The increase in fill height of 150 $mm$ has the affect of reducing the shear stress measured by as much as 35%. The stress reduction reduced for the cells further away from the centre span, the reason for this being that the increase in fill represents a 100% increase in fill depth at the crown and only a 11% increase at the abutment, this increase influencing the measured shear. The increase in height also seems to have the affect of smoothing the stress response so that trends become clearer. The addition of fill also contributes further dead weight, adding to the strength of the bridge. The stresses registered in arch 2 were significantly lower, due to increased stiffness of the primarily loaded arch not allowing as much load distribution through the bridge structure. This increased stiffness reduces the movement occurring and the load being transfered to arch 2.

### 4.6.3 Fill Pressure results

#### 4.6.3.1 Transverse loading

The fact that only the cell directly below the loading position is influenced suggests that there is very little load spread directly through the fill. Figure 4.19 shows the the influence lines for the horizontal line of soil pressure cells. The graphs show the large reduction in measured pressure as the load moves away from the line of cells. This reduction is even more marked compared to the stress changes. This is as would be expected since the fill is non-cohesive and therefore does not transmit load in the same way as the arch barrel. The pressure changes produced for loading lines $B$ and $C$ must be due to arch movement affecting the normal pressure and not directly from the load, since they are remote enough from the load to remain unaffected at the original load level.

The pressure measured for the vertical line of soil pressure cells is shown in Figure 4.20. Again an indication of the load dispersal through the fill can be gained from these graphs. When the load is over the line of cells the expected distribution is obtained, with the measured pressure decreasing with depth. For loading line $B$ it is clear that the highest reading are for the cells at greater depth, with cell N4 giving virtually no change in pressure. For loading line $C$ the pressure changes are due to arch movement and direct influence from the load, this is inferred by pressure increases being quite uniform for different depths of cell. The Kulite cell again records very small pressure readings, all negative representing a pressure decrease.

#### 4.6.3.2 Increased load level

For an increase in load level the fill pressure readings increase depending upon the position of the cell relative to the arch. Very little load spread can be identified due to the large peak values which mask any of the smaller trends. A very similar response is seen in Figure 4.22($b$) where the increased pressure reading are increased by between 120 and 80%. The load spread to the adjacent cells seems to be unaffected with the graphs looking similar apart from the increased pressure readings.

Increasing the load level influences the transverse positions by an unknown amount since loading lines close to the soil pressure cells were not completely tested. It was however noticed that the pressure in the fill for loading line 7 drops very quickly in the transverse direction.

#### 4.6.3.3 Increased fill height

The increase in fill height has the affect of reducing the pressure reading by about half. The factors are different for each cell since other factors are affecting this reduction and have been previously discussed in section 4.5.2.2. A difference between Figure 4.21($c$) and previous results is that the pressure distribution is clearly spread over a larger area. This is because there is greater depth between the load and the cells through which to distribute the load. Cell N1 also shows an interesting response when the load is remote with a clear increase in pressure being indicated for loading positions 4 and 5. This is due to movement of the arch into the fill in the area of this cell, also with the increased fill height results in pressure increases. Other cells show similar affects but to a lesser, less visible degree.

Increasing the fill height has the affect of reducing the pressure readings for the vertical line of cells from reading obtained from previous tests. Again small pressure distribution through the structure is indicated. Loading position 11 results indicate that the increase in fill height distributes the applied load further with an increase in pressure reading for cell N5.

### 4.6.4 Deflection results

The deflection results are a meaningful way to understand some of the other results discussed previously. The results are from the 12 deflection gauges placed under the two arches in both the longitudinal and transverse directions. Loading would be within the elastic limit of the bridge, this was checked with the unloaded deflections also being recorded showing how the structure returned to its original position. Deflections show how the arches barrels are affected by the applied loads.

Influence lines, as shown in Figure 4.23, have been constructed to enable the deflected shape of the arch at all loading positions to be drawn. A negative displacement represent an arch movement into the fill and a positive displacement movement away from the fill. This graph shows how the arch sways away from the load and into the fill on the remote site of the arch. This must therefore be utilising both the passive and active strength of the fill. The affect is not quite symmetrical but it is difficult to draw clear conclusions from these results since the measured displacements are small and differences difficult to identify. The lack of symmetry may be due to the presence of the secondary arch which would support observations made in previous sections.

The deflected shape of the arch for each loading position can be obtained by taking the displacement of all dials for each loading line, to produce an deflected shapes of the arch. These graphs are shown in Figure 4.24. Deflections have to be exaggerated, by a magnification factor, $D_{mag}$, to give a visible representation of the displacements. Figure 4.24($c$) shows the deflected shape for loading position 6, over the the centre of the arch. All values to draw these graphs are taken from Figure 4.23 using the magnification factor listed.

The arch by the nature of its construction is very stiff, therefore deflection reading were expected to be quite small. The maximum deflection recorded during any of the tests was $0.6mm$. The load positions presented are chosen to show the difference in behaviour when the load is applied across arch 1. For these load positions arch 1 is the active arch and arch 2 is the passive, since arch movement is due to the load and from load distribution respectively.

It can be clearly seen that the load causes a sway to occur for the arch under the load. There seems to be some symmetry between the different sides of the arch both in the size and direction of displacements. When the load is placed over the centre of the span the displaced shape is again symmetrical, with the major displacement occurring directly under the load. Deflection results tend to be consistent for all the tests performed along the line of instrumentation therefore only one case has been shown here.

The transverse loading influence line results in Figure 4.25 show a few interesting affects. The maximum displacements occur when the load is at loading position 5 in all cases, the loading position directly over the line of transverse dials. When

the height of fill is small the transverse load dispersal is smaller than for larger fill heights. When the load is remote from the dials indicated very similar load dispersal is observed. The position of the load does have some transverse affect on the displacements measured.

Comparisons with previous tests have been performed throughout this chapter to quantify the affect of the increase in load level and the increase in fill height. Since comparisons with current theory have already been performed by Prentice[20] it was felt unnecessary to repeat this exercise here.

## 4.7 Conclusions

The objectives of these tests were to produce a study of the behaviour of the structure to applied loads, in particular the affect of the second arch on the structure as well as the soil-structure interaction. Investigating the affect of increasing the fill depth, the load level and changing the load type are also included. Instrument analysis was used to measure stress distribution in the fill and on the arch extrados and deflections measured on the arch intrados.

- The tests performed were shown to be repeatable.
- It is clear that multi-span bridges cannot be analysed as a series of single spans.
- Line loads at the same contact pressure are more critical than patch loads on a multi-span arch bridge.
- There is interaction between both arches and the fill in all loading cases to a varying degree, so the whole structure is used to carry the load.
- The two arches acted in an active and passive manner according to the load position.
- Peak pressure and stress reading were higher than applied values, for the reasons postulated.
- The most critical load position was near the quarter point of arch 1, on the abutment side. This position although not producing the peak stress values

but did have the most significant affects on the bridge and in particular the second arch.

- Results show the response of the primarily loaded arch were not symmetrical between the abutment and the pier/second arch side of the arch. The pier side tended to be more flexible.

- Cracks in the arch barrel opened during loading, closing again when the applied load is removed. It was found they had an affect on the loading behaviour of the bridge.

- Increasing the fill height significantly decreases the stresses transfered to the arch barrels. This stress decrease is proportional to the original fill height over that arch barrel.

- The increase in fill height reduces arch movement due to the increased restraint from the additional dead weight.

- Stresses decrease in magnitude, dispersed through the fill and arch movement, with distance and depth from the applied load.

- The cell adjacent to the crown of arch 1 on the abutment side records the maximum shear stress.

- Increasing fill depth does not always produce the predicted decrease in stress applied to the arch barrel. The pressure recorded for some loading positions are higher than for lower fill levels.

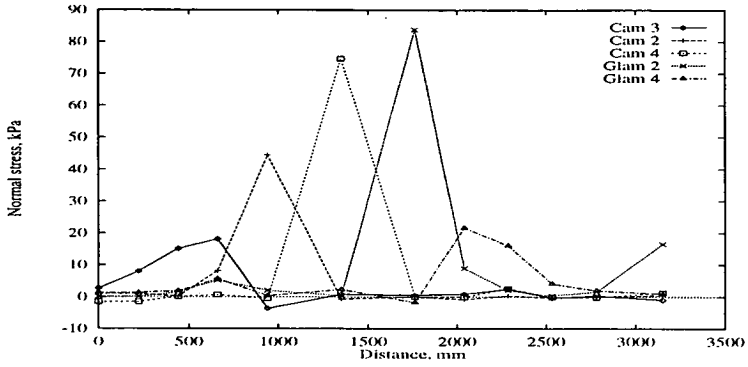


(a) Loading line 'a'

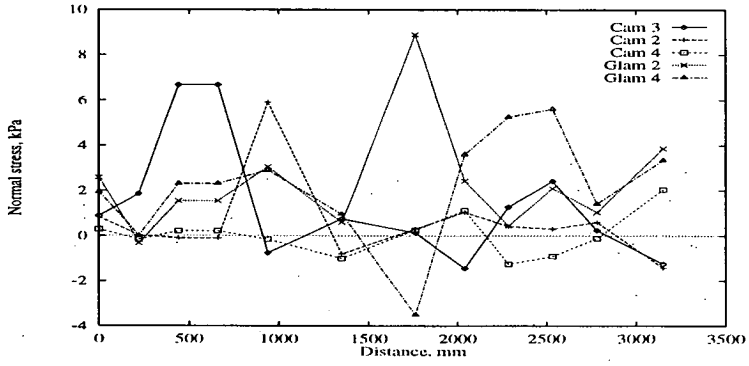


(b) Loading line 'b'

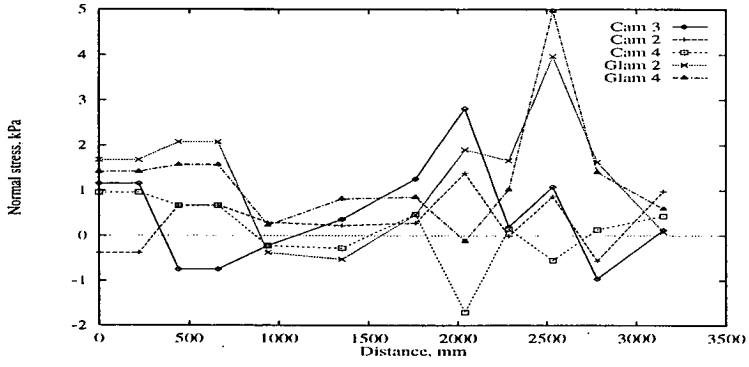


(c) Loading line 'c'

Figure 4.15: Normal stress on Arch 1 (Transverse loading)

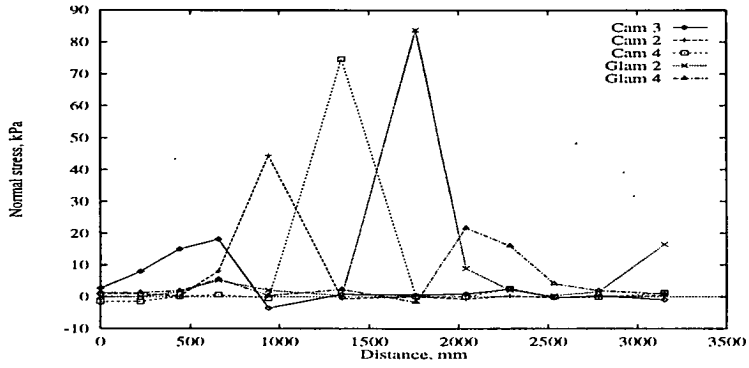


(a) Applied load = 41 kPa, fill height = 150 mm

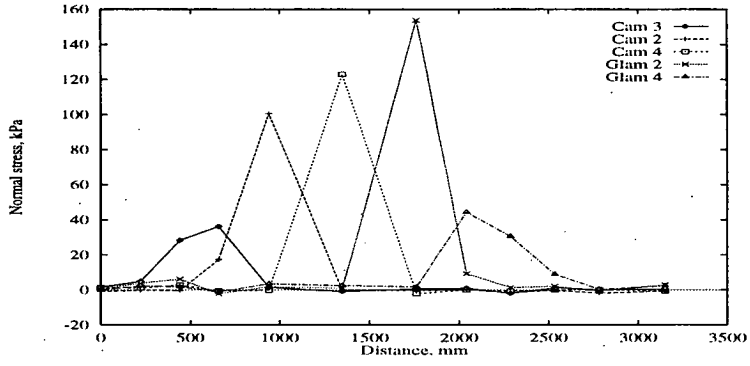


(b) Applied load = 82 kPa, fill height = 150 mm

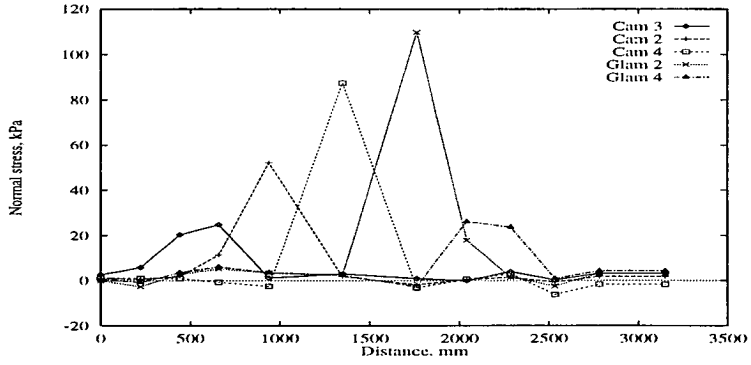


(c) Applied load = 82 kPa, fill height = 300 mm

Figure 4.16: Change in load level and fill height. Normal stress on Arch 1

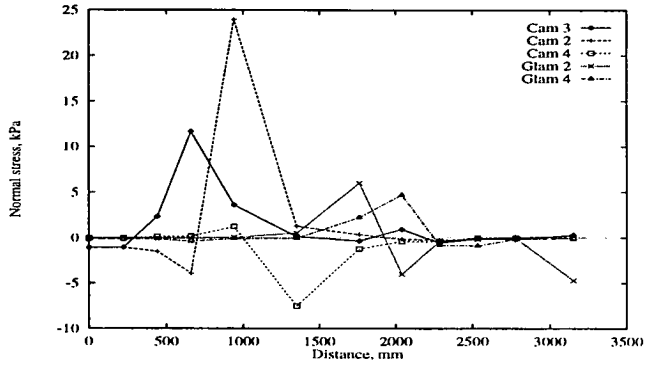


(a) Loading line 'a'

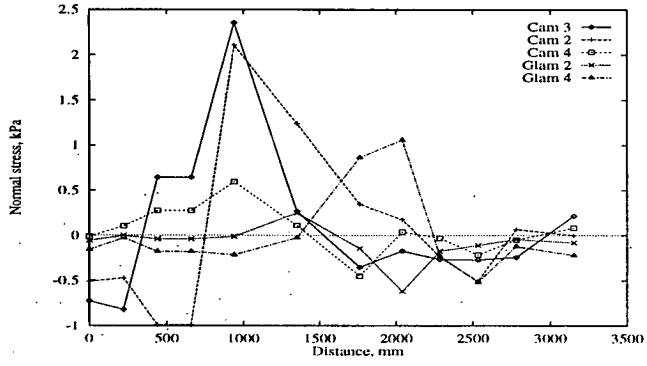


(b) Loading line 'b'

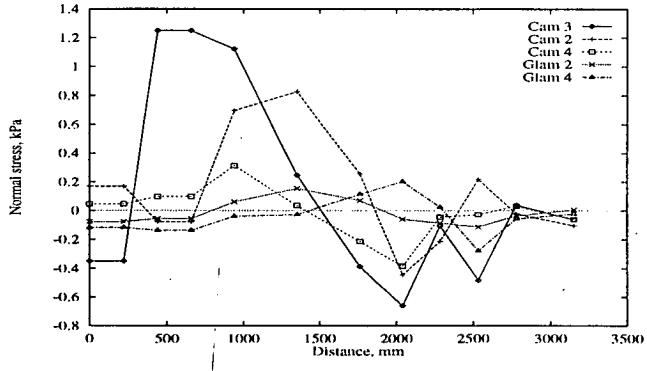


(c) Loading line 'c'

Figure 4.17: Shear stress on Arch 1 (Transverse loading)

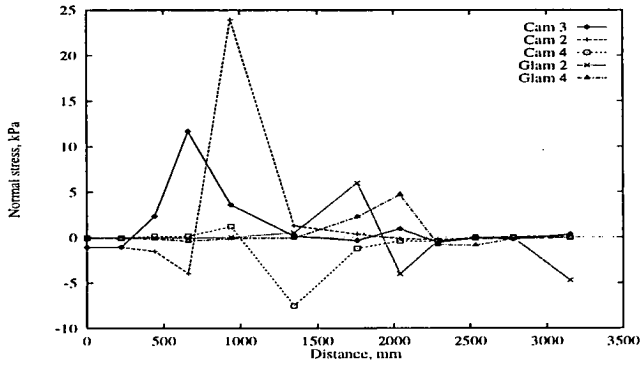


(a) Applied load = 41 kPa, fill height = 150 mm

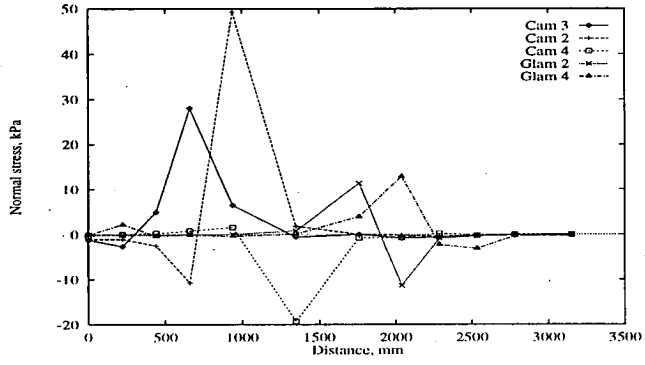


(b) Applied load = 82 kPa, fill height = 150 mm

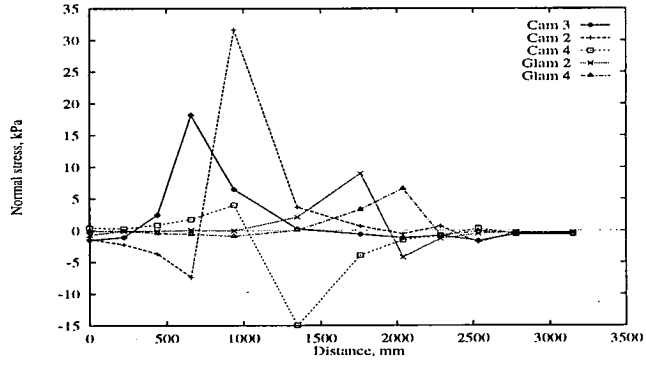


(c) Applied load = 82 kPa, fill height = 300 mm

Figure 4.18: Change in load level and fill height. Shear stress on Arch 1

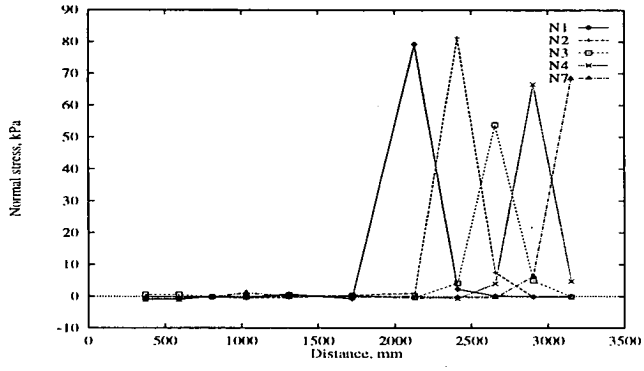


(a) Loading line 'a'

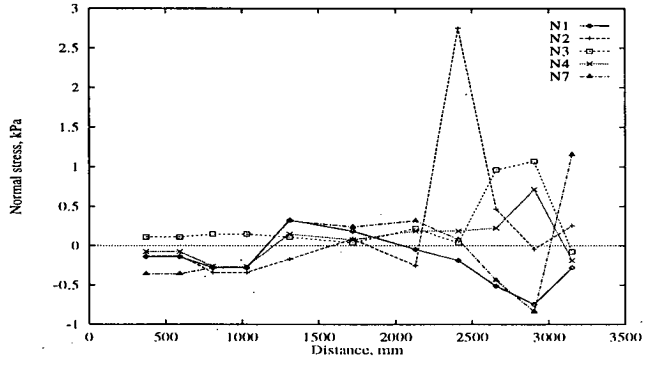


(b) Loading line 'b'

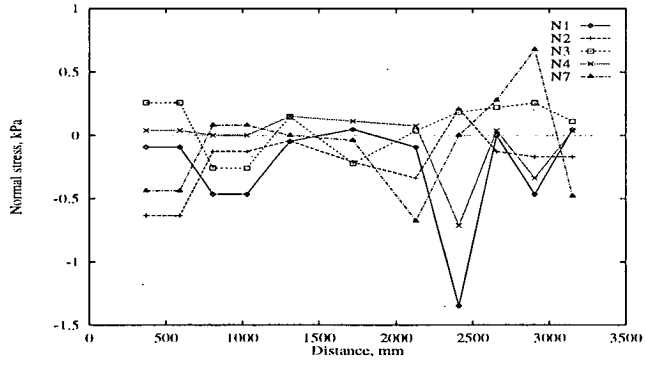


(c) Loading line 'c'

Figure 4.19: Horizontal soil cell influence lines (Transverse loading)

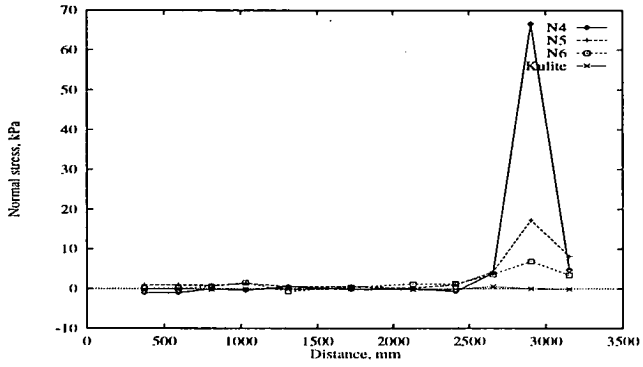


(a) Loading line 'a'

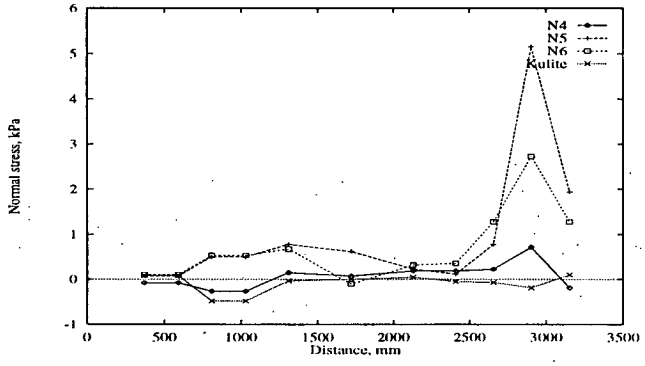


(b) Loading line 'b'

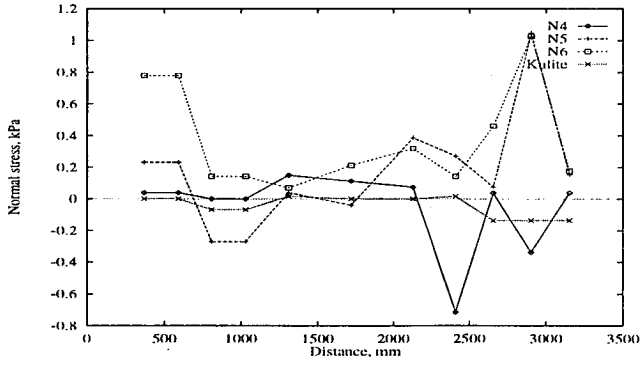


(c) Loading line 'c'

Figure 4.20: Vertical soil cell influence lines (Transverse loading)

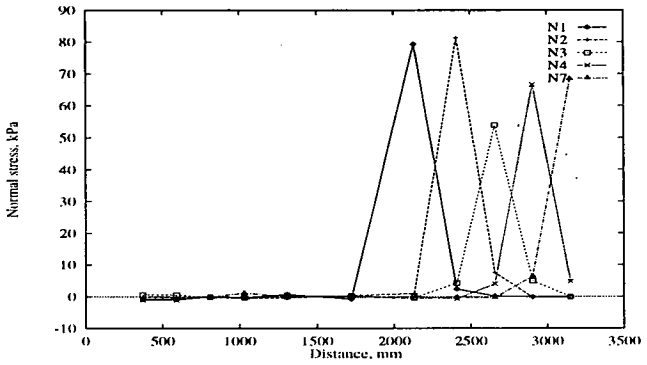


(a) Fill height = 150 mm, applied load = 41 kPa

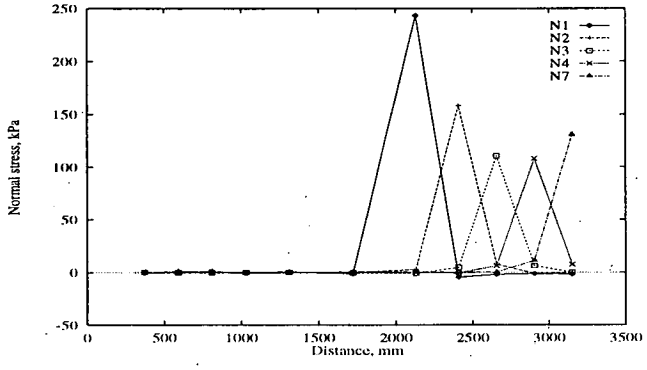


(b) Fill height = 150 mm, applied load = 82 kPa

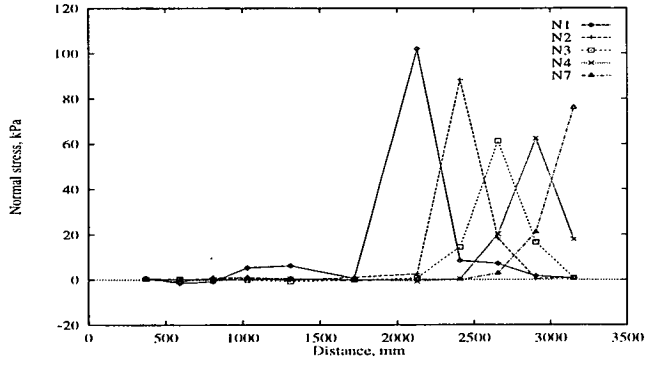


(c) Fill height = 300 mm, applied load = 82 kPa

Figure 4.21: Horizontal soil cell influence lines (1996-1998)

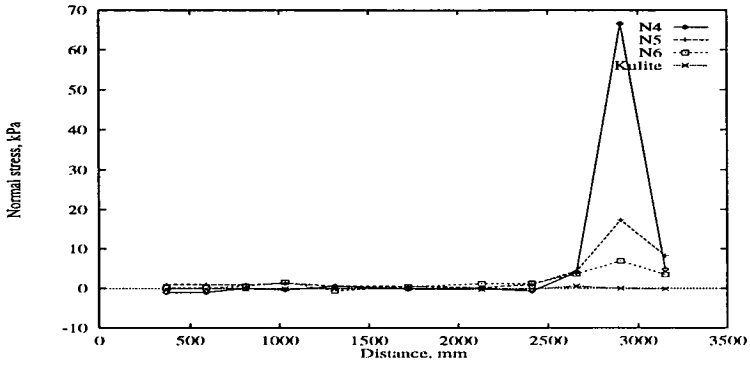


(a) Fill height = 150 mm, applied load = 41 kPa

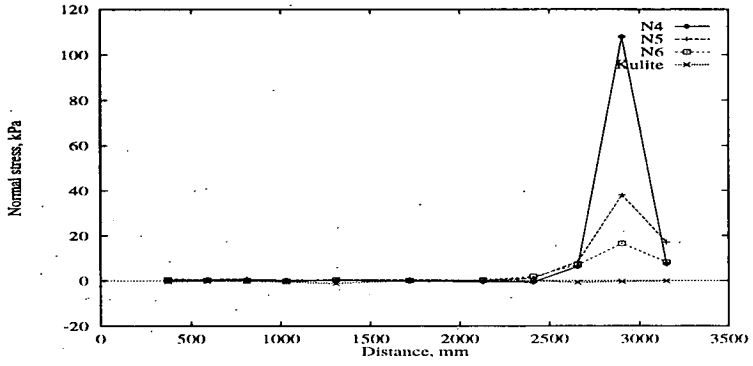


(b) Fill height = 150 mm, applied load = 82 kPa

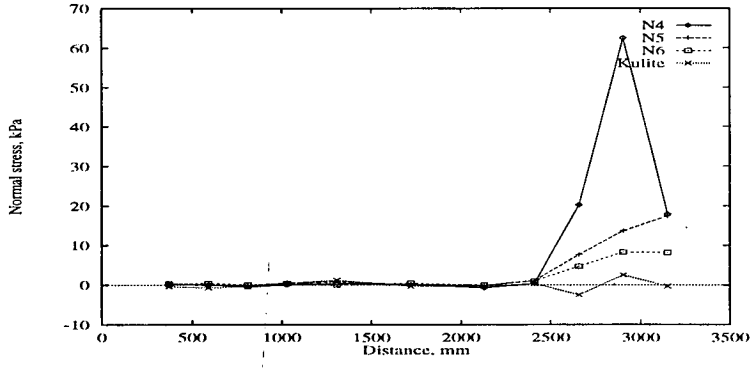


(c) Fill height = 300 mm, applied load = 82 kPa

Figure 4.22: Vertical soil cell influence lines (1996-1998)

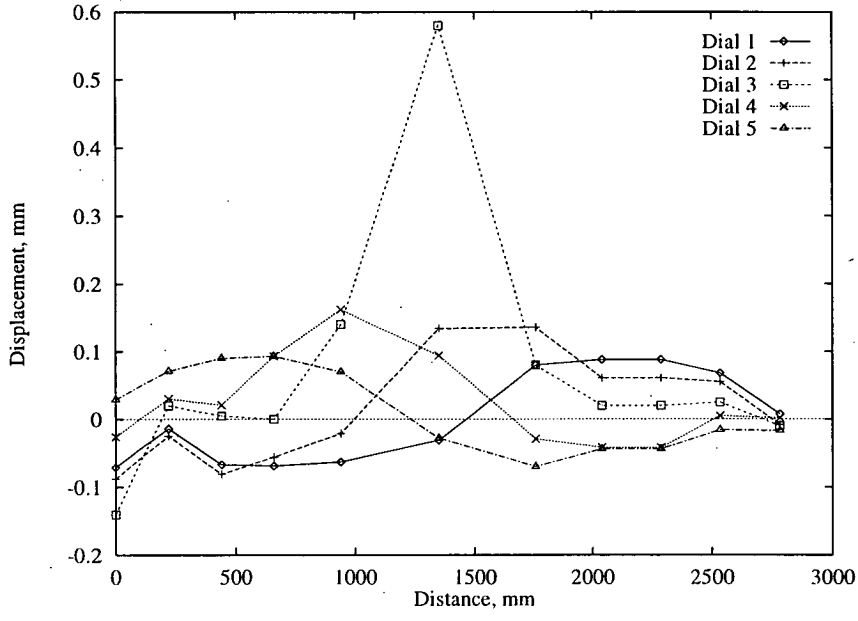


Figure 4.23: Displacement influence line, load = 81kPa, fill height = 300mm

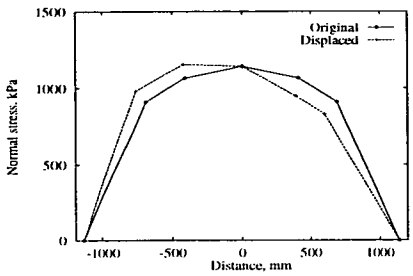


(a) Position 4, $D_{mag} = 1500$

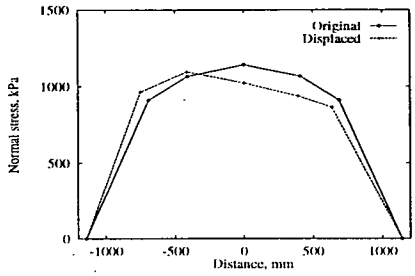


(b) Position 5, $D_{mag} = 1000$

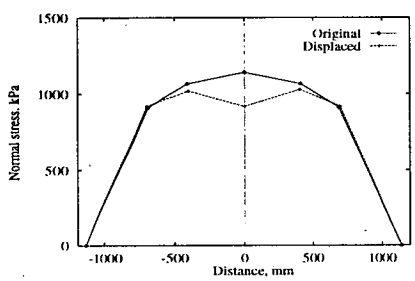


(c) Position 6, $D_{mag} = 500$

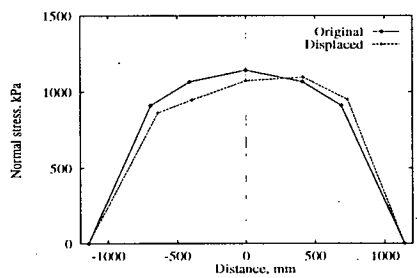


(d) Position 7, $D_{mag} = 1000$

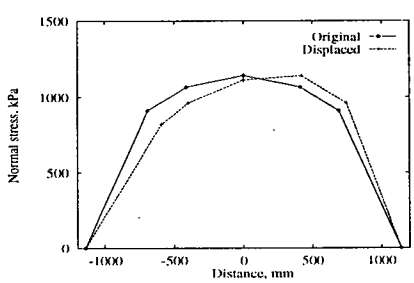


(e) Position 8, $D_{mag} = 1500$

Figure 4.24: Deflected shape of arch. Load positions 4-8

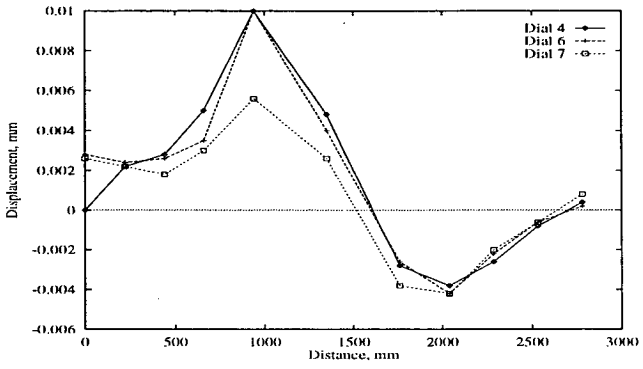


(a) Loading line 'a'

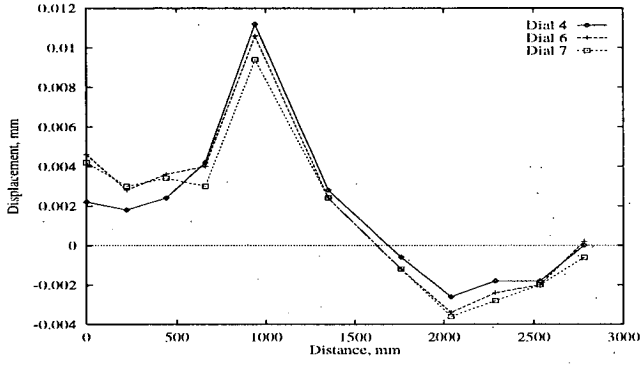


(b) Loading line 'b'

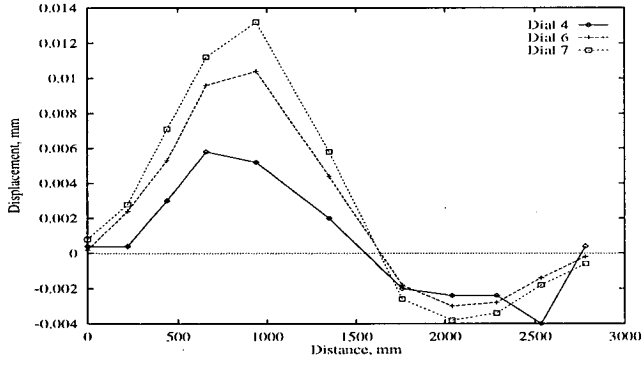


(c) Loading line 'c'

Figure 4.25: Transverse deflection results

# Chapter 5

# Thermal analysis of Kimbolton Butts bridge

## 5.1 Introduction

The research described in this chapter is an element of the process of monitoring an instrumented masonry arch bridge. This area of research investigates the thermal loading of the structure and how this affects arch behaviour. Some of these thermal effects have been shown to have a significant influence on stresses and strains throughout arch bridges, particularly with respect to the arch and fill interaction.[125] The work presented here examines the capability of linear finite element techniques to model and analyse the thermal loading problem induced by the range of observed temperatures. Features of arch-fill interaction and that of the road surface and spandrel walls are described and the approach to the numerical analysis is outlined using the data obtained during the construction of the arch bridge. It has been shown previously[20] that thermal effects produce changes of a significant magnitude to affect the behaviour of the bridge structure, and as such represents an important factor in arch bridge assessment.

Today there are a number of different methods available for the assessment of masonry arch bridges. The majority of these provide information about the predicted ultimate failure load and mechanism, based on the arch geometry and material properties of the structure. Any changes therefore in the arch geometry has been shown to have a large affect on the line of thrust and subsequent failure load, thus the extent of any thermal effects may be of importance. The serviceability criteria of a structure is also important since this is the actual limit at which the bridge can be safely used. Thus the elastic phase of analysis of the structure is as important as the ultimate failure load, and as such requires investigation to gain further understanding.

## 5.2 Arch Construction & Instrumentation

The potential to construct and instrument a full scale bridge, important to enable the overall objectives of this type of investigation, arose in 1992, when Cambridgeshire County Council designed and constructed of a new arch bridge. The elevation and relevant dimensions of the arch are shown in Figure 5.1. A 650mm thick brick spandrel wall is connected to the barrel at each side. The road pavement was 450mm thick, consisting of 250mm of asphalt surfacing and 200mm

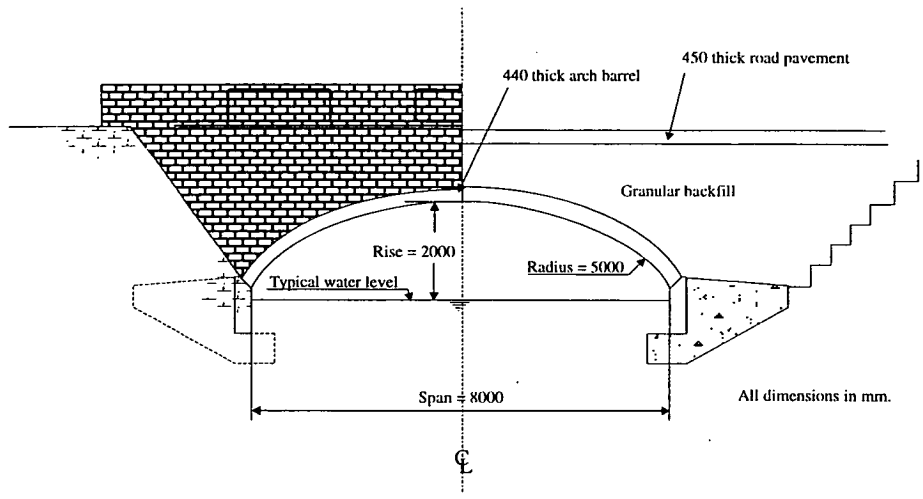


Figure 5.1: Kimbolton Butts bridge, elevation

of Type 1 sub-base. Instrumentation of the structure was jointly undertaken by the University of Edinburgh and the Transport Research Laboratory (TRL), to achieve the following objectives:

- Monitor the soil pressure in the fill, and the stresses and strains on the voussoirs of the arch barrel.
- Identify the affects of changes in temperature on fill pressures.
- Compare measurements with elastic finite element analyses.

The layout of the instrumentation installed within the bridge structure is shown in Figures 5.2 & 5.3. These consist of pressure cells on the arch extrados and within the fill, strain gauges on the arch extrados and thermocouples distributed throughout the structure. The pressures normal to the extrados were measured using Gage Techniques[126] vibrating wire gauge (VWG) pressure cells. The vertical pressure in the fill was measured using Soil Instruments[127] pressure gauges. As shown in Figure 5.3, a total of 24 strain gauges[126] were installed by TRL. Two thermocouples were also installed in the arch and the fill respectively. Control cells were utilised to ascertain the influence of thermal changes on the instrumentation. Full details of all instrumentation can be found in the official TRL report.[17] A suitable data-logger capable of storing up to 13,650 readings was also installed in the cable termination manhole, connected to the instrument cables and programmed to take readings at appropriate intervals.

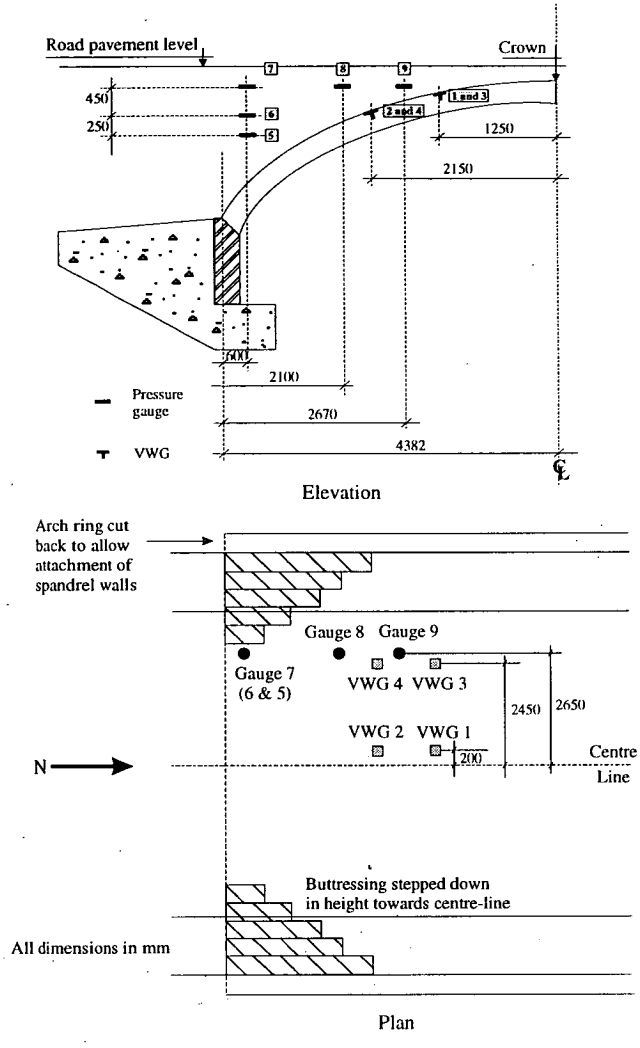


Figure 5.2: Distribution of stress gauges within the bridge

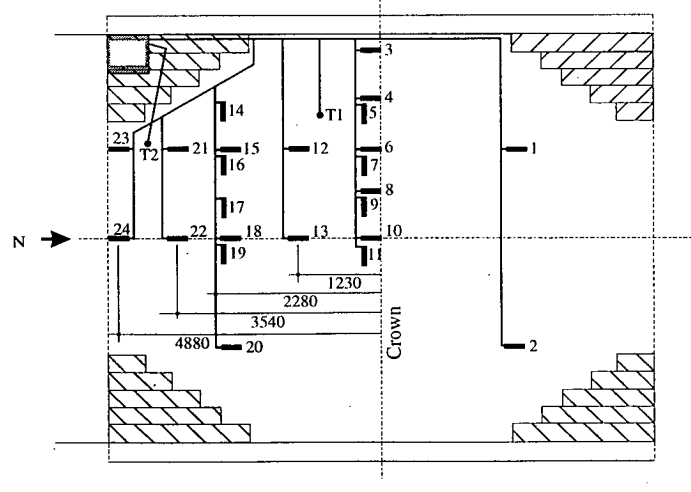


Figure 5.3: Strain gauge distribution

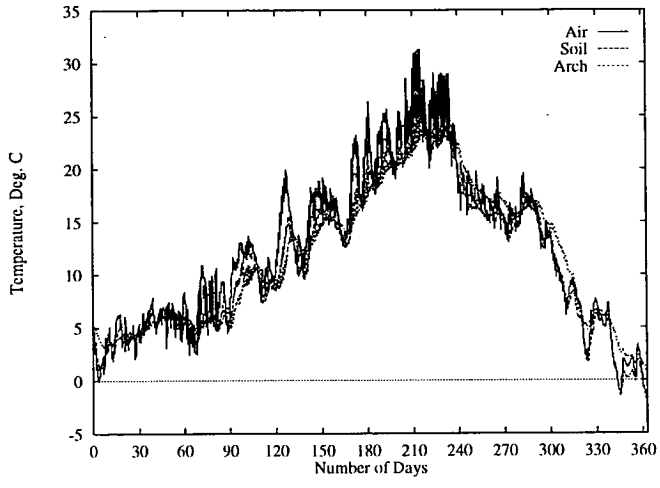


Figure 5.4: Variation of temperature throughout the bridge structure during a yearly cycle (January-January)

### 5.2.1 Temperature variations

The distribution of temperature recorded at the three locations is easily definable and follows expected daily and seasonal patterns, as shown in Figure 5.4. The maximum reading of 31 °C is from the air temperature occurring in the month of August, while a minimum value of below 0 °C was recorded in January of each year. This range is significant with respect to the analysis of the stress and strain results since it has been shown to be cyclic and repeatable. Temperature fluctuations in the fill are in synchronisation with those of the air indicating that heating and subsequent cooling of the material takes place at approximately the same rate. Temperature fluctuations in the arch are slightly out of synchronisation with the others due to the nature of the material. A more meaningful discussion of the different temperature distributions was carried out in conjunction with the analysis of the respective stress and strain results.[20]

### 5.2.2 Normal stress on extrados

Figure 5.5 shows the normal stress measured by VWG gauges 1, 2 and 3 throughout the same time period as the previous temperature measurements. VWG 4 readings are not included since spurious results are obtained from the cell not consistent with the other cells or any of the temperature variations. The

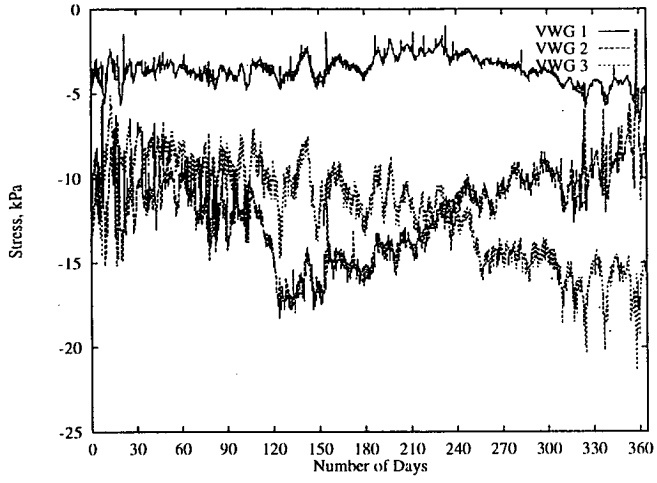


Figure 5.5: VWG stresses for gauges 1-3

stress fluctuations are of a variable nature. Gauge 2 indicates a greater degree of sensitivity than Gauges 1 & 3, where a significant difference in stress readings of up to 20 kPa in any given day is evident. Temperature correction was unnecessary for these cells due to the nature of their construction. Although small variations are evident throughout the year, no global permanent changes in stress have taken place.

### 5.2.3 Vertical pressure in fill material

The pressure gauges within the fill have a significant sensitivity to temperature variations and therefore the measured values require some correction using the results obtained from the dummy cell. Figure 5.6 shows the corrected variation in pressure with time for VWG's 5 to 9. As the gauges come close to the surface and closer to the mid-line of the bridge the reduction in pressure for the same temperature changes is observed to increase, by a maximum value of 50 kPa. This affect has been explained by the increasing temperature reducing the stiffness and so the restraining effects of the road surface on the soil.[20]

### 5.2.4 Strain on extrados

All strains are calculated from a base value taken from each instrument at the time of installation on the arch. The global values of strain at gauges 19 to 24, shown in

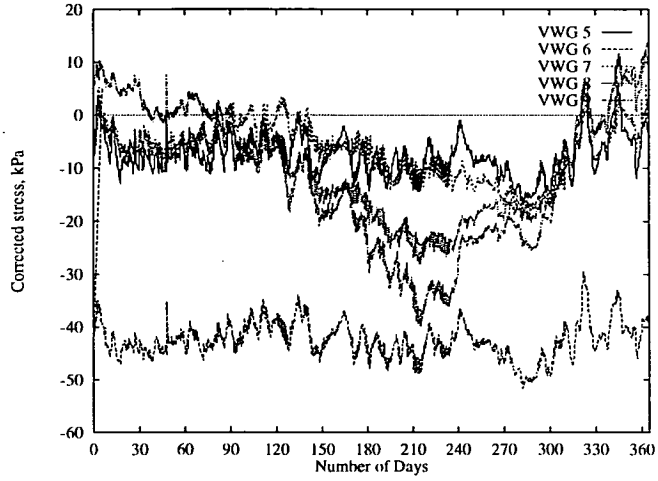


Figure 5.6: VWG stresses for gauges 5-9

Figure 5.7*a*, are indicative of the actual strains on the arch extrados induced from the placement of the fill material and road surfacing. The smaller fluctuations are a function of the temperature variations. The results at these gauges are representative of the fluctuations at most other gauges. The strain gauge results have been corrected for temperature sensitivity by exactly 12 $PPM/^oC$, or 12 micro-strain of compressive strain, to produce Figure 5.7*b*. Strain gauge 10, not shown here, results in the maximum overall reduction in compressive strain of 208 micro-strain for the range of temperatures recorded. A positive reading indicates an increase in tensile strain.[17] These changes in length and therefore strain are thought to be due to the fact that the arch barrel is only partially restrained by the abutments which is normally the case in arch bridges. As the temperature increases, the arch barrel tends to expand and lengthen, which in turn causes a reduction in the compressive strain on the extrados. This behaviour is purely elastic and strain returns to approximately the same level for equivalent temperatures at the beginning and end of the collection period. It should also be noted that the maximum reduction in strain occurred close to the centre line of the arch while the minimum reductions occurred closer to the springings. The average reduction in uncorrected strain of all the gauges is 82 micro-strain, a strain requiring significant loading during the load tests.

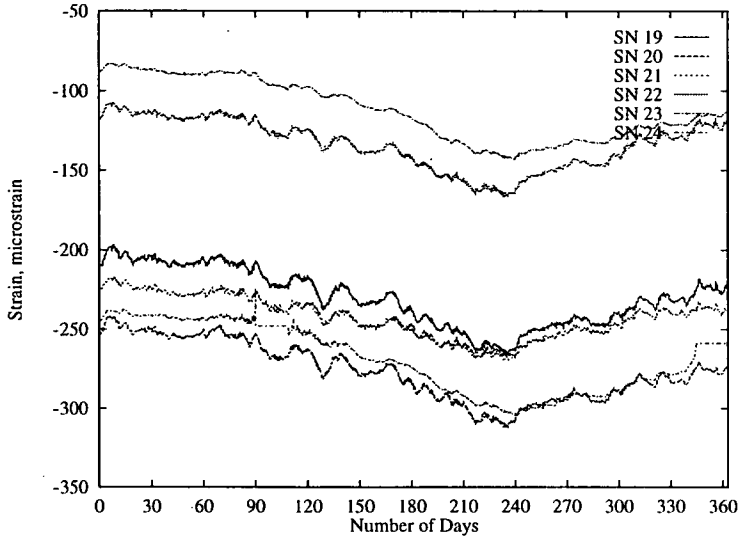


(a) Uncorrected strain

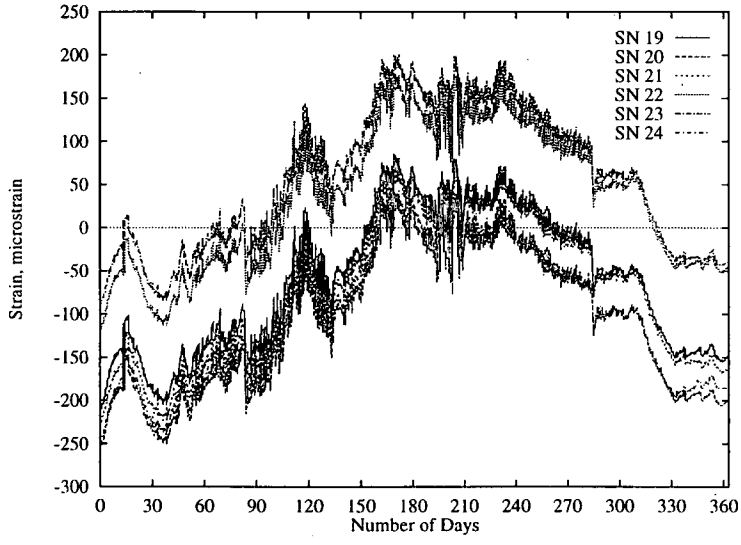


(b) Corrected strain

Figure 5.7: Strain gauge readings, Sn 19 - 24

## 5.3 Thermal modelling and analysis

### 5.3.1 Choice of assessment package

It was obvious from the previously presented results that significant and repeatable thermal effects had been observed, some of these changes having some complicated 3-D effects. The thermal analysis of a cross section of the structure ignoring the spandrel walls, (2-D analysis), and a section including the spandrel wall, (3-D analysis), was therefore required to try and replicate these observed affects. ABAQUS[128] was chosen to perform this analysis since it provides a comprehensive suite of programmes useful in many fields of finite element analysis, including the necessary thermal option. The package was also well known within the department and so seemed to be the natural choice for the analysis. The ABAQUS finite element system includes the following programmes:

- ABAQUS/Standard, a general-purpose finite element programme;
- ABAQUS/Pre, an interactive preprocessor that can be used to create finite element models and the associated input file for ABAQUS.
- ABAQUS/Post, an interactive postprocessor that provides contour plots, animations, and tabular output of results from the results files.

At the time of analysis the pre-processor package was not available. Since initial modelling would be complicated, particularly for the 3-D analysis, an alternative pre-processor was required which had to be powerful enough to create the required model and also compatible with ABAQUS requirements. *Hypermesh*[129] was chosen as the suitable alternative since it provides a powerful modelling tool with many of the required element types and allowed exporting of the model data in suitable formats.

Since ABAQUS analysis modules are batch programmes, so the objective for a successful analysis is to assemble an input file which describes a suitable problem in order that ABAQUS can provide a suitable analysis. Input files for complex simulations can be large, but can be managed by using features built into the programme's input structure. Typical soil model types are allowed for, in addition linear and non-linear behaviour can be modelled. All data definitions in ABAQUS

| Model type | No. of elements | No. of nodes | Displacement (mm) |
|---|---|---|---|
| 2-D | 240 | 435 | 1.678 |
| 2-D | 704 | 1025 | 1.677 |
| 2-D | 960 | 1587 | 1.677 |
| 3-D | 656 | 948 | 1.454 |
| 3-D | 960 | 1587 | 1.454 |

Table 5.1: Affect of element number on vertical displacement at the crown

are accomplished with option blocks which are sets of data describing a part of the problem definition. The user chooses those options that are relevant for a particular application. Options are defined by lines in the input file. Each option is introduced by a keyword line followed by the necessary data lines.

It is normal to validate a computer package being used to analyse any specific structure, in some cases this involves achieving convergence of results. It has been shown that as the elements get smaller, producing almost constant strain conditions, the accuracy of results is generally improved. This however can produce problems due to the size of input files and subsequent output files required for such suitably large meshes. From both the idealised 2-D and 3-D analysis it was shown that increasing mesh density above a certain level has little further influence on stresses, strains or deflections recorded for the model. The size of the mesh and the respective sizes of the individual elements has a great affect on the size of the output files, but a decreasing influence on the resulting values. As can be seen in Table 5.1 it is clear that for subsequent runs with increasing element numbers the results for displacements quickly converge. Since further increase in accuracy is not required it was decided that a suitably large mesh had been used to give accurate enough results. Nominal meshes shown in Figures 5.8 & 5.9, were used for the subsequent thermal analysis.

Only a brief parametric study has been performed since the geometric and material properties are all accurately known. The load dispersal throughout the fill for various meshes were tested by varying some of the material properties and their influence was found to be small. The material properties included the modulus of elasticity, Poisson's ratio, density and thermal expansion. Normal and

| Parameter | Units | Fill | Arch | Surfacing |
|---|---|---|---|---|
| Density ($\rho$) | $N/mm^3$ | $16.5 \times 10^{-5}$ | $22 \times 10^{-5}$ | $14.5 \times 10^{-5}$ |
| Young's modulus (E) | $N/mm^2$ | 5.6 | 10000 | 200 |
| Poisson's ratio ($\nu$) | - | 0.4 | 0.2 | 0.4 |
| Thermal expansion ($T_e$) | $K^{-1}$ | $1.23 \times 10^{-7}$ | $6 \times 10^{-6}$ | $1.23 \times 10^{-5}$ |

Table 5.2: Bridge material properties

shear stresses are plotted over regions and have been shown to be insignificant on the overall stress distributions through the soil. A non-linear elastic analysis was used to model the arch within the dead and thermal range of loading, which has previously been shown to be within the anticipated elastic range of the arch bridge structure.

### 5.3.2 Finite element model

Since no significant differences have been measured between the different sections of the bridge it was felt justifiable to analyse only one quarter of the structure for both the 2-D and 3-D analysis, saving greatly on processor time and memory. This was felt justifiable since the bridge has previously been well documented, and the parameter being investigated is the thermal loading which is applied uniformly across the entire structure. The main reason why a 3-D analysis package was required, allowing the affects of changes in the transverse properties of the bridge to be investigated, is because the presence of the spandrel walls has a large influence on the stiffness of the bridge structure and many other affects.

The bridge was modelled using 8-node isoparametric brick elements. Each element has 8 Gauss points, allowing accurate readings to be obtained throughout the element, especially around the vicinity of the instrumentation. The meshes chosen for the final analysis, (Figures 5.8 & 5.9), represent the different problems being investigated, the first ignoring the affects of any spandrel wall, and the second with the affects of these walls included. The properties of the materials used in the analysis are summarised in Table 5.2. These values have been extensively described in the report by Fairfield,[130] and do not require further expansion here. The arch barrel properties are those recommended by the TRL

and Page et al[4] and for the surfacing based on those suggested by NAASRA.[131] These values also coincide with ranges suggested by Jackson.[132]

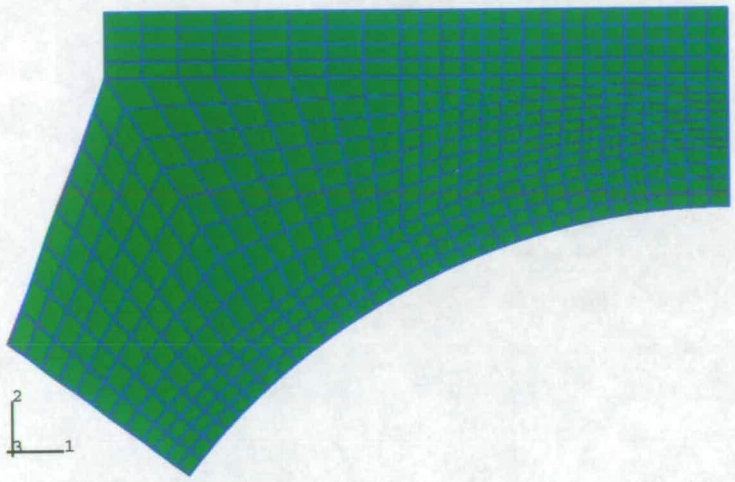


Figure 5.8: 2-D model used for the analysis

The axes direction numbers, 1, 2, and 3, shown in Figures 5.8 & 5.9 have been defined to be the $x$, $y$ and $z$ axes respectively. Nodal restraints were defined to correctly restrain the model at the abutments and springings, while at centre span the edge is unconstrained only in the y direction. The importance of the pre-processor was apparent at this stage since this allowed selection of node or element sets, greatly simplifying restraining of the structure. The model initially undergoes gravity loading to achieve the correct dead load conditions representing the present state of the structure, at the initial bridge temperature. After the gravity loading was completed the model was loaded thermally over the range of temperatures observed, applied via the temperature input parameter incorporated into the analysis package. The dead weight and initial displacements were checked after each loading stage in order to give confidence in the model. After each loading stage the stresses, strains and deflections are recorded for the model and stored for later analysis with ABAQUS/post. The ABAQUS input data file used for the 3-D analysis is included in Appendix C.

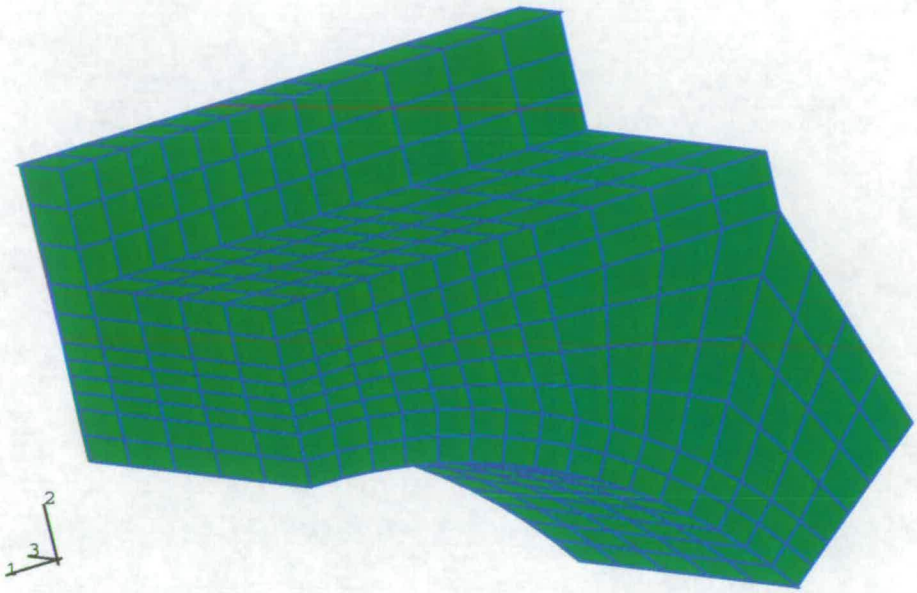


Figure 5.9: 3-D model used for the analysis

## 5.4 Output from FE model

### 5.4.1 Output Variables

The output variables requested from the input file for an analysis are given sign conventions prescribed from the input data and then defined by ABAQUS. The sign conventions are important since all output from ABAQUS is given with these prefixes. Figure 5.10 shows how the sign conventions are attributed, with the prescribed numbers relating to each axis of the model. For example 1, 2 and 3 relate to X, Y, and Z axes respectively. The strain axis sign convention is identical to that for the stress apart from the prefix is E instead of S being assigned. Deflection output has the prefix U, shown as U1, U2 and U3 which correspond to the X, Y, and Z axes respectively.

- S11 - XX direct/normal stress

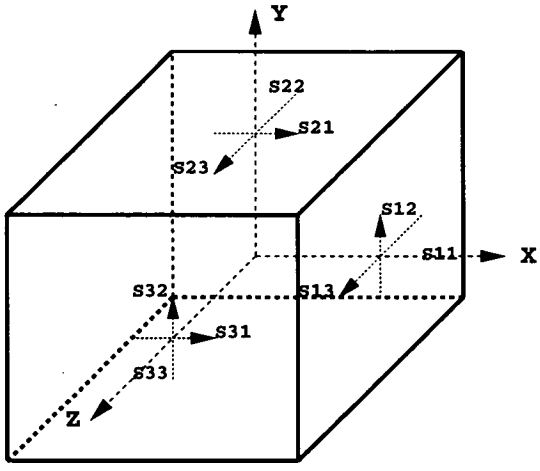


Figure 5.10: Sign convention for elements

- S22 - YY direct/normal stress
- S33 - ZZ direct/normal stress
- S12 - XY shear stress
- S13 - XZ shear stress
- S23 - YZ shear stress

### 5.4.2 Deflection

From the dead loading only conditions a small deflection is recorded at the centre of the span, reducing as the springing is approached. These readings are as expected being due to the elastic compression of the arch bridge material under its own dead weight. It is the same displacements that would occur when "centring" supporting the bridge during construction was removed. Readings from the actual bridge were however not taken so direct comparisons cannot be made at this stage.

Deflection results due to the applied thermal loading indicate a small but not insignificant rise of the centre of the span. The deflections produced by the different analyses are shown in Figure 5.11, and are obviously dependent upon the distance from the spandrel wall. The displacements are taken from along line A in Figure 5.12. A uniform displacement is recorded for the idealised 2-D

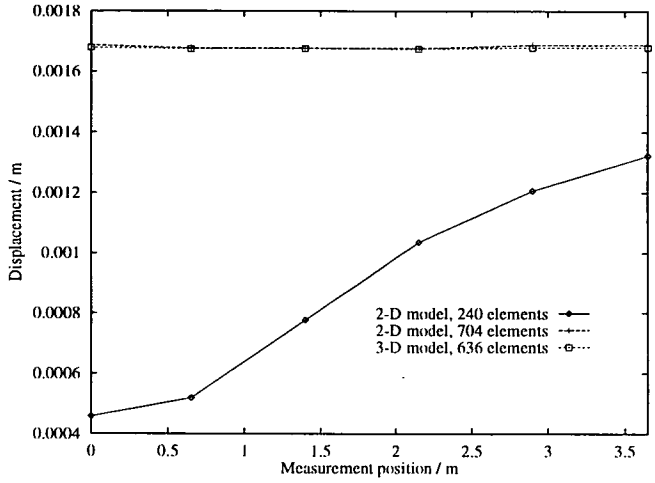


Figure 5.11: Vertical displacement across the centre span (line A in Figure 5.12)

models while for the 3-D including the spandrel wall, the deflection results at the centre of the span increase as they get further away from the restraining affects of the spandrel wall towards the centre line of the bridge. Even far away from the spandrel wall the restraining and stiffening affects of the wall are still having some affect. The presence of the spandrel wall seems to reduce the upwards displacement of the arch barrel close to it, while away from it, the deflection increases. The deflections produced from the different models are almost unaffected by the number of elements used in the model.

### 5.4.3 Stress & strain output

The stress and strain output from the different models show a gradual change in each value throughout the bridge structure produced by the thermal loading. The main stress changes observed are generally produced in the arch barrel, as would be expected since the arch barrel is restrained, has the second largest expansion coefficient and elastic modulus used in the model, and is the main load bearing structure of the arch bridge. The largest increases in stress is in the area of the quarter span. The changes in strain are produced throughout the whole structure, but with the main changes being within the fill material. All plots of these values cannot be shown due to the lack of space, but various figures are shown as an illustration. It has also been shown that the presence of the spandrel walls has a large affect on the stresses and strains throughout

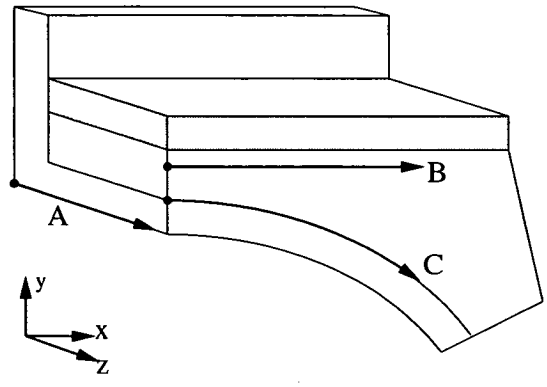


Figure 5.12: Defining where results have been obtained

the structure. The values are similar for all meshes without the spandrel walls attached, but significantly different readings are obtained with the spandrel wall attached. The maximum values are similar but the values of strain produced are generally reduced in magnitude, and this affect increased for the fill closer to the spandrel wall.

From the recorded strain results it is has been shown that the average strain increase is of the order of 200 micro-strain, with a peak increase of the gauges in line to the arch of 300 micro-strain. It can be seen in Figure 5.14 that for the shear strain along the extrados that a similar distribution is produced, with the maximum increase in strain being closer to the centre of the span and then reducing the further away from the crown, resulting in an decrease in strain past about 1/4 span. The maximum increase in tensile strain along the lines shown is of a similar magnitude and distribution.

For the normal stress on the extrados results showed a smaller change in the measured values, of only a few kPa. Comparisons of normal pressure and shear strain plots are shown in Figures 5.13 & 5.14 respectively. These plots show two lines of stress going through the fill to give an idea of the variation in this area.

For the stresses and strains a similar affect is produced by the addition of the spandrel wall as was seen for the deflections. For the stresses, there is an increase the further away from the restraining affects. This is also produced for the strains. The measurement position axis in Figure 5.14 is the angle taken from a vertical line going through the crown.

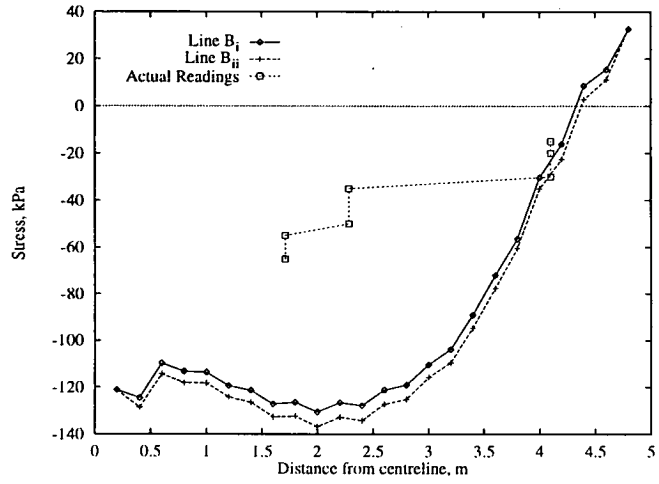


Figure 5.13: Stress in the fill (along line B in Figure 5.12)

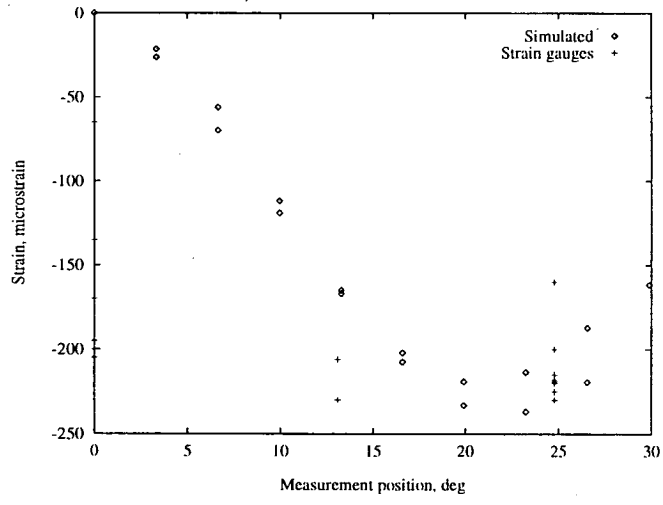


Figure 5.14: Measured and calculated strain along the arch extrados (line C in Figure 5.12)

### 5.4.4 ABAQUS post output

Using the ABAQUS post processor enables the input and output models and files to be viewed in greater detail. Different orientations of the model can be chosen and the desired output variables can be viewed in the form of contours. This has advantages over looking at tables of output results, since trends and affects are made much more easily identifiable.

It is possible with ABAQUS post to view variables in the major axes giving contours for each desired output. For the 3-D analysis especially it is initially obvious that the major stress changes produced in the brick arch barrel and spandrel wall are much greater than any in the fill material. These high stresses mask the stress changes within the fill on the contour plots, so values are required to be taken and plotted separately. The stress within the fill reduces with the rise in temperature. Plots for this output is shown in Figure 5.15.

For the strain results, the spandrel wall again has a marked affect on the outputs. When the contour plots are viewed this gives a clearer view of how the strains vary. For E22 there is an increase in strain in the arch barrel and the road surface at the crown. A similar reduction in strain is produced in the fill, whose affect increases the further away from the spandrel wall the element is. As the quarter span is approached the strain reduction is not as much. Almost the opposite affect is shown for the E11 strain, with the strain decreasing near the quarter span, this affect again reducing closer to the crown. The E11 strain increases for the arch barrel but decreases in the road surface. A better way of showing this is with the output files from the ABAQUS post, plots of variations of either stress, strain or deflection are possible. Examples of which are available in Figure 5.16.

## 5.5 Live load monitoring

Further load tests on the structure were suggested to be useful for future work by the previous author[20] of the original load tests. This however proved impossible since the structure was flooded in 1998 due to a period of sustained rain. This flooding unfortunately compromised the protection provided for the data-logger and the power supply unit causing permanent corrosion of the unit and also

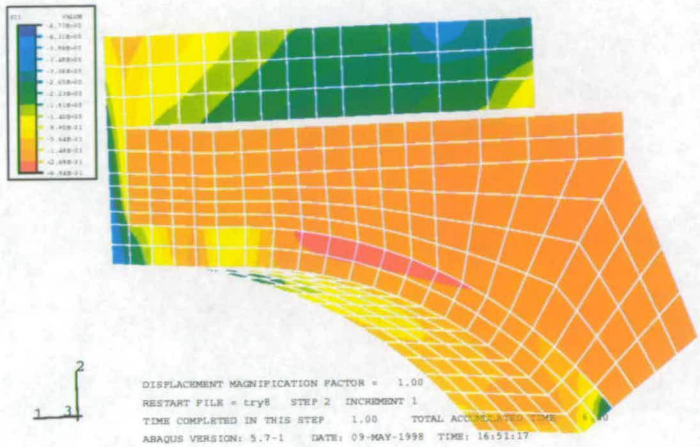


(a) S11 stress

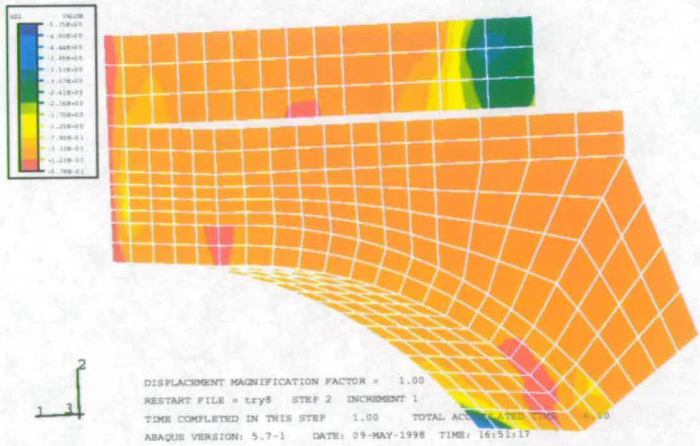


(b) S22 stress

Figure 5.15: Stress throughout 3-D structure

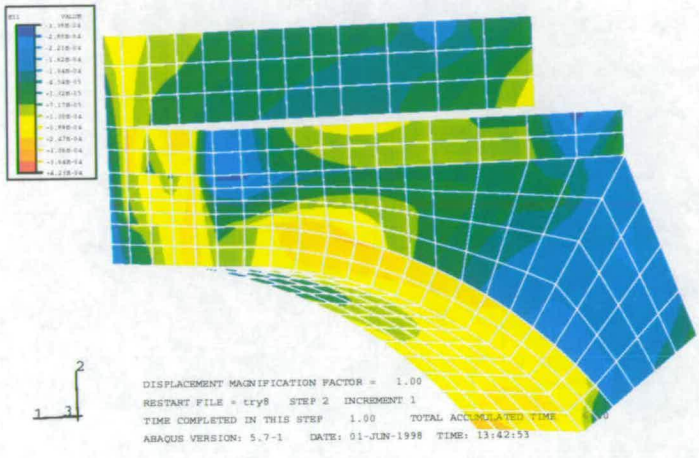


(a) E11 strain

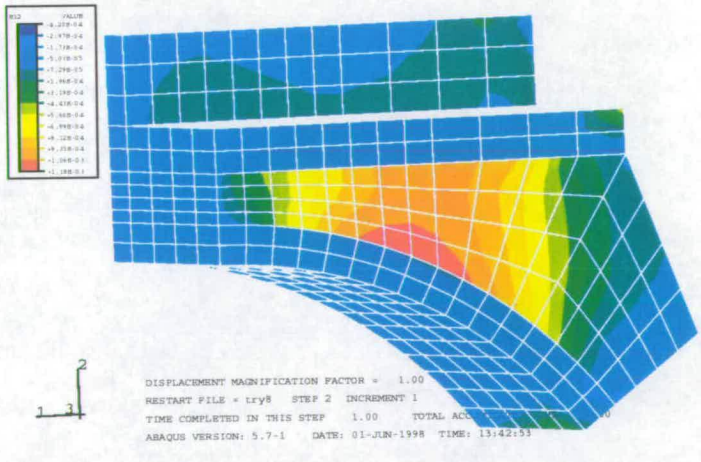


(b) E22 strain

Figure 5.16: Strain throughout 3-D structure

the loss of the previous two months stored data. The loss of the data logging equipment then precluded load tests being repeated in order to see if any changes had occurred during the monitoring period of the structure. Up to this point almost four years recorded data had been successfully logged and analysed, resulting in a large quantity of information with which to relate to other methods of assessment.

Shortly before the data logging equipment was lost a single working day live load monitoring was conducted. This involved collecting readings from all instrumentation at a much greater frequency than previously in order to get the live traffic load response of the structure. To enable the collection period to be varied the data collection programme required altering. The collection period was however governed by the time taken for the data logger to take reading from all the instruments. The time for this to occur was about 20 seconds, so a collection frequency was chosen to be every 30 seconds. One obvious drawback of this rate was that the reading from all instrumentation would not all be instantaneous, and so dissipation of the load was difficult to calculate throughout the structure. When a reading is recorded at one cell, the value recorded at another is not necessary due to the same loading case and may be from another vehicle or more likely the same vehicle at another position on the bridge.

The results, which present a significant quantity of data, indicates which of the cells placed within the structure were still working correctly and how the stresses and strains vary within the structure. The cells which are working correctly, considered to give relatively constant readings, can then be inspected to obtain useful information. It was initially clear that quite a high percentage of the different instruments were giving strange readings, the actual reasons for this being unclear. Whether it is due to the instrument being unable to respond to the data-logger or the fact that the instrument is no longer working, is not clear.

It is clear from the data trends that the change in measured values are much smaller than those recorded for the change in temperature. In fact the change in measure stress is on average less than 1 $kN/m^3$. These values may have missed the peak value while a vehicle was on the structure, and also indicate that load distribution is very quickly dissipated since large peak values were not recorded.

## 5.6 Conclusions

1. Significant overall temperature ranges were recorded over the time period at all three locations with a maximum temperature in air of approximately 31°C and a minimum of -3°C.

2. No significant global changes in pressure or strain were observed for the cells on the extrados or in the fill over the collection period.

3. A reduction in stress and compressive strain was observed for a corresponding increase in temperature at the cells.

4. Results from the model show that large stresses are produced in the arch barrel and spandrel wall, much greater than that produced in the fill material.

5. Temperature correction highlighted an overall reduction in compressive strain with a corresponding increase in temperature.

6. A reduction in compressive strain was found to be reproduced from the thermal analysis.

7. The thermal analysis produces similar trends to that observed over the collection period.

8. FE analysis reproduced many of the thermal affects successfully.

# Chapter 6

# Discontinuous modelling of masonry arches

## 6.1 Introduction

This section investigates the potential use of new discrete based techniques in analysing masonry arch bridges. The discontinuum elements differ from continuum elements mainly due to the existence of contacts between discrete blocks or particles which make up the structural system being modelled. Over the last ten years numerous investigations have been conducted utilising finite element modelling of the arch and soil-structure interaction has proved to be a useful tool providing useful data particularly at lower load levels, up to 40% of the estimated failure load. However at higher load levels these methods have not been completely satisfactory due to the nature of the arch bridge mechanism. It has initially been hypothesised that discrete computerised techniques would provide a natural framework to analyse the various phenomena of a complex back-fill arch bridge interaction problem and the discontinuous nature of masonry. These problems include such things as block deformation, large displacements and rotations, load dispersal through the fill, as well as displacement discontinuities. Interface properties between the arch and the fill material and joint properties between the voussoirs are also investigated.

Three different computational tools, a discrete Discontinuous Deformation Analysis method (DDA), a discrete element based analysis using a Particle Flow Code (PFC), and a non-linear finite element method (DIANA) have been used for this purpose, and comparisons have been made with an experimental model. For each package the structural response has been traced up to and beyond the collapse load and the collapse mechanism has been identified. The specific capabilities and limitations of each package are demonstrated and some sensitivity analysis is also included.

To give the three packages a constant structure to model it was decided that the numerical techniques would be compared to a semi-circular single span arch previously developed and tested to failure by Fairfield.[19] Details of the structure are available and the arch dimensions and failure mechanism are shown in Figure 6.1. A line load was applied to the structure at $\frac{1}{3}$ of the span until failure occurred due to the formation of four hinges at a failure load of 38.1 kN.

This research has been undertaken with help from various EPSRC Grants, and the results from this work has already been presented in the final grant report.

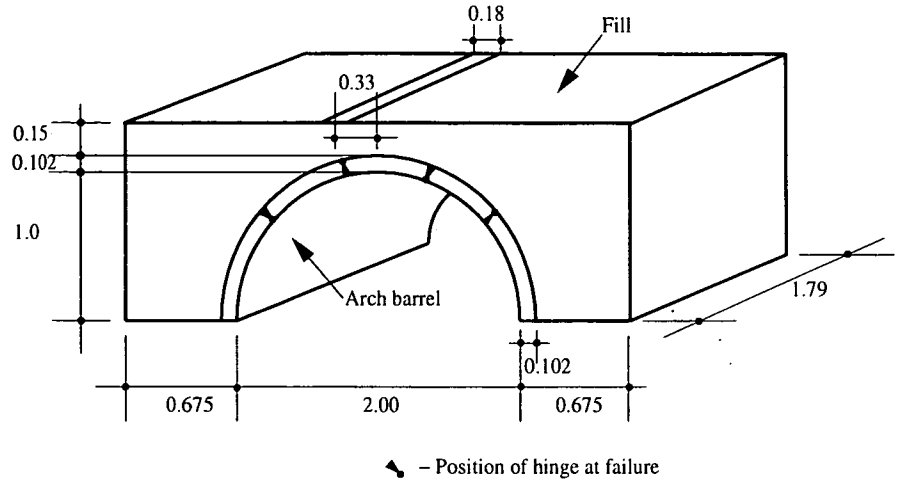


Figure 6.1: The backfilled semi-circular arch experimental model

## 6.2 Discontinuous deformation analysis, DDA

### 6.2.1 Introduction

DDA is a numerical method initially developed to model the behaviour of discontinuous materials such as fractured rock masses.[70,71] This computer based method is capable of analysing a system of discontinuous blocks under general static or dynamic loading, with rigid body movement and deformations occurring simultaneously. Arch analysis involves interaction between discrete elements often with large displacements and finite strains. DDA incorporates dynamics, kinematics and the elastic deformation of blocks and models actual displacements of the individual blocks. This allows predictions to be made as to the mode of failure and amount of displacement required. The present package is based on original computer programmes written by Gen-hua Shi, and its new conversion for UNIX and windows environments make it more useful to practising engineers.

Both static and dynamic analysis requires the use of time steps. For each time step block displacements are kept small, giving a first order approximation shown in Equation 6.1. Shi further expressed these small displacements,$u$ and $v$, of the block centre as a shape function of rigid body motion and small straining of an element as in Equation 6.2.

$$\begin{bmatrix} u \\ v \end{bmatrix} = \begin{bmatrix} a_0 + a_1 x + b_1 y \\ a_0 + a_2 x + b_0 y \end{bmatrix} \tag{6.1}$$

$$\begin{bmatrix} u \\ v \end{bmatrix} = \begin{bmatrix} 1 & 0 & -(y-y_0) & (x-x_0) & 0 & \frac{(y-y_0)}{2} \\ 0 & 1 & (x-x_0) & 0 & (y-y_0) & \frac{(x-x_0)}{2} \end{bmatrix} \begin{bmatrix} u_0 \\ v_0 \\ r_0 \\ \epsilon_x \\ \epsilon_y \\ \gamma_{xy} \end{bmatrix} \tag{6.2}$$

Where $u_0$, $v_0$ and $r_0$ are the rigid body movements at the centroid $(x_0, y_0)$, and $\epsilon_x$, $\epsilon_y$ and $\gamma_{xy}$ represent the components of the 2-D infinitesimal strain tensor. These six components describe the displacement field for each block deformation vector $\mathbf{D_i}$.

The formulation used is based on the minimisation of potential energy of the system of blocks, and uses the penalty method to prevent penetration of the blocks. This method detects blocks with vertices in contact and then applies numerical penalties, analogous to stiff springs, to these contacts to prevent inter-block penetration. Three types of contacts are considered in DDA, 'vertex to vertex', 'edge to edge' and 'vertex to edge', generally reducing solely to 'vertex to edge' contact problems. For instance, consider blocks $i$ and $j$ shown in Figure 6.2, where the vertex of one block penetrates another block through the edge defined by points $P_2$ and $P_3$. Assuming deformation increments of the two blocks are denoted by $D_i$ and $D_j$ respectively, the penetration in the direction normal to the block side can be expressed as a function of these deformation increments, Equation 6.5.[63]

Any penetration at these contacts adds so much energy to the system, because of the large penalties, that the lowest energy solution will be the one where there is no penetration. This factor acts as both the strength and the weakness of such packages. It is also assumed that the blocks are totally elastic, and the shear resistance at the block contacts are purely frictional and obey the Mohr-Coulomb law. Mechanical interactions, such as loading, block inertia, elastic deformation and displacement constraints due to block contacts and

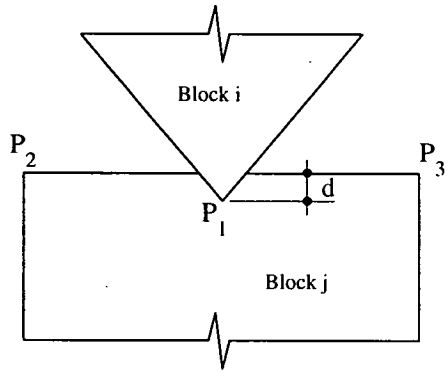


Figure 6.2: Illustration of the vertex-edge contact

boundaries, are formulated in terms of a displacement parameter set. Each six-number displacement parameter describes the displacements of the centre of mass of each block, from which the corresponding locations of the block vertices can be determined. For each time step, the displacements of each block are calculated by setting up and solving the system of equations. The total potential energy is minimised until the state of the contacts becomes constant, a post-iteration contact check is performed, then the positions of the blocks is updated and the programme goes to the next time step. Stresses and strains are constant across the region of each block regardless of size or shape.

DDA uses an implicit formulation, meaning that equilibrium is satisfied at the end of each time step rather than at the beginning, guaranteeing numerical stability. Because of the dynamic equations used, small time steps have to be taken, an accumulation of which gives the displacements and deformations required. The more influence the individual material discontinuities have, the more appropriate the DDA model. A particular strength of the DDA package is that the data it uses is readily available. The geometry, loads acting on the system, material strengths and deformation properties are all known, or easily found for the arch bridge problem.

A distinction is made between the contribution to the potential energy of the whole system arising from the internal strain energy of the block itself and the potential energy associated with any contact conditions or constraints. Minimisation of this potential energy leads to the formation of a system of equations with mixed degrees of freedom (centroid displacement components and strain field parameters) for all blocks.

$$\begin{bmatrix} K_{11} & K_{12} & \dots & K_{1i} & \dots & K_{1n} \\ K_{21} & K_{22} & \dots & K_{2i} & \dots & K_{2n} \\ \vdots & \vdots & & \vdots & & \vdots \\ K_{i1} & K_{i2} & \dots & K_{ii} & \dots & K_{in} \\ \vdots & \vdots & & \vdots & & \vdots \\ K_{n1} & K_{n2} & \dots & K_{ni} & \dots & K_{nn} \end{bmatrix} \begin{bmatrix} D_1 \\ D_2 \\ \vdots \\ D_i \\ \vdots \\ D_n \end{bmatrix} = \begin{bmatrix} F_1 \\ F_2 \\ \vdots \\ F_i \\ \vdots \\ F_n \end{bmatrix} \tag{6.3}$$

$$\left[\underline{\mathbf{K}}\right]\left[\underline{\mathbf{D}}\right] = \left[\underline{\mathbf{F}}\right] \tag{6.4}$$

Each $K_{ij}$ element is a $6 \times 6$ sub matrix, defined by contacts between blocks when $i = j$, and by material properties when $i \neq j$.

$$d = \frac{A}{L} + G^T D_i + H^T D_j \tag{6.5}$$

where $A$ is the area of the triangle defined by the points $P_1$, $P_2$ and $P_3$ and $L$ is the original length of the segment $P_2$ to $P_3$. $G$ and $H$ are the vectors dependent on the initial geometries of both blocks. Depending on the inter-block contact stress state, the contact conditions between these blocks will either allow sliding with no penetration and no tension or impose a no sliding, no penetration and no tension condition. The presence of penalty springs at all positions of contacts contributes to the overall strain energy of the system, which in turn effects the system stiffness matrix as well as the load vector. The formulation leads to a secant iterative scheme until the zero penetration condition is satisfied at all contact points.

Another method which improves the treatment of contacts is the use of the augmented Lagrangian method.[133] This solves for the contact force, $\lambda_i$, with an iterative combination of the Lagrangian multiplier and the previous contact penalty spring method. For consecutive iterations the new contact force is found from Equation 6.6. This method allows contact forces to be found without problems associated with ill-conditioned system matrix as with the penalty method. The selection of the penalty stiffness still effects the convergence rate.

$$\lambda_{i+1} = \lambda_i + (p \times d) \tag{6.6}$$

### 6.2.2 Implementation

The programme is designed to be run in two parts, the first which describes the shape of the system by defining the blocks from the data supplied in a geometry file. The second part performs the transient analysis using the data supplied to it by the analysis file. This allows an analysis with different parameters to be performed without the need to rerun the geometry file. This data is specified using consistent S.I. unit for length, mass, force, time, etc. Further information on the DDA method and how it has been improved can be found in the relevant literature.[76,134]

#### 6.2.2.1 Defining the geometry

Block geometry is input using line segments representing individual block edges, each line being defined by two endpoints, with $x$ and $y$ coordinates and an integer corresponding to the material type. Each line segment may extend beyond the region being defined, since the actual block is defined only as an area enclosed by intersecting line segments.

The DDA programme itself or other editing packages may be used to generate the input files using the predefined input structure shown below. This structure allows the joint and point coordinates which are defined separately to be created within a defined grid, each type defining areas or points of different material or restraint. With DDA all lines with only one intersection are 'trimmed' as they cannot be a block edge, then a search is performed to determine which lines are connected in order that they define unique blocks.

| | |
|---|---|
| 0.01 | *(minimum edge-node distance)* |
| 4 | *(number of line segments)* |
| 0 | *(number of boundary lines - not implemented)* |
| 0 | *(number of material lines - not implemented)* |
| 0 | *(number of rock bolts - not implemented)* |
| 1 | *(number of fixed lines or points)* |
| 1 | *(number of measured points)* |
| 0 | *(number of loading points - not implemented)* |
| 1 | *(number of hole points)* |

10 10 30 10 1 *(coordinates and material type of each line segment)*
10 10 20 20 2
20 20 30 10 2
20 10 20 20 1
21 11 21 11 *(coordinates of endpoints of each fixed line)*
22 12 22 14 *(coordinates of measured, loading and hole points)*

There are three different types of block points which can be specified: fixed, measured and hole. Fixed points are used to prevent a block from moving, and are made using very stiff springs, in the same way as penetration is prevented. Measured points allow the displacements of various points to be recorded and saved during an analysis. If more than one measured point has been used then the results for each point appear on subsequent lines. Hole point, not used in this analysis, are used to indicate tunnels and other excavations. Load is applied to the model with a rectangular block at $\frac{1}{3}$-span with correct cross section and properties.

The output from this geometry subroutine is a graphical representation of the points and blocks that are defined by these lines. There are three output files produced from the successful running of the geometry file.

- block file ... contains a list of the block vertices and joint types which are used in the analysis subroutines
- data file ... Information about how successfully the geometry programme has run
- dcps file ... The postscript file of the section modelled.

#### 6.2.2.2 Running the Analysis

This is performed using another programme file, the input dialogue for which contains the information of the parameters necessary for the analysis. These are listed below with an explanation for each following. Further information can be obtained by referencing the user's manual.[135]

| | |
|---|---|
| 0 | *(0 indicate static analysis, 1 indicates dynamic analysis)* |
| 500 | *(number of time steps)* |
| 1 | *(number of block materials)* |
| 4 | *(number of joint materials)* |
| 0.01 | *(maximum allowable displacement ratio)* |
| 0.01 | *(upper limit of time interval in each time step)* |
| $g_0$ | *(stiffness of contact spring, F/L. Usually 0)* |
| $k_1$ $k_2$ ... $k_i$ | *(number of interpolation nodes, fixed or loading points)* |
| $t_i$ $x_i$ $y_i$ | *(time, displacement or load x and y at time ti)* |
| $m_a$ $w_x$ $w_y$ $E$ $u$ | *(material properties)* |
| 0 0 0 | *(block material properties: x, y, xy components of initial stress)* |
| 0 0 0 | *(block properties: x, y, xy incremental strains)* |
| 0 0 0 | *(block properties: x, y, xy components of initial velocities)* |
| 37 3500 3450 | *(joint properties: friction angle, cohesion, tensile strength)* |
| 32 0.0 0.0 | |
| 1.4 | *(factor of over-relaxation)* |

Where:

| | |
|---|---|
| $g_0$ | stiffness of contact spring |
| $k_i$ | number of interpolation nodes, fixed or loading points |
| $m_a$ | mass per unit area |
| $w_x$ | weight per unit area in x-direction |
| $w_y$ | weight per unit area in y-direction |
| $E$ | Young's modulus |
| $u$ | Poisson's ratio |

Dynamic analysis allows the velocities of the blocks to be maintained throughout the analysis, while the static option resets the block velocities to zero at the start of each time step. In this study static analysis is used in order to reduce the potentially noise effects produced by a dynamic analysis. The maximum allowable displacement ratio is the maximum displacement allowed per time step divided by half the vertical dimension of the region defined by the geometry. Contacts can be detected if block vertices are within a distance of 2.5 times this value. The recommended range is 0.001-0.01. The analysis subroutine models the behaviour of the system of blocks as it progresses through each time step. The analysis is

performed until further convergence (inter block penetration less than a required tolerance) cannot be achieved. Four output files are created after each analysis:

- Results.txt ... contain data about the contacts, iteration convergence, maximum displacement and size of time step
- a.txt ... ... contain data about the contacts, iteration convergence, maximum displacement and size of time step
- Blocks.out ... contains the coordinates of the blocks at chosen intervals throughout the analysis allowing replay of results
- Disp.dat ... lists the number and coordinates of the measured points for each time step.

### 6.2.3 Model improvements

#### 6.2.3.1 Mesh discretisation

The method utilised to produce realistic shaped elements for the fill material is to use a Veronai tessellation technique to create the input mesh. This method has previously been used by Tran[136] for the micro modelling of concrete structures for the analysis of damage due to cracking. A procedure based on the Delaunay triangulation,[137,138] is used initially to produce simpler and more realistic shaped elements.

Initially the area was covered with regularly distributed points in the $x$ and $y$ plane, where the distance between the points may be imagined as the average radius of each polygon. All points are then randomly moved by a small distance in order to create a random mesh. A triangle mesh is created from these points based on the Delaunay triangulation technique. Finally the Veronai polygons are calculated by connecting the centre of each adjacent triangle, until the final polygons are produced. A valid Delaunay triangulation is shown in Figure 6.3. This method produces a fill as an area of randomly generated particles of a definable average size. Figure 6.18*a* shows the 2-D model of a standard arch where the area of the fill has been discretised using the Veronai polygons.

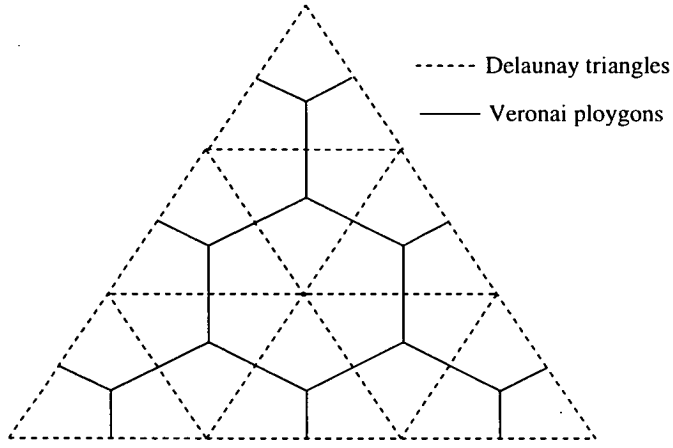


Figure 6.3: Illustration of Delaunay triangulation and Veronai tessellation

A further development was a sub-block system for dividing the arch voussoirs with strong jointed blocks. This was done in order to provide a better stress distribution across the voussoir since DDA assumes the stress being constant for each block. This was done as it was felt that the constant stress state could effect the failure mode and therefore load produced.

#### 6.2.3.2 Displacement control procedure

In this type of procedure the analysis is conducted by applying prescribed displacements to selected points within a structure. This is required to trace the structural response beyond the ultimate load level and get post peak behaviour. A displacement point can be selected within DDA and its displacement constrained using two stiff springs in the $x$ and $y$ directions. Assuming a displacement, $(\delta)$ is given to a predefined point within the model as shown in Figure 6.4. The displacement constraint computed from the spring stiffness at that point along the $x$ and $y$ directions are denoted by $u$ and $v$ respectively. Thus the actual displacement of the the spring, $(d)$ is given in Equation 6.7.

$$d = \delta - \sqrt{u^2 + v^2} \tag{6.7}$$

Assuming that the prescribed displacements at the point along the $x$ and $y$ directions are denoted by $\delta_x$ and $\delta_y$ respectively, and the corresponding spring

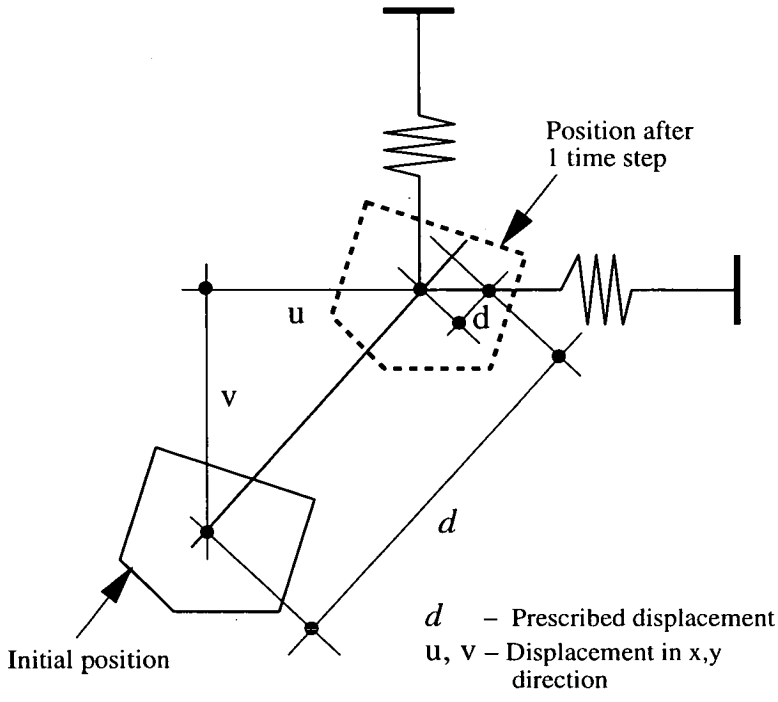


Figure 6.4: Illustration of prescribed displacement at a point

displacements are $d_x$ and $d_y$, then;

$$\begin{aligned} d_x &= \delta_x - u \\ d_y &= \delta_y - v \end{aligned} \tag{6.8}$$

If two springs with an equal stiffness of $p$ are used in the $x$ and $y$ directions, then;

$$\begin{aligned} f_x &= p \times (\delta_x - u) \\ f_y &= p \times (\delta_y - v) \end{aligned} \tag{6.9}$$

The spring strain energy can then be calculated as well as the contribution to the stiffness matrix and the force matrix due to the spring.[138]

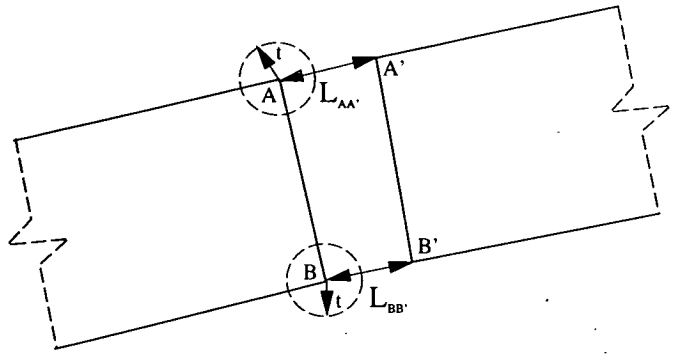


Figure 6.5: Joint between voussoirs

#### 6.2.3.3 Failure criteria

Within DDA the arch barrel is idealised as a set of rigid voussoirs linked together with mortar joints. In this section a simple procedure is presented to identify the different modes of failure by observing the separation between block joints. The application of DDA to masonry arch bridge analysis involved an iterative process with small movements in the structure for each time-step with an appropriate load increment. This is continued up to the collapse, and thus the relative displacements between the voussoirs is monitored.

A failure mechanism is identified by defining some rules for the failure possibilities. Evaluating the relative displacements between each adjacent voussoir within the arch allows the formation of hinges to be detected. The interpretation for a failure mode is illustrated by considering a joint between two adjacent blocks shown in Figure 6.5. The distance between points $A$, $B$ and $A'$, $B'$ are given by $L_{AA'}$ and $L_{BB'}$ respectively. A tolerance factor, $t$, is introduced to allow a defined displacement to occur before a hinge is indicated, meaning the hinge will not be highlighted until either $L_{AA'}$ or $L_{BB'}$ go outside the circle of radius $t$.

The possible hinge criteria are illustrated in Figure 6.6. Example $(a)$ demonstrates a safe solution to the analysis, when there has been relative displacement, but it has not exceeded the tolerance factor and so a hinge has not officially formed. There are two main types of failure presented, hinge formation at the intrados or extrados, $(b)$ and $(c)$ respectively, and a shear failure, $(d)$, although a combination of the two will also be detected. A failure mechanism will be present when at least four of these failures have been detected.

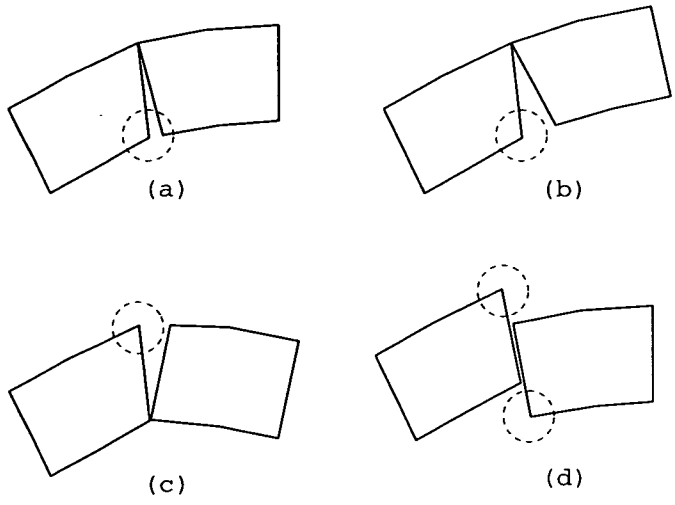


Figure 6.6: Failure mechanisms considered

## 6.3 Particle flow code, PFC

### 6.3.1 Introduction

The present particle flow codes, $PFC^{2D}$ and $PFC^{3D}$ have been developed from a distinct element method originally validated for research into granular assemblies by Cundall and Strack.[139] Granular material generally acts as a set of distinct particles, which displace independently from one another and interact at contact points. The measurement of the stresses and strains within real material samples are difficult and numerical models offer a powerful way of modelling assemblies of idealised particles. In PFC the equilibrium contact forces and displacements of an assembly are found through a series of calculations tracing the movement of individual particles. These movements are a result of disturbances originating at boundaries, a dynamic process. PFC is based upon the idea that for a chosen time step the disturbances produced can only propagate from one particle to its immediate neighbours. The resulting forces acting on each particle due to these interactions are determined after each time step. In this way the calculation method is an explicit time-stepping scheme involving many thousands of time-steps. For each time step the programme alternates between Newton's second law (force = mass × acceleration) and a force displacement law at the contacts, each integrated twice for each particle to give new particle positions and velocities. Based on these new positions new contact forces and hence the

next positions are calculated. The time-step calculation is automatic and can change during a simulation according to the number of contacts around each particle and the instantaneous stiffness value.

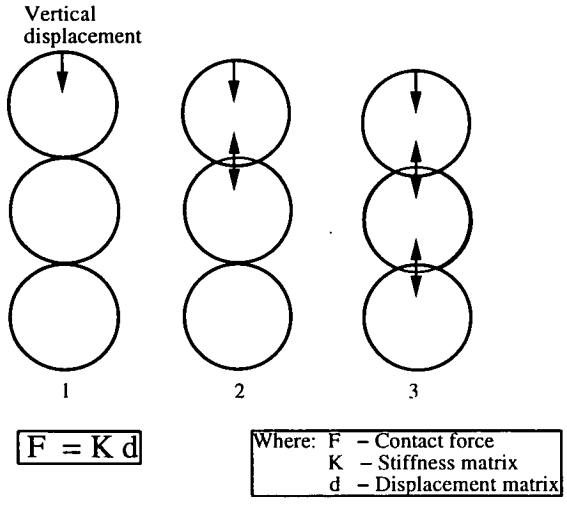


Figure 6.7: Figure showing the time stepping scheme of load propagation

Particles are allowed to overlap each other at contact points as shown in Figure 6.7. The size of the overlap produced by the applied force is related to the contact force by the relative stiffness of the particles. In this iterative way the new contact forces found can be used to find the displacements over the next time step. Two circular particles are taken to be in contact only when the distance between their centres is less than the sum of their radii.

A compacted state for an assembly of particles cannot be specified within PFC2D since there is no unique way to pack particles within a given volume. Methods exist by which uniform distributions of particles can be defined but these shapes are not always suitable to model all different types of area. A method analogous to physical compaction can be used until a required porosity of fill is obtained; this is suitably comparable to the method actually used for the fill material. For the present 2-D package the choice of number of particles is however limited to 500. The main disadvantage of this package is that block boundaries are not linear and 'bumpy' by the nature of the particles forming the solids. $PFC^{2D}$ has been designed to operate specifically on small computers and operates in a DOS command driven version.

### 6.3.2 Implementation

#### 6.3.2.1 Different models considered

Since PFC has not previously been used for arch bridge analysis, it was thought important that an investigative study was performed. This involved the modelling of the arch voussoir, the arch barrel and the fill material. Each stage was tackled sequentially in order that the affects of input parameters could be investigated before a more complicated model was investigated.

1. The main problem with the formation of a voussoir was the fact that blocks formed by joining particles could only transmit forces and moments through the particle contacts. However assuming that the particles were infinitely strong, by applying strong inter-particle contacts this was quite easily achieved.

2. The voussoir blocks formed not having linear edges and containing voids made it necessary to change the effective thickness and density of the arch barrel to account for this affect.

3. Due to the problem of having a finite number of particles to model in $PFC^{2D}$ the investigation of all the soil-structure interaction effects could not be directly investigated with $PFC^{2D}$, but was attempted with $PFC^{3D}$.

#### 6.3.2.2 Defining the geometry

Much of the investigation of the package has involved comparisons between the idealised 2-D single span structure previously discussed in Section 6.1 and described by Fairfield[19] and Prentice.[20] The same $2m$ span has been modelled with and without the fill material. Particles are defined and their properties prescribed to form the structure. An Excel spreadsheet has been utilised for this purpose by which the number of particles required for the thickness of the arch barrel can be changed and the radii, number and position of each ball can be calculated. It is important at this stage that contacts are only slight since the material properties prescribed to the particles are affected directly by this initial overlap. The contact between balls however are important since these allow

interaction to occur between adjacent particles, without which analysis would be impossible.

Two models of this arch have been investigated with PFC, the first modelling the arch barrel only and the second with fill material included. For each model runs have been performed to model and predict the following requirements:

1. the dead load is correct and the model is stable
2. the soil structure interaction has been correctly modelled and influences of change in material properties are known
3. the load is applied to the fill surface in a correct method
4. a failure load and mechanism is obtained for each model

#### 6.3.2.3 Material properties

Material properties are defined for either particles, walls or the contacts between the combination of the two. Once a set of particles have been defined and given an identification number, properties can be prescribed to suitable particle ranges. A joint generator exists such that contact properties can be modified along prescribed lines. In this way the model can be traversed by a set of week planes (corresponding, for example, to mortar joints). When trying to compare a simulated material (comprising of bonded particles) with real materials a trial and error process is required, since no complete theory exists to predict all required properties. Guidelines are given for this although this is by no way covering all possible problems.

Since the materials used for this model are known then choice of property inputs are simplified greatly. The materials and properties used in these models are shown in Table 6.1. Here $kn$ and $ks$ are the normal and shear stiffness of the ball surface, $n_b$ and $s_b$ are the normal and shear contact bond strengths and $pb$ strength are the parallel bond strengths. These bonds consist of those described at contact points and those represented by parallel bonds, to resist bending.

Friction angle is an important aspect of the analysis within $PFC^{2D}$. The recommended procedure is to fit the contact models and known properties for

| Material | Density $kg/m^3$ | Friction coef. - | Normal stiffness ($kn$) $N/m$ | Shear stiffness ($ks$) $N/m$ | Normal strength ($n$-$bond$) $N$ | Shear strength ($s$-$bond$) $N$ | Parallel bond ($pb$-$*$) $N/m^2$ |
|---|---|---|---|---|---|---|---|
| Arch | 1517 | 0.6 | $1e^9$ | $1e^9$ | $1e^{10}$ | $1e^{10}$ | $1e^{20}$ |
| Mortar | - | 0.4 | $1e^8$ | $1e^8$ | $5e^3$ | $5e^3$ | 0 |
| Fill | 1800 | 0.6 | $1e^8$ | $1e^8$ | 0 | 0 | 0 |

Table 6.1: Material and joint properties used for PFC arch analysis

each application. The friction coefficient used in the package is used to represent the peak friction angle for each material. It has also been shown that the peak friction angle does not increase linearly as a function of the particle friction angle. The relationship accounting for contact properties and problem scale effects can be obtained by running numerical tests.[139] The friction coefficient for both the mortar joint and the fill material has been varied and discussed later in Section 6.3.3. It has become evident that the friction coefficient, $k$, relates to the friction angle by the relationship shown in Equation 6.10.

$$\phi = tan^{-1}\ k \tag{6.10}$$

A higher density than the measured value has been used for the particles in the arch barrel and the fill to give a correct dead load. Increasing the number of particles used during modelling does not decrease the density required, due to the circular shape of the particles producing voids in the final arch ring and fill.

#### 6.3.2.4 Void ratio discussed

For a perfectly packed assembly of identically sized particles the area of the voids compared to the area of the circles remains at a constant ratio. Since all circle are of equal diameter the triangle formed by joining their centres is an isosceles triangle. Therefore:

$$\sin\varphi = \cos\phi = \frac{\sqrt{3}R}{2}, \quad where \quad \varphi = \frac{\phi}{2} = 60^o$$

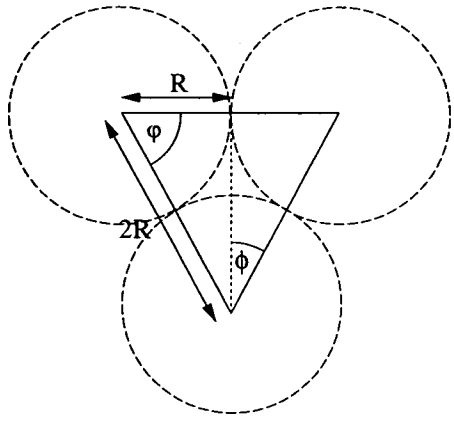


Figure 6.8: The void area between identical circles.

The area of the triangle, $A_\triangle$, formed by joining the three centres is given by:

$$A_\triangle = \sqrt{3}R^2$$

And the area of the void, $(A_V)$, is equal to the area of the triangle minus the area of the three wedges.

$$A_V = R^2\left(\sqrt{3} - \frac{\Pi}{2}\right)$$

Since both the area of the triangle and the void increase with respect to $R^2$, then the particle size does not effect the void ratio of the sample, so long as packing is consistent.

#### 6.3.2.5 Modelling requirements

Due to the spherical nature of the particle used in this package several problems were initially encountered in the modelling of the arch barrel. Initial arch only

stability was difficult to achieve while the combined diameter of the particles was equal to the required thickness of arch. This had the effect of falsely producing a different hinge position, reducing the effective ring thickness and increasing the density of these particles, making this effect worse. This effect is illustrated in Figure 6.9, where the formation of hinges can only occur at particle contacts producing a smaller effective ring thickness than is represented by the combination of diameters. This effect reduces as the number of particles used to model the ring thickness is increased. Since ring thickness has such an important effect on the failure load it was felt important to make the effective ring thickness equal to the experimental arch dimension, although this would produce a larger actual ring thickness.

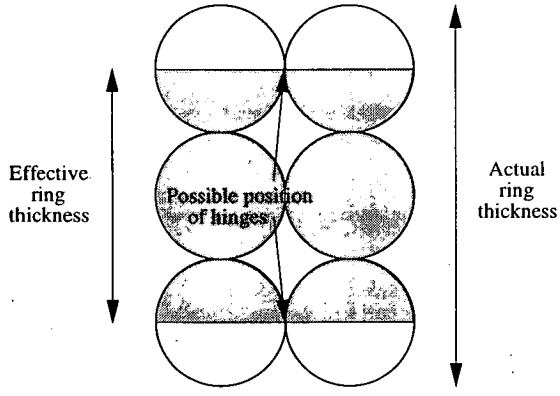


Figure 6.9: Actual and desired ring thickness

As the number of particles is limited for $PFC^{2D}$, this resulted in the number of particles available for the arch ring also to be limited. This made the effective and actual ring thickness an important parameter during the following investigation. The above method however still required a slight tensile force to be applied along the mortar joints to achieve stability. This minor force, shown in Table 6.1, was required to account for the area of the particle lying out side the effective thickness of the arch barrel. The failure mechanism produced without this force relates well with relevant theories already introduced, Figure 2.5($c$) in chapter 2.

An equilibrium condition is reached for the arch barrel, allowing initial stability, dead load and uniformity of loading to be checked. Before any fill material is placed the joints between the arch voussoirs are made very strong, analogous to placing a supporting structure under the arch to maintain arch stability during the loading process. Fill is then placed under an increased gravity loading to

achieve the required porosity. Joint and voussoir properties are then returned to the values required for the analysis and the model is allowed to relax to again reach an equilibrium. Dead loads, initial arch displacements and other model properties can be checked at this stage and material properties varied accordingly to achieve correlation with experimental data before any live loads are applied. Once a stable model had been created the effect of different parameters could be investigated.

#### 6.3.2.6 Loading to failure

Relevant loading of an assembly of particles can be performed by either gravity, displacement or a load controlled method. In this way the model can be checked to see how it is performing and a failure load can be obtained for each run. The method of loading chosen for a majority of the runs was to load the model with a displacement controlled procedure, but due to the nature of the package a loading rate had to be chosen that would not effect the failure load. For this reason loading rates were varied in order to find the limits that effect the failure load. Figure 6.10 shows clearly that once the loading rate falls to $1e^{-7}$ m/s the failure load becomes stable. These variations are due to the large failure peaks produced by the relatively large displacements producing large inter-penetration of particles produced between steps.

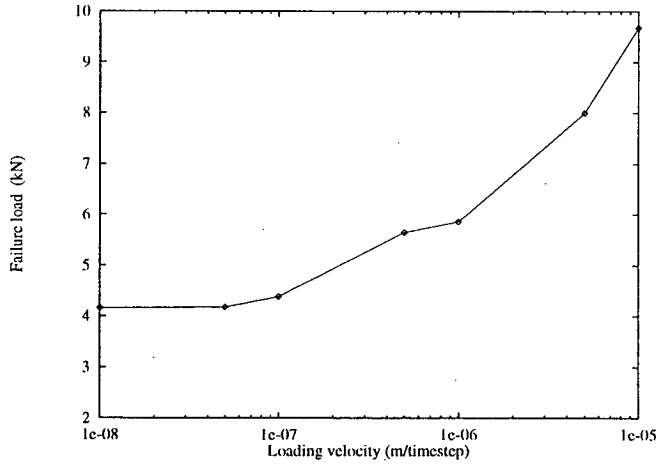


Figure 6.10: Variation of failure load vs loading rate

Failure occurs when the bonds set up at the beginning of an analysis are broken at a sufficient number of places to form enough hinges to form a failure mechanism.

The failure load is found by monitoring the restraining walls placed around a model and recording the maximum force applied to each at a particular moment. This has the added advantage that the load distributed to each support can be monitored throughout providing some interesting results. The peak support reaction for each support does not have to coincide with the ultimate failure load since the value depends upon the formation of other hinges, not necessarily the final one. The support closest to the load gives the largest reaction just before the formation of the third hinge, while the support further away gives a peak reading with the formation of the final hinge. This indicates the way in which the arch redistributes the load with the formation of hinges, hence the formation of hinges does not indicate arch ultimate failure.

At any stage during an analysis the present state of the model can be saved to a designated file which can be recalled at a later date. This is particularly useful since it allows properties to be investigated for a model without the need to rerun the entire programme which leads to a great saving in computational time. The output requested for specific particles or walls during the analysis can be viewed using various commands built into *PFC*. Information is only collected for parameters if requested, this helps cut down on the size of output files but does require careful analysis so as not to miss anything important.

### 6.3.3 Parametric study

Work has been performed to find suitable input material values for the arch analysis, and the following section is an overview of the work performed. Choice of model dimensions, contact and material properties, loading types and rates are all presented, including explanations as to the affect of each of the parameters and why specific values have been chosen. The values used during this study are presented in Table 6.1. The parameters which have been investigated are presented in Table 6.2, in each case only the selected parameter under investigation was varied.

The arch barrel and fill material represent the load bearing part of the structure while the mortar joints represent the planes of weakness inherent in brick work. The normal and shear stiffnesses, ($kn$ and $ks$ respectively) are a measure of the contact stiffness, and so also are a measure of force/displacement at that contact.

| Arch properties | Loading | Fill properties |
|---|---|---|
| n-bond | Position | Particle size |
| s-bond | Width | Height |
| Density | Velocity | Density |
| Friction angle | | Friction angle |

Table 6.2: Summary of main parameters investigated

The normal and shear bond strength, *n-bond* and *s-bond* respectively are forces that keep particles in contact with each other. The mortar and fill friction angles have been investigated but are discussed later with comparisons made with the other analysis methods used in the chapter.

#### 6.3.3.1 Mortar bond strength properties

As the mortar joint properties have been varied it is clear from Figure 6.11 that the normal bond strength *n-bond* has the most influential effect on the failure load. The shear bond strength *s-bond* has very little effect since the predominant type of failure present is a mechanism failure without slipping. The *s-bond* however cannot fall below a given value since this prevents a shear failure mechanism, and so is required to give initial arch stability.

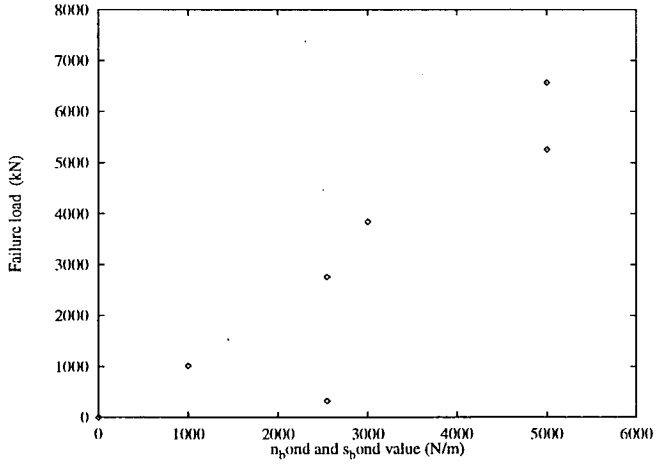


Figure 6.11: Variation of failure load vs combined s-bond, n-bond values

#### 6.3.3.2 Loading position

For the arch only analysis, shown in Figure 6.12($a$) the critical position for the load is at the centre of the span, at the crown. Tests were also conducted varying parameters at different load positions but similar trends have been observed. Since comparisons are being made with an actual arch test, loaded at $\frac{1}{3}$ span, this is the loading position chosen for the parametric study. Figure 6.12($b$) shows clearly that the critical loading position had moved away from the crown towards the $\frac{1}{3}$ span position. Both of these results correlate very well with observed and theoretical predictions for a semi-circular arch.

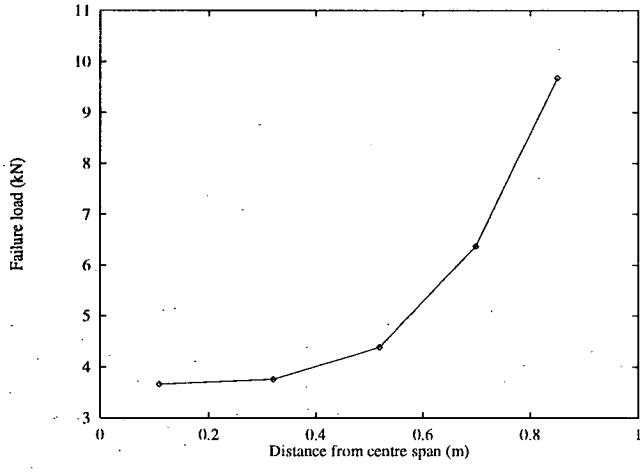


(a) Arch only

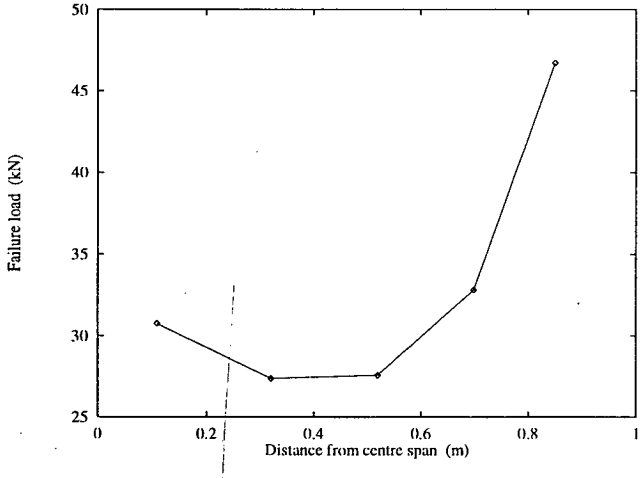


(b) Arch and fill

Figure 6.12: Variation of failure load vs loading position

#### 6.3.3.3 Width of loading

Since with $PFC^{2D}$ the load could only be applied to the arch directly the width of load applied to the arch could be investigated. In this way the fill distribution effects could be neglected from this analysis to give more direct results. It is clear that as the loaded width increases so does the failure load. Where there are two identical loaded widths, at two slightly different loading positions, the position closer to the crown gave the lower failure load in all cases. The width of the loaded area also has some effect on the position of the hinges being produced and therefore the failure mechanism.

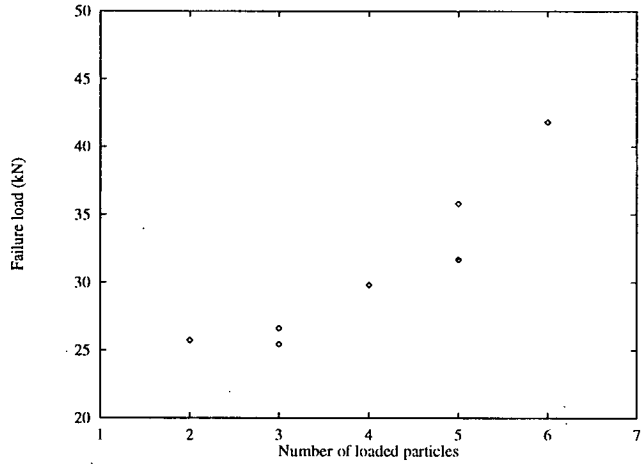


Figure 6.13: Variation of failure load vs loaded width

#### 6.3.3.4 Fill density

A model was tested with varying values for fill density resulting in the failure load increasing with increasing density. This relationship is not linear, indicating an interesting effect with the failure mechanism changing slightly with the hinges formed moving towards the springings with decreasing fill density. When the density is reduced greatly to 100 and 10 $kg/m^3$ this has the effect of reducing the failure load further. Density values below theses values did not run correctly since particle were removed from the model by the forces imparted from the loading. This value is still greater however than the arch only failure load, and indicates the possible isolation a soil structure interaction effect, neglecting density. At these falsely low densities the failure mechanism changed with hinges forming at

the springings rather than the usual positions. The fill at these values contributes very little to the dead load of the structure and hence the increase in failure load can only be due to other interaction effects. This shows an increase in capacity of 14% solely due to the interaction between the fill and the arch barrel.

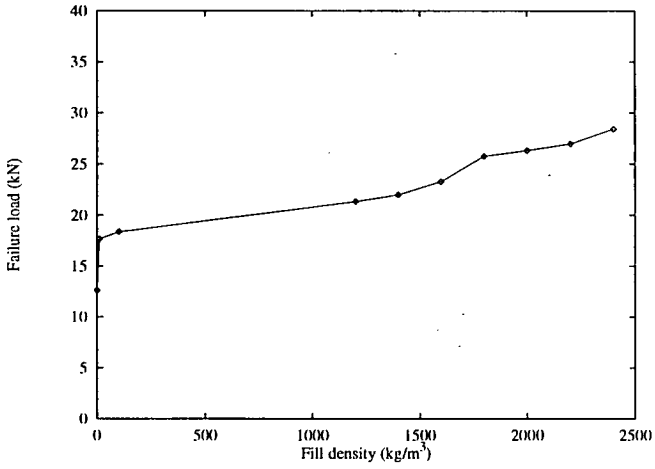


Figure 6.14: Variation of failure load vs fill density

#### 6.3.3.5 Fill height

Varying fill height produces the results shown in Figure 6.15. Again the response to the varying height is not linear, providing important results to do with a critical depth of fill required for initial stability for this shape of arch. The critical height of fill required seems to be at $0.2m$. Over this value the failure load again falls predictably with a constant failure mechanism but below this value another failure mechanism is produced affecting the failure load produced. The height of fill therefore has a very meaningful effect on the failure mechanism and therefore the failure load.

This parametric study has produced relationships which compare well with theoretical work and also compare well with the parametric studies conducted earlier in in chapter 3, with the comparisons of modern assessment methods. This gives confidence in the results obtained and the discrete element analysis methods being utilised.

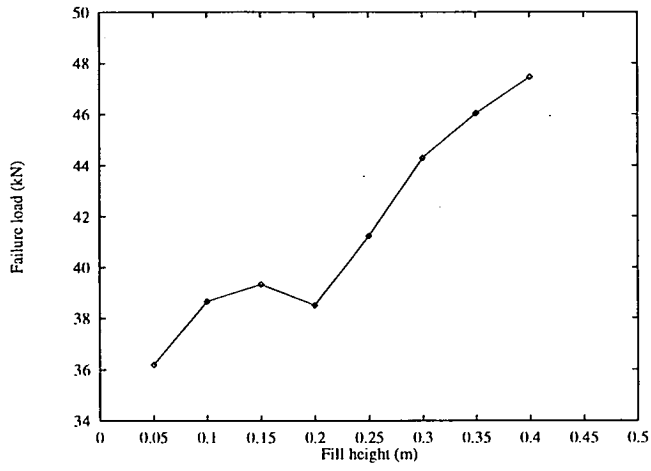


Figure 6.15: Variation of failure load vs fill height

## 6.4 Finite element model, DIANA

Recent advances in finite element analysis techniques include the development of joint and interface elements. These improvements can be used to model planes of weakness as well as potential failure mechanisms within the conventional finite element technique in a similar way as discrete element methods perform. It is this factor which allows comparison with the previously discussed discrete element methods.

The non-linear finite element analysis has been performed using DIANA.[140] Other packages were considered but it was thought that DIANA offered the most suitable capabilities since it was developed predominantly for the analysis of cohesive and frictional materials. DIANA was initially developed as a series of research codes at the University of Delft, Netherlands. There exists an extensive library of interface elements and non-linear interface material laws which are suitable for modelling the structural response of the structure beyond the peak strength. This finite element work has been largely performed by Thavalingham.[141] A more in depth discussion of this analysis package has been performed elsewhere in work presented by Thavalingham[141] and in the grant report.[142]

### 6.4.1 Modelling the arch

The finite element model used during the analysis is shown in Figure 6.18($c$). Four-noded quadrilateral isoparametric plane stress elements were used to model the arch voussoirs while similar elements were used to model the fill material with the inclusion of a plasticity based modelled on the Drucker-Prager failure criterion. Interfaces, such as those between the arch voussoirs and the fill material were modelled with interface elements of varying thicknesses. The use of these interface elements is to allow the formation of hinges and failure planes within the finite element model. In this way the programme would behave more as a discontinuous method of analysis.

Again loading is by a displacement controlled procedure which enables the failure load to be predicted by monitoring the force required to produce the required displacement. This method of analysis tends to produce a much smoother formation of zones of failure, representing the hinges, than the previous discrete element methods.

## 6.5 Comparisons of packages

For each package a failure load analysis has been performed using the same input parameters in order to make direct comparisons possible. As well as this a parametric study investigating the friction angle for the fill and the mortar joints has been conducted.

### 6.5.1 Parametric study

A sensitivity analysis has been performed with the three packages by varying the friction angle of the mortar joints and the fill material. Friction angles for the mortar joint were varied between $30^o$ and $40^o$, and the fill angle was varied between $30^o$ and $44^o$. The friction angle of the arch-fill interface was taken as 75% of the fill friction where required. Figure 6.17 shows the 3-D plots used to illustrate the effect that changes in these values have on the failure load.

The results suggest that changing the friction angle for the mortar joints between voussoirs provided little effect on failure loads. An exception for this is the PFC package that does show some reduction in failure load with decreasing friction angle. The change of the fill friction angle has a significant effect on the failure load for all packages, although the effect produced is not consistent.

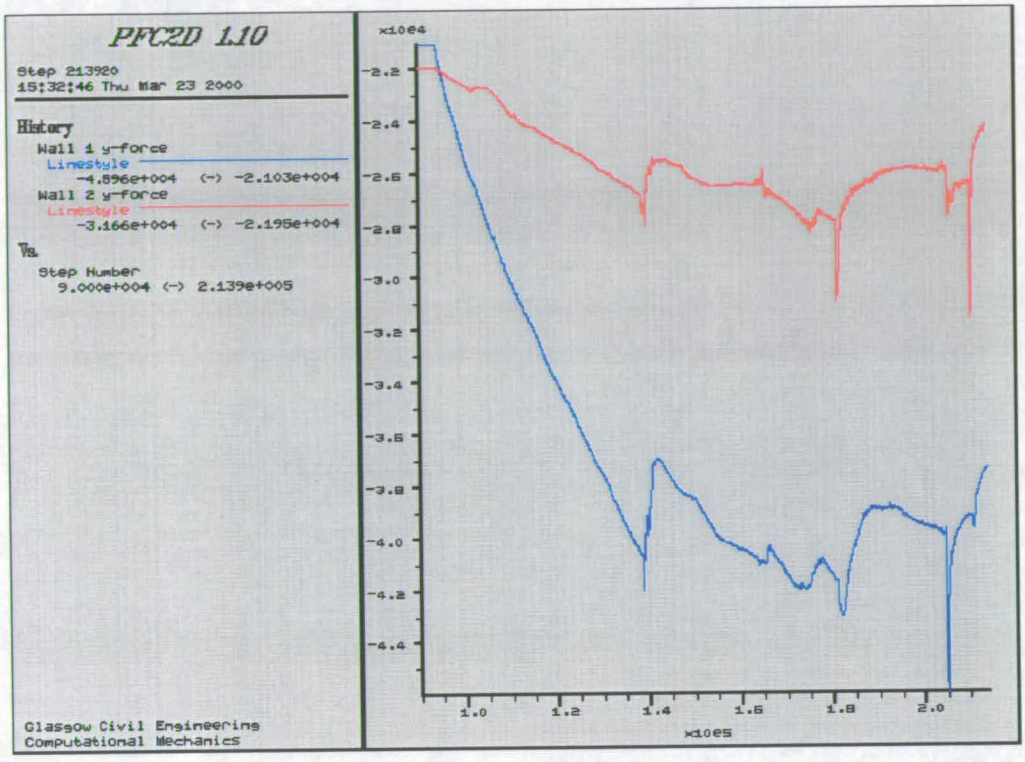


Figure 6.16: Load distribution to the springings of the arch

Table 6.3 compares the effect of the change in fill density, $\Delta\rho$ and fill height, $\Delta h$, on the failure load produced with the four assessment methods used earlier in Chapter 3 produces close comparisons. The structures analysed are different, both of which are however semicircular but of very different dimensions. This probably explains the effect of the change in density being quite close while the change in fill height not being very close due to some scale effects.

### 6.5.2 Failure load and mechanism

The deformed models obtained from the three analysis packages are shown in Figure 6.18. It is initially obvious that the three packages produce very similar failure modes, with the placement of hinges being as identical as allowed for

| Analysis method | $\Delta\rho$ $(kg/m^3)$ | Failure load (kN) | $\Delta h$ (m) | Failure load (kN) |
|---|---|---|---|---|
| PFC | 1000 | 6 | 0.3 | 9 |
| MEXE | - | - | 0.6 | 30 |
| ARCHIE | 1000 | 8 | 2.4 | 15 |
| CTAP | 1000 | 8 | 1.0 | 3 |

Table 6.3: Comparison of PFC with other assessment methods

within each model. Even for these relatively simple models the comparisons with the actual experimental failure load and mechanism is very close. It is also clear that the formation of the hinges is a progressive process with the failure mode only being formed by the formation of a mechanism. Up to this point load can be increased due to the redistribution of the load due to the formation of hinges, allowing further arch movement.

This process is also indicated by the way in which the springing forces vary throughout the loading process to failure, as shown in Figure 6.16. There exist peaks in the measured response at the springings, each relating to an increase in required applied load directly before the formation of a hinge. The load then reduces as the arch barrel moves to redistribute the applied load. It is noticeable that the peak values coincide, with the larger amount of the force going to the restraining wall closest to the load. When comparing the theoretical load required for the formation of the hinges to the experimental[19] the results shown in Table 6.4 were found. A close correlation between the percentage of the total load and the creation of the hinges has been initially found. Although this is a relatively simple model the closeness to actual results gives confidence in results obtained.

| Hinge | Expt. load kN | % | Theoretical load kN | % |
|---|---|---|---|---|
| 1 | 11.4 | 30.0 | 9 | 26 |
| 2 | 21.3 | 56.0 | 27 | 78 |
| 3 | 32.7 | 86.0 | 31 | 89 |
| 4 | 38.1 | 100 | 34.6 | 100 |

Table 6.4: Comparison of load required to produce hinge formation

It is also clear that the discrete element methods allow soil-structure redistribution of the load into the fill due to arch barrel movement. This has been detected by both deflection results for the arch and also increased load being applied horizontally to the retaining walls. These walls are to remote to be directly effected by the applied load so any increase must be due to soil-structure interaction. The arch movement is a sway of the arch away from the load and into the fill on the remote side of the arch. These results again compare well with previous experimental and theoretical work.

The collapse loads predicted by each of the packages, shown in Figure 6.19, shows a relatively good comparison between the different methods. These results, expressed as a percentage of the actual failure load, are compared with the experimental test and other assessment methods as shown in Table 6.5. It is clear that the failure loads produced are close to the actual failure load of the arch, and more importantly the failure mechanism is closely replicated by each package. This give confidence both in the failure load and the method of analysis. DIANA tends to produce the failure load relatively smoothly, but it is produced only by a large required displacement. This displacement is much greater than that experienced during the load test to failure. The displacement required by PFC and DDA are much closer to the actual results.[19] The failure load is obtained from the peak load required to produce the prescribed displacement from each graph. The reason why the graphs appear to fluctuate is due to the redistribution of the applied load already mentioned. A post failure load-displacement relationship is obtained for the two discrete packages making the failure load easier to identify, this is however not possible for DIANA.

| Analysis method | Expt. | MEXE | MARCH | MAFEA | DIANA | PFC | DDA |
|---|---|---|---|---|---|---|---|
| Failure load / kN | 38.1 | 10.6 | 15.0 | 21.4 | 48.6 | 42.5 | 32.0 |
| % of experimental | 100 | 28 | 40 | 56 | 128 | 112 | 84 |

Table 6.5: Comparison of failure loads of the experimental, discontinuous frameworks and analytical methods

It is also clear from the results from the present assessment methods that the strength of the arch is greatly underestimated. The closest failure load being predicted by MAFEA providing a failure load of 56% that of the experimental. The MEXE method gives the lowest failure load, only 28% of the experimental

but this is not surprising since the size of the arch is outside the accurate range for MEXE predictions.

## 6.6 Conclusions

Two different discontinuous modelling frameworks are presented and comparisons have successfully been made with a non-linear finite element analysis and experimental results. As the loading applied to the arch increases there is a progression in regions of the arch from the elastic response to plastic and discontinuous behaviour. If collapse loads are to be correctly assessed the inclusion of discontinuities is required to give realistic failure predictions. Research into discrete element analysis techniques has been successful at a basic level and the nature of the methods leaves great scope for future research.

Several other conclusions have also been made during the course of this research:

- Discretised assessment methods have been shown to produce realistic and accurate failure loads.
- Displacement controlled loading procedure has successfully been utilised to achieve the collapse load and failure mechanism.
- The modelling framework presented can give reliable and realistic failure predictions.
- Sensitivity analysis shows the significance of the backfill to the strength of the entire structure, not just acting as dead weight.
- Arch only analysis compares well with plastic failure methods.
- The analysis is easy to generate and perform with known parameters.
- Zones of fill displacement have been identified due to an applied load and subsequent arch movement.
- The effects of varying material parameters has been investigated and the results compare well with previous theory and model tests.

- Discrete element analysis has successfully been identified as being a being suitable for both 2D and 3D arch bridge problems.

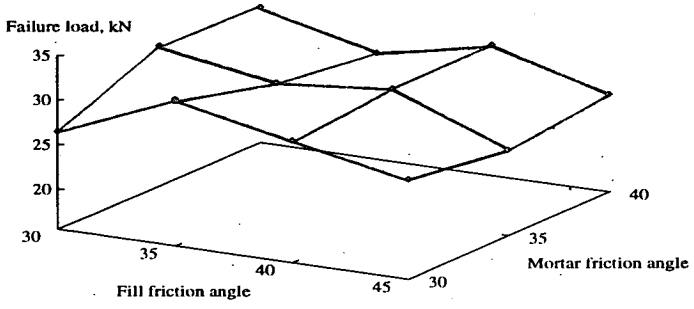


(a) DDA analysis

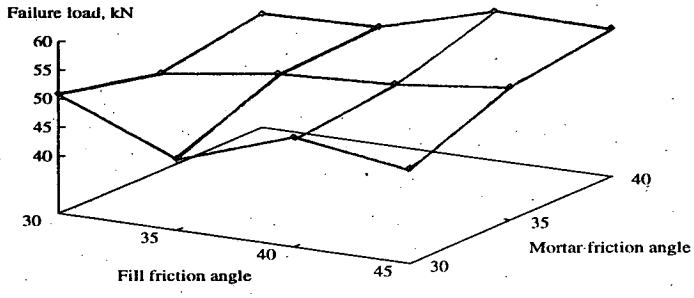


(b) PFC analysis

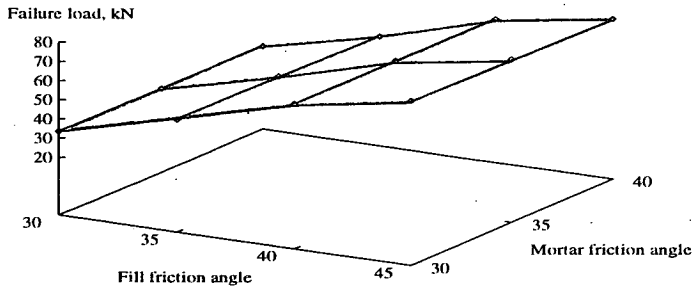


(c) DIANA analysis

Figure 6.17: The effect of fill and mortar friction angle on the failure load

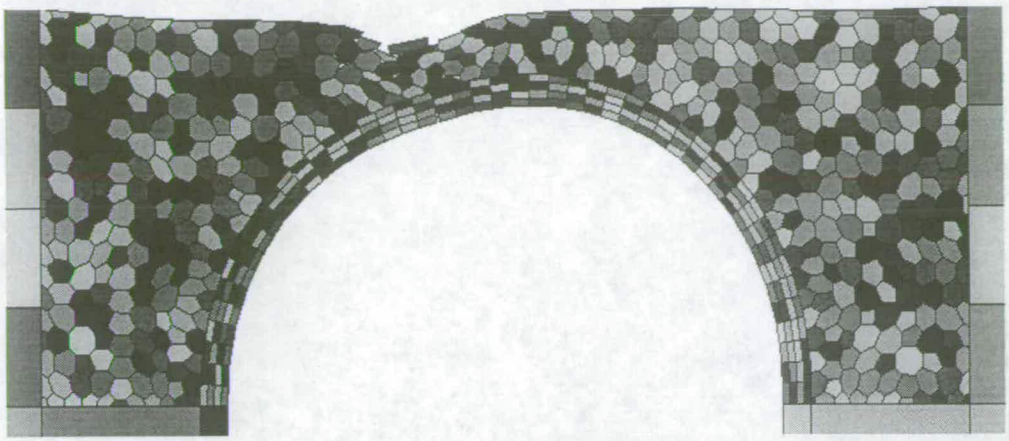

(a) DDA analysis

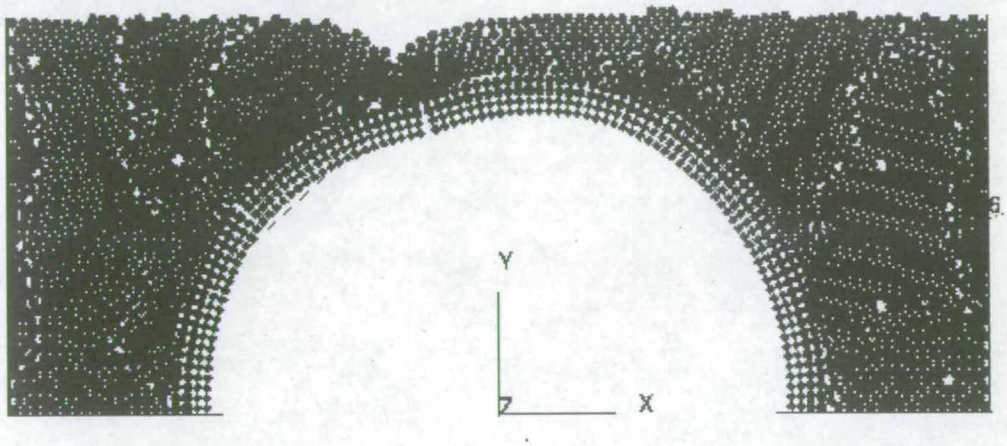


(b) PFC analysis

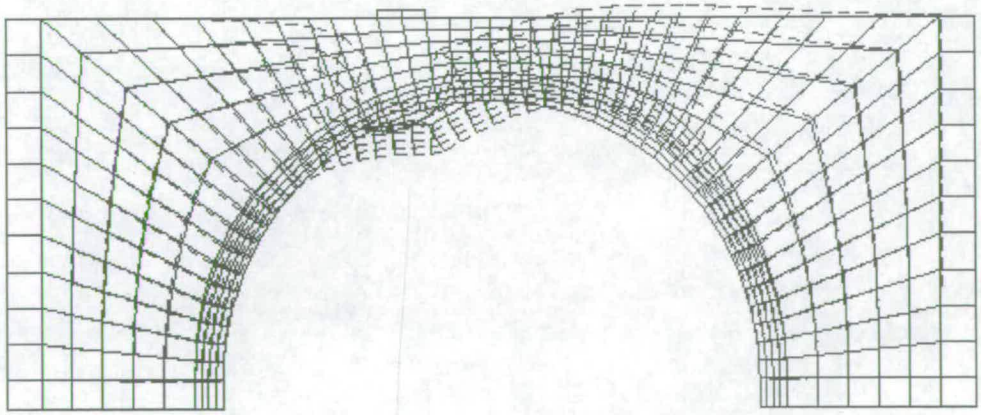

(c) DIANA analysis

Figure 6.18: Failure mechanisms produced by different analysis methods

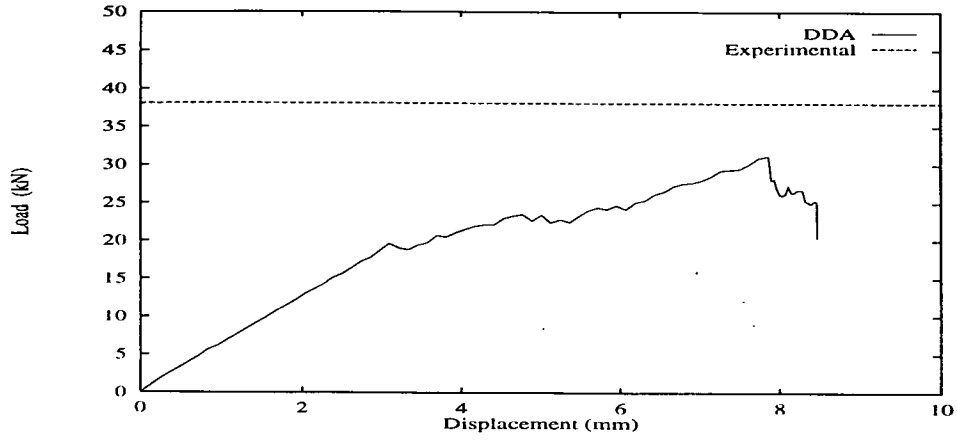


(a) DDA analysis

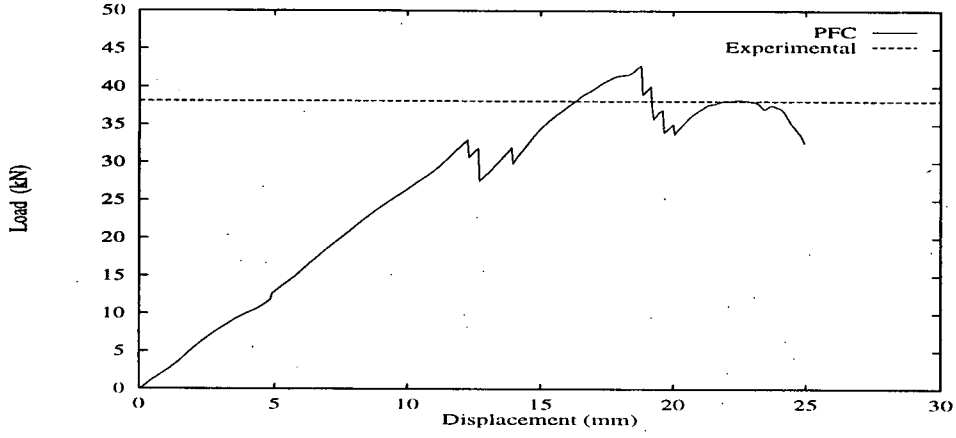


(b) PFC analysis

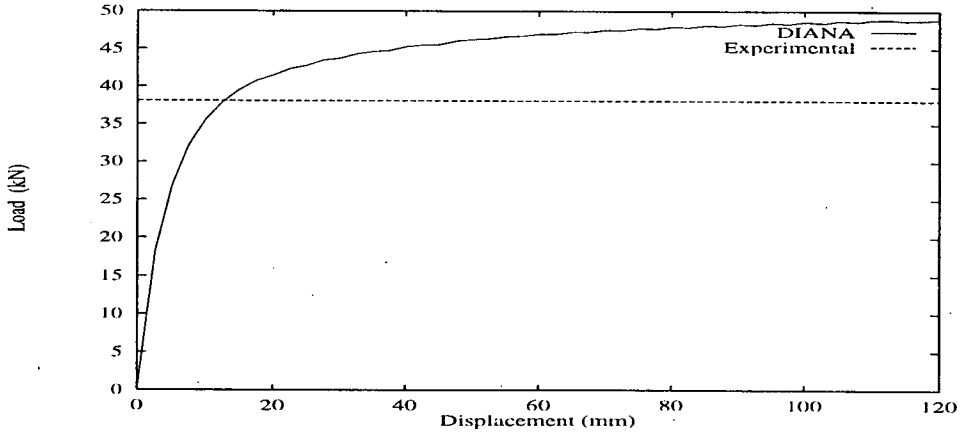


(c) DIANA analysis

Figure 6.19: Failure loads produced by different analysis methods

# Chapter 7

# Conclusions

## 7.1 Introduction

This chapter presents a summary of the conclusions derived from the findings presented in this thesis. It presents an amalgamation of the conclusions written at the end of each chapter and serves to eliminate duplication of conclusions drawn thus far and to draw particular attention to conclusions applicable to the entire thesis.

A parametric study was undertaken investigating four masonry arch bridge assessment programmes. Comparisons have highlighted differences which suggest that arch analysis is inaccurate for more than one of the methods and has identified many of the problems with the current arch assessment methods. Specific parameters have been identified as being crucial for an accurate assessment of these structures. The inclusion of other parameters in arch assessment have also been investigated. Discontinuous modelling frameworks are presented and comparisons have successfully been made with a non-linear finite element analysis and experimental results. As the loading increases there is a progression in regions of the arch from the elastic response to plastic and discontinuous behaviour. If collapse loads are to be correctly assessed, the inclusion of discontinuities is required to give realistic failure predictions. Research into discrete element analysis techniques has been successful at a basic level; the nature of these methods leaves great scope for future research.

## 7.2 General conclusions

1. Masonry arch bridge assessment is a complicated process, however a quick and accurate method of arch assessment is desired.

2. The discontinuous nature of the masonry arch failure mechanism presents many difficulties to the present arch assessment methods.

3. Arch dimension and material property parameters have been identified as affecting arch strength which are not presently included in arch assessment methods.

4. Soil-structure interaction has been shown to be crucial to arch stability and strength.

## 7.3 Specific conclusions

### Comparison of assessment methods

1. Despite the importance of arch assessment in maintaining a safe transport network throughout the UK there still exist uncertainties and inconsistencies in many of the assessment methods used today.

2. It is important that more than one method is utilised during an assessment programme to produce reliable predictions of arch strength.

3. Arch dimensions and material properties affect the assessment methods by varying degrees with what should be consistent assessment packages.

4. ARCHIE gives the most consistent set of results for the range of bridge investigated in the arch assessment programme.

5. There is scope for the improvement of modern assessment methods, particularly in an interactive role.

### Line and patch load tests

6. The tests performed were shown to be repeatable.

7. Line loads are more critical than patch loads on a multi-span arch bridge.

8. There is a degree of interaction between both arches and the fill in all loading cases .

9. Peak pressure and stress readings were higher than applied values, for the reasons postulated.

10. Results show that the responses of the primarily loaded arch were not symmetrical between the abutment and the pier side of the arch.

11. Increasing the fill height decreases the stresses transfered to the arch barrels and reduces arch movement due to the increased soil-structure interaction.

12. Zones of influence are primarily in the longitudinal rather than the transverse direction, due to relative arch movement.

## FE modelling of thermal effects

13. A temperature increase produces an expansion of the arch, resulting in an upward movement at the crown.

14. Results from the model show that large stresses are produced in the arch barrel and spandrel wall, much greater than those produced in the fill material.

15. Temperature correction highlighted an overall reduction in compressive strain on the arch extrados with a corresponding increase in temperature.

16. The ABAQUS thermal analysis produces similar trends to that observed over the collection period and also highlighted many other significant affects.

## Discrete element analysis

17. Discrete element analysis has been shown to be particularly suited to masonry arch failure mechanisms.

18. The collapse load rises as the fill density and height increase, comparing well with previous tests.[20]

19. Displacement controlled loading procedure has successfully been utilised to detect the collapse load.

20. The loading rate is critical for this type of analysis, as it directly affects the failure load produced.

21. Discretised assessment methods have been shown to produce realistic, identifiable and accurate failure mechanisms.

22. Zones of fill displacement and arch movement have been identified due to applied loads.

23. Discrete element analysis has successfully been identified as being suitable for both 2D and 3D arch bridge problems.

# Chapter 8

# Recommendations for further work

## 8.1 Introduction

This chapter is included to summarise areas of research which have been highlighted during the course of this research. It is clear that the following suggestions are outside the initial aims set out in chapter 1, since further research was limited by time constraints. The following suggestions are presented in a logical progression based on the work already presented.

## 8.2 Assessment packages

A comprehensive parametric study has been conducted with four arch bridge assessment methods using initially semicircular dimensions, yielding some useful conclusions. A similar study investigating other arch configurations. such as shallower segmental arches, would undoubtedly give many other useful results. This segmental shape is common and so the affect of this shape has to be of great relevance to these packages.

The packages used in the arch assessment programme are being updated as new methods of arch analysis are available. The affects of each improvement would be very useful to investigate and to compare to other methods.

Inclusion of other assessment packages not previously included would allow comparisons to be made to the present assessment methods and allow relationships to be formulated for each package.

## 8.3 Kimbolton Butts bridge

Although the data-logging equipment was permanently destroyed due to the aforementioned flooding of the structure, the capability to reinstall this equipment still exists. This would enable further load tests to be performed on the structure to see if its response has changed greatly over the 6 years in which it has been in service.

Large changes in stress and strain have been observed in the arch barrel and spandrel wall from the finite element analysis. If a method of measuring these

stresses could be utilised this would provide a direct method of comparison between theoretical and measured results.

## 8.4 2m double span arch tests

Research of this structure involved the testing of different load levels and fill heights with nominal line and patch loads. The results from this comprehensive series of tests have indicated to this author and to Prentice[20] areas of load dispersal, both in the fill and on the arch extrados and transverse displacement of the arch barrel.

Future research should concentrate on testing the affects of either a surfacing layer or a spandrel wall and parapet added to the present structure. The influence of these and the 3-D effects from patch loads tests could also be included. Failure load tests providing obvious comparisons with previous tests and direct comparisons with various assessment methods, including the discrete element analysis methods already introduced. This would give more proof with regard to the suitability of this type of analysis to the failure load of these structures.

A large amount of work investigating a 2m double span arch bridge, has previously been completed and documented by previous authors and by this author. Future research should concentrate of different arch profiles, which almost definitely would have to be a flatter arch profile. This arch shape generally has a shallower covering of fill at the crown thereby affecting the interaction involved. However, valuable insight would be gained on the affect on the collapse load of the various material and dimensional parameters.

The present bridge structure has been extensively tested; a failure load test would thus give a large amount of information which would be useful for comparisons to be made with a previous single span failure test. This would help highlight affects of the second arch on failure load and mechanism.

Many of the tests already conducted have been invaluable in the initial investigation into the new discrete analysis methods developed previously in this thesis. Future tests would undoubtedly provide similarly useful results for the identification of affects and subsequent calibration.

## 8.5 Discretised model analysis

The identification of discrete methods of analysis which closely replicate the structural behaviour of bridges at failure has presented many areas of further research, both for 2-D and 3-D analysis.

If soil-structure interaction influences could be isolated and investigated, the positive affect of each could be noted. This would identify the critical material parameters which affect these mechanisms.

The option is also available of the inclusion of a material failure mechanism, which would replicate the affects of such things as masonry block material or mortar failure, due to some maximum strength parameter. This would allow different failure mechanisms to form, as apposed to the mechanism failure with no material failure, which has already considered. Mortar failure could be included to see how initial dead loading affects the initial dead load state.

Zones of movement are easily identified within these packages, and significant movements have already been seen. There is scope to relate these zones with previously conducted tests and also with the formation of hinges, which are identified within each package.

The number of parameters previously tested in actual arch model tests is large enough to enable further tests to be completed. The obvious subjects for future research are arch dimensions or arch material properties, in fact those investigated in chapter 3 for the current assessment methods.

The 3-D nature of the packages used has opened the opportunity of further investigation of the components of a typical masonry arch structure, such as: spandrel walls, wing walls, parapets and different road pavement layers. Careful comparison with results from specific instrumented field and model tests would be a vital part of this investigation, as research is still at an early stage. With the ever increasing power of computer based analysis methods it is envisaged that such an analysis could be completed for a standard arch assessment, although at present this is not economic for reasons of both time and cost.

Investigation of different arch profiles, preferably of more segmental arches, would be of great interest, as this would present a new set of problems for this type of

analysis. Such arch shapes differ from the previously investigated semicircular shape in the ways that the fill interacts, and the arch barrel transmits the load to the abutments and foundations. This makes the investigation of abutment thrust and displacements essential, and has already been shown to be possible.

The research presented in this thesis has wider application within engineering, particularly within the study of other masonry structures out-with the masonry arch bridge. These include studies into other arches used in many other historical structures and has been shown already to be applicable to concrete problems.

## 8.6 Summary

Recommendations have been made relating to each area of research developed in this thesis. The work has been conducted as either continued research, looking at expanding existing knowledge, or at the initial stages of new research. The work completed is assessment-driven and has been carried out in places in conjunction with the engineers actually assessing the arch bridge stock. It is hoped that the knowledge and understanding gained into the behaviour of arch bridges will help to develop a practicable, accurate and economic solution for the analysis assessment of masonry arch bridges.

# References


[1] H Falter and A. Bogle. Conceptual design of renaissance arch bridges. In *Arch Bridges - History, analysis, assessment, maintenance and repair. Proc. Second Int. Arch Bridge Conf.*, pages 45–52. A.A. Balkema, October 1998.

[2] J. Heyman. *The masonry arch.* Ellis Horwood Ltd., Chichester, England, 1982.

[3] M. Gilbert. On the analysis of multi-ring brickwork arch bridges. In *Arch Bridges - History, analysis, assessment, maintenance and repair. Proc. Second Int. Arch Bridge Conf.*, pages 109–118. A.A. Balkema, October 1998.

[4] J. Page. *Masonry arch bridges; State of the art review.* HMSO, London, 1993.

[5] A. Kumar. Interactive assessment of masonry arch bridges. In *Arch Bridges - History, analysis, assessment, maintenance and repair. Proc. Second Int. Arch Bridge Conf.*, pages 195–204. A.A. Balkema, October 1998.

[6] P.L. Berry and D. Reid. *An introduction to Soil Mechanics.* McGraw-Hill Book Company, 1987.

[7] BS 6100, British Standards Institution, London. *Glossary of building and engineering terms*, 1985.

[8] BD21/97. Department of Transport, HMSO, London. *The assessment of highway bridges and structures*, 1993.

[9] BS 5390, British Standards Institution, London. *Code of practice for stone masonry*, 1976.

[10] E. Benvenuto. Bridge-building and modern structural mechanics. In *Arch Bridges - History, analysis, assessment, maintenance and repair. Proc. Second Int. Arch Bridge Conference*, pages 3–13. A.A. Balkema, October 1998.

[11] G. Riva and P. Valle. Construction knowledge between the 18th and the 19th century applied to arched systems in venice. In *Arch Bridges - History, analysis, assessment, maintenance and repair. Proc. Second Int. Arch Bridge Conf.*, pages 57–64. A.A. Balkema, October 1998.

[12] M. Chalana. Brick bridges and historical transportation systems. In *Arch Bridges - History, analysis, assessment, maintenance and repair. Proc. Second Int. Arch Bridge Conf.*, pages 53–56. A.A. Balkema, October 1998.

[13] M. Bellono and S. D'Agostino. Construction conception and structural conservation of masonry arch bridges. In *Arch Bridges - History, analysis, assessment, maintenance and repair. Proc. Second Int. Arch Bridge Conference*, pages 353–359. A.A. Balkema, October 1998.

[14] D. Ridley-Ellis. A model for optimum arch design (MOAD). University of Edinburgh; http://www.nottingham.ac.uk/evxdjr/, 1998.

[15] J. Page. Assessment of masonry arch bridges. In *Proceedings of the Institution of Highways and Transportation National Workshop*, Leamington Spa, England, March 1990.

[16] T. G. Hughes and M. J. Blackler. Arch bridge assessment, art or science? Talk to Institute of Structural Engineers - Masonry Arch Structures, July 1997.

[17] J. Page, C. Beales, and D.A. Ives. Structural monitoring of Kimbolton Butts bridge, Cambridgeshire. Project report, TRRL, Crowthorn, 1993.

[18] J. Page. Load test to collapse on the three span masonry arch Rotherham road railway bridge. Project report, TRRL, Crowthorn, 1994.

[19] C.A. Fairfield. *Soil-structure interaction in arch bridges.* Phd thesis, University of Edinburgh, 1994.

[20] D.J. Prentice. *An appraisal of the geotechnical aspects of multi-span arch bridges.* Phd thesis, University of Edinburgh, 1996.

[21] M. Corradi. Empirical methods for the construction of masonry arch bridges in the 19th century. In *Arch Bridges - History, analysis, assessment, maintenance and repair. Proc. Second Int. Arch Bridge Conference*, pages 25–36. A.A. Balkema, October 1998.

[22] C. Inglis. Applied mechanics for engineers. *Cambridge University Press*, 1951.

[23] BD21/93. Department of Transport, HMSO, London. *The assessment of highway bridges and structures*, 1993.

[24] T. G. Hughes and M. J. Blackler. A review of the UK masonry arch assessment methods. *Proc. Instn Civ Engrs Structs & Bldgs*, 122:305–315, August 1997.

[25] R.J. Bridle and T.G. Hughes. The arch revival: the Cardiff arch analysis procedure. In *Highways and Transportation*, Oct 1989.

[26] R.J. Bridle and T.G. Hughes. An energy method for arch bridge analysis. In *Proc. Instn. Civ Engrs, Part 2, 89*, Sept 1990.

[27] T. G. Hughes. The assessment of a multi-span masonry arch bridge. *Proc. of 1st Int. Conf. on Arch Bridges*, 1995.

[28] M.A. Crisfield. A finite element computer program for the analysis of masonry arches. Technical Report Laboratory Report 1115, Department of Transport, Crowthorne, 1984.

[29] J. Heyman. The assessment of strength of masonry arches. In *Arch Bridges - History, analysis, assessment, maintenance and repair. Proc. Second Int. Arch Bridge Conf.*, pages 95–98. A.A. Balkema, October 1998.

[30] J. Heyman. The stone skeleton. *Int. Jour. Solids & Structures*, 2:249–279, 1966.

[31] J. Heyman. The safety of masonry arches. *Int. Journ. Mech. Sci.*, 11:363–385, 1969.

[32] J. Heyman and C. Padfield. Two masonry arch bridges. *Inst. Civ Engrs*, 52:319–330, 1972.

[33] J. Heyman. Coulomb's memoir on statics. *Cambridge University Press*, 1972.

[34] J. Heyman. The estimation of the strength of masonry arches. *Proc. Inst. Civ Engnrs.*, 66:921–937, 1980.

[35] A. De Rubeis. Definition of the geometrical factor of safety of masonry arches. In *Arch Bridges - History, analysis, assessment, maintenance and repair. Proc. Second Int. Arch Bridge Conf.*, pages 119–122. A.A. Balkema, October 1998.

[36] W.J. Harvey and F.W. Smith. Semi-circular arches. *Proc. Instn. Civ. Engrs*, 83:845–849, 1987.

[37] W.J. Harvey and F.W. Smith. The behaviour and assessment of multi-span arches. *The Structural Engineer*, 69(24), Dec 1991.

[38] W.J. Harvey, F.W. Smith, and X. Wang. Arch-fill interaction in masonry bridges - an experimental study. In *Proceedings of Centenary Year Bridge Conference - Bridge Assessment, Management and Design*, Cardiff, 1994.

[39] M.A. Crisfield and A.J. Packham. A mechanism program for computing the strength of masonry arches. Research report, TRRL, Crowthorne, 1987.

[40] J. G. Cabrera, A. W. Beeby, and D. J. Van der Cruyssen. Mechanism analysis of masonry arch bridges with lateral soil pressure. In *Seventh International Conference on Structural Faults and Repair*, volume 1, pages 97–102, Edinburgh, July 1997.

[41] T. E. Boothby. Elastic plastic stability of jointed masonry arches. *Engineering Structures*, 19:345–351, 1997.

[42] A. Kooharian. Limit analysis of voussoirs. In *Proceeding of American Concrete Institution*, 1953.

[43] P. Clemente, A. Occhiuzzi, and A. Raithel. Limit behaviour of stone arch bridges. *Journal of Structural Engineering*, July 1995.

[44] C. Melbourne and M. Gilbert. The application of limit analysis techniques to masonry arch bridges. In *Proc. of the Centenary Year Bridge Conference: Bridge Assessment, Management and Design*, Cardiff, 1994.

[45] A. Sinopoli, M. Corradi, and F. Foce. Modern formulation for pre-elastic theories on masonry arches. *Journal of Engineering Mechanics*, pages 204-213, March 1997.

[46] A. Sinopoli, M. Corradi, and F. Foce. Lower and upper bound theorems for masonry arches as rigid systems with unilateral contacts. In *Proceedings of the Second International Conference on Arch Bridges*, pages 99–108, Venice, Italy, October 1998. A.A. Balkema Publishers.

[47] M. Como. Minimum and maximum thrust states in statics of ancient masonry bridges. In *Arch Bridges - History, analysis, assessment, maintenance and repair. Proc. Second Int. Arch Bridge Conference*, pages 133–137. A.A. Balkema, October 1998.

[48] W.J. Harvey, F.W. Smith, and R. Barthel. Some notes on the behaviour in arch bridges. In *Arch Bridges - History, analysis, assessment, maintenance and repair. Proc. Second Int. Arch Bridge Conf.*, pages 315–319. A.A. Balkema, October 1998.

[49] K.D.S. Towler and F. Sawko. Limit state behaviour of brickwork arches. In *Proc. 6th International Brick Masonry Conference*, Rome, 1982.

[50] K.D.S. Towler. The non-linear finite element analysis of bridgemill masonry arch bridge. *Masonry International*, 5, 1985.

[51] M.A. Crisfield. Nonlinear analysis of concrete and masonry structures. *Bergan et al, Finite element methods for nonlinear problems*, 1986.

[52] A.R. Mari. A general method for the analysis of curved beams and space frames. Technical report, Department of Construction Engineering, Universitat Politècnica de Catalunya, Barcelona, Spain, 1985.

[53] C. Molins and P. Roca. Capacity of masonry arches and spacial frames. *Journal Of Structural Engineering, ASCE*, 124, 1998.

[54] P. Roca, C. Molins, T.G. Hughes, and C. Sicilia. Numerical simulation of experiments in arch bridges. In *Arch Bridges - History, analysis, assessment, maintenance and repair. Proc. Second Int. Arch Bridge Conference*, pages 195–204. A.A. Balkema, October 1998.

[55] B.S. Choo, M.G. Coutie, and N.G. Gong. Analysis of masonry arch bridges by a finite element method. In *Proc. of Fourth Rail Bridge Centenary International Conference*, pages 381–392, Edinburgh, 1990.

[56] B.S. Choo, M.G. Coutie, and N.G. Gong. The application of the finite element method to the cracking in masonry arch bridges. In *Proc. of the International Conference on Applied Stress Analysis*, pages 476–485, Nottingham, 1990.

[57] J. A. Hodgson and P. S. Fasholé-Luke. Finite element analysis of the multi-ring brickwork arch. In *Seventh International Conference on Structural Faults and Repair*, volume 1, pages 135–142, Edinburgh, July 1997.

[58] M. Cardinale, G.and Orlando and P. Spinelli. Static & dynamic response of a masonry arch bridge over Arno River. In *Seventh International Conference on Structural Faults and Repair*, volume 1, pages 129–134, Edinburgh, July 1997.

[59] C. Sicilia. A study of 3-D masonry arch structures using centrifuge models and finite element analysis. http://www.cf.ac.uk/uwc/engin-/research/concmas/cs-1.html, 1999.

[60] B.T. Rosson and T.E. Boothby. Hardening and shakedown of masonry arch joints. In *Arch Bridges - History, analysis, assessment, maintenance and repair. Proc. Second Int. Arch Bridge Conference*, pages 195–204. A.A. Balkema, October 1998.

[61] A.F. Ashour and S.W. Garrity. An upper bound analysis for the strength assessment of masonry arch bridges. In *Arch Bridges - History, analysis, assessment, maintenance and repair. Proc. Second Int. Arch Bridge Conference*, pages 139–146. A.A. Balkema, October 1998.

[62] I.M. May and J. Tellett. Non-linear finite element analysis of reinforced and unreinforced brickwork. In *Proc. of the British Masonry Society*, volume 1, pages 96–99. London, Stoke-on-Trent, 1986.

[63] N. Bićanić. From continua to discontinua - Modelling of progressive discontinuities in concrete. *Computational Modelling of Concrete Structures*, 1998.

[64] P.A. Cundall. A computer model for simulating progressive large scale movements in blocky rock systems. *Proc. Int Symp. on Rock Structure*, 11, 1971.

[65] P.A. Cundall and D.L. Strack, O. A discrete numerical model for granular assemblies. *Géotechnique*, 29:47–65, 1979.

[66] P.A. Cundell and R.D. Hart. Numerical modelling of discontinua. In G. et al Mustoe, editor, *1st US Conference on Discrete Element Methods*, 1989.

[67] N. Bićanić. From continua to discontinua- Modelling of progressive discontinuities in concrete. *Computational Modelling of Concrete Structures*, 1998.

[68] C. Hogue. Shape representation and contact detection for discrete element simulations of arbitrary geometries. *Engineering Computations*, 15(2–3):374–392, 1998.

[69] J.R. Williams and G.W. Mustoe. Model analysis for the analysis of discrete elements. *Computers and Geotechnics*, 4:1–10, 1987.

[70] G.H. Shi. *Discontinuous Deformation Analysis - a new numerical method for the statics and dynamics of block systems.* PhD thesis, Dept. of Civil Engineering, Univ. of California, Berkely, 1988.

[71] G.H. Shi. Numerical manifold method. In Y. Ohnishi, editor, *Proc. ICADD-2 Conference on Analysis of Discontinuous deformation*, Kyoto University, July 1997.

[72] T. Ng. Small-strain response of random arrays of spheres using discrete element methods. *Journal of Engineering Structures*, pages 239–244, March 1996.

[73] A. Munjiza, D.R.J. Owen, and N. Bićanić. A combined finite/discrete element method in transient dynamics of fractured solids. *Engineering Computations*, 12:145–174, 1995.

[74] Y.M. Cheng. Advancements and improvement in discontinuous deformation analysis. *Computers and Geotechnics*, 22(2):153–163, 1998.

[75] L.R. Jing. Formulation of discontinuous deformation analysis (DDA) - an implicit discrete element model for block systems. *Engineering Geology*, 49(3–4):371–381, 1998.

[76] C.T. Lin, B. Amadei, J. Jung, and J. Dwyer. Extensions of discontinuous deformation analysis for jointed rock masses. *Int. Journal of Rock Mechanics and Mining Sciences and Geomechanics Abstracts*, 33(7):671–694, 1996.

[77] R.J. Owen, D. Peric, N. Petrinic, C.L. Brookes, and P.J. James. Finite/discrete element models for assessment and repair of masonry structures. In *Arch Bridges - History, analysis, assessment, maintenance and repair. Proc. Second Int. Arch Bridge Conf.*, pages 173–180. A.A. Balkema, October 1998.

[78] C. Melbourne and H. Tao. The behaviour of open spandrel brickwork arch bridges. In *Arch Bridges - History, analysis, assessment, maintenance and repair. Proc. Second Int. Arch Bridge Conf.*, pages 263–269. A.A. Balkema, October 1998.

[79] G. Mirabella Roberti and F. Calvetti. Distinct element analysis of stone arches. In *Arch Bridges - History, analysis, assessment, maintenance and repair. Proc. Second Int. Arch Bridge Conf.*, pages 173–180. A.A. Balkema, October 1998.

[80] P.A. Cundell and R.D. Hart. Development of generalised 2-D and 3-D distinct element programs for modelling jointed rock. Misc. paper SL-85-1, U.S. Army Engineering Waterways Experiment Station, U.S Army Corps of Engineers, 1985.

[81] T. G. Hughes and R. Pritchard. In situ measurement of dead and live load stresses in a masonry arch. *Engineering Structures*, 20(1–2):5–13, 1998.

[82] K. Hellmich. Determination of the load carrying capacity of masonry arch bridges based on measurements. In *Seventh International Conference on Structural Faults and Repair*, volume 1, pages 77–81, Edinburgh, July 1997.

[83] T. E. Boothby and J. A. Laman. Development of load rating procedures for U.S. masonry arch bridges. In *Seventh International Conference on*

*Structural Faults and Repair*, volume 1, pages 179–187, Edinburgh, July 1997.

[84] A.W. Hendry *et al.* Load test to collapse on a masonry arch bridge at Bargower, Strathclyde. TRRL contractor report 26, Department of Transport, Transport Research Laboratory, Crowthorne, 1986.

[85] D. E. Boothby, T. E.and Domalik and V. A. Dalal. Service load response of masonry arch bridges. *Journal of Structural Engineering*, 124(1):17–23, 1998.

[86] C. Melbourne. *Arch Bridges - Proceedings of the First International Conference on Arch Bridges.* Thomas Telford Services Ltd., Bolton, England, September 1995.

[87] T.G. Hughes, M.C.R. Davies, and P.R. Taunton. The influence of soil and masonry type on the strength of masonry arch bridges. In *Arch Bridges - History, analysis, assessment, maintenance and repair. Proc. Second Int. Arch Bridge Conf.*, pages 321–330. A.A. Balkema, October 1998.

[88] D. Peng, C. Fairfield, and A. Sibbald. Experimental validation of flat arch analysis techniques. In *Seventh International Conference on Structural Faults and Repair*, volume 1, pages 121–128, Edinburgh, July 1997.

[89] N. Davey. Tests on road bridges. Technical report, National Building Study, Research Paper No.16, HMSO, London, 1953.

[90] D.A. Ponniah. Stress dispersal in arch bridges. In *Third International Conference on Structural Faults and Repair*, pages 311–316, London, 1987.

[91] D.A. Ponniah. Geotechnical considerations in bridge testing. In *Third International Conference on Structural Faults and Repair*, pages 329–336, London, 1987.

[92] D.A. Ponniah and K. Blackie. Further considerations in the soil-structure interactions of arch bridges. In *Fourth International Conference on Structural Faults and Repair*, pages 301–306, London, 1989.

[93] C.A. Fairfield and D.A. Ponniah. Increasing arch bridge capacity economically. In *Fifth International Conference on Structural Faults and Repair*, volume 1, pages 329–335, Edinburgh, 1993.

[94] C.A. Fairfield and D.A. Ponniah. Arch bridge backfill properties. In *Fifth International Conference on Structural Faults and Repair*, volume 3, pages 269–273, Edinburgh, 1993.

[95] C.A. Fairfield and D.A. Ponniah. Soil pressure measurement for arch bridge assessment. In *Fifth International Conference on Structural Faults and Repair*, volume 3, pages 283–288, Edinburgh, 1993.

[96] C.A. Fairfield and D.A. Ponniah. Heavy axle load tests on a new brickwork arch bridge. In *Fifth International Conference of structural Masonry for Developing Countries*, Santa Catarina, 1993.

[97] D.A. Ponniah and C.A. Fairfield. Earth pressure measurements at Kimbolton Butts Bridge, Cambridgeshire. In *Centenary Bridge Conference*, Cardiff, 1994.

[98] D.A. Ponniah, C.A. Fairfield, and D.J. Prentice. Heavy axle loads on a new brickwork arch bridge. Report, Institute of Civil Engineers, 11 Upper Belgrave street, London, 1996.

[99] D.A. Ponniah, D.J. Prentice, and C.A. Fairfield. The effect of overlying fill on stresses in a new arch bridge. In *Proceedings of the US-Europe Workshop on Bridge Engineering*, Barcelona, July 1996.

[100] D.J. Prentice and D.A. Ponniah. Testing of multi-span model masonry arch bridges. In *Proceedings of the Conference on Bridges Assessment, Management and Design*, Cardiff, 1994.

[101] D.J. Prentice and D.A. Ponniah. Installation of data acquisition equipment in Kimbolton Butts bridge. In *Proceedings of the First International Conference on Arch Bridges*, Bolton, 1995.

[102] D.J. Prentice and D.A. Ponniah. New techniques in the elastic analysis of arch bridges using image processing. *British Society for Strain Measurement*, Nov 1996.

[103] F. W. Sumon. Repair and strengthening of a damaged arch with built-in ring separation. In *Seventh International Conference on Structural Faults and Repair*, volume 1, pages 69–75, Edinburgh, July 1997.

[104] C. Peaston and B. S. Choo. Predicting the capacity of spayed concrete strengthened masonry arch bridges: A comparison of experimental and analytical data. In *Seventh International Conference on Structural Faults and Repair*, volume 1, pages 91–95, Edinburgh, July 1997.

[105] S. Thorburn, W.J. Larnach, M.J. Tomlinson, and T. Whitaker. Soil-structure interaction - a state of the art report. Report, The Institution of Structural Engineers, 11 Upper Belgrave street, London, April 1978.

[106] S. Thorburn and Burland J.B. Soil-structure interaction - the real behaviour of structures. Report, The Institution of Structural Engineers, 11 Upper Belgrave street, London, March 1989.

[107] S. Thorburn. The real behaviour of structures - soil structure interaction. *The Institution of Civil Engineers*, Feb 1985.

[108] M.N. Viladkar, P.N. Godbole, and I. Noorzaei. Modelling of interface for soil-structure interaction studies. *Computers and Structures*, 52(4):765–779, 1994.

[109] K. Runesson, H. Tangfors, and N. Wiberg. Interaction problems in soil-structure mechanics with material non-linearity. *Computers and Structures*, 12:581–592, 1980.

[110] B. Gosy. Soil-foundation-structure interaction. *ASCE- Structure Division*, 104:749–761, 1978.

[111] A. Sinopoli. *Arch Bridges - History, analysis, assessment, maintenance and repair. Proceedings of the Second International Conference on Arch Bridges.* A.A. Balkema Publishers, Venice, Italy, October 1998.

[112] NAVFAC. Design Manual - soil mechanics, foundations and earth structures. Report DM-7, US Navel Facilities Engineering Command, Washington DC, 1971.

[113] D.R. Carder, R.G. Pocock, and R.T. Murrey. Experimental retaining wall facility - lateral stress measurements with sand backfill. TRRL Report 766, Dept. of the Environment, Transport and road research Laboratory, Crowthorne, 1977.

[114] M.G. Katona, J.M. Smith, R.S. Odello, and J.R. Allgood. CANDE - a modern approach for the structural design and analysis of buried culverts. Report FHWA-RD-77-5, Federal Highway Administration, Washington DC, October 1976.

[115] CIRIA. Design and construction of buried thin-walled pipes. *Research Report*, July 1978.

[116] BA16/93. Department of Transport, HMSO, London. *The assessment of highway bridges and structures - Advice Note*, 1993.

[117] Military Engineering Experimental Establishment. MEXE. In *Classification of masonry arch bridges.* Christchurch, 1952.

[118] W.J. Harvey. *ARCHIE and MULTI operation manual*, 1991.

[119] S.F. Broomhead *et al.* Masonry Arch Finite Element Assessment, MAFEA documentation. Report no. 1,2,3,4 and 5, Track & Civil Engineering Group, BR Research, PO Box 2, London Road, Derby, DE24 8YB, 1996.

[120] S Lee. Load behaviour of multi-span arch bridges. Master's thesis, University of Edinburgh, 1996.

[121] BS5400. British Standards Institution, London. *Highway bridge live loads*, 1978.

[122] F.D.C. Henry. The design and construction of engineering foundations. 1986.

[123] T.W. Lambe and R.V. Whitman. *Soil Mechanics.* John Wiley and Sons, 1996.

[124] M.E. Harr. *Foundations of theoretical soil mechanics.* McGraw-Hill Book Company, 1966.

[125] C.A. Fairfield and D.A. Ponniah. Model tests to determine the effect of fill on buried arches. *Proc Instn Civ Engrs Structs & Bldgs*, 104, Nov 1994.

[126] Gage Technique Ltd., Trowbridge, UK. *Equipment operating instructions*, 1972.

[127] Soil Instruments Ltd., Uckfield, E. Sussex. *User's Manual*, 1991.

[128] Hibbitt, Karlsson, and Sorensen Inc. *ABAQUS User's Manual*, 1998.

[129] Altair Computing Inc., 1757 Maplelawn, Troy, MI. *Hypermesh User's Manual*, 1995.

[130] C.A. Fairfield and D.A. Ponniah. Earth pressure measurements at Kimbolton Butts bridge, Cambridgeshire. Technical report, TRRL, Crowthorne, 1993.

[131] NAASRA. Pavement design; A guide to the structural design of road pavements. Technical report, National Association of Australian State Road Authorities, Revesby, Australia, 1987.

[132] N. Jackson. *Civil engineering materials.* Macmillan Press, 4th edition, 1988.

[133] C. Lin. *Extensions to the DDA method for jointed rock masses and other blocky systems.* PhD thesis, University of Colorado, 1995.

[134] B. Amedei, C. Lin, and J. Dwyer. Recent extension to the DDA method, simulation of discontinuous media. Technical report, TSI Press, Albuquerque, 1996.

[135] G.H. Shi and M.R. Yeung. *Discontinuous Deformation Analysis programs, User's Manual.*

[136] T.X. Tran, A. Dorfmann, and Y.B. Rhie. Micro-mechanical modelling of cracking and damage of concrete structures. *Computational Modelling of Concrete Structures*, 1998.

[137] T.K.H. Tam and C.G. Armstrong. 2-D finite element mesh generation medial axis sub-division. *Advances in Engineering Software*, 13:313–324, 1993.

[138] A. Thavalingam. Delaunay triangulation on three dimensional surface for element analysis, 1991. Misc. dissertation. Queen's Univ. of Belfast, UK.

[139] Itasca Consulting Group. *Particle flow code in 2 dimensions.* Volume I: User's Manual. Thresher Square East, 708 South Third Street, Minneapolis, 55415, USA, 1995.

[140] *DIANA - Finite element analysis, User's Manual.* TNO Building and Construction Research, Delft, Netherlands, 6.1 edition.

[141] J.I. Robinson, A. Thavalingham, D.A. Ponniah, and N. Bicanic. Comparative predictions of the collapse load for masonry arches including backfill interaction. *Masonry International*, 2000.

[142] D.A. Ponniah and N. Bicanic. Discrete element/finite element modelling of backfilled interaction in masonry arch bridges. Technical report, Universities of Edinburgh and Glasgow, 1999.

# Appendix A

The spreadsheet shown here represent the MEXE analysis method used for the parametric study and subsequent arch bridge assessment program.

**Analysis by the 'Modified MEXE method'**

From BA 16/97 The Assessment of Highway Bridges and Structures

First find the Provisional axle load (P.A.L.)

P.A.L. = 740*(d+h)^2/L^1.3

| | | | | | | |
|---|---|---|---|---|---|---|
| Span | L = | 10.45 (m) | where | | d= | arch barrel thickness |
| Rise | Rc = | 5.22 (m) | | | h= | depth of fill |
| Dept of fill (mm) | h = | 1.76 (m) | | | L= | arch span |
| Arch barrel thickness | d = | 0.7 (m) | | | ^ = | to the power of |
| Rise at 1/4 span | Rq = | 4.521 (m) | | P.A.L. = | | 211.96 |
| span/rise factor | Fsr = | 1.000 | | | | |
| profile factor | Fp = | 0.689 | where | Fp = | 0.6886376 | Fp = 2.3*((rc-rq)/rc)^0.6 |
| | | | | rc = | 5.22 | rq = 4.52052 |
| material factor | Fm = | 0.842 | where | Fm = | 0.8422764 | Fm = ((Fb*d)+(Ff*h))/(d+h) |
| | | | | Fb = | 1.2 | Ff = 0.7 |
| joint factor | Fj = | 0.900 | where | Fj = | 0.9 | Fj = Fw + Fd + Fmo |
| | | | | Fw = | | 0.9 width |
| | | | | Fd = | | 1.0 depth |
| | | | | Fmo = | | 1.0 mortar factor |
| condition factor | Fc = | 0.640 | where | Fc = | 0.64 | Fc = combination of defect factors |
| | | | | defects = | | 0.8 Unfav. defects = 0.8 |

Modified axle Load = 70.81 where M.A.L. = P.A.L. * Fsr * Fp * Fm * Fj * Fc

Figure A.1: MEXE analysis spreadsheet used

# Appendix B

The graphs shown in this appendix are those relating to Chapter 3. They include the graphs presenting the data from the parametric study performed on the four assessment methods discussed. They are presented in order with which they are discussed within the text and as such should be used a reference.

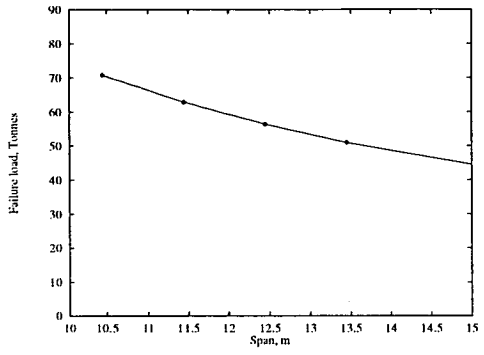


(a)

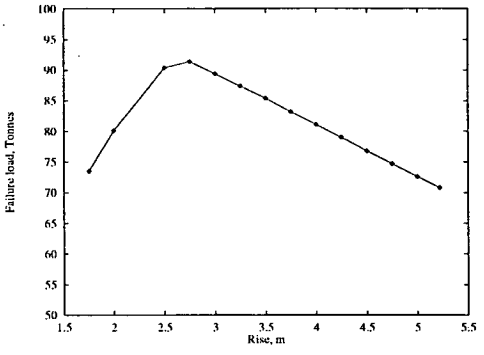


(b)

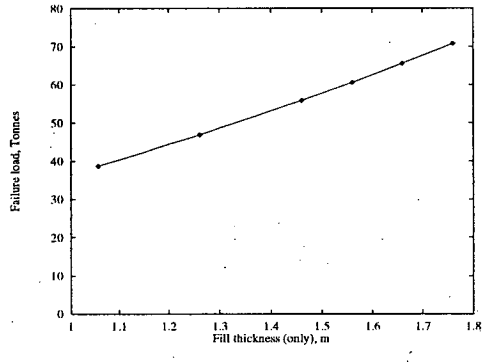


(c)

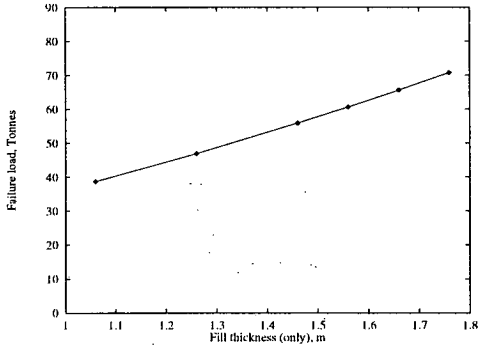


(d)

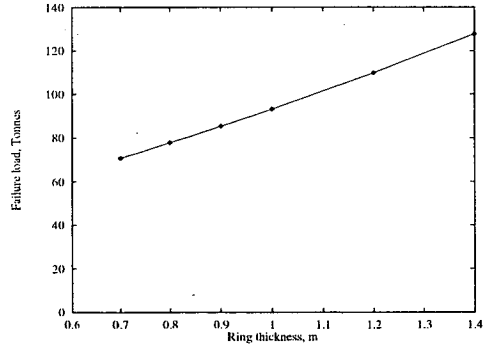


(e)

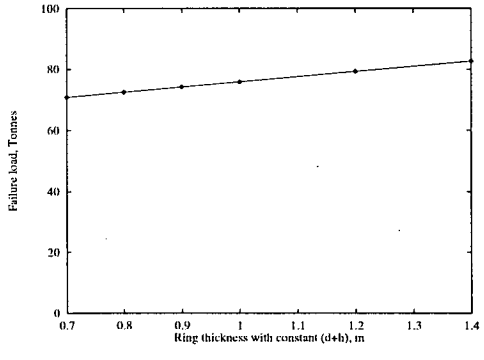


(f)

Figure B.1: Mexe parametric study results

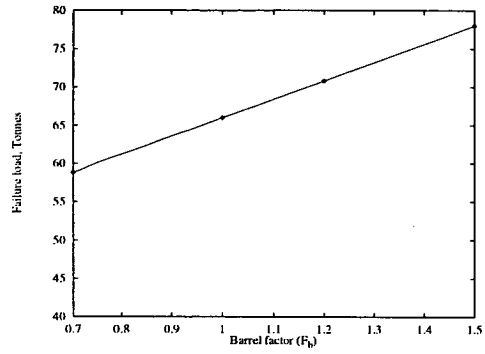


(a)

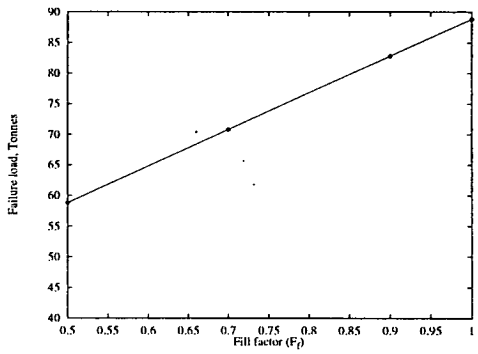


(b)

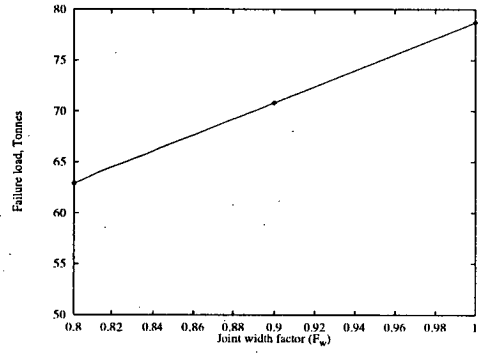


(c)

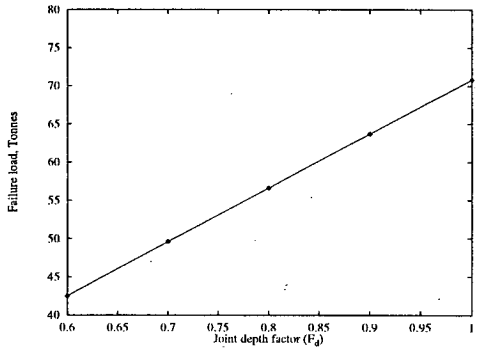


(d)

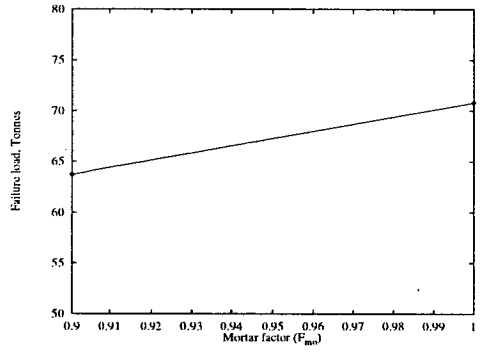


(e)

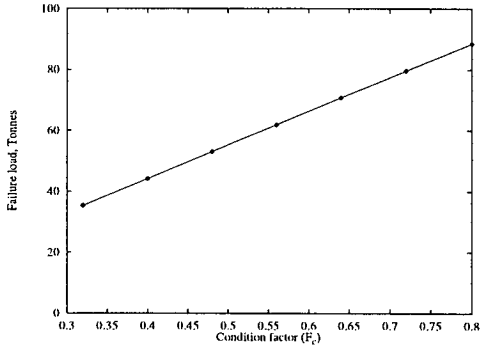


(f)

Figure B.2: Mexe parametric study results

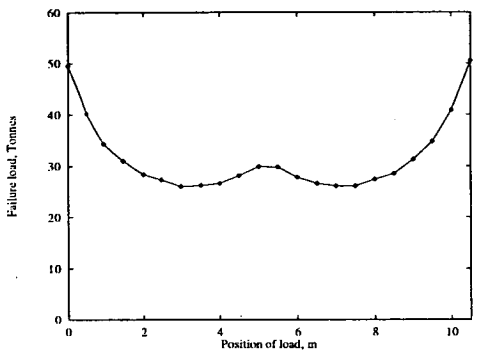


(a)

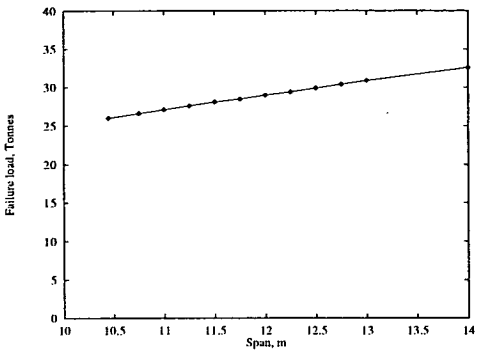


(b)

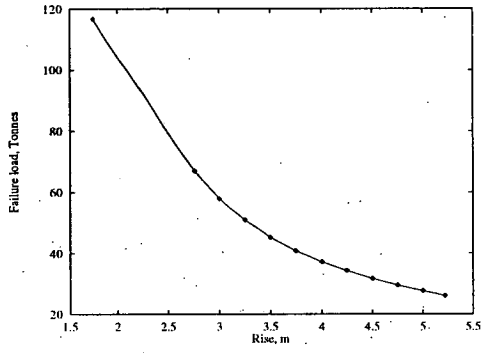


(c)

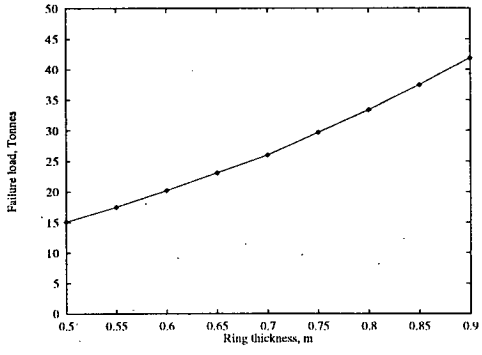


(d)

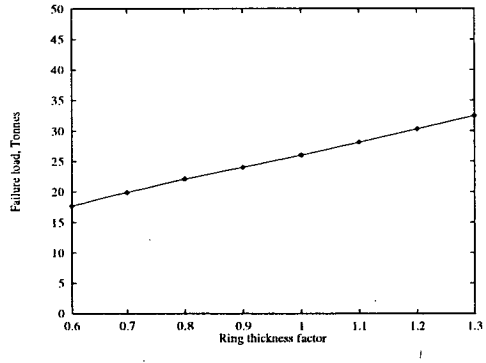


(e)

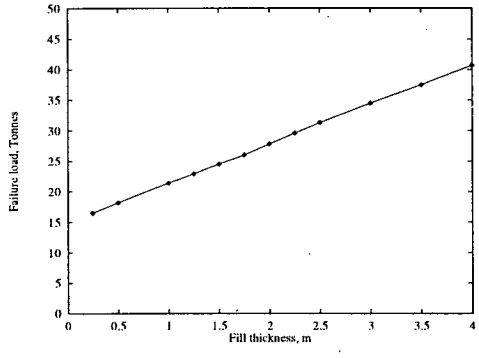


(f)

Figure B.3: Archie parametric study results

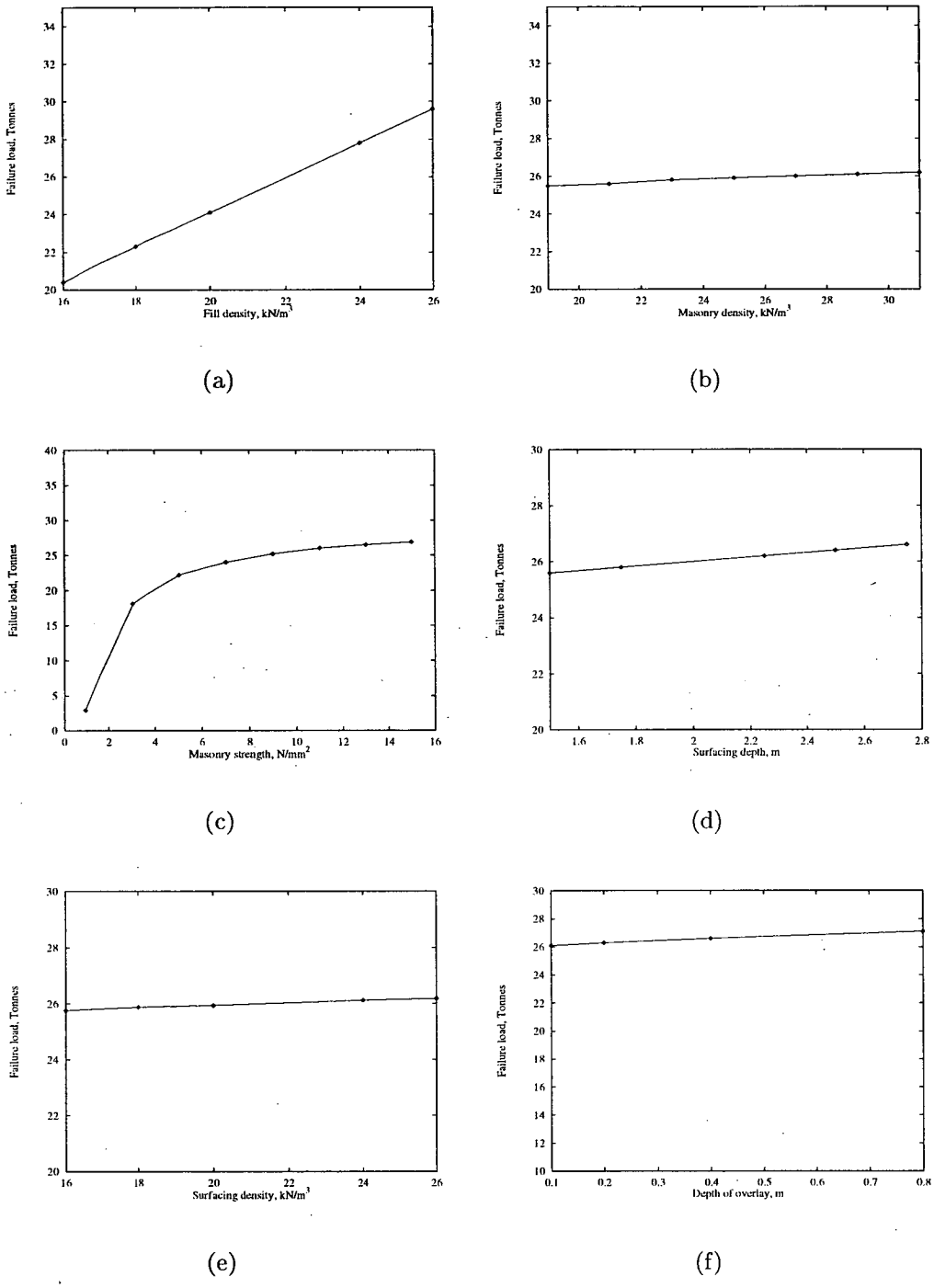


Figure B.4: Archie parametric study results

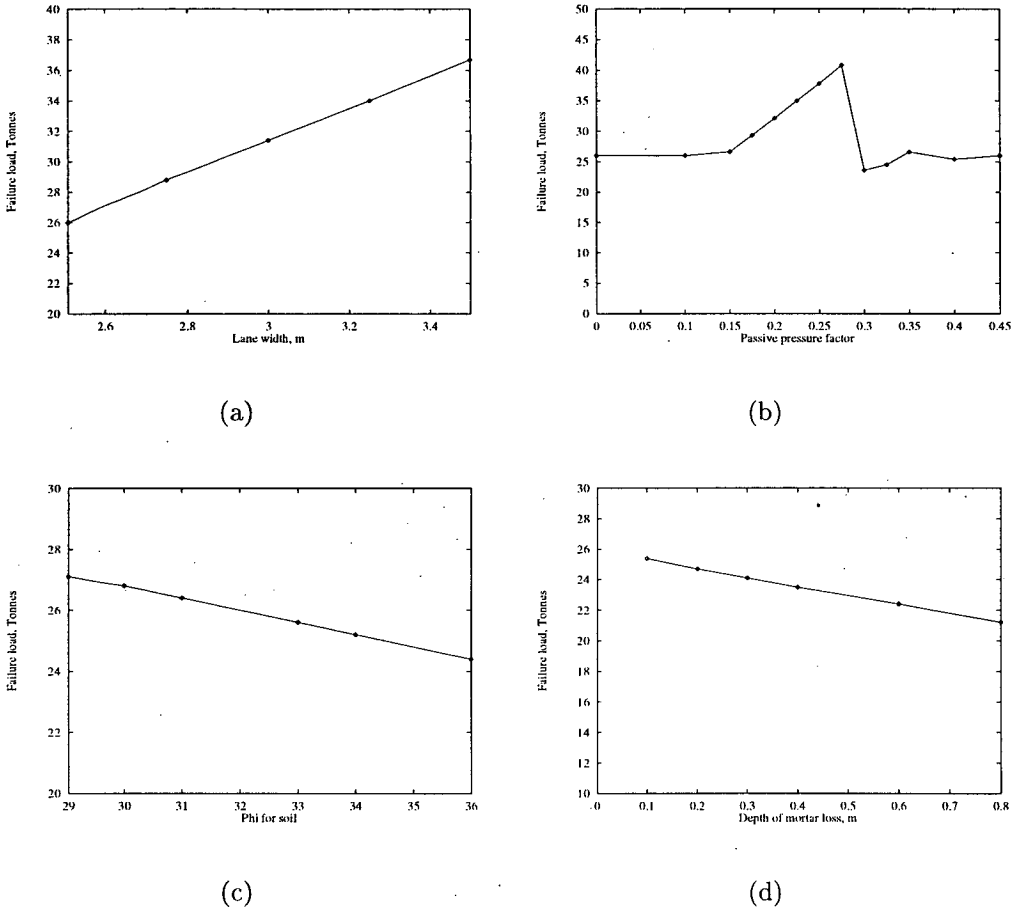


Figure B.5: Archie parametric study results

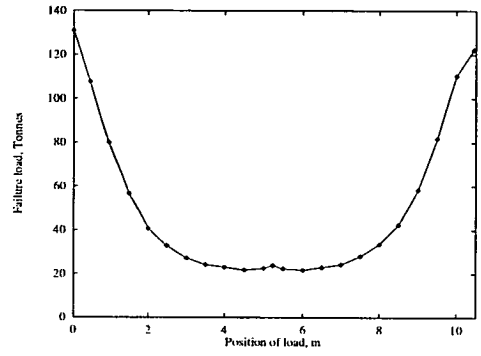


(a)

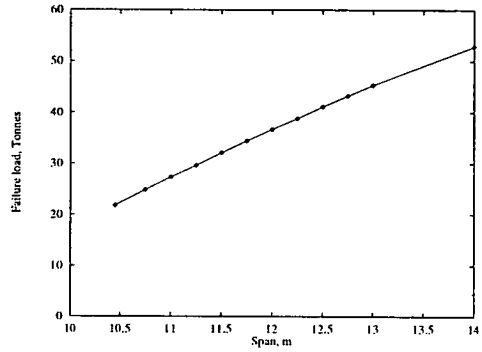


(b)

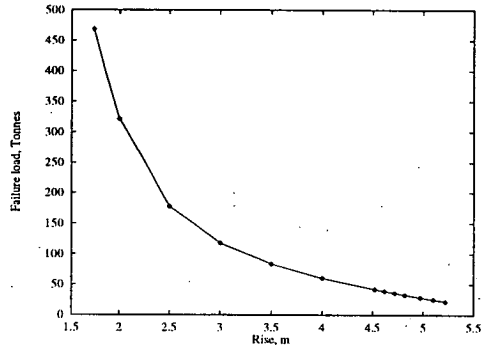


(c)

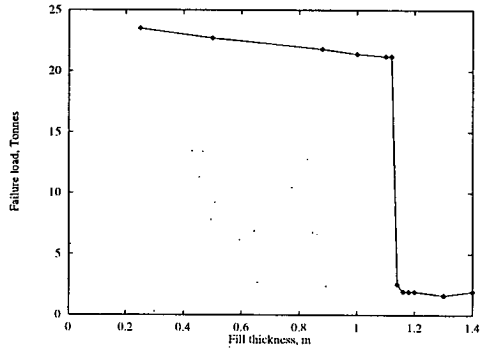


(d)

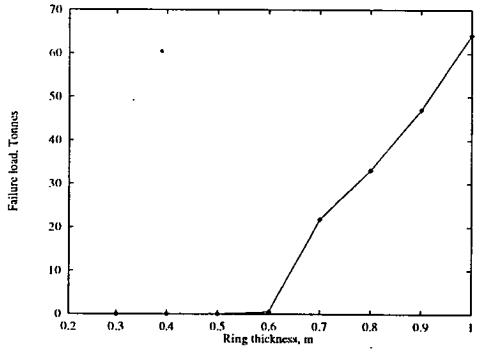


(e)

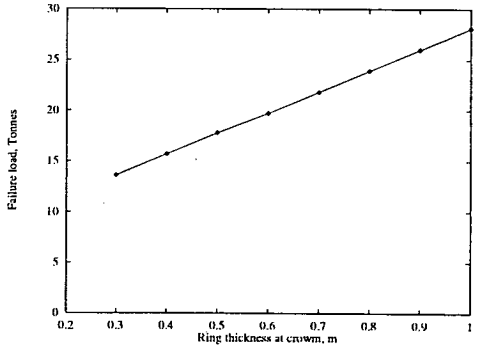


(f)

Figure B.6: Ctap parametric study results

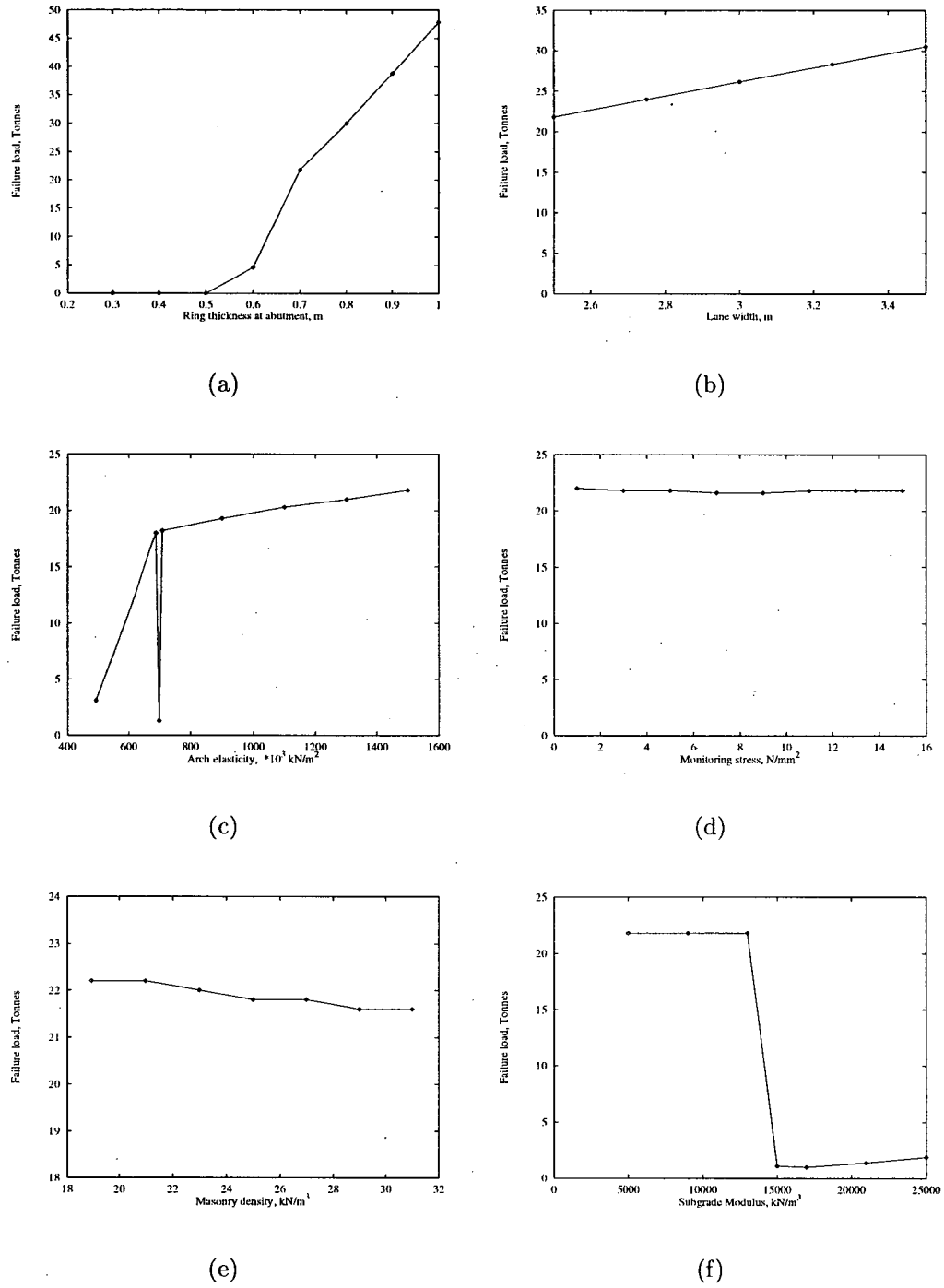


Figure B.7: Ctap parametric study results

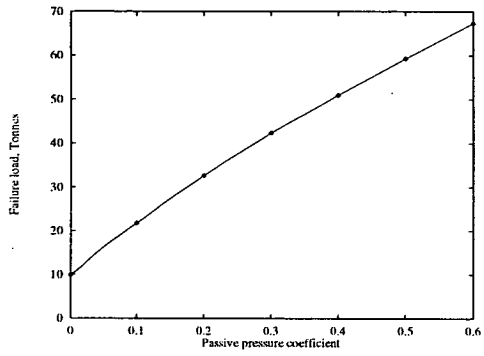


(a)

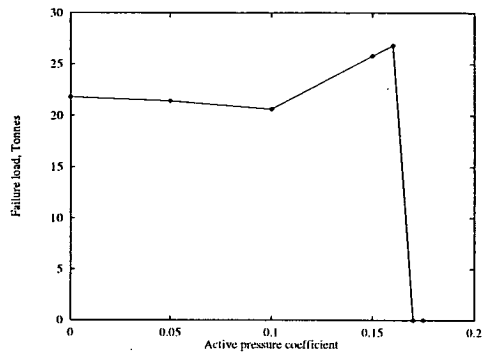


(b)

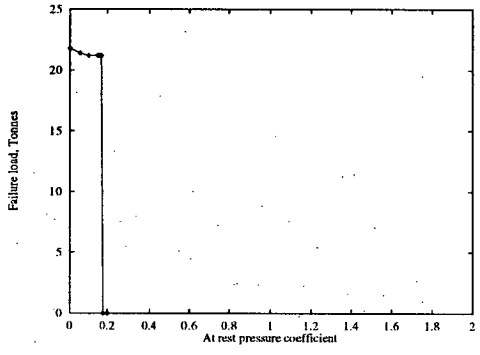


(c)

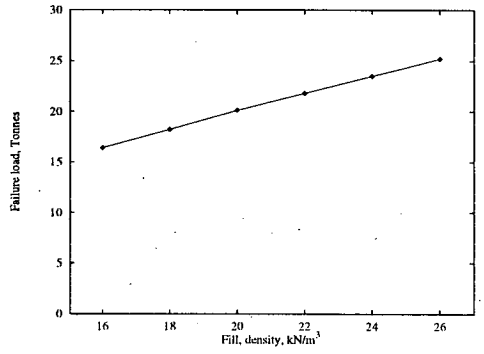


(d)

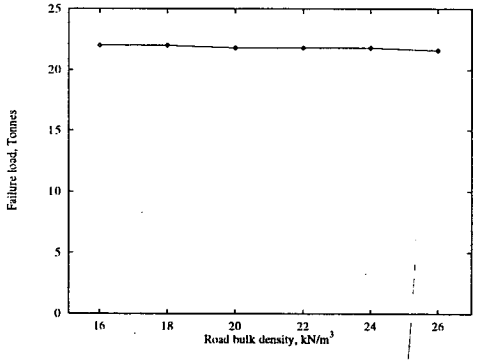


(e)

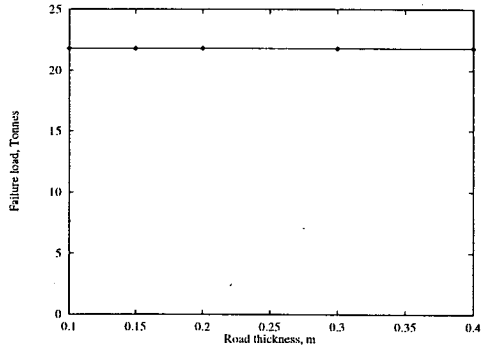


(f)

Figure B.8: Ctap parametric study results

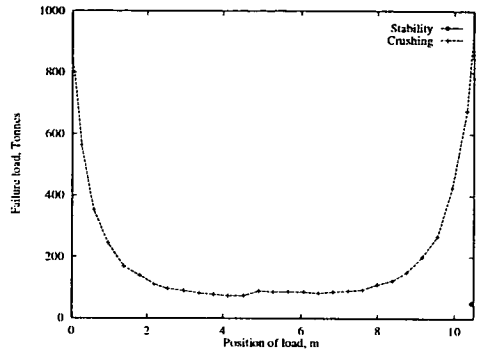


(a)

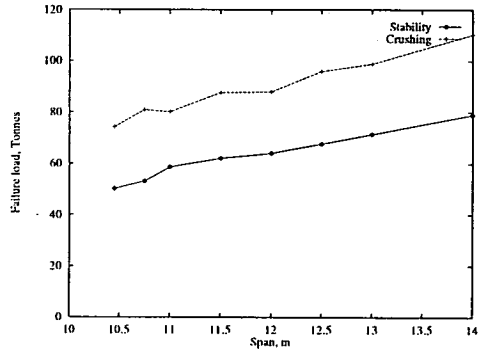


(b)

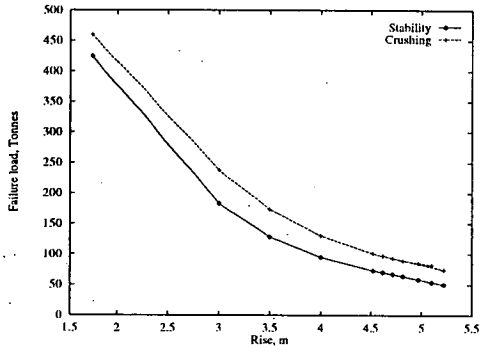


(c)

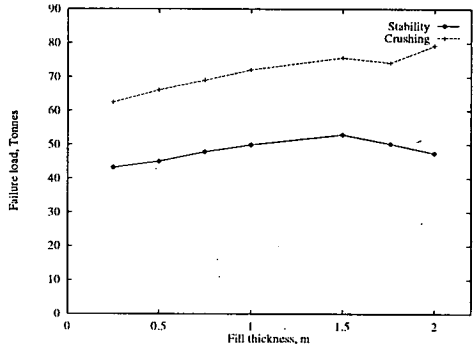


(d)

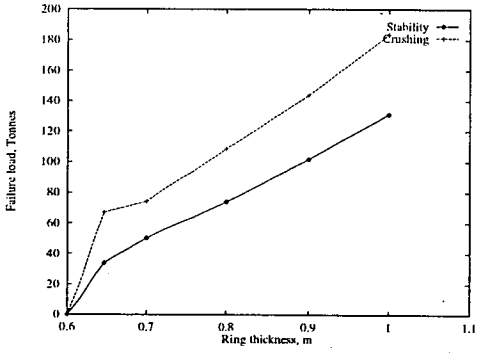


(e)

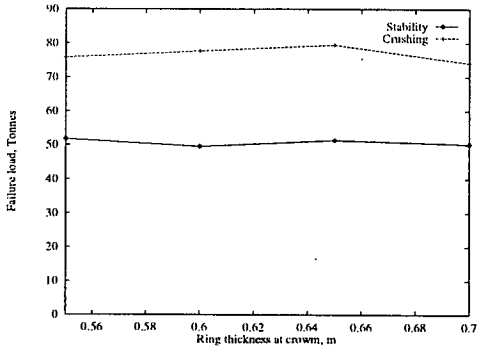


(f)

Figure B.9: Mafea parametric study results

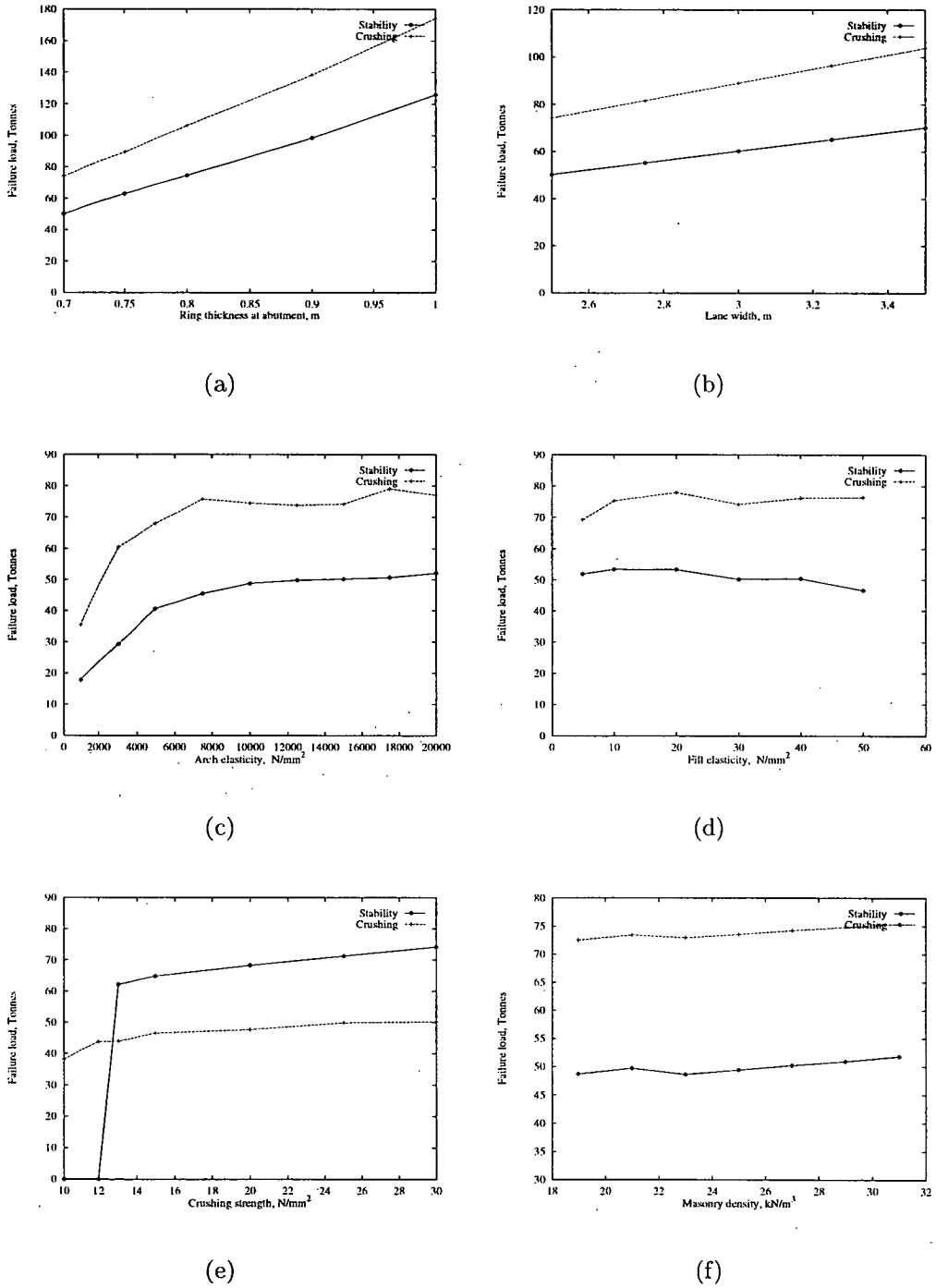


Figure B.10: Mafea parametric study results

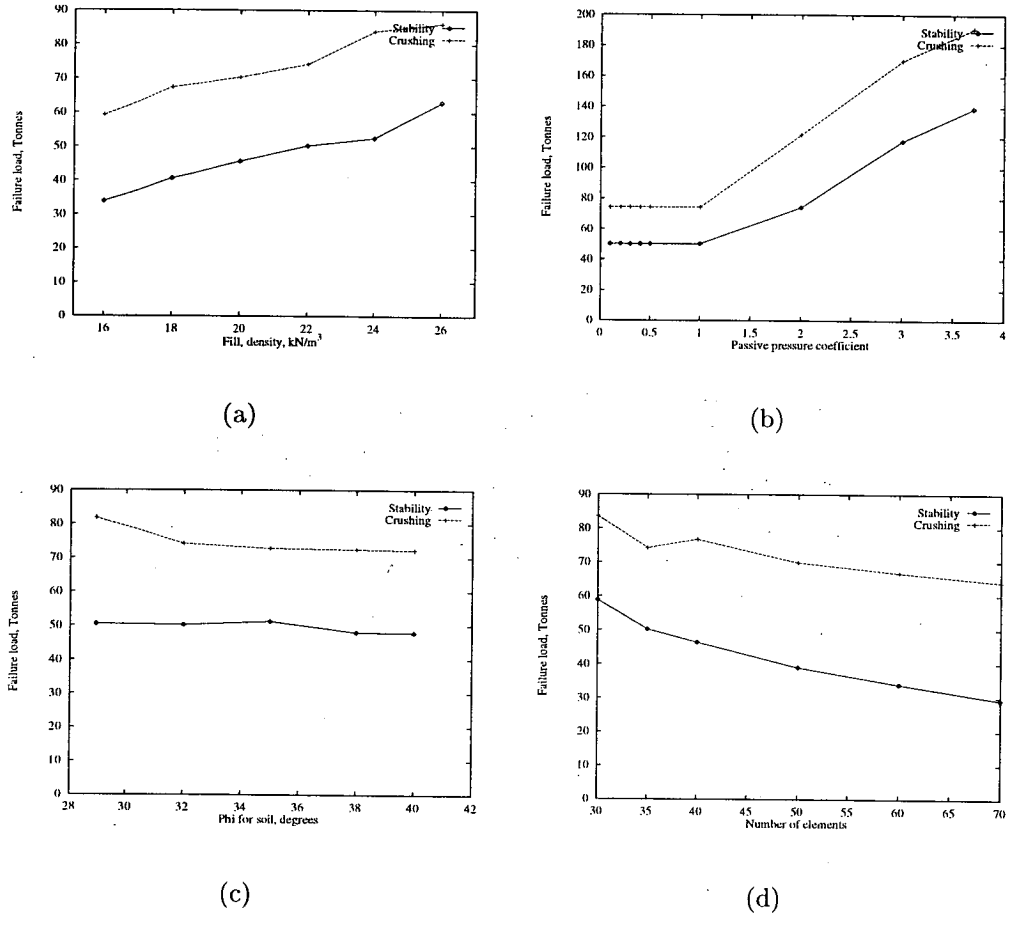


Figure B.11: Mafea parametric study results

# Appendix C

This is the input file used for the 3-D thermal analysis of Kimbolton Butts Bridge using ABAQUS.

```
 **
**
**
*HEADING
FIRST TRY AT THE IMPORTING IF DATA TO A FILE, FOR THE BRICK, FILL AND
TARMAC SECTIONS OF THE BRIDGE STRUCTURE.
**
**NODE GENERATION
**
*NODE, INPUT=all-arch.res, NSET=ALL
**NODE
**
**ANY EXTRA NODES THAT NEED ADDING
**
**NOT IN THIS CASE PUT IF REQUIRED THEN-*NSET, NSET=TARMAC1
**7000,-4,2,0
**
**NODE GENERATION
**
*ELEMENT,INPUT=el-brick.norm, TYPE=C3D8,ELSET= BRICK
*ELEMENT,INPUT=el-fill.norm, TYPE=C3D8,ELSET= FILL
*ELEMENT,INPUT=el-tarmac.norm, TYPE=C3D8,ELSET= TARMAC
**
```

```
**MATERIAL DEFINITION
**
*MATERIAL, NAME=BRICK
*ELASTIC
1E+10,0.2,20
*DENSITY
22000
**SAME VALUES FOR SAME TEMPERATURE, IF VARY THEN NEED OTHER VALUES
**PLASTIC
**300,0,20
*EXPANSION
6E-6,20.0
**ETC.
*MATERIAL, NAME=FILL
*ELASTIC
6E+6,0.4,20
*DENSITY
16000
**SAME VALUES FOR SAME TEMPERATURE, IF VARY THEN NEED OTHER VALUES
***PLASTIC
**300,0,20
*EXPANSION
1.23E-7,20.0
**ETC.
*MATERIAL, NAME=TARMAC
*ELASTIC
2E+8,0.3,20
*DENSITY
14500
**SAME VALUES FOR SAME TEMPERATURE, IF VARY THEN NEED OTHER VALUES
***PLASTIC
**300,0,20
*EXPANSION
1.23E-5,20.0
**ETC.
**
```

```
**INITIAL TEMPERATURE
**
*INITIAL CONDITIONS,TYPE=TEMPERATURE
ALL,20.0
**
**LOADING CONDITIONS
**
*STEP,AMPLITUDE=STEP,INC=30,NLGEOM
GRAVITY LOADING
*STATIC
0.5,5
**
**FIXED BOUNDARY CONDITIONS
**
*NODE, INPUT=leftside.data, NSET=LEFTSIDE
*BOUNDARY
LEFTSIDE,1,3
*NODE, INPUT=rightside.data, NSET=RIGHTSID
*BOUNDARY
RIGHTSID,1
RIGHTSID,3
**
**INITIAL LOADING
**
*DLOAD,OP=NEW
BRICK,GRAV,-9.81,0,1,0
FILL,GRAV,-9.81,0,1,0
TARMAC,GRAV,-9.81,0,1,0
*TEMPERATURE,OP=NEW
ALL,20.0
**
**
*NODE PRINT,FREQ=9
U
*NODE FILE,FREQ=9
U
```

```
**
*EL PRINT,POSITION=NODES,FREQ=9
S
E
THE
***EL FILE,POSITION=NODES,FREQ=0
**S
**E
*RESTART,WRITE
*END STEP
**
**
**
*STEP,AMPLITUDE=RAMP,INC=500,NLGEOM
THERMAL LOADING
*STATIC
**8,140,0.1,20.0
*TEMPERATURE
ALL,50.0
**BRICK,50.0
**FILL,50.0
**TARMAC,50.0
*NODE PRINT,FREQ=9
U
*EL PRINT,POSITION=NODES,FREQ=9
S
E
THE
***EL FILE,POSITION=NODES,FREQ=0
**S
**E
*RESTART,WRITE
*END STEP
```

# Appendix D

This appendix shows the published papers written and presented during the course of this thesis.

# TEMPERATURE EFFECTS IN A NEW BRICKWORK ARCH BRIDGE

J. I. Robinson
Civil & Environmental Engineering
University of Edinburgh
The Kings Building
Edinburgh EH9 3JN
Scotland

Dr D. Prentice
Civil & Environmental Engineering
University of Edinburgh
The Kings Building
Edinburgh EH9 3JN
Scotland

Dr D. Ponniah
Civil & Environmental Engineering
University of Edinburgh
The Kings Building
Edinburgh EH9 3JN
Scotland

KEYWORDS: Arch bridges; data acquisition; instrumentation; stress; strain; temperature

## ABSTRACT

This paper presents the results from long term monitoring of a single span brickwork arch bridge at Kimbolton Butts, Cambridgeshire, England. The monitoring has been ongoing since December 1994, and is part of a combined research programme into masonry arch bridges being carried out at the University. Various instruments were installed in the arch bridge during construction, which have enabled the long term monitoring of stress and strain levels throughout the bridge. This paper is concerned with the results obtained from this monitoring. A description of the bridge will be given, followed by a discussion on both the theory and the relevance of the tests, and how the monitoring was carried out. The results have been analysed and a number of conclusion have been drawn based on the effect the temperature has on stress levels within the arch.

## INTRODUCTION

Under ever increasing axle loads the importance of the masonry arch in Britain's infrastructure has never been more significant than at the present time. It is estimated that there are over forty thousand highway arch bridges in the UK in need of urgent reassessment due to recent European Community Directives (Page, 1993). Current assessment methods are considered to be conservative and improvements to these methods could lead to substantial savings. The research described in this report is an element of an on-going study into soil-structure interaction which has been shown to be an important factor in the assessment of arch bridges (Fairfield and Ponniah, 1994).

The instrumentation of a full scale bridge is important to the overall objectives of such an investigation, particularly where continual monitoring of a full scale arch can be carried out over a long period of time. Such an opportunity arose in 1992, when Cambridgeshire County Council undertook the design and construction of a new arch bridge on the B660 at Kimbolton Butts, Cambridgeshire. Instrumentation of the structure was jointly undertaken by the University of Edinburgh and the Transport Research Laboratory (TRL), to achieve the following objectives:

- Monitor the soil pressure in the fill, and the stresses and strains in the voussoirs of the bridge.
- Identify the effects of traffic work hardening and changes in temperature on fill pressures.
- Compare measurements with elastic finite element analyses.

## CONSTRUCTION DETAILS

The construction of the bridge was completed in 1992 and the main construction details are shown in figure 1. It has a span of 8m and a rise of 2m with a total width of arch of 10.1m. The arch barrel is constructed in engineering brick and laid in four courses to give a total thickness of 440mm. A 650mm thick brick spandrel wall is connected to the barrel at each side. The foundations are constructed in mass concrete to a depth of approximately 14m where they are founded on Oxford clay.

Prior to backfilling of the bridge, the arch barrel, spandrel and wing walls were waterproofed with a suitable material and a drainage fabric was placed on the extrados. The fill material was then laid in equal increments up to a height of 50mm above crown level. The Carrstone fill is a brown, silty, ferruginous SAND with some gravel. From tests undertaken at the University of Edinburgh the maximum dry unit weight of the fill was measured at 16.5 kN/m$^3$ with an angle of shearing resistance of 35° (Fairfield and Ponniah, 1993). The road pavement was 450mm thick, consisting of 250mm of asphalt surfacing and 200mm of Type 1 sub-base.

## INSTRUMENTATION

The layout of the instrumentation is shown on Figures 2 and 3, and consisted of pressure cells on the extrados and within the fill, strain gauges on the extrados, and thermocouples at three locations.

Pressure cells:

The pressures normal to the extrados were measured using Gage Techniques Ltd.'s vibrating wire gauge (VWG) pressure cells (Gage Technique Ltd., 1972). The cells have a working stress range of 0 to 500kPa and a sensitivity of 0.1% and can be calibrated against external pressure from a change in the frequency of vibration in the wire. The vertical pressure in the fill was measured using Soil Instruments Ltd. pressure gauges which consists of two circular active faces separated by oil of a similar elastic modulus to the surrounding fill (Soil Instruments Ltd., 1991). These cells have a similar working stress range to the ones described above.

Both types of cells were calibrated in-house while embedded in a sample of the Carrstone fill. The cells on the arch barrel were placed in pre-counterbored holes in the extrados and set in a surround of dental plaster to hold it in position during backfilling. Particular care was taken in the placement of the fill around the cell. The cells in the fill were installed in a similar manner but in a 100mm deep pocket with 50mm of the fill hand compacted above the cell before normal compaction resumed. The cables were run through semi-rigid ducts to the cable termination manhole shown in Figure 3, accessed from the top of the bridge. An additional Soil Instruments Ltd. cell which was subject to no externally applied pressure was also placed in this manhole.

Strain gauges on arch extrados:

As shown in Figure 3, a total of 24 Gage Technique 200mm vibrating wire strain gauges were installed by TRL on the extrados of the arch. Full details of these can be found in the official report by TRL (Page *et al,* 1993). The majority of the gauges were positioned on the south side of the crown but cells 1 and 2 were specifically located on the north side to assess the uniformity of the arch behaviour. The gauges were fixed to the barrel onto "header" bricks and positioned so that they always spanned two mortar joints.

Thermocouples :

Two type T thermocouples were installed in the arch and the fill by TRL. The instruments were of the copper-constant type with insulated, unducted wires and could be read to the nearest 0.1°C. All wires were again taken back to the cable termination manhole. A type K thermocouple was installed in this manhole at the same time as the data acquisition equipment. This was specifically carried out to allow a correlation between the air temperature and the results from the dummy pressure gauge also situated in the manhole.

## DATA ACQUISITION EQUIPMENT

A suitable datalogger was installed in the cable termination manhole which could be connected to the instrument cables and programmed to take readings at appropriate intervals. Part of the work was carried out at Edinburgh University and then installed in the manhole on-site at Kimbolton. The main requirements for the datalogger were;

- capable of monitoring of over 30 channels.
- robust and weatherproof.
- of suitable dimensions to fit in the manhole (450 x 450 x 600mm depth).
- enable a minimum of 4 readings a day from each instrument.
- capacity to store readings up to a month at a time.

After investigation into suitable systems, the Datataker 600$^{TM}$ datalogger developed by Data Electronics (Australia) and distributed in this country by Gage Technique Ltd. was selected as being most suitable (ref). The microprocessor based datalogger is powered by a battery and can measure 10 differential or 30 single ended analogue inputs with a further capacity of 30 channels available from an external expansion module.The battery backed RAM is capable of storing up to 13,650 readings with an additional 340,000 readings available on a removable memory card. It is of robust modular construction of powder coated steel and can operate at temperatures of between -20°C to 70°C which is more than sufficient for the likely range expected in this case. The waterproof enclosure also houses the battery power supply, connection cables and channel expansion cards.

upstream footpath. At this point the cables for the 10 VWG's pressure cells were taken into a junction box and wired to a 10-way Plessey socket. The 24 strain gauges were wired into an equivalent 25-way Plessey socket in a separate junction box. These were connected to the datalogger via a serial cable and a wiring block.

The datalogger is programmed via a laptop computer where the information is entered as a series of commands which are downloaded into the datalogger. These commands instruct the Datataker™ what channels to read, when, and how often. The time intervals for data collection was set at 6 hours starting at midnight, which was considered to be sufficient to record the likely daily and seasonal temperature fluctuations. Downloading of data is again carried out using the portable laptop computer and each time data are downloaded the program is terminated and restarted.

## PRESENTATION OF RESULTS

The datalogger was installed in the bridge on 12th December 1994 which represented a time lapse of almost 2 years since the bridge was constructed. Since then data collection has been continuous and has encompassed two full cycles of seasonal variations. The results presented and discussed in this paper are only a representative sample of the total due to the limitation of space.

Results two years after construction:

The distribution of stresses over a two year period from the time of installation are based on a zero reading taken prior to backfilling of the arch, and is shown in Figure 4. The initial increase in the results is a function of the placement of the arch fill. All the cells then show a reduction in stress from the time of installation, to the point of commencing datalogging. This reduction is of the order of 5 to 10 kPa for most of the cells. This could be partly due to the locked-in stresses during the placement of the sand fill which have dissipated over the 22 month time period.

Results from datalogger installation onwards:

A total of two years worth of data has been collected for the bridge. The results presented in this paper are based on one years worth of data from Dec. 1994 to Jan. 1996. Only one years data is shown as this highlights results in greater detail, and the second years results are very similar. All four daily readings are shown in each case to highlight the different responses to variations in both the daily and the seasonal temperature fluctuations.

*Analysis of temperature variations:*

The distribution of temperature of the three locations is easily definable and follow an expected pattern, as shown in Figure 4. The maximum reading is from the air temperature with a peak value of approximately 31°C occurring in the month of August. The daily fluctuations are also much more pronounced than in the soil or arch extrados, especially in mid summer where changes of approximately 7°C have been recorded. The temperature reaches a minimum value of almost 0°C in January of each year which is significant with respect to the analysis of the stress and strain results.

A similar distribution is evident from the temperature monitored in the fill but the daily fluctuations are lower. The minimum readings are similar to those taken in air but the maximum temperature is slightly less with a value of 27°C. This is as expected since the fill material is not exposed to direct climatic changes and will not undergo such large daily temperature variations. However, it is interesting to note that the recorded temperature fluctuations are in synch with those of the air indicating that heating and subsequent cooling of the material takes place at approximately the same rate.

The same cannot be said for the variations in the temperature of the arch barrel. It can clearly be seen that the temperature peaks and troughs are out of synch from those of the air and fill with the peaks occurring after a certain time lag. This is due to the nature of the brickwork material which retains heat for a longer period of time thus registering a maximum value after the actual peak air temperature. In line with this, the daily fluctuations are also considerably less pronounced than either of the other two plots discussed above. In addition and again as expected, the range of values is less significant than those of the air temperature with maximum and minimum temperatures of 23 and –3°C respectively. However, a more meaningful discussion of the different temperature distributions can be carried out in conjunction with an analysis of the respective stress and strain results as presented in the following sections.

*Normal stress on extrados:*

Figure 5 shows the normal stress at gauges 1 to 3 on the arch extrados compared to the temperature measured from the thermocouple nearest the instruments. The stress fluctuations are of a variable nature. Gauges 2 and 3 indicate a greater degree of sensitivity than VWG 1, where a significant difference in stress readings of up to 20 kPa in any given day is evident. No temperature correction was carried out for any of these cells since, due to the nature of their construction, the effects of this was considered insignificant. Although small variations are evident throughout the year, no global permanent changes in stress have taken place, with the stresses returning to approximately the same values as at the start of the collection period.

*Vertical pressure in fill material:*

The pressure gauges in the fill material have a higher sensitivity to temperature and therefore have been corrected using the results obtained from the dummy cell placed in the manhole. The temperature correction below has been derived from a regression analysis on the results.

$$\sigma = \left[-0.11 + (2.59 \times T_x)\right]$$

where: $\sigma$ is the apparent pressure as a function of the surrounding temperature, $T_x$.

Figures 6 to 10 show the variation in pressure with that of fill temperature at VWG's 5 to 9 respectively. For VWG's 5 to 6 the corrected stress distribution is seen to be reasonably flat over the total time period, however for VWG 7, which is closest to the surface, a reduction in pressure is observed with the temperature increase. A similar pressure reduction is also observed for the corrected stress distributions at VWG's 8 and 9, which are at the same depth as VWG 7, but for VWG's 8 and 9 this reduction effect is more obvious. This effect could be explained by the increasing temperature reducing the stiffness and so the restraining effects of the road surface on the soil. Fluctuations are also evident and the surrounding soil does undergo some changes in stress due to the temperature variations but these are relatively small.

*Strain on extrados:*

All strains are calculated from a base value taken from each instrument at the time of installation on the arch. The global values of strain at gauges 23 and 24, shown in Figure 11, are indicative of the actual strains on the arch extrados induced from the placement of the fill material and road surfacing. The smaller fluctuations are then a function of the temperature variations. The results at these gauges are representative of the fluctuations at most other gauges.

The strain gauge results have been corrected for temperature sensitivity by exactly 12 ppm/°C, or 12 microstrain of compressive strain. A typical example, as shown in Figure 12, the final corrected result for strain gauge 10 is obtained in which an overall reduction in compressive strain of 208 microstrain is experienced over the 24°C temperature rise. This is due to the fact that the arch barrel is only partially restrained by the abutments which is normally the case in arch bridges. As a result, the temperature increases, the barrel tends to expand or lengthen which in turn will cause a reduction in the compressive strain on the extrados, as observed in gauge 10. However, this behaviour is purely elastic and the strain returns to approximately the same level for equivalent temperatures at the beginning and end of the collection period. Similar analyses are being carried out for the other instruments and results are being produced for publication.

## CONCLUSIONS

1. Datalogging equipment was successfully installed in Kimbolton Butts bridge and readings of the stress, strain and temperature at the relevant instruments subsequently successfully recorded.

2. Significant overall temperature ranges were recorded over the time period at all three locations with a maximum temperature in air of approximately 31°C.

3. No significant global changes in pressure were observed for the cells on the extrados or in the fill over the collection period.

4. A reduction in stress was observed for a corresponding increase in temperature at the cells in the fill under the road surfacing. This was accentuated closer to the crown due to the effects of differential thermal expansion coefficients of the various constituent materials.

5. No significant global changes in strain were observed in any of the gauges from the time of installation on the extrados.

6. Temperature correction highlighted an overall reduction in compressive strain with a corresponding increase in temperature.

The author would like to thank: the EPSRC, the Highways Agency, Cambridgeshire County Council and the Transport Research Laboratory. The author expresses his gratitude for the assistance of the Technical Staff in the department and in particular that of Mr Kevin Broughton.

REFERENCES

Fairfield, C. A. and Ponniah, D. A., "Fill pressure measurements: Kimbolton Butts Bridge, Cambridgeshire", Sub-Contractor's Rep., TRL, Crowthorne, 1993.

Fairfield, C. A. and Ponniah, D. A., Model tests to determine the effect of fill on buried arches. Proc Instn Civ Engrs Structs & Bldgs, 104, Nov, 1994.

Gage Technique Ltd., "Equipment operating instructions", Gage Tech., Trowbridge, 1972.

Page, J., Masonry Arch Bridges - State of the Art Review. HMSO Publications, 1993.

Page, J., Beales, C. and Ives, D. A., "Structural monitoring of Kimbolton Butts Bridge, Cambridgeshire", Project Rep. PR/BR/26/93, TRL, Crowthorne, 1993.

Soil Instruments Ltd., "User's manual, No. 34", Uckfield, E. Sussex, 1991.

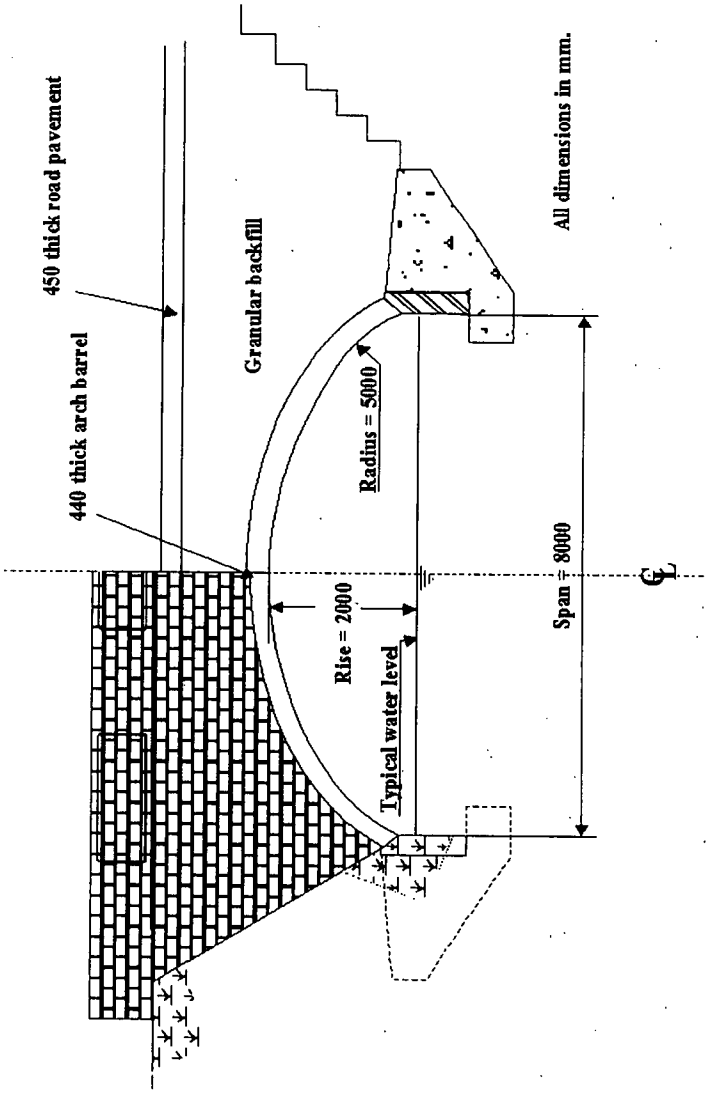


Figure 1 Construction details of Kimbolton Butts Bridge

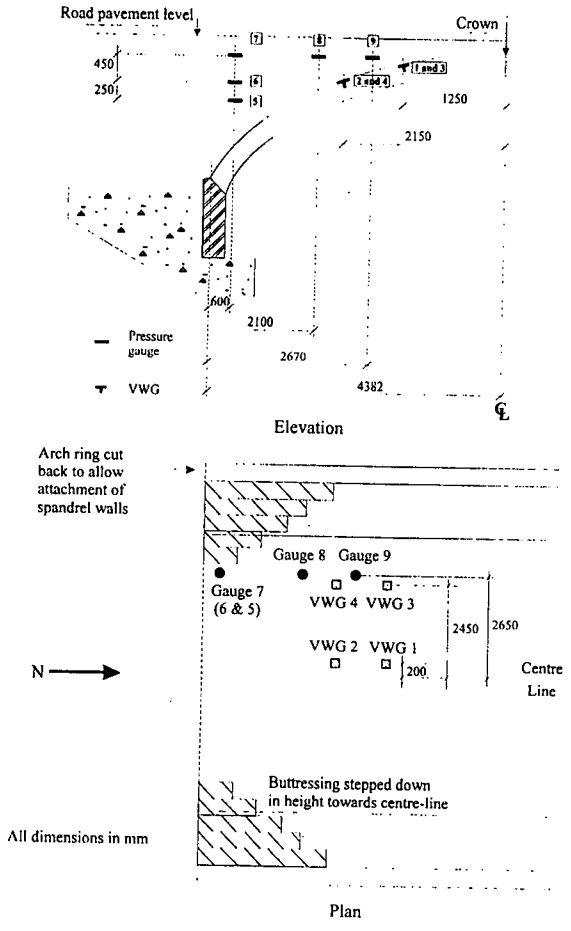


Figure 2 Location of VWG's and pressure cells in bridge

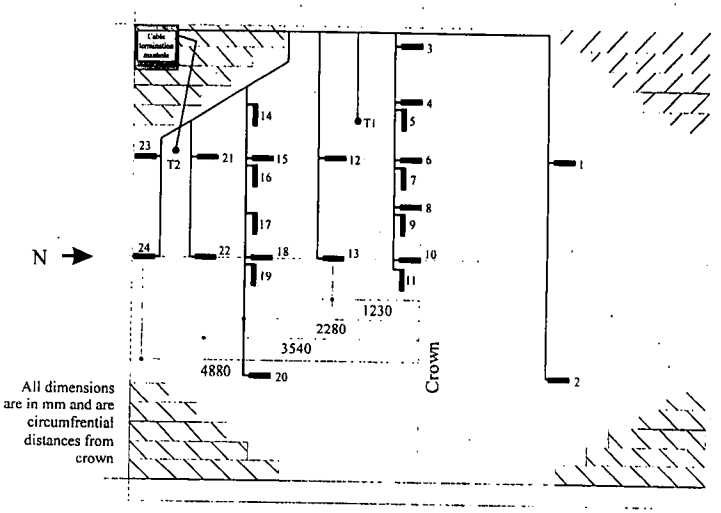


Figure 3 Layout of strain gauges cells

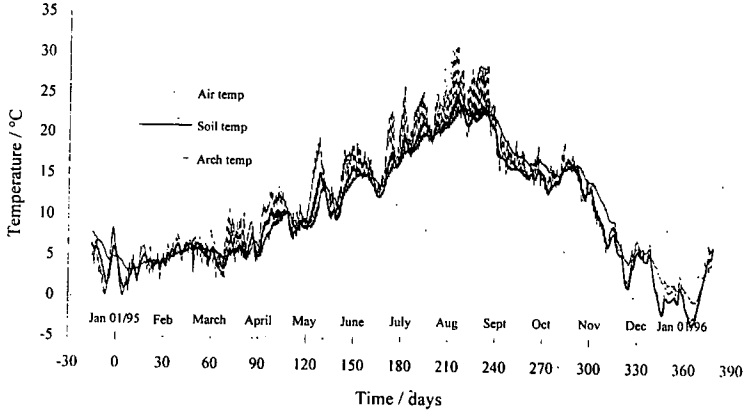


Figure 4 Temperature fluctuations in arch, fill and air

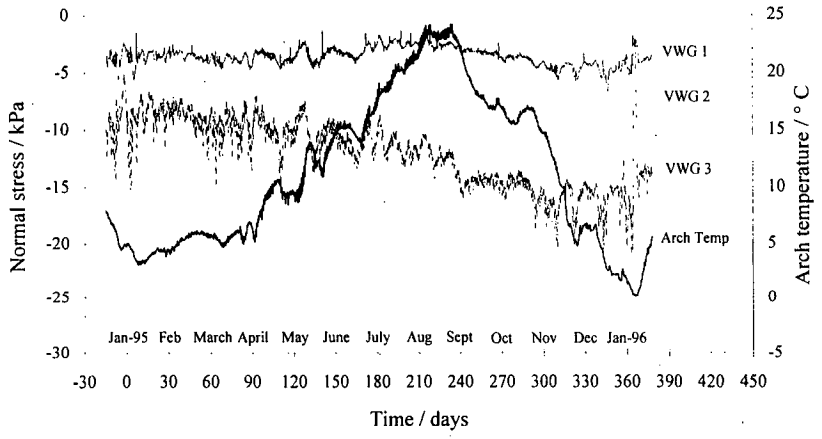


Figure 5 Normal stress on extrados at gauges 1 to 3

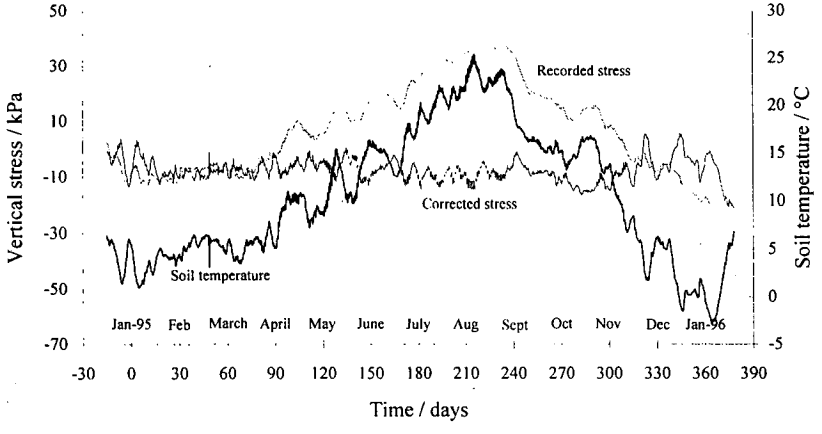


Figure 6 Variation in recorded and corrected stress with soil temperature at VWG 5

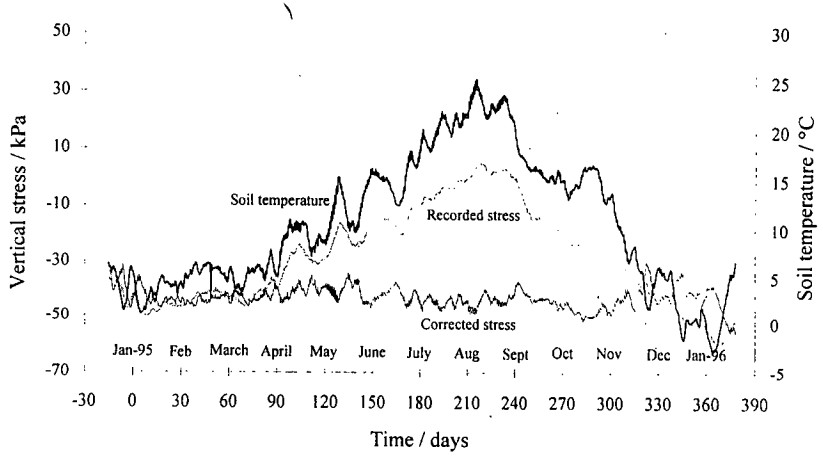


Figure 7 Variation in recorded and corrected stress with soil temperature at VWG 6

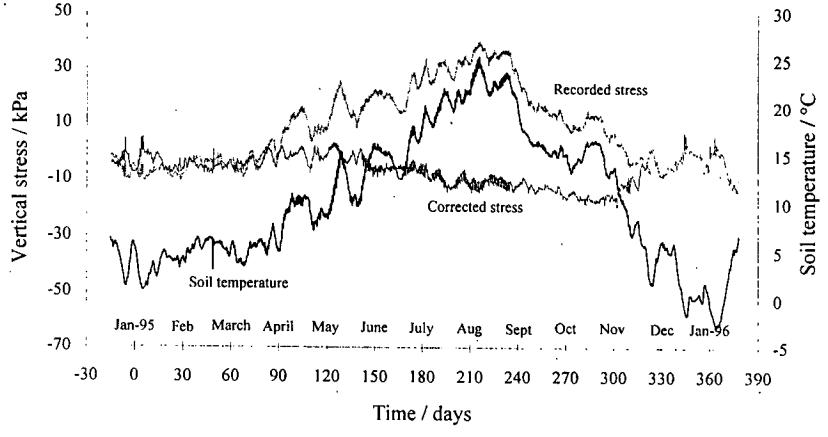


Figure 8 Variation in recorded and corrected stress with soil temperature at VWG 7

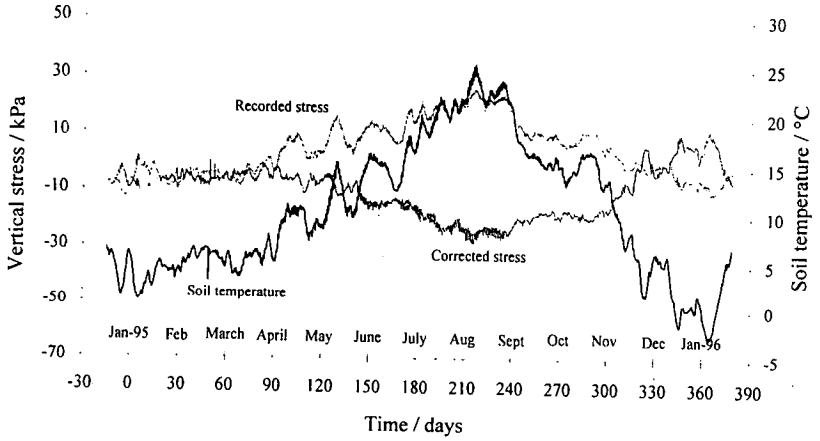


Figure 9 Variation in recorded and corrected stress with soil temperature at VWG 8

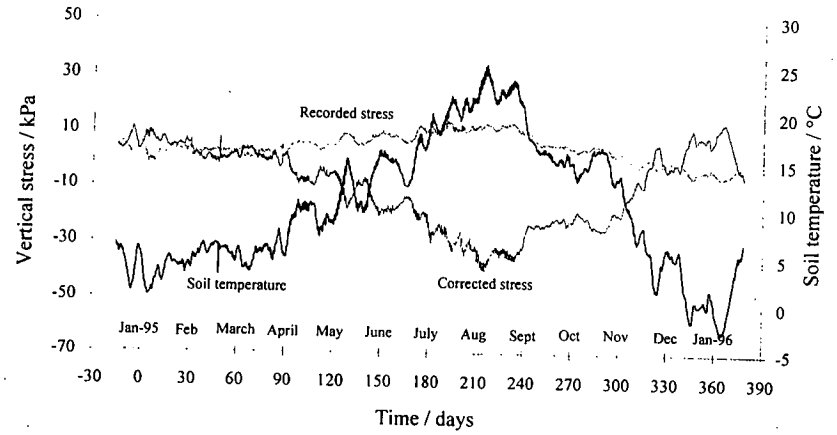


Figure 10 Variation in recorded and corrected stress with soil temperature at VWG 9

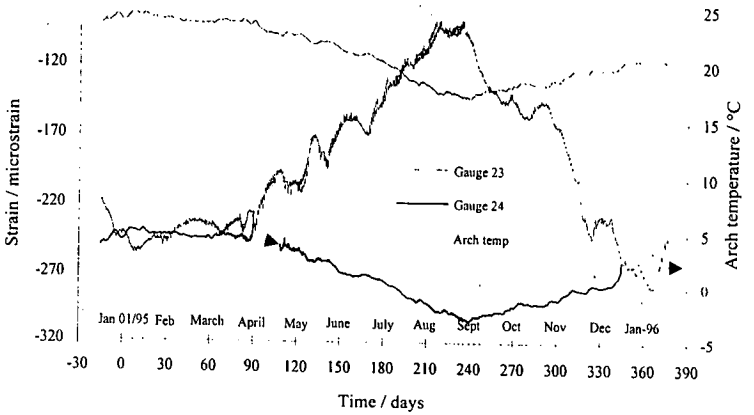


Figure 11 Corrected strain distributions at gauges 23 and 24 with the arch temperature

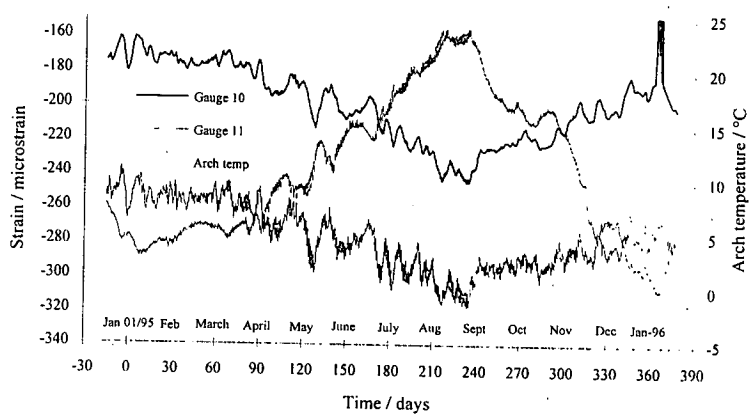


Figure 12 Corrected strain distributions at gauges 10 and 11 with the arch temperature

# A COMPARATIVE STUDY OF MASONRY ARCH ASSESSMENT METHODS

**J.I. Robinson, M. O'Flaherty, P.Stewart, D.A. Ponniah**

School of Civil & Environmental Engineering, University of Edinburgh

## Abstract

From the beginning of 1999 gross vehicle and axle weight restrictions were relaxed to admit the more onerous European Community vehicle types (Directive 85/3/EEC) onto UK principle routes. This required the reassessment of the load carrying capacity of a significant number of masonry arch bridges assessed relative to loading from any convoy of vehicles up to 40/44 tonnes gross weight. It has previously been found that the current methods used for this assessment programme are conservative and often result in the need for costly repair work. This paper presents the results from an investigation performed looking at four of the masonry arch assessment packages currently available. A series of parametric studies has been performed investigating the dimensional and input parameters for each package. A statistical package has then been used with the different packages to make comparisons between each. A bridge assessment programme has been completed and the information gained used to compare the predicted failure loads produced by each package.

**Keywords:** Masonry arch bridge, assessment, failure load, finite element.



## Introduction

By the end of 1999 all bridge structures in the UK had to have capacities of at least 40 tonnes live loading,[1] in order to standardise lorry loads throughout the community. Currently in the UK a national assessment programme is being undertaken, and where necessary structures are being strengthened to meet this new criteria.

The age and general lack of documentation of much of the present bridge stock has meant that the load carrying capacity is usually only ever an estimation based on external measurements. Recently efforts have been made to improve the accuracy of masonry arch assessment, including specific work by Pippard,[2] Heyman,[3] Harvey,[4] Choo[5] and Hughes.[6] The theories behind each method of assessment has been previously documented in great detail,[1-3] and so has not been included here. This paper focuses on differences between some of these current assessment methods and the failure loads produced by certain specified input data, relating these to each method.

This work hopes not only assists in the assessment and maintenance of the present bridge stock but also to provide useful insights for the design of new masonry arch bridges. Masonry arch bridges provide a low maintenance structures compared with steel or concrete options, providing a cheaper longer term structure, as well as being more aesthetically pleasing. Therefore the need for a quick, accurate and reliable assessment method is therefore of great importance not only to maintain the present stock of arch bridges but to advocate the building of new structures.

## Current assessment methods

The new load criteria introduced by the European Union has helped focus attention on the need for an accurate, efficient method of assessing highway arch bridges. While underestimating the strength of a bridge could result in needless and expensive work being carried out, an overestimation could prove even more costly. Given this situation, it was felt important to investigate the differences between the present assessment methods. This was performed in two sections, the first of which by performing a parametric study. The four assessment methods used in this study were modified MEXE,[1,7] ARCHIE,[8] CTAP[9,10] and MAFEA.[11]

The modified MEXE method is based upon an empirical formula using solely the arch dimensions. The ideal arch is assumed parabolic in shape, with a span to rise ratio of four, built of good quality masonry with well pointed undamaged joints. With these dimensions and using a series of equations and factors based on the dimensional and qualitative properties of the arch, a modified axle load ($MAL$) is calculated. The $MAL$ is then multiplied by an appropriate axle factor to calculate the allowable axle loading for the arch. A full list of information required can be found in the relevant parts of the code.[1,7] Several limitations have already been placed upon this method. Larger spans ($L < 12m$), and abnormally shaped arches (flat, noticeably deformed or heavily skewed) produce rogue results.

ARCHIE is based on plastic theory, assuming that the arch will fail as a four-hinged mechanism. It was first introduced in 1988 by Harvey[8] to overcome shortcomings he saw in the assessment methods at that time. The three main developments of the program were the modelling of the fill (including load dispersal, dead load and horizontal pressure), the creation of a zone of thrust in place of the line of thrust and the calculation of a required ring depth for a given magnitude and position of load.



CTAP (Cardiff TRRL Assessment Package) was developed by Bridle and Hughes[9,10] and based on Castigliano's elastic strain energy theorem. This method has been extended to produce a theoretical failure load for a two-dimensional arch with passive horizontal interaction with the fill for different arrangements of applied loading. Numerical integration is employed to find the forces and moments in each section and then progressively thin the arch ring, in each case only areas in compression are considered and the process repeated until convergence. If this convergence is not possible the load increment is reduced until a solution is found, resulting in the collapse load for a given load position.

MAFEA[11] (Masonry Arch Finite Element Analysis), was developed jointly by British Rail and Nottingham University and combines elastic theory with finite element modelling. It models the arch barrel with tapered beam elements which allow for both rigid body movement, changes in sectional properties and material failure. In this way two types of failure, crushing and stability, can be modelled. The quantity and complexity of input data required is large, however predefined data within the package can be utilised to produce an effective assessment.

The second part of the study was performed using data obtained from an assessment programme, where all masonry arch bridges in East Lothian were to be assessed for load capacity. Data was collected in the form of the basic arch dimensions: span, rise, ring thickness and fill thickness. This dimensional data was then processed using the aforementioned arch assessment packages. Work during this period provided the essential data which many of the findings later in this paper are based upon.

## Parametric study

Before any direct comparisons could be made between the different packages it was important to investigate the influence of each input parameters on a specific package. For this reason a comprehensive parametric studies were undertaken using the parameters shown in Table 2. The basic arch dimensions used were those of Bargower, a semi-circular arch bridge previously documented.[12] Failure loads (or in MEXE's case the $MAL$) were calculated from the standard set of parameters, by isolating and varying each parameter in turn while keeping all others constant. In the parametric studies this process was repeated for each parameter in turn to give a series of individual relationships. An example of the results produced by varying one of the input parameters, in this case the span, is illustrated in Figure 1. This shows the relationships between the span and output failure load for each package.

## Arch assessment program

Ninety-nine arch bridges were inspected in East Lothian and the dimensional information recorded was used with the four assessment packages already introduced to assess each structure. Of the data gathered there were ten multi-span bridges which for the purpose of this study have been treated as individual spans. This has already been shown to be conservative but is necessary for the comparison. Other structures with spans less than $2m$ were also surveyed although an assessment was not required. Dimensional information was only collected for each bridge and therefore the other factors required for each package had to be kept constant and at realistic values to give comparable results. The input parameters for the assessment packages are given in Table 3.



The MEXE assessments of the arch dimensions obtained in East Lothian were performed initially with constant (worst case) modification factors. Only structures failing this analysis required a second site visit to find actual modification factors with which to re-analyse the structure. Failure loads for a single axle configuration were investigated here. MAFEA considers both stability and crushing therefore both were investigated in order to find the lowest failure load. MAFEA recommends properties to be used with a provisional assessment and these are the values which have been adopted here. Although some of the values used for all packages are obviously conservative these values are recommended if the properties of materials are not known, which is often the case in actual arch bridge assessment problems. The failure load results produced by the four assessment packages are shown in Table 1.

**ANALYSIS** Analysis of the results shown in Table 1 were then analysed using a statistical package, $SPSS$ for Windows, under the option for non-linear regression. The failure load results were specified as being dependent upon the four dimensional parameters; span, rise, ring thickness and fill thickness. The predicted failure load, $W$, is specified in the form shown in Equation 1.

$$W = k \times L^A \times r_c{}^B \times d^C \times h^D \tag{1}$$

## Discussion of results

**PARAMETRIC STUDY** This study highlighted some of the differences that exist between the assessment methods. Table 2 presents the overview of results from this parametric study, showing a comparative view of how a change in each

parameter effects the failure load produced. Column 'A' indicates the importance with which a change in each parameter has been judged to affect the failure load, while column 'B' indicates the effects of this change for an increase in the parameter. Each parameter has been classed in order of importance to that package and also relative to the others. This is achieved by analysing the change in failure load affected by the change in the parameter. Care was taken to ensure that this change in parameter did not miss any affects that are induced. Hence this method is not solely a numerical classification, but also a subjective judgement made considering the failure load range and the range of the parameter. The meaning of symbols in Table 2 are:

- 1 - Accuracy of *primary* importance to package
- 2 - Accuracy of *secondary* importance to package
- 3 - Accuracy of *tertiary* importance to package
- + - Indicates increase in failure load for increase in parameter
- - - Indicates decrease in failure load for increase in parameter
- None - Indicates no effect in failure load for increase in parameter
- *** - Indicates where a parameter is not required for specific package

Figure 1 shows a standard set of results obtained from the parametric study. It clearly shows the difference between the computerised packages and MEXE. The computer packages predict an increase in strength for larger spans while MEXE predicts a decrease. Also, of the three computer packages, ARCHIE is the least sensitive to changes in span as it has a smaller failure load range over the change in parameter. By looking at these plots in this way enabled Table 2 to be constructed.

ARCHIE, CTAP and MAFEA consider the ring thickness to be of primary importance, and for MEXE it is taken as secondary, making this parameter vital



for accurate assessment. However measuring the actual ring is difficult and so seldom performed since this requires coring. MEXE considers the total crown thickness (d+h) in calculating the provisional axle load, despite the fact that the arch ring is undoubtedly going to have a greater load capacity than that of the fill. Although the material factor treats the ring and fill thickness separately, this has less influence than that of the provisional axle load. For the two packages which allow entry of the ring thickness at the abutments and at the crown separately, both consider the ring thickness at the abutments to be of greater importance. This was however felt to be an affect produced by the original arch shape being assessed.

Rise was also found to be an important parameter by all packages. For MEXE it is not just the rise which is having a large effect here, but also the span/rise ratio. In MEXE the rise can have both a positive and negative effect on the failure load, which arises from the assumption that a span to rise ratio of four being an optimum. By increasing the span or the span/rise ratio, which has the effect of flattening the arch, ARCHIE, CTAP and MAFEA all agree that this will increase the strength of the bridge. MEXE on the other hand favours steeper arches.

For both MEXE and ARCHIE, an increase in fill thickness increases the capacity of the structure. For the two elastic methods however, the fill thickness has a detrimental effect on the failure load (shown by column B). This is due to the fact that large dead loads can cause excessive thinning of the arch ring, and thus lower the arch's capacity.

CTAP treats the pressure coefficients as of primary importance. The sensitivity with which CTAP treats these parameters makes an accurate assessment rather difficult, unless the soil has actually been tested. For a large number of bridge assessments, soil testing is perhaps not economically viable. The crushing strength

has a large bearing on the results of MAFEA. This is the only material property in all of the packages which is considered to be of primary importance. Hence a close approximation of the crushing strength is pivotal in obtaining an accurate result.

**Assessment and analysis** Table 1 shows the arch assessment results produced from the analysis of all surveyed dimensional data. The results have been ordered in ascending failure loads from the ARCHIE assessment. From examination of this table it becomes clear just how much variation in results there is. Figure 2 has also been constructed to show the failure loads produced by each assessment package relative to ARCHIE. This allows trends to be more clearly identified.

The MEXE analysis tends to produce consistently low results, again related to the PAL load limit and the application of constant modification factors. ARCHIE produces what appears to be the most consistent set of failure loads along with MAFEA whose trend seems to be quite similar. There are several exceptions within the MAFEA assessment (zero failure loads produced) when the arch fails under its own dead load. These initial failures are generally for arches with abnormally high span:ring thickness or span:rise ratios. CTAP produces a good comparison with ARCHIE for lower loads but produces large failure loads for arches with shallow profiles and large fill depths. This is due to the elastic cracking analysis struggling to fail the structures since crushing failure is not considered. If the load/stress plots for each bridge were analysed then a stress cut-off could be used to identify a failure load. This is however somewhat subjective and considered out-with the aims of this assessment.

From the statistical analysis of these results the unknowns $A$ to $D$ and $k$ in equation 1 were found for each package and are shown in Table 4. To represent how well these equations related to the actual package results, the package failure



loads were plotted against those produced by the derived equations as shown in Figure 3. A forty five degree line has also been plotted to represent where the data points would lie if a perfect correlation had been obtained. The correlation coefficients $r^2$ have also been recorded giving a numerical value as to the accuracy of the fit. The CTAP graph, shown in Figure 3(d), displays rather nicely the effect seen when the failure loads were originally assessed. That is the failure loads for the stronger bridges are being over estimated due to the lack of an option for a crushing failure mode in the package. This results in a right shift in the plot once the failure loads rise above forty tonnes.

In order to more clearly illustrate the relationships produced from the analysis of these results the effects of the coefficients on each parameter have been plotted in Figure 4. These graphs show the effects of the powers on the span, rise, ring and fill thickness for the four packages. The relative sensitivity on the y-axis is simply the arch dimension to the corresponding power. Table 4 showed that the original MEXE analysis produced a poor correlation. It was subsequently realised that this was due to the standards[1] specifying a PAL limit of seventy tonnes. Hence the analysis was repeated for the thirty eight bridges which met this criteria (PAL $<$ 70t), resulting in a much better correlation of results.

The results show that the MEXE may be more sensitive to changes in fill depth than in changes in any other parameter which supports the code when it says that MEXE may not be suitable to bridges where the fill depth is greater than the ring depth.

Figure 4(b) shows the interesting relationship between the rise and the relative sensitivity. All three computer packages show a similar relationship, with the sensitivity (or strength) decreasing as the rise increased, whereas the MEXE line shows an opposite response. This can be related to the results obtained from the parametric studies, in which similar conclusion relationships were discovered.

Of the other packages ARCHIE tends to give the best regression relationship, which is reflected in the graphs in Figure 4. CTAP and MAFEA both show a trend in the results but the correlation between the actual assessments and the SPSS predictions is rather weaker than that displayed by the ARCHIE assessment. The correlation for MAFEA may be weaker due to allowing two different failure criteria, crushing and stability, but the individual results were not recorded for this comparison to be made.

The MEXE regression analysis for the restricted range produced constants that form equation 2. Upon closer inspection this equation is very similar to the equation for calculating the $PAL$,[1] for the modified MEXE method.

$$W = 760.7 \times \left( \frac{r_c^{0.22} \times d^{1.037} \times h^{0.744}}{L^{1.057}} \right) \qquad (2)$$

With careful consideration it is felt that the development of such equations could provide the assessing engineer with an extra tool to assist in their work. Such a simple relationship could easily be completed in the field and could highlight bridges that are likely to need careful surveying. This could save having to travel back to structures to do a full survey after the initial results show a possible problem and this would save both time and resources.

## Conclusions

1. MEXE is sensitive to fill depth and insensitive to ring thickness when compared to the other three packages.

2. MEXE considers flatter arches to be weaker when compared to the computerised packages which will favour this shape for increased strength.

3. CTAP does not give conservative results for flat or very strong arches.

4. Masonry strength is a sensitive parameter when it is used, especially for MAFEA when large structures are assessed.

5. ARCHIE gives the most consistent set of results over the range of bridges investigated.

6. CTAP and MAFEA behave similarly to changes in dimensional parameters.

7. There is a wide variation in some of the assessment failure loads.



## References

[1] BD21/97. Department of Transport, HMSO, London. *The assessment of highway bridges and structures*, 1997.

[2] J. Page. *Masonry arch bridges; State of the art review.* HMSO, London, 1993.

[3] J. Heyman. *The masonry arch.* Ellis Horwood Ltd., Chichester, England, 1982.

[4] W.J. Harvey. Application of the mechanism analysis to masonry arches. *The Structural Engineer*, 66(5), Mar 1988.

[5] B.S. Choo, M.G. Coutie, and N.G. Gong. Analysis of masonry arch bridges by a finite element method. In *Proc. of Fourth Rail Bridge Centenary International Conference*, pages 381–392, Edinburgh, 1990.

[6] T. G. Hughes and M. J. Blackler. A review of the UK masonry arch assessment methods. *Proc. Instn Civ Engrs Structs & Bldgs*, 122:305–315, August 1997.

[7] BA16/97. Department of Transport, HMSO, London. *The assessment of highway bridges and structures - Advice Note*, 1997.

[8] W.J. Harvey. *ARCHIE and MULTI operation manual*, 1991.

[9] R.J. Bridle and T.G. Hughes. The arch revival: the Cardiff arch analysis procedure. In *Highways and Transportation*, Oct 1989.

[10] R.J. Bridle and T.G. Hughes. An energy method for arch bridge analysis. In *Proc. Instn. Civ Engrs, Part 2, 89*, Sept 1990.

[11] S.F. Broomhead *et al.* Masonry Arch Finite Element Assessment, MAFEA documentation. Report no. 1,2,3,4 and 5, Track & Civil Engineering Group, BR Research, PO Box 2, London Road, Derby, DE24 8YB, 1996.

[12] A.W. Hendry *et al.* Load test to collapse on a masonry arch bridge at Bargower, Strathclyde. TRRL contractor report 26, Department of Transport, Transport Research Laboratory, Crowthorne, 1986.



Table 1: East Lothian arch failure load predictions

| Bridge Name | Span (m) | Rise (m) | Ring (m) | Fill (m) | ARCHIE tonnes | MEXE tonnes | CTAP tonnes | MAFEA tonnes |
|---|---|---|---|---|---|---|---|---|
| GIFFORD VILLAGE | 7.67 | 3.02 | 0.36 | 0.367 | 4.00 | 16.10 | 4.70 | 7.00 |
| BLANCE BURN | 3.40 | 1.40 | 0.335 | 0.085 | 4.40 | 11.60 | 4.40 | 10.10 |
| JANEFIELD | 2.40 | 1.05 | 0.30 | 0.20 | 5.50 | 22.60 | 5.10 | 9.90 |
| SMEATON | 4.46 | 2.02 | 0.30 | 1.13 | 5.60 | 23.80 | 6.70 | 18.10 |
| KEITH | 7.30 | 3.69 | 0.41 | 0.82 | 5.70 | 33.10 | 7.10 | 0.00 |
| PENCAITLAND (1) | 3.60 | 1.60 | 0.30 | 1.10 | 7.50 | 23.00 | 8.10 | 22.90 |
| FASENY | 7.34 | 2.14 | 0.45 | 0.319 | 7.50 | 21.50 | 8.60 | 14.00 |
| TYNINGHAM DAM | 6.10 | 1.55 | 0.40 | 0.30 | 7.60 | 20.40 | 7.90 | 14.50 |
| QUARRYFORD | 6.00 | 2.52 | 0.42 | 0.78 | 7.70 | 30.80 | 8.60 | 15.00 |
| LINTON LINN (1) | 12.45 | 4.18 | 0.49 | 0.91 | 7.80 | 36.20 | 9.80 | 9.20 |
| GARVALD | 6.13 | 1.63 | 0.44 | 0.216 | 8.30 | 18.50 | 8.80 | 16.00 |
| OLDHAMSTOCKS | 10.10 | 4.26 | 0.56 | 0.45 | 8.40 | 22.80 | 10.30 | 14.90 |
| LINTON LINN (2) | 12.50 | 4.26 | 0.49 | 1.17 | 8.70 | 45.20 | 10.90 | 0.00 |
| HADDINGTON RAILWAY | 8.60 | 1.57 | 0.40 | 0.58 | 9.10 | 24.20 | 9.20 | 11.30 |
| SALTOUN (1) | 4.32 | 1.27 | 0.36 | 0.46 | 9.20 | 30.20 | 9.40 | 11.215 |
| BOLTON | 4.04 | 1.325 | 0.42 | 0.20 | 9.40 | 20.40 | 9.60 | 11.131 |
| SALTOUN (2) | 10.53 | 3.99 | 0.59 | 0.44 | 9.40 | 24.00 | 11.20 | 11.046 |
| TYNE WATER (3) | 3.91 | 1.43 | 0.44 | 0.21 | 9.70 | 22.50 | 10.10 | 10.962 |
| ROCKVILLE | 4.47 | 1.548 | 0.46 | 0.241 | 10.00 | 23.50 | 10.70 | 10.877 |
| DUNGLASS NEW | 26.33 | 6.91 | 0.86 | 1.48 | 10.10 | 42.50 | 16.60 | 10.792 |
| MORHAM | 4.70 | 1.83 | 0.47 | 0.40 | 10.10 | 29.80 | 10.60 | 10.708 |
| WEST SALTOUN | 15.63 | 2.24 | 0.60 | 0.11 | 10.20 | 6.60 | 9.60 | 10.623 |
| WHITTINGHAME (1) | 9.75 | 2.911 | 0.57 | 0.456 | 10.70 | 27.90 | 12.10 | 10.538 |
| SAMUELSTON | 21.40 | 3.38 | 0.75 | 0.13 | 10.90 | 7.30 | 10.90 | 10.454 |
| UGSTON | 8.60 | 1.28 | 0.40 | 0.61 | 10.90 | 22.30 | 11.60 | 10.369 |
| SMEATON RAILWAY (1) | 7.90 | 1.68 | 0.43 | 0.68 | 11.10 | 36.90 | 12.20 | 10.285 |
| PENCAITLAND (2) | 5.40 | 1.20 | 0.35 | 0.75 | 11.30 | 33.30 | 12.20 | 10.20 |
| "STATION ROAD " | 3.365 | 1.502 | 0.37 | 0.871 | 11.30 | 23.70 | 12.00 | 10.115 |
| ALDERSTON HOUSE (1) | 2.50 | 1.16 | 0.33 | 0.70 | 11.60 | 23.40 | 11.60 | 10.031 |
| SMEATON RAILWAY (2) | 7.85 | 1.65 | 0.43 | 0.76 | 12.00 | 39.90 | 12.70 | 9.946 |
| ALDERSTON HOUSE 2 | 2.50 | 1.08 | 0.33 | 0.58 | 12.10 | 24.60 | 12.30 | 9.862 |
| TYNE WATER (2) | 4.01 | 1.46 | 0.47 | 0.30 | 12.40 | 29.00 | 13.30 | 9.777 |
| GILCHRISTON | 5.50 | 1.22 | 0.38 | 0.69 | 12.70 | 33.80 | 13.70 | 9.692 |
| GLENKINCHIE | 3.69 | 1.331 | 0.39 | 0.673 | 13.10 | 26.70 | 14.30 | 9.608 |
| MERRYHATTON | 9.10 | 1.60 | 0.44 | 1.00 | 13.30 | 36.80 | 15.30 | 9.523 |
| GIFFORD | 12.07 | 2.87 | 0.63 | 0.644 | 14.10 | 34.60 | 16.60 | 9.438 |
| ALDERSTON HOUSE 3 | 2.50 | 1.15 | 0.36 | 0.68 | 14.80 | 23.70 | 15.60 | 9.354 |

*continued on next page*

| Bridge Name | Span (m) | Rise (m) | Ring (m) | Fill (m) | ARCHIE tonnes | MEXE tonnes | CTAP tonnes | MAFEA tonnes |
|---|---|---|---|---|---|---|---|---|
| TENTH GREEN | 2.30 | 1.00 | 0.30 | 0.80 | 15.30 | 23.70 | 17.20 | 9.269 |
| BROXBURN A1087 | 7.64 | 1.64 | 0.52 | 0.54 | 15.60 | 36.00 | 18.00 | 9.185 |
| SPILMERSFORD | 20.45 | 3.42 | 0.775 | 0.72 | 15.60 | 20.60 | 18.50 | 9.10 |
| ORMISTON STATION | 4.24 | 1.47 | 0.46 | 0.64 | 16.20 | 28.50 | 18.70 | 22.90 |
| BLACKHALL | 3.11 | 0.45 | 0.25 | 0.29 | 16.30 | 15.60 | 18.90 | 16.50 |
| HOPES HOUSE | 6.90 | 1.30 | 0.47 | 0.59 | 16.50 | 35.80 | 19.00 | 22.60 |
| WATERLOO | 21.95 | 3.52 | 0.88 | 0.30 | 16.80 | 12.20 | 19.10 | 0.00 |
| STENTON | 4.27 | 1.43 | 0.55 | 0.19 | 17.30 | 28.30 | 19.40 | 31.70 |
| LITTLE KNOWES (SOUTH) | 3.75 | 0.71 | 0.35 | 0.28 | 18.30 | 20.50 | 58.60 | 22.00 |
| WHITTINGHAME (2) | 4.70 | 1.52 | 0.43 | 1.15 | 18.90 | 29.50 | 24.20 | 41.30 |
| COLSTON WATER | 12.30 | 1.25 | 0.60 | 0.62 | 20.10 | 18.90 | 31.40 | 3.50 |
| GRANTS BRAES | 15.50 | 1.57 | 0.71 | 0.26 | 20.60 | 10.00 | 27.60 | 1.60 |
| FILTER STATION | 5.33 | 0.92 | 0.44 | 0.41 | 20.90 | 25.70 | 25.50 | 25.40 |
| THORNTON BURN | 5.50 | 1.34 | 0.56 | 0.26 | 21.20 | 30.70 | 24.30 | 36.30 |
| INCH | 5.16 | 0.985 | 0.465 | 0.34 | 21.90 | 26.60 | 26.40 | 28.80 |
| SETON FARM | 3.40 | 0.833 | 0.43 | 0.065 | 22.00 | 18.80 | 25.50 | 29.10 |
| ALDERSTON HOUSE 4 | 2.75 | 0.84 | 0.32 | 0.67 | 22.30 | 27.80 | 41.40 | 32.50 |
| DUNGLASS OLD | 10.00 | 4.45 | 0.70 | 4.00 | 23.30 | 35.80 | 46.80 | 0.00 |
| HUMBIE DEAN (1) | 2.92 | 0.93 | 0.34 | 0.82 | 24.00 | 27.20 | 29.80 | 41.30 |
| THORNTON | 5.80 | 2.78 | 0.62 | 2.04 | 24.00 | 28.00 | 31.70 | 44.50 |
| CROOK ROAD | 5.80 | 0.89 | 0.46 | 0.48 | 24.00 | 28.20 | 77.30 | 27.80 |
| LOCH | 2.09 | 0.76 | 0.25 | 0.94 | 25.50 | 25.10 | 58.30 | 33.60 |
| CUDGEL HOUSE | 3.06 | 1.52 | 0.50 | 1.02 | 25.70 | 22.50 | 31.10 | 33.40 |
| GAMUELSTONE | 3.20 | 1.11 | 0.34 | 1.36 | 26.60 | 25.40 | 47.90 | 39.40 |
| SPILMERSFORD APPR'CH | 6.12 | 1.04 | 0.47 | 1.03 | 27.80 | 30.50 | 44.10 | 26.40 |
| LUGGATE BURN | 3.32 | 0.86 | 0.46 | 0.10 | 28.00 | 24.00 | 51.60 | 36.70 |
| GOSFORD SANDS | 3.35 | 0.25 | 0.42 | 0.907 | 29.30 | 17.70 | 149.90 | 0.00 |
| NEWLANDS | 3.68 | 1.13 | 0.48 | 0.64 | 31.40 | 28.90 | 44.40 | 28.50 |
| SMEATON TROWS | 3.03 | 0.67 | 0.33 | 0.67 | 32.80 | 27.90 | 84.60 | 29.20 |
| LYARS | 3.84 | 0.75 | 0.46 | 0.135 | 33.60 | 20.00 | 112.20 | 38.90 |
| WEST LATCH | 2.20 | 0.91 | 0.37 | 0.67 | 34.70 | 25.10 | 44.10 | 42.50 |
| EAST BEARFORD | 6.15 | 1.60 | 0.72 | 0.36 | 34.80 | 43.20 | 51.20 | 54.50 |
| SPOTT 1 | 5.00 | 0.74 | 0.42 | 1.43 | 37.00 | 23.80 | 71.2 | 26.10 |
| ST. LAWRENCE HOUSE | 4.59 | 1.44 | 0.605 | 0.79 | 40.20 | 30.80 | 60.70 | 50.10 |
| GOLF | 2.00 | 0.85 | 0.40 | 0.40 | 40.70 | 26.10 | 54.30 | 32.20 |
| SPOTT 2 | 5.60 | 0.91 | 0.54 | 0.80 | 41.80 | 28.70 | 149.90 | 35.40 |
| LITTLE KNOWES (NORTH) | 2.56 | 0.29 | 0.38 | 0.50 | 41.90 | 18.20 | 112.40 | 0.00 |
| PARK HILLS | 4.24 | 0.55 | 0.48 | 0.29 | 44.60 | 21.90 | 149.90 | 33.60 |

*continued on next page*



| Bridge Name | Span (m) | Rise (m) | Ring (m) | Fill (m) | ARCHIE tonnes | MEXE tonnes | CTAP tonnes | MAFEA tonnes |
|---|---|---|---|---|---|---|---|---|
| BROOMRIGG | 3.08 | 0.53 | 0.40 | 0.32 | 48.00 | 25.90 | 149.90 | 37.10 |
| MORHAM BANK | 2.70 | 0.57 | 0.37 | 0.47 | 51.70 | 27.70 | 149.90 | 35.90 |
| LEASTON | 2.74 | 0.49 | 0.37 | 0.49 | 52.30 | 25.00 | 149.90 | 37.00 |
| PILMUIR | 2.15 | 0.60 | 0.31 | 0.58 | 52.50 | 28.80 | 149.90 | 36.20 |
| MAINSHILL | 2.36 | 0.42 | 0.36 | 0.32 | 53.40 | 25.90 | 149.90 | 37.40 |
| BILSDEAN (1) | 6.10 | 1.58 | 0.65 | 1.25 | 55.30 | 38.00 | 149.90 | 42.50 |
| PEFFER BURN | 3.60 | 0.50 | 0.50 | 0.60 | 56.00 | 21.80 | 149.90 | 42.40 |
| BILSDEAN (2) | 6.13 | 1.28 | 0.66 | 1.19 | 56.20 | 34.60 | 149.90 | 40.00 |
| SANDYFORD B6369 | 2.79 | 0.66 | 0.35 | 1.00 | 56.30 | 28.00 | 149.90 | 34.30 |
| HARELAW | 2.64 | 0.51 | 0.37 | 0.56 | 57.50 | 26.00 | 149.90 | 36.10 |
| MILL LADE (2) | 2.45 | 0.40 | 0.40 | 0.408 | 57.70 | 24.50 | 149.90 | 37.90 |
| ALDERSTON HOUSE 5 | 2.50 | 0.89 | 0.42 | 0.75 | 58.00 | 26.80 | 149.90 | 51.40 |
| BRANXTON | 2.23 | 0.43 | 0.34 | 0.13 | 58.30 | 24.00 | 149.90 | 38.50 |
| TRANENT RAILWAY | 7.50 | 1.70 | 0.80 | 1.20 | 59.00 | 43.20 | 149.90 | 54.00 |
| NORTH MARVINGSTON | 2.65 | 0.44 | 0.41 | 0.63 | 61.00 | 23.90 | 149.90 | 37.60 |
| MILL LADE (1) | 2.50 | 0.40 | 0.44 | 0.35 | 63.00 | 24.70 | 149.90 | 43.40 |
| BLACKFORD | 2.31 | 0.40 | 0.435 | 0.14 | 65.70 | 27.70 | 149.90 | 28.80 |
| TYNEHOLM HOUSE | 2.40 | 0.79 | 0.48 | 0.18 | 68.00 | 31.30 | 149.90 | 51.90 |
| MORHAM MAINS | 2.20 | 0.43 | 0.39 | 0.56 | 71.00 | 26.70 | 149.90 | 40.00 |
| PENSHIEL | 2.24 | 0.73 | 0.40 | 0.59 | 73.50 | 28.10 | 149.90 | 42.50 |
| MORHAM MAINS | 2.23 | 0.45 | 0.42 | 0.81 | 83.10 | 26.30 | 149.90 | 65.90 |
| LUFFNESS CULVERT | 2.00 | 0.55 | 0.42 | 0.18 | 83.70 | 32.70 | 149.90 | 63.30 |
| TRANENT ACCESS | 2.43 | 0.94 | 0.37 | 2.42 | 102.50 | 23.70 | 149.90 | 155.20 |
| SPITTALRIGG | 2.15 | 0.71 | 0.46 | 0.61 | 106.70 | 28.20 | 149.90 | 52.70 |

| Parameter varied | Package | | | | | | | |
|---|---|---|---|---|---|---|---|---|
| | MEXE | | ARCHIE | | CTAP | | MAFEA | |
| | A | B | A | B | A | B | A | B |
| Span | 2/1 | - | 2 | + | 1/2 | + | 1/2 | + |
| Rise at centre | 2 | +/- | 1 | - | 1 | - | 1 | - |
| Ring thickness | 2 | + | 1 | + | 1 | + | 1 | + |
| Ring thickness at crown | *** | *** | *** | *** | 2 | + | 3 | + |
| Ring thickness at abutment | *** | *** | *** | *** | 1 | + | 1 | + |
| Fill thickness | 2 | + | 2 | + | 2 | - | 2 | +/- |
| Ring thickness factor | *** | *** | 2 | + | *** | *** | *** | *** |
| Passive pressure factor | *** | *** | 2/3 | +/- | 1 | + | 2/1 | + |
| At Rest pressure factor | *** | *** | *** | *** | 1 | - | *** | *** |
| Active pressure factor | *** | *** | *** | *** | 1 | + | *** | *** |
| Masonry strength | *** | *** | 2 | + | *** | *** | 1 | + |
| Arch elasticity | *** | *** | *** | *** | 3 | + | 3 | + |
| Fill elasticity | *** | *** | *** | *** | *** | *** | 3 | - |
| Masonry density | *** | *** | 3 | + | 3 | - | 3 | + |
| Fill density | *** | *** | 3 | + | 2 | + | 2 | + |
| Surfacing density | *** | *** | 3 | + | 3 | - | *** | *** |
| Phi for soil | *** | *** | 3 | - | *** | *** | 3 | - |
| Surfacing depth | *** | *** | 3 | + | 3 | None | *** | *** |
| Depth of mortar loss | *** | *** | 2 | + | *** | *** | *** | *** |
| Depth of overlay | *** | *** | 3 | + | *** | *** | *** | *** |

Table 2: Summary of combined parametric study



| Parameter | Package | | | |
|---|---|---|---|---|
| | ARCHIE | CTAP | MAFEA | MEXE |
| Ring thickness factor | 1.0 | - | - | $F_b = 1.0$ |
| $K_p$ | 0.1 | 0.6 | 0.1 | $F_f = 0.7$ |
| $K_o$ | - | 0.5 | - | $F_w = 0.9$ |
| $K_a$ | - | 0.4 | - | $F_m = 0.9$ |
| Masonry strength | 3.0 | 3.0 | 3.0 | |
| $E$ arch | - | 1500 | 1500 | $F_d = 0.9$ |
| $E$ fill | - | - | 30.0 | $F_c = 0.8$ |
| $\rho_m$ | 20.0 | 20.0 | 20.0 | - |
| $\rho_f$ | 18.0 | 18.0 | 18.0 | - |
| $\rho_s$ | 23.0 | 23.0 | - | - |
| $\phi$ soil | 25.0 | - | 35.0 | - |
| Surfacing depth | 0.1 | 0.1 | - | - |
| Distribution angle | 27 | 27 | 27 | - |
| Wheel size | - | 0.3 | 0.3 | - |
| Sub-grade modulus | - | 9000 | - | - |

Table 3: Arch bridge assessment input parameters

| Variable | Package | | | | |
|---|---|---|---|---|---|
| | ARCHIE | MEXE | MEXE($W_p \leq 70$) | CTAP | MAFEA |
| A | -1.406 | -0.127 | -1.057 | -0.292 | -1.035 |
| B | -0.410 | 0.083 | 0.222 | -0.878 | -0.324 |
| C | 2.423 | 0.280 | 1.037 | 1.735 | 1.633 |
| D | 0.262 | 0.156 | 0.744 | 0.364 | 0.619 |
| k | 1722.92 | 43.83 | 760.72 | 328.71 | 631.55 |
| $r^2$ | 0.755 | 0.286 | 0.828 | 0.544 | 0.580 |

Table 4: Results of the SPSS analysis

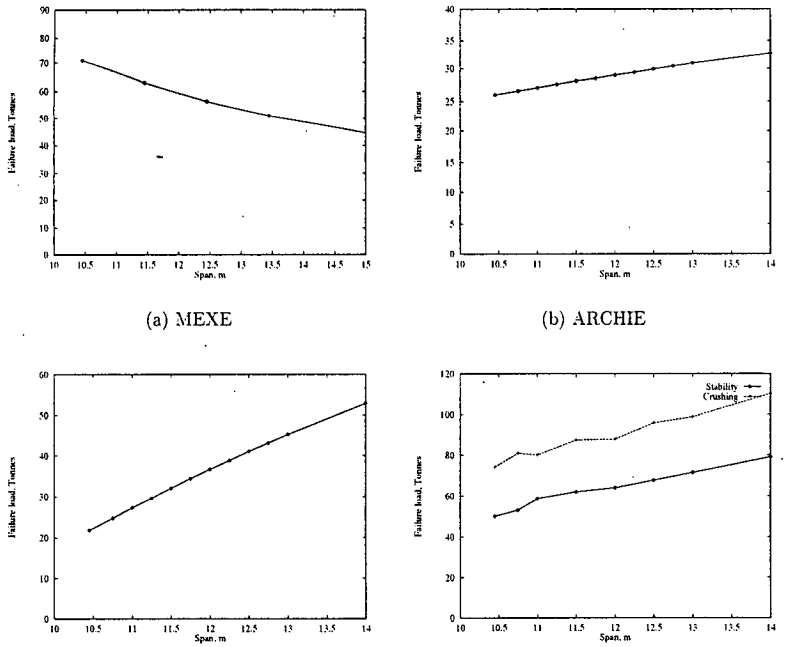


(a) MEXE

(b) ARCHIE

(c) CTAP

(d) MAFEA

Figure 1: Effect of change of span on failure load



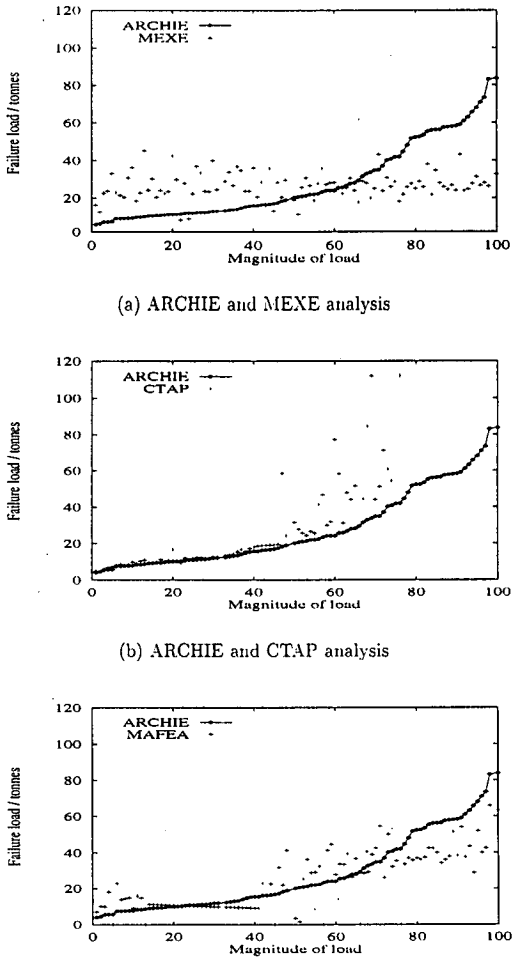


(a) ARCHIE and MEXE analysis

(b) ARCHIE and CTAP analysis

(c) ARCHIE and MAFEA analysis

Figure 2: Failure load results from the arch bridge assessment program

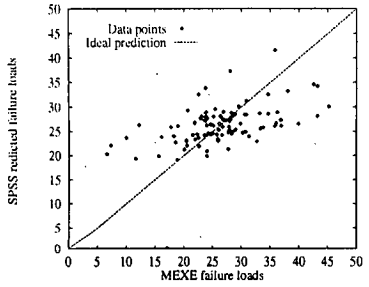


(a) MEXE correlation

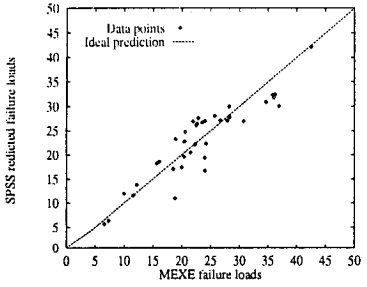


(b) MEXE correlation ($W_p \leq 70$ tonnes)

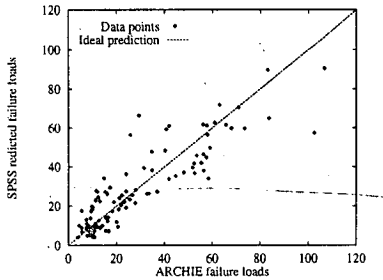


(c) ARCHIE correlation

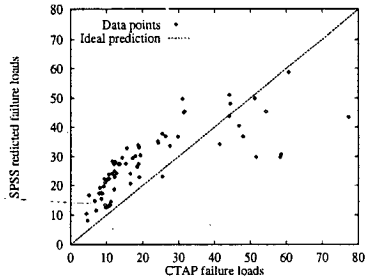


(d) CTAP correlation

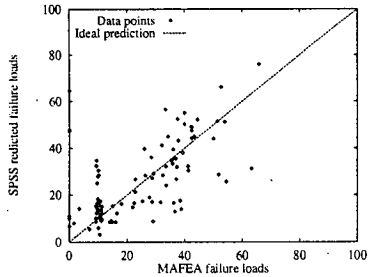


(e) MAFEA correlation

Figure 3: Correlation of each package to the SPSS predicted failure loads



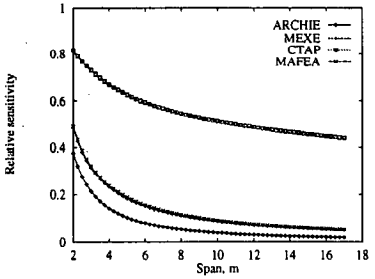


(a) SPSS sensitivity to span

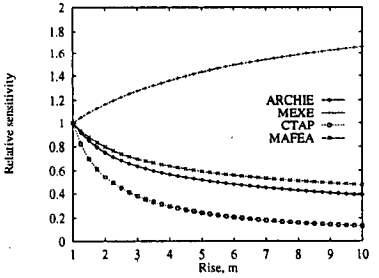


(b) SPSS sensitivity to rise

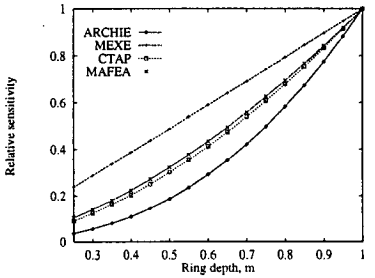


(c) SPSS sensitivity to ring thickness

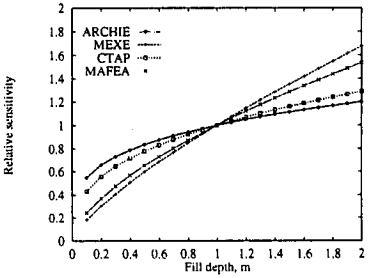


(d) SPSS sensitivity to fill depth

Figure 4: Effect of change of parameter on sensitivity of package